Development of Nonlinear Ultrasound Techniques for Multidisciplinary Engineering Applications

Malfense-Fierro, Gian-Piero

Award date:
2014

Awarding institution:
University of Bath

Development of Nonlinear Ultrasound Techniques for Multidisciplinary Engineering Applications

Gian Piero Malfense Fierro

A thesis submitted for the degree of Doctor of Philosophy

University of Bath
Department of Mechanical Engineering
October 2014

COPYRIGHT

Contents:

NOMENCLATURE

a	Lagrangian (material) coordinate
a_1	propagation distance
A	material dependent constant
A_1 & A_2	frequency amplitudes of the first and second harmonics of the recorded time domain waveforms
A_3	frequency amplitude of the third harmonic of the recorded time domain waveform
A_2^H	second order Huang coefficients of the material
A_3^H	third order Huang coefficients of the material
b	Burgers vector
c_L	Lamb wave speed (phase velocity)
c_p	primary wave (P-wave) speed
c_S	secondary wave (S-wave) speed of the plate material
C	material dependent constants and are the crack growth intercept in the crack growth exponent
C_{crk}	concentration of cracks in the interior of the material
d_0	distance between middle lines of the crack surface
E	Young modulus (or nonlinear and hysteretic modulus)
E_0	linear modulus
f	fraction of total fatigue life
$f = \omega/2\pi$	frequency
f_{dip}, $f_{T\text{-}N}$ & $f_{pT\text{-}N}$	are the volume fractions of material consisting of dipoles of density L (Taylor-Nabarro dislocation lattice structure of density $L_{T\text{-}N}$ and polarized Taylor-Nabarro dislocation lattice structure of density $L_{pT\text{-}N}$ respectively)
G	shear modulus
G_2	quadratic nonlinearity parameter
G_{2E}	experimental quadratic (second order) nonlinearity parameter
G_{2T}	theoretical quadratic (second order) nonlinearity parameter
G_3	cubic nonlinearity parameter
G_{3E}	experimental cubic (third order) nonlinearity parameter
G_{3T}	theoretical cubic (third order) nonlinearity parameter
h	dipole height ($y=h$)
$h_s = 2^{1/2}h_0$	h_0 is the characteristic height of the rough surface irregularities
k	wave number
ΔK	stress-intensity range

L	half of the distance of the length of dislocation between the pinning points
m	material dependent constants
M_1^+ & M_1^-	second order intermodulation products
M_2^+ & M_2^-	third order intermodulation products
n	material dependent constant
N	number of fatigue cycles
N_0	crack concentration
$N(\varphi,\theta)$	function of the crack distribution within the angles φ and θ
R	Schmid factor
R	current size of defect
R_0	initial size of defect
R_{crk}	radius of the crack
R_f	final crack length
$R_{f2/f1}$	second harmonic nonlinear acoustic moment
$R_{f2+f3/f1}$	second and third harmonic nonlinear acoustic moment
$R_{f3/f1}$	third harmonic nonlinear acoustic moment
$T = 1/f$	the period
U_x	component of the displacement vector in the Cartesian system coordinates (x, y, z)
U_y	component of the displacement vector in the Cartesian system coordinates (x, y, z)
U_z	component of the displacement vector in the Cartesian system coordinates (x, y, z)
V_0	speed of sound
$\Delta V(\varphi)$	volume variation of a single crack
α	linear coefficients of elasticity of the crack
β	nonlinear quadratic coefficients of elasticity of the crack
β'	normalised nonlinearity parameter
β^{crk}	crack growth contribution to the total nonlinearity parameter β
β_D	difference-frequency nonlinear parameter
β_{dp}	plastic contribution from the dislocation dipoles
β_{e}	elastic or lattice contribution to β
β_I	nonlinearity parameter for wave mode I
β_{lat}	contribution from the anharmonicity of the crystal lattice
β_S	sum-frequency nonlinear parameter
γ	nonlinear cubic coefficients of elasticity of the crack

ε	total longitudinal strain associated with the motion of dislocations in the dipole configuration
ε_e	elastic component of strain associated with the motion of dislocations in the dipole configuration
ε_{pl}	plastic component of strain associated with the motion of dislocations in the dipole configuration
$\Delta\varepsilon$	strain amplitude change over the last period
$\lambda = 2\pi/k$	wavelength
λ_I	eigenvalues
Λ	dislocation dipole density
$\Lambda_{(I)(I)(I)}$	diagonal terms
ρ	density of the medium
σ_0	compressive stress
$\|\sigma_0\|$	magnitude of the initial (residual or internal) longitudinal stress in the material
σ_{nn}	normal stress
ν	Poisson's ratio
ϕ	initial phase angle
ω	circular frequency (rad/sec, $\omega = 2\pi f$) of the propagating wave
Ω	conversion factor from the dislocation displacement in the slip plane to longitudinal displacement along an arbitrary direction

TABLE OF FIGURES

ACKNOWLEGDEMENTS

First to my mother, who has deeply been missed over the last few years, your grace and tenacity will forever be a great source of motivation and humility. To my father, thank you for your unconditional support; financial and other. Your never ending desire to improve the lives of those around you has been a great inspiration and your lessons on life will never be forgotten. My brother, your ability to have the contrary perspective about any subject matter will continue to entertain me.

To my supervisor Dr Michele Meo, I would like to thank you for offering me the opportunity to undertake the PhD in the first place. Your intellectual generosity, flexibility and tolerance of me during this long process has been critical, as has been your encouragement and support.

To all my fellow colleagues and friends who have been there through the good and bad times, thank you. To Dr F.Ciampa, Dr F. Pinto and Dr S. Pickering for you technical assistance throughout these long years.

This piece of research (Baseline-free Estimation of the Residual Fatigue Life using a Modulated Nonlinear Ultrasound Method) was funded and made possible by the Defence Science & Technolongy Laboratory (DSTL), (completed under MOD contract DSTLX-1000065588 – MAST Project CDE 23726). The study can be found in Chapter 4.1.

ABSTRACT

Mankind's constant pursuit of knowledge founded on innovation and creativity has led to a more complex world. A world governed by structures stretching high into the skies, objects flying faster than the speed of sound and exploration of the stars. These advancements have manifested in structures with complex geometrical designs, new building and engineering materials and the need for constant structural health monitoring (SHM). Structures comprising of a handful of components to those enlisting thousands are not impervious to failure. The 'perfect' material, one that will never fail, does not exist and may never. The need to remove the possibility of failure from the ever growing list of materials, components and structures has never been greater. There is an abundance of well suited techniques for a myriad of engineering problems, all suited for individual problem areas but all suffering from different weaknesses. There is no complete solution, only partial, short-lived solutions which are eclipsed by the next.

The objective of this PhD is to explore a new and interesting non-destructive testing and evaluation (NDT/E) technique; nonlinear ultrasound. The work looks at assessment of both metallic and composite structures. As of recently, the technique has become well studied and documented, which has highlighted the associated benefits. Theoretically it builds on the fundamental theories of ultrasound testing techniques, but provides solutions that have amplified sensitivity in early damage detection. The techniques follow the main principle that the excitation of damaged regions results in clapping/rubbing mechanisms that give rise to further harmonic production, these further harmonics can be correlated to damage.

Nonlinear ultrasound techniques were used to assess various systems that are prone to failure, these systems included adhesively bonded structures, bolted structures, structures susceptible to fatigue, compression loaded structures and impact damage of a composite plate. A series of experiments were undertaken which evaluated the ability of novel nonlinear ultrasound techniques to detect damage within these systems.

Initially the primary principles of nonlinear ultrasound techniques those that affect the accuracy and repeatability of these methods were explored. The effects of hysteresis, input and output voltages of piezoelectric transducers (PZTs), modal analysis, and various nonlinear parameters were evaluated. This allowed for a clear understanding of what factors affect the accurate generation of data from these techniques.

After determining various influences on results, adhesive and bolted joints were evaluated. With the aim to determine accurate nonlinear techniques that would be able to assess kissing bonds in metallic and composite joints, cracks in loaded structures and the loosened state of an individual bolt. A novel frequency specific nonlinear acoustic moment

method was used to evaluate the presence of kissing bonds. The acoustic moment experiments provided good kissing bond detection probability in both metallic and composite joints. Further experiments explored the effects of structurally loading on the production of nonlinear responses. The results provided valuable insight into the potential for these techniques to assess defects in loaded structures. Thus kissing bond detection as well as the loaded state of the structure was possible using the nonlinear acoustic moment method developed.

Joints account for a large proportion of mechanical and engineering structures, robust evaluation techniques would provide great savings in terms of maintenance, complete failure and lifetime service costs. The main finding was the ability to measure the loosened state of an individual bolt. Individual bolt loosened state was possible by using only two PZTs while assessing a system which included four bolts. This piece of research provides significant advancement in SHM of these structures, which has implications for small and large scale industrial joints.

Fatigue failure is the most prominent failure mechanism in metallic structures, an investigation into a baseline-free method using nonlinear ultrasound was undertaken. A fatigued component was examined over its useful life using a modulated nonlinear ultrasound technique, where the development of a nonlinear ultrasound theory was used to assess the residual fatigue life by comparing the nonlinear modulated response to a theoretical model. Findings showed good correlation between the theoretical and experimental results, paving the way for further studies of baseline-free methods. A baseline-free testing method would provide a great leap forward in current testing procedures; the work highlights the potential of such methods.

Further studies explored the possibility of using a computational model to predict damage levels in a material from a measured experimental nonlinear parameter. The findings of this research found good correlation between the second harmonic measured experimentally and that of the computational model.

A novel nonlinear ultrasound based thermosonic technique was developed using a dual frequency excitation method. The investigation looked at determining barely visible impact damage (BVID) of a composite plate. The speed and accuracy of the method provided many advantages over current testing methods, which can be slow and deliver inconsistent results. The research relied on the determination of damage-specific resonance frequencies (DSRF), which results in focused heating at the damaged zones. The methodology explored could be used in an autonomous setup which would provide rapid assessment of composites and higher probability of damage detection.

Finally the nonlinear ultrasound research completed establishes the broad range of applications for these techniques. The ease of adaptability of the techniques from metallic to

composite, loaded and unloaded structures and their ability to improve other NDT/E techniques shows the great potential of nonlinear ultrasound. Through methodical application of the various nonlinear ultrasound techniques to other SHM problems there is a great degree of certainty that these methods would provide further benefits.

In loving memory of my mother,
Corina Malfense Fierro

‘non est ad astra mollis e terries via’
‘There is no easy way from the earth to the stars.’

1. INTRODUCTION

1.1. Motivation

The research looks at ways to examine and define the extent of damage a material has received during its useful life, focusing on nonlinear ultrasound methods and a broad range of applications such as: fatigue life evaluation, location of impact damage using thermosonics, assessment of loaded structures, kissing bonds and debonding of joints and determination of the condition of bolted tension joints. The emphasis is to determine accurate and robust methods to evaluate multidisciplinary engineering problems such as fatigue and loosening of bolts. Initially nonlinear ultrasound techniques are used to investigate damage of metals, with the aim to apply similar methods or approaches to composite material evaluation.

Over the last sixty years NDT has been an area of continued growth, the need for such methods has increased dramatically in recent years due to the need for [1]: product safety, in-line diagnostics, quality control, health monitoring, security testing, etc. Over the last two decades due to the high cost of inspection of composite materials compared with metallic structures, development of a reliable and effective NDT/E method to detect the occurrence of critical failure modes in composites has been pursued [2-5].

Currently there are over two dozen NDT techniques that are available for metallic and composite material evaluation. Some of these methods include: acoustic emission testing (AE), electromagnetic testing (ET), infrared and thermal testing (IR), magnetic resonance imaging (MRI), NMR spectroscopy, scanning electron microscopy (SEM), ultrasonic testing (UT) and visual inspection (VT) to name a few. These methods although essential for the testing of materials are not without drawbacks, which include: time, cost and defect discovery concerns.

One main area of concern with current NDT methods is the large amount of time needed to test components for damage, as components need to be brought to test facilities and undergo lengthy inspections. While other areas of concern are the damage that occur in components during service as they play a key role for condition monitoring and residual life estimation of in-service components or structures [6]. Thus methods of NDT which may lead to testing a component while attached to their larger structure and methods to decrease inspection time will be explored.

The aim is to evaluate the suitability and effectiveness of nonlinear ultrasonic NDT/E methods which are currently available or which may become available in the near future. The great demand for NDT methods is further amplified as methods usually overlap many fields of engineering such as: aerospace engineering, civil engineering, electrical engineering and material science among others. Of the many methods of NDT available ultrasonic methods are among the most popular due to their capability, flexibility and relative cost effectiveness.

Ultrasonic testing can be broadly defined into two groups those based on principles of linear acoustics and those based on principles of nonlinear acoustics. Linear acoustics include transmission, reflection, scattering, mode-conversion and absorption of acoustic energy caused by a defect [7-12]. Nonlinear acoustics include harmonic generation, frequency mixing and modulation of ultrasound by low-frequency vibration [13-15]. While linear techniques identify cracks by detecting the amplitude and phase change of the response signal caused by defects when a consistent probe signal is applied, nonlinear techniques correlate defects with the presence of additional frequency components in the output signal [16]. The current shift away from linear ultrasonic techniques is mainly due to the fact that the sensitivity of nonlinear methods to study damage evolution appears to be a few orders of magnitude higher [17], while linear techniques are only sensitive to gross defects rather than micro-damage [6].

The effectiveness of ultrasonics as a measure of a structures integrity comes from the fact that elastic waves propagating through a nonlinear medium give higher order harmonics [18]. These higher order harmonics give a direct measure of the acoustic nonlinearity parameter (β, referred to as G_{2E}) [19], it has been shown experimentally that there is a good correlation between the fatigue damage and the acoustic nonlinearity parameter in metallic materials [13, 20-22]. The increase of acoustic nonlinearity can be attributed to microcracks on the surface of aluminium alloy [13], while it has also been found that the contribution of dislocation dipoles is even more significant in polycrystalline materials since the monopole loop lengths in these materials are much shorter than ones used in earlier investigations [23]. While application of Cantrell's model [24] using aluminium alloy under fatigue loading yields excellent agreement between theory and experiment. Higher order harmonics have been extensively investigated with regard to metallic materials and have shown good correlation with damage.

The robustness of nonlinear methods to geometry and moderate environmental variations (temperature) makes these techniques attractive for field applications. Nonlinear ultrasonic methods have recently focused on guided ultrasonic waves, Lamb waves, as they have unique advantages over other ultrasonic techniques that use bulk waves in that they can efficiently interrogate large areas and geometrically complex or inaccessible components [25].

Current research has focused on structural health monitoring (SHM) with regard to composite material structures, which looks to create structures capable of producing real time information about their condition. These systems usually use a network of built-in sensors to provide real-time data acquisition [26], either employing active sensors (create acoustic signals to detect damage) or passive sensors (detects structure vibrations/impacts). Other methods include the development of a SMART layer which can be mounted to the surface of composites or embedded inside composites [27]. This could ultimately be used to record dynamic signals such as foreign object impact [28, 29]. Although SHM systems are the next level in non-destructive testing of materials it is unlikely that all the components of a structure will be equipped with these capabilities, this still leaves space for alternative methods.

1.1.1. Bolted Joints, Adhesive Joints and Kissing Bonds

Adhesive bonding of aluminium and other materials has been used for many years in industries such as aircraft construction; primarily to reduce weight, create rigid structures and improve the durability of these structures. Adhesive bonds are used in some form or another in most products that are produced from labels on products to protective coatings on automobile parts to joints that provide structural integrity. The focus is on structural adhesive joints where failure of the joint can lead to critical failure in the larger structure. Birch (1994) [30] outlines many advantages of adhesively bonded joints, these benefits can be found during the design, production and service life of the joints. In design they allow for a larger choice of materials, have good fatigue behaviour, result in stiffer/stronger joints, smooth aerodynamic appearance and weight saving. In production joining and sealing operations are combined, there are no metallurgical damage due to panel coatings and production can be rapid and automated. In service there is reduced corrosion of the joints, improved fatigue behaviour, improved vibration and harshness characteristics.

The disadvantages of adhesive joints are that they are inherently weak in peel, the bond strength decreases with temperature and they cannot be easily dismantled for in-service repair. The bonding of two aluminium components relies on two mechanisms that determine the strength and durability of the bond. Which are the mechanical interlocking of the adhesive polymer into a micro-roughened surface and the chemical bonding between the adhesive and the aluminium oxide or pre-treatment. In order for good adhesion to occur the adhesive must be spread over and achieve effective and uniform wetting of the aluminium surface, without the accurate application at the adhesion phase, kissing bonds can occur.

These errors, of poor cohesion result in the degradation of the strength and other mechanical properties of the adhesive, and can be caused during manufacture or by environmental affects [31]. There are numerous definitions of what exactly a kissing bond is, but for the purpose of this work it refers to contact between two layers where adhesive has not covered the entire surface of the joint, resulting in an adhesive free gap (dry-contact bond). Chapters 3.1 and 3.2 focus on kissing bond detection (as well as crack detection) using various nonlinear ultrasound techniques, with the main aim to understand the underlying factors that may affect the accuracy of these techniques while looking to develop more accurate testing procedures. A multitude of tests were conducted such as: transmission and reflection tests, single and dual frequency tests, loaded structures and a variety of nonlinear ultrasound techniques.

Bolted joints are used in numerous engineering industries due to relative low cost, ability to be disassembled, strength and are compatible with most materials. Some of the general issues relating to bolted joints are the size of joints, micro-slip/hysteresis, damping problems, difficulty of modelling and controlling, assembly and fabrication times. Joints are usually used as connectors between multiple parts of a larger structural system and play important roles in dealing with

stiffness, vibration, damping, stability, and loading. As part of larger assemblies they are used to resist tensile, shear loads and moments.

These joints are usually made up of bolts, washers and nuts that are used to apply a preload to the joint, the washers are used to distribute load in a clamped member while the nut allows for the disassembly of the joint. Preloading of the bolt can be simply described by a series of springs: where k_b refers to the bolt stiffness and k_m refers to the members stiffness. In a joint with two bolted components this can be described as two in-line springs with the same or different stiffness (depending on material of the member).

Typically joints are designed to result in bolt failure this is done as the bolts are less expensive and easily replaced. Evaluation of the loosened state of the bolt can have large implications on structural health monitoring (SHM) of joints, as current maintenance programs are systematically carried out. The development of *in-situ* systems with the ability to assess individual as well as group bolt states would advance the monitoring of structures incorporating bolted joints.

A wind turbine section was used to test the ability of nonlinear ultrasound methods to evaluate individual as well as group bolt loosened states. The ability to detect individual bolt loosening would have great significance in improving maintenance and monitoring of such structures. Thus an extensive evaluation of potential methods was undertaken to assess the effectiveness of nonlinear methods in Chapter 3.3.

1.1.2. Fatigue and Impact Damage

Fatigue failure often leads to catastrophic failure of components and structures and materialises in bridges, aircraft and machine components, with failure occurring due to dynamic stresses over time. Fatigue failure is also one of the most common metallic failure mechanisms (90% of all service failures due to mechanical causes), underlining the importance of reliable, accurate and robust testing techniques. One of the main issues relating to the discovery and evaluation of fatigue is the magnitude of external forces which may be so small that the effect does not results in any detectable damage. Current methods employ systems of designing against fatigue. These methods take into account factors such as mean stress, notches, environment and surface finish. Although designing for fatigue results in structures that are perceived to be much stronger, failure still occurs due to uncertainties in the repeated cyclic plastic deformation which may exceed design parameters. Plastic deformation can be caused by maximum tensile stress of sufficiently high values, large amount of variation or fluctuation in the applied stress and sufficiently large number of cycles of the applied stress. Other elements contributing to fatigue failure include stress concentration, corrosion, temperature, overload, metallurgical structure, residual stress and combined stress. Designing for fatigue has also become more difficult due to the increase in sophistication in machines and structures which can lead to poor design of parts and components.

It is understood that cyclic plastic deformation is the major contributor to the fatigue process, without repetition of this process fatigue would not occur [32]. Plastic strain, applied only once, does not cause any changes to the substructure of materials, while multiple repetition of this very small plastic deformation leads to cumulative damage and ultimate failure. Elastic deformation is totally reversible unlike plastic deformation which causes irreversible changes. Thus plastic deformation can be considered the most decisive phenomenon in the fatigue process. Other factors such as fatigue hardening and/or softening, microcrack nucleation and crack propagation all have significant effects on the fatigue life performance of material.

The crack nucleation and propagation phases of fatigue are of particular importance. As it is believed that measurable ultrasound responses at various points over the fatigue life can be generated by fatigue cracks. Fatigue cracks are usually induced by incisions on the surface of the material [32]. Fatigue cracks always nucleate from free surfaces of cyclically loaded metals and propagate from positions where cyclic-plastic deformation is higher than average, in places with plastic-strain concentration (connected to stress concentration). Crack initiation areas usually occur at fatigue slip bands, grain boundaries and surface inclusions. For the experiments conducted in Chapter 4 fatigue cracks were induced near high stress concentration areas, this was done to ensure fatigue cracks propagated in the correct regions.

Due to the importance and broad implications of fatigue failure, one of the main pieces of work focused on was the development of a baseline-free estimation method for residual fatigue life using nonlinear ultrasound modulation (Chapter 4.1). As has been mentioned there are countless fatigue related issues and failure mechanisms, thus the work focuses on the propagation of a known fatigue crack of a military aircraft rib which was a simple sub-structural component.

Composite structures are highly susceptible to impact damages (especially in the aerospace industry) which can lead to large reductions in the strength of components and can ultimately lead to failure. One of the main concerns relating to impact damage is the fact that considerable internal damage may occur with minimal visual detectability (Barely Visible Impact Damage, BVID). Due to the difficulty of detection, BVID may be undetected and lead to catastrophic failure of key structures.

Aircraft structures can be subjected to numerous BVID sources which can be broadly categorised into two groups of damage: those that involve high-mass, low-velocity and wide area impact known as blunt impact (such as collisions with ground vehicles) and low-mass, high-velocity impact (hail, birds and tire fragments). Many locations of aircrafts are exposed to these sources of BVID damage such as the fuselage, nacelles, wing surfaces and control surfaces. Thus there is a high need for BVID NDT/E techniques for the detection and localisation of damage that are accurate, efficient and provide quick assessment. Due to the importance of BVID detection and localisation a novel thermosonic technique was explored (Chapter 5).

1.2. Thesis Objective

The main focus of this thesis is to develop novel nonlinear ultrasound methods for the detection, localisation and imaging of defects in materials. The experimentation was broken down into various stages with clear objectives, starting with:

(i) The evaluation of the critical factors that may affect nonlinear ultrasound testing techniques, such as: material hysteresis, input voltage levels, amplification, resonance frequency of materials and structural loading effects (among others).

(ii) Examination of various nonlinear ultrasound techniques, such as single frequency excitation, dual-frequency excitation and nonlinear acoustic moments.

(iii) Testing of different materials, metallic and composite materials.

(iv) Experimentation assessed the ability of nonlinear techniques to accurately evaluate five main damage detection issues. These included: detection of kissing bonds in metallic and composite joints, the potential of nonlinear methods to improve the probability of damage detection of loaded structures, prediction of the loosened state of a bolted joint, residual fatigue life estimation and the evaluation of low impact damage in composite materials.

(v) Finally, the incorporation of nonlinear methods with other techniques. The fundamental nonlinear theory of the generation of further harmonics was incorporated with a thermosonics method in order to improve the probability of damage detection.

The preliminary investigations were conducted to provide robust testing methodologies and techniques which could be applied to many different engineering problems. Initially, a solution was sought for loaded structures (bonded or compression loaded structures) where linear and other techniques have difficulty in assessing damage. Subsequently an experiment was conducted to establish a baseline-free testing method using dual frequency nonlinear ultrasound. With the main advantage and innovation of this method being that pretesting of the structure (no baseline) would not be needed in order to measure the extent of damage. A computational model was also developed to replicate nonlinear responses in materials and predict the damaged state of a fatigued structure.

Furthermore considerable work focused on determining the loosened state of a bolted structure (wind turbine, in this case) considering the importance of such joints in many engineering fields. This work looked to provide clear evidence of the advantages of using nonlinear over other more conventional methods.

Due to the large perceived benefits of nonlinear ultrasound methods, a brief investigation into other NDT techniques that could benefit from nonlinear ultrasound mechanisms and phenomena lead to the exploration of a nonlinear ultrasound based thermosonics method for the

evaluation of impact damage in composite structures. While the thesis covers a broad range of seemingly diverse areas; the approaches developed and research all relate to nonlinear ultrasound. The variety of solutions found, from loaded to non-loaded structures, metallic to composite materials, and fatigued specimens to bolted structures, show the wealth of diversity of these new and exciting testing techniques.

Current industry standard testing techniques rely heavily on linear ultrasound methods, and therefore there has yet been mainstream adoption of nonlinear ultrasound testing methods, this body of work looks to bridge this gap by providing robust real world nonlinear ultrasound solutions to a few of the many problems troubling many engineering professions.

1.3. Thesis Outline

The literature review (Chapter 2) highlights the importance and vast research that has been undertaken in the field of non-destructive testing and evaluation (NDT/E). Chapter 2 focuses on the development of ultrasound testing procedures for NDT/E. The Chapter builds the basic foundation of the propagation of waves in materials and then describes differences in linear and nonlinear techniques. The various advantages and disadvantages of ultrasound techniques are discussed with the aim of establishing areas where further research could provide great improvement in damage detection and evaluation. The accuracy of ultrasound techniques in detecting damage in metallic and composite materials are evaluated, while the necessity for a fatigue life prediction method is explored by investigation of prior studies. The main aim of this chapter is to build the foundation and reasoning of why the work investigated is important and worthwhile.

Chapter 3 focused on the key factors and testing techniques that may affect the accuracy of nonlinear ultrasound testing methods, such as: hysteresis, input voltage, modelling techniques, resonance frequency testing, reflection and transmission testing and single or dual frequency excitation techniques. The measurement of the second and third order nonlinearity parameters for a single frequency excitation technique is discussed (Section 3.1.1) and the modulated (dual frequency) nonlinear parameters are derived (Section 3.1.2). A novel technique (derived in Section 3.2.1) called nonlinear acoustic moments was used to assess a metallic and composite loaded structure. After determining the importance of the key factors and identifying weaknesses of various nonlinear ultrasound approaches, a bolted structure was evaluated using all the nonlinear methods in order to determine the loosened state of the bolts.

Chapter 4 develops a novel baseline free estimation method for the residual fatigue life of a metallic structure using a modulated nonlinear ultrasound technique. This method takes into account key factors determined in Chapter 3 relating to the nonlinear behaviour of the structure as well as the modulated nonlinearity parameters. A theoretical approach (described in 4.1.1) is evaluated against experimental fatigue data of the modulated nonlinearity parameters. Furthermore the chapter looks to develop a finite element model to assess the nonlinear elastic behaviour of a

fatigued structure. This work builds on methodologies developed in the baseline free estimation method and looks to estimate further harmonic responses using the commercially available software LS-DYNA.

Chapter 5 establishes a novel thermosonic technique that uses nonlinear ultrasound phenomena to determine damage specific resonance frequencies as well as a dual-frequency excitation method, which ultimately led to an improvement in the technique. Chapter 6 presents the conclusions, main findings and potential for future work of the thesis.

2. Ultrasonic Theory

This chapter focuses on the background theory and research of ultrasound techniques. Section 2.1 defines the basic principles of wave propagation, discussing Rayleigh and Lamb Waves. Section 2.2 outlines early findings proving the propagation of waves in metallic structures, while discussing important early studies. Section 2.3 briefly explains the damage process of metallic materials showing the need for damage detection techniques and Section 2.4 explains various linear ultrasound techniques.

Nonlinear ultrasound techniques are broken down into four main sections (in Section 2.5), which include: early nonlinear studies, damage precursors and fatigue using nonlinear methods, nonlinear modulation and the use of nonlinear methods for various other damage types (such as creep, hardening and thermal ageing).

Sections 2.6 highlighting the difficulty of assessing damage progression in composite materials and explores nonlinear ultrasound techniques that have produced robust results in the evaluation of composite damage. Section 2.7 provides a brief summary of the literature review.

2.1. Wave Propagation

Ultrasonics is generally defined as the band between 20 kHz and 1 GHz over which is conventionally known as the hypersonic regime [33]. Throughout this report frequencies above 1kHz have been referred to as ultrasonics, this has been done to describe a large range of sound waves which possess similar characteristics and which can be generated using piezoelectric transducers. Ultrasonic methods can be broken down into cavitation, guided waves, SAW, linear ultrasonics, nonlinear ultrasonics and medical imaging among others. For the purpose of nonlinear ultrasonic non-destructive techniques; Rayleigh and Lamb waves have been focused on by many researchers. The basic wave equation and solution can be defined; respectively as:

$$\frac{\partial^2 \psi}{\partial x^2} = \frac{1}{V_0^2}\frac{\partial^2 \psi}{\partial t^2}$$

Eq. (2.1)

$$\psi = A\sin k\left(x - V_0 + \phi\right)$$

Eq. (2.2)

Where: V_0 is the speed of sound, ϕ is the initial phase angle, the wavelength $\lambda = 2\pi/k$, k is the wave number, the period $T = 1/f$, and frequency $f = \omega/2\pi$. It was first discovered by Rayleigh (1896) [34] that the propagation of finite-elastic waves through a medium result in the presence of nonlinear terms in the wave equation, which cause intense acoustic waves to generate new waves at frequencies which are multiples of the initial sound wave frequency. Other early work [35, 36]

contributed to the theoretical treatment of nonlinear elasticity, while acoustic harmonic generation was first verified experimentally in air by Thuras, et al. (1934) [37].

Rayleigh waves are synonymous with surface acoustic waves (SAW) they are confined to within a wavelength or so of the surface along which they propagate, are independent of longitudinal and shear BAW modes (which propagate independently at different velocities) and their longitudinal and shear motions are intimately coupled together and travel at a common velocity [33]. They are also considered to be guided waves when they are propagating along the stress-free boundary of an elastic half-space and the wave speed in an elastic half-space is non-dispersive (i.e. independent of the frequency) [12]. Other important studies include those from Viktorov (1964) [38] where the nonlinearity of the waves was first discussed, Rischbieter (1967) [39] where their applicability to steel and aluminium was established and Vella, et al. (2009) [40] where the theory of thermoelasticity was used to derive exact expressions for the nonlinear force and stress fields. Further nonlinearity research was extended to anisotropic materials and derived generalisations [41, 42].

Displacement and velocity components of Rayleigh waves are in the *x* and *z* directions, with no coupling with the transverse waves with displacement along *y*, this can be seen in Figure 2.1 below [33]:

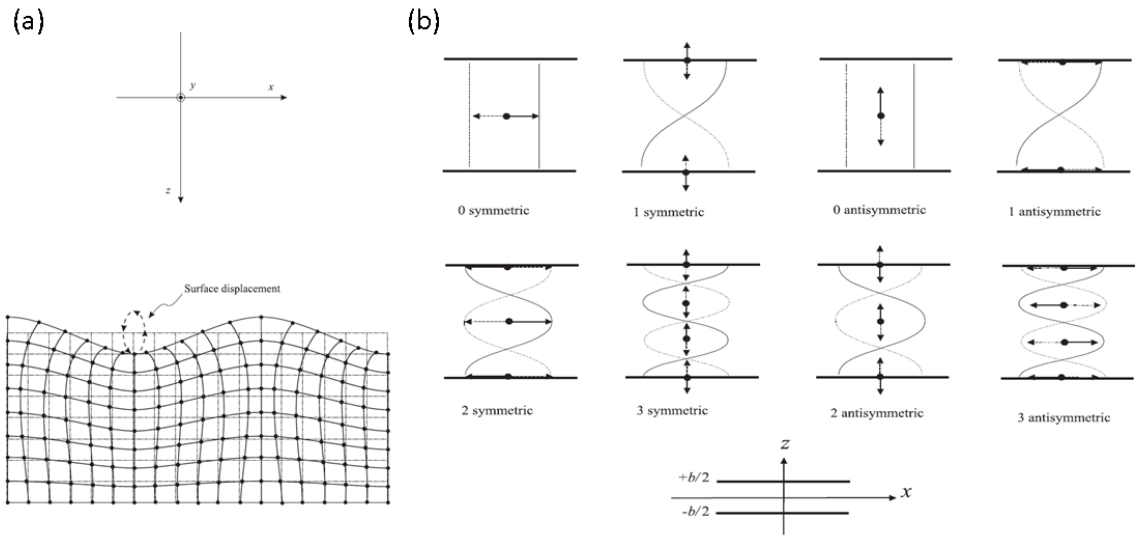

Figure 2.1: (a) Coordinate system for Rayleigh wave propagation, and grid diagram for near-surface mechanical displacement due to Rayleigh waves. (b) Coordinate system used for Lamb waves, with displacement variations for the lowest four modes in the limit $\beta S \rightarrow 0$ [33].

Lamb waves are guided waves that propagate in a plate, they propagate through a waveguide and satisfy the stress-free boundary conditions of the waveguide, are dispersive (dependent on frequency) and are more complicated than Rayleigh waves [12, 33]. Lamb waves propagating through a plate whether in air or immersed in a liquid result in energy being leaked into the surrounding medium [12], this is the case for any Lamb wave propagating through a plate that is

not in a vacuum. Although the magnitude of energy leaking into air is negligible and can generally be ignored, the same cannot be said for a plate immersed in liquid in which case the energy should not be ignored. Early work using lamb waves conducted by Deng (2009) [43] investigated the second harmonic generation in an isotropic material. de Lima, et al. (2003) [44] formulated the second harmonic generation for isotropic elastic waveguides which took into account all the modes of the secondary wave field and Lee, et al. (2008) [45] suggested additional conditions for generating cumulative nonlinear Lamb waves.

Dispersive waves are characterised as having a phase speed independent of wavenumber, thus all waves of any wavenumber propagate at the same speed (there is no change in shape). The differences between dispersive and non-dispersive waves are highlighted in Figure 2.2 below:

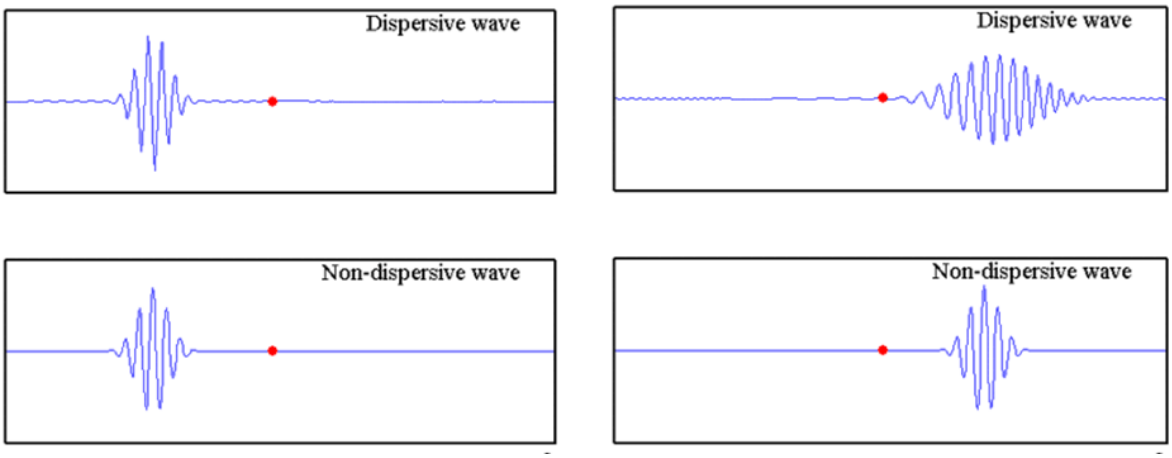

Figure 2.2: The image above shows how dispersive wave differs from a non-dispersive wave after an initiating point (red dot, with the wave moving from left to right)

For a linear, elastic, isotropic plate (homogeneous, in a vacuum) of thickness 2*h* the phase velocity dispersion curves for a Lamb waves are obtained by solving the following dispersion equations [12]:

$$\frac{\tan(\eta h)}{\tan(\beta h)} = \frac{\left(2k^2 - k_S^2\right)^2}{4k^2\eta\beta}$$

Eq. (2.3)

$$\frac{\tan(\eta h)}{\tan(\beta h)} = \frac{4k^2\eta\beta}{\left(2k^2 - k_S^2\right)^2}$$

Eq. (2.4)

Where:

$$k = \frac{\omega}{c_L}$$

Eq. (2.5)

$$\eta = \sqrt{k^2 - k_p^2}$$

Eq. (2.6)

$$\beta = \sqrt{k^2 - k_S^2}$$

Eq. (2.7)

$$k_p = \frac{\omega}{c_p}$$

Eq. (2.8)

$$k_S = \frac{\omega}{c_s}$$

Eq. (2.9)

Where: c_L is the Lamb wave speed (phase velocity), c_p is the primary wave (P-wave) speed, c_S is the secondary wave (S-wave) speed of the plate material, ω is the circular frequency (rad/sec, $\omega = 2\pi f$) of the propagating wave. Dispersion curves are used to determine the relationships between wave velocity and frequency for the tested material. Both symmetric and antisymmetric modes can be solved using the dispersion equations, and dispersion curves show all the constructive interference zones that could occur as the waves reflect inside a structure (demonstrating the kinds of waves and modes that could actually propagate) [46].

The dispersion curves are solved by fixing the frequency (ω) to determine the Lamb wave speed or by fixing the Lamb wave speed (c_L) to determine the frequency (it is assumed that all other values are known) [12]. One of the difficulties in determining the dispersion equation is that solutions of the dispersion equations result in many roots thus it is important to ensure that a very small step size is used (to insure no roots are missed) [12]. Mode shapes S_0 (symmetric) and A_0 (antisymmetric) which are determine using the dispersion equations can be described by Figure 2.3 below, which shows the dispersion curves for a brass plate [33]. Details for computing these phase and group velocity dispersion curves can be found in Rose, et al. (2000) [47].

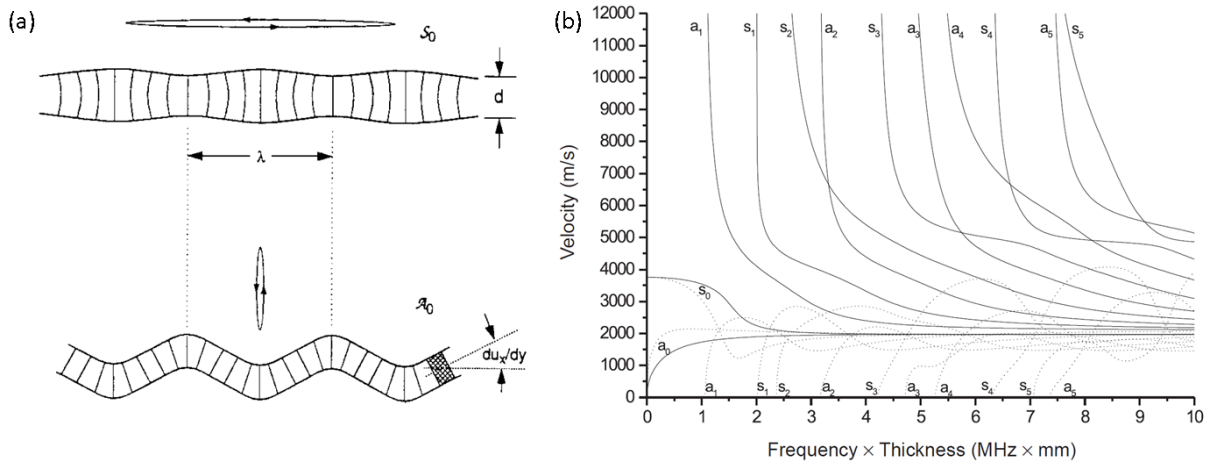

Figure 2.3: (a) Mode shapes of S_0 and A_0 modes showing the deformation of particle planes and the retrograde elliptical motion at the plate surface. (b) Phase (-) and group (…) velocities of Lamb modes in a brass plate as a function of frequency x thickness [33].

Rose (2002) [46] discusses important factors of designing a guided wave experiment including the use of dispersion curves as they contain a great amount of information that can be used to design and analyse experiments. Rose (2002) [46] discusses: the importance of taking into account phase velocity and frequency spectrum principles, the source influence concept (using an experimental versus theoretical results), selection of guided wave modes for the particular experiment, the distribution of in-plane displacement, out-of-plane displacement and actual stress across the thickness of the structure, the influence of the vibration pattern along the thickness which varies, wave structure considerations to establish maximum penetration power for the structure and ability to establish maximum sensitivity to a defect either on the surface of the structure or at the centreline or elsewhere.

This section discussed the complexities involved in using guided lamb waves and presents basic wave propagation theory in materials. This thesis looks to develop and evaluate non-dispersive longitudinal waves which are a function of both time and space. Piezoelectric sensors attached to the surface of the materials tested are used to generate these waveforms. Generally continuous frequency specific sinusoidal waves were used to excite the various materials studied. Simple waveforms are used as it is expected that defects will be represented by changes to the waveform and additional frequency components caused by defects will be represented in the response signals (nonlinear effects of damage). The nonlinear effects caused by defects will be discussed in Chapter 2.5, while the next section gives a brief history of ultrasound as a damage detection tool.

2.2. Ultrasound as a Damage Detection Tool

This chapter briefly discusses the progression of ultrasound from purely scientific experiments into a non-destructive testing tool.

Hughes, et al. (1953) [48] derived expressions for the velocities of elastic waves in stressed solids using Murnaghan's theory of finite deformations and third order terms in energy. The experiments conducted measured the transmission time of elastic pulses through the material, with the velocities of longitudinal and shear waves being determined as a function of applied stress (hydrostatic pressures and simple compression were applied to the specimens). Three materials were used in the experiments polystyrene, iron and pyrex glass. Shortcomings of the research were that it was only conducted on perfectly elastic solids i.e. solids where strains are a function of stresses and temperature (thus a strain-energy function exists). This limited the solution to a few materials and problems as solids may be anelastic or plastic and deformations may be so large that infinitesimal theory is not accurate.

Toupin, et al. (1961) [49] showed that the variation of sound speeds with initial stress and that the measured magnitude of the acoustoelastic effect can be used to determine the third-order elastic constants of an isotropic material. The experiment analysed plane waves of small amplitude propagating in an initially deformed and stressed elastic material.

Truell, et al. (1969) [18] evaluated how an ultrasonic wave would propagate in solid state physics. This research established a mathematical proof of how waves propagate through Al_2O_3 (Aluminium Oxide) including compressional and transverse waves. Truell, et al. (1969) [18] also investigated preparation methods for materials whether a single crystal or not and evaluated how elastic anisotropy affects wave propagation including how the orientation may become important for velocity and attenuation measurements. This research ultimately provided early scientific proof for the use of ultrasonic waves in metallic materials.

Acoustoelasticity is an ultrasonic technique that has been used to determine residual stress of various metallic materials [50-53]. The method relates the changes in the stress state to corresponding changes in the speeds at which various plane waves propagate through a material. Studies undertaken by Fukuoka, et al. (1978) [51] were based on the fact that an initially isotropic material becomes anisotropic under stress. A mild-steel circular plate with a concentrically patch-welded joint was measured using the acoustoelastic method to give an acoustical stress measurement, which was found to agree well with conventional destructive methods as well as theoretical predictions. A similar experiment was performed by Scott, et al. (1979) [52], where acoustoelastic measurements were used to non-destructively determine the in-plane residual stress variation in extruded cylindrical billets. The results were shown to be rapid, accurate and reliable and were able to determine the absolute residual stress values from only longitudinal wave data.

These early studies built the fundamental principles from which many ultrasound techniques have been developed. The follow section briefly discusses the damage process of materials, while

Sections 2.4 and 2.5 discuss the development of linear and nonlinear ultrasound techniques for the detection and evaluation of damage in metals.

2.3. Damage process of a material

It is important to understand the basic principles relating to cyclic deformation and crack initiation in materials. These factors affect the remaining useful life of the material as well as its ultimate failure. There are five stages leading up to and including failure of a material, these can be classified as [54]:

(i) Substructural and microstructural changes which cause nucleation of permanent damage.
(ii) The creation of microscopic cracks.
(iii) The growth and coalescence of microscopic flaws to form 'dominant' cracks, which may eventually lead to catastrophic failure.
(iv) Stable propagation of the dominant macrocrack.
(v) Structural instability or complete failure.

Factors such as minimum shear stress and strain required for crack formation, delamination (composite materials, discussed in Section 2.6) and the affect they have on the fatigue life of the material are important factors to consider. The effectiveness of NDT/E techniques relies on how early damage can be assessed. A method that can only determine damage at the macrocrack level is not as effective as one that can measure damage at a microcrack level. Thus there has been a great emphasis in both industry and research for techniques that provide early detection of damage. Nonlinear ultrasound techniques are believed to provide detection of damage before linear techniques. The next sections discuss the ability of linear and nonlinear ultrasound techniques to evaluate damage at the various stages of failure of a material (Chapters 2.4 and 2.5.)

2.4. Linear Ultrasonic Development and Theories

Traditional ultrasonic techniques are based on linear theory and normally rely on measuring some particular parameter in order to determine the elastic properties of the material or detect defects [55]. Linear techniques usually focus on the measurement of the velocity of sound, attenuation, transmission coefficients and reflection coefficients [7-9, 11]. If defects are present the phase or amplitude of the output signal changes, although the frequency of the input and output signals remain the same [6].

Linear ultrasonic techniques rely on the propagation of vibrations through a medium, where deviations from the equilibrium state of the medium caused by these vibrations are assumed to be small (the propagating wave is assumed to have small amplitude or low intensity) [6].

Common linear ultrasonic tests use a transmission basis, which detects irregularities within and on the surface of materials. High frequency sound waves are transmitted as beams or rays of energy through a test specimen to a receiving device [56]. Defects are then evluated by energy losses in transmitting the ultrasonic waves through the test specimen, which may lead to deflection or scattering of energy rays by irregular surfaces and losses in passing energy rays through an air pocket [56]. Due to the solid to air interface defects can be determined by using a receiving device.

Nielson (1976) [57] investigated the use of acoustic emission (AE) for detection of defects as they arise during fabrication, focusing on three main areas inspection during welding to detect defects as they are formed (arc welding, electro slag welding, electron beam welding, resistance spot welding and other welding methods), inspection immediately after welding to detect delayed cracking and inspection during stress relief to detect reheat cracking. The outcome of the experiment found that AE was a useful tool to provide information about delayed and reheat cracking during welding. Nielson (1976) [57] found the welding process to be hostile to AE techniques due to noise thus stages of quietness were introduced and reheat cracking was successfully investigated by the AE technique.

Linear ultrasonic techniques (such as transmission) have often been used in rock mechanics and mining sciences because wave propagation velocity and attenuation can be used to determine dynamic properties of rocks [58, 59]. Mogi (University of Tokyo) conducted an extensive study of AE in rocks in the early 1960s, where he found that the propagation of cracks as a function of time by using a source location technique and pointed out the linear relationship on a log-log scale between number and magnitude of AE [60]. Later it was found that although wave propagation velocity and attenuation are correlated, attenuation has been found to be more sensitive to weathering condition, anisotropy, grain dimensions and porosity of a rock [58, 61-65].

The 60s and 70s saw rapid growth in the use of acoustic emission techniques for materials research and assessment of structural integrity [66, 67]. There was a large array of tests developed such as tensile tests, fracture mechanics tests, structural evaluations, stress corrosion testing, production monitoring, stress rupture testing, weld material qualification, very small parts quality assurance and high explosive cracking (to name a few AE developments). AE is used to provide early and ample warning of impending failure, detection and location of hidden flaws and detection of AE associated with subcritical flaw growth [68]. The AE tests described earlier detect various mechanical occurrences to evaluate the condition of a material, generally these test detect propagating defects or flaws, location of propagating defects or flaws, gross or localised yielding, pressure vessel burst strength, early warning of impending failure, effective welding process parameters and monitoring of welding processes [68].

Kikuta, et al. (1975) [69] explored the initiation of cracks using the AE technique for detecting and monitoring propagation of delayed crack induced by hydrogen embrittlement in high strength steel. Okada, et al. (1974) [70] researched the AE technique to distinguish between the active path corrosion and the hydrogen embrittlement in stress corrosion cracking of high strength

and stainless steels. Sakamoto, et al. (1973) [71] studied the cracking at solidification of pure iron with various contents of sulphur by means of the AE technique.

Graham, et al. (1975) [82] investigated the use of AE in the frequency domain in order to determine the frequency content of individual acoustic emission bursts, identify source mechanisms (dislocation motion, crack propagation, phase transformations and twinning) for insight into the physical parameters associated with their operations and distinguish between AE generated by the source mechanisms and those produced by extraneous noise sources (enabling filtering of noise). Graham, et al. (1975) [72] established a method for easily determining the broadband frequency content of acoustic bursts which allow quick formation of different types of AE and extraneous background noise in the AE test environment. Graham, et al. (1975) [72] also determined that the frequency content of the acoustic burst is related to the mechanism which produced it and was not affected substantially by mode conversion during multiple reflection in a solid and that several distinctive types of frequency spectra suggested that determination of noise bursts from different sources can be accomplished in some cases by frequency content alone.

Kelly, et al. (1975) [83] investigated the detection and location of flaw growth in metallic and composite structures Kelly, et al. (1975) [73] by using a multichannel real-time acoustic emission location system. The study contributed to the field considering that most of the previous work on AE locational techniques were restricted to metallic structures and location of the source were found by post-test analysis. Kelly, et al. (1975) [73] found that the AE source location techniques provided accurate information on the location of defects in a variety of materials and structures, the AE location techniques provided a powerful tool for verification of integrity of pressure vessels and other structures and it was desirable to perform a AE characterisation of an unfamiliar material prior to testing a structure of that material.

Novel scan patterns were explored by Highmore, et al. (1987) [74] to determine whether they were useful for flaw sizing and characterisation, as significant sizing and characterisation errors had been made at the time by the best inspection teams and methods struggled with regard to irregularly-shaped and complex flaws. Highmore, et al. (1987) [74] methods involved increasing the range of angles of the ultrasound incident on the flaw, focusing on the two probe Time-of-Flight Diffraction (TOFD) method, probe skewing and probe separation scanning. The beam skewing method found beneficial effects of the TOFD configuration for surface-breaking and buried flaws of irregular shapes. Flaw edges not visible using conventional TOFD arrangements were visible using the skewed probe arrangement, although the images did exhibit significant amounts of ‘clutter’ attributed to the finite ultrasonic pulse length, the inherent probe beam spread and possible mis-registration of the composite skewed scans and further work was suggested to improve these images. The probe separation method found that although it was possible to demonstrate the effects on a simple through-thickness flaw, further work was needed to determine the effects on a more complex real flaw [74]. Methods which have applications to a large range of

varying flaws provide significant advantages in terms of damage detection, benefits from using nonlinear ultrasound techniques are highlighted in the next section.

Many studies of ultrasonic techniques and their potential applications have been completed over the years, ultrasonic researchers have explored: changes in the ultrasonic wave attenuation in spheroidal graphite iron test pieces subjected to fatigue load [75], titanium tubing using ultrasonic lamb waves generated by an electromagnetic acoustic transducer [76], ultrasonic angle beam examination for welds of ferritic steels with acoustic anisotropy [77], contactless ultrasonic inspection with fibre-optics [78], flaw size estimation in brazed joints by ultrasonic testing [79] and automisation of inspection with Rayleigh waves on curved and complex surfaces [80].

Recent applications and research into linear ultrasonic techniques has provided a great amount of work that can be used in many facets of engineering [81-91]. Modern techniques rely on guided wave propagation where a boundary is required [46]. Whereas classic surface wave propagation includes surface waves, Lamb waves and Stonely waves.

Rose, et al. (2000) [83] describes the use of ultrasonic guided waves for detection of flaws in aircraft components. The wide range of applications for aircraft components are shown in Table 2.1 below.

Guided Wave Inspection Applications	Guided Wave Benefits
Fuselage wall thinning:	Guided waves can travel long distances and large zones can be tested without continuously moving the probe.
Lap splice joints:	By using through transmission guided waves travel across a joint, where the amount of energy that leaks can be controlled by varying the incidence angle
Tear strap:	Due to difficulty of access of a tear strap, guided waves show great flexibility as the energy can be launched from the outside of the structure into the inside of the structure
Honeycomb structures:	Due to the skin being a natural wave guide, guided waves can test large zones by limiting energy leakage into the core
Helicopter blades:	Can be inspected due to their ability to travel long distances guided waves can test these large areas
Landing gear:	Is constantly subjected to impact loading, guided waves can be generated for cylindrical geometries by simply being placed at an accessible point and the frequency and angle tuned

Table 2.1: Guided wave applications and advantages [83]

Rose (2002) [56] summarises the benefits of using guided waves to determine defects in materials. Benefits include inspection over long distances from a single probe position and mode/frequency tuning to establish wave resonances and excellent overall defect detection potential. The sensitivity of guided waves are often greater than that obtained in standard normal beam ultrasonic inspection or other NDT techniques, while the ability to inspect structures under water, with coatings/insulation, multiply layers or concrete provide excellent sensitivity. The cost effectiveness of guided waves is low due simplicity and speed of inspection (often less than 1/20 cost of standard normal beam ultrasonic and other inspection techniques). Two of the most common guided wave techniques have been highlighted by Rose (2002) [46] and can be seen in the figure below:

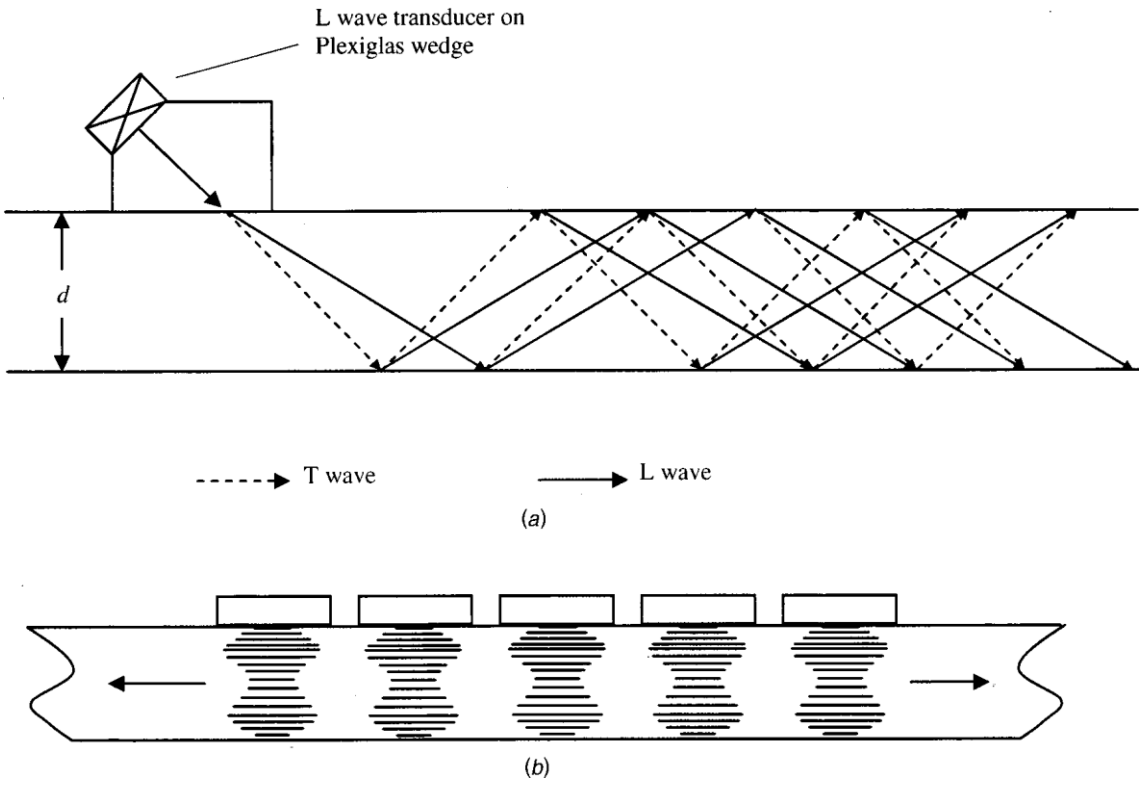

Figure 2.4: Techniques for the generation of guided waves – (a) oblique incidence and (b) comb transducer [46]

Although linear ultrasonic techniques are sensitive to gross defects or open cracks (areas where there is an effective barrier to transmission) they are less sensitive to evenly distributed micro-cracks or degradation, leading the way for nonlinear ultrasonic techniques. The figure below shows a comparison of the sensitivity of linear and nonlinear ultrasonic methods to fatigue damage detection:

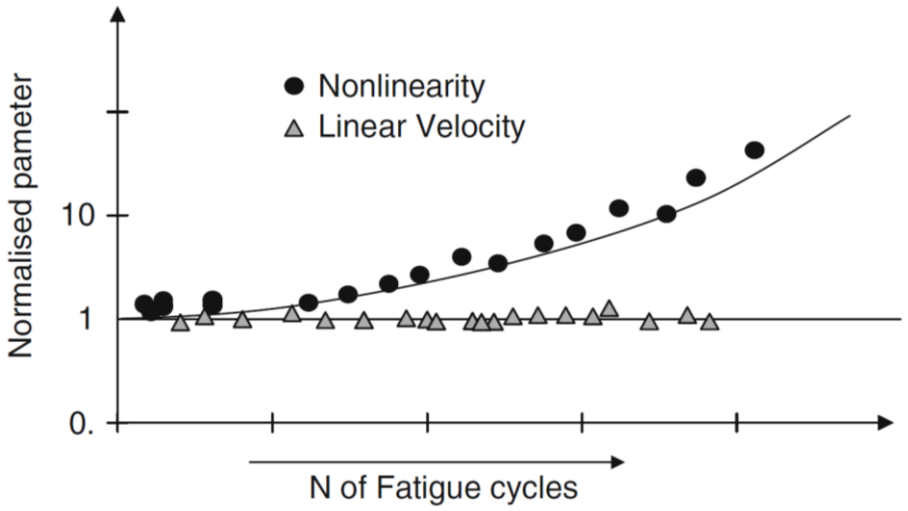

Figure 2.5: Variation of linear and nonlinear parameters with fatigue cycles [92].

The main reason for using nonlinear ultrasound techniques instead of linear methods is that the former is not sufficiently sensitive to the microscopic degradation of a materials integrity. The next Chapter establishes the principle theory governing nonlinear ultrasound techniques while describing the effectiveness of defect detection for many material damage types.

2.5. Nonlinear Ultrasonic Development and Theories

This Chapter establishes the various damage detection capabilities of nonlinear ultrasound techniques. These include micro-damage and plastic deformation detection using nonlinear ultrasound techniques as well as the examination of the relationship between the nonlinear parameter, damage precursors, fatigue and creep. The ability of nonlinear ultrasound methods to detect creep, hardening and thermal ageing is briefly discussed in order emphasise the broad capabilities of these methods.

2.5.1. Early Nonlinear Ultrasound Studies

A significant proportion of empirical academic study focuses on the effects of fatigue on the nonlinearity parameter. The importance of such research is that it may provide a quick, simple and cost effective method of evaluating a components residual fatigue life and thus predicting the likelihood of failure. The need for such evaluation techniques arises due to the limitations in current material testing techniques. It becomes too expensive and time consuming to test all the potentially fatigued components of a structure (of which there may be many) hence many parts are being abandoned after they have reached their estimated fatigue life (calculated using an estimated number of cycles to failure).

Hikata, et al. (1964) [21] suggested that the effectiveness of ultrasonic techniques rely on a set of conditions. These conditions require that an induced sinusoidal ultrasonic wave of a given frequency and of sufficient amplitude results in distortion of the fundamental frequency as it propagates generating second and higher order harmonics of the fundamental frequency. The amplitudes can then be measured and used to provide information on the coefficients of the second and higher order terms of the stress-strain relation for a nonlinear solid. It was established that the stress-dependent part of the second harmonic in high-purity single crystals is due to dislocation motion.

There are two basic nonlinear effects that can be used for material evaluation, the first is the dependence of the ultrasonic velocity on an external stress applied to the specimen (acousto-elastic effect) and the harmonic generation as an acoustic wave of finite amplitude propagating through the medium [22]. Acousto-elastic and harmonic generation techniques have been used to measure third-order elastic constants for various materials [48, 49, 53, 93].

Suzuki, et al. (1964) [20] and Hikata, et al. (1964) [21] evaluate the nonlinear parameter (higher order harmonics) as a damage detection tool, their work forms the basis of how damage effects the parameter and relationships that exist. Figure 2.6 shows the experimental setup of a pulse echo technique for ultrasonic measurements used by Hikata, et al. (1964) [21]. The system relied on two attenuation measurement units, the first employed the driving pulse to the fundamental frequency transducer while the second received and displayed the echoes at the

fundamental frequency. The system allowed calibration of the first attenuation unit, as well as filtering of the undesired frequencies generated in the electrical system.

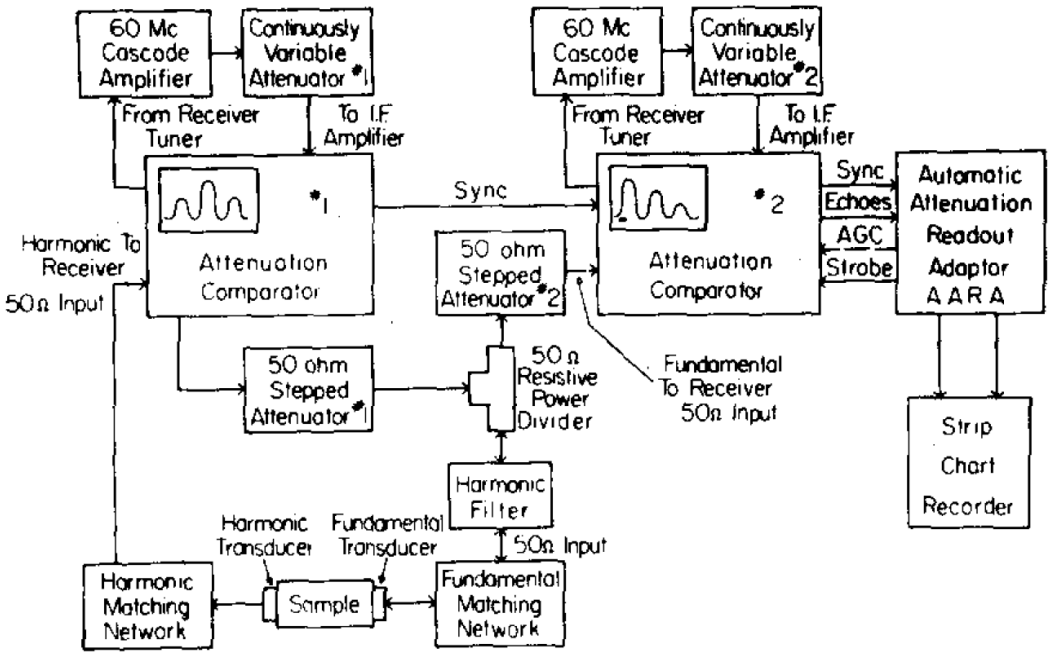

Figure 2.6: Block diagram of the equipment used in measuring the amplitudes and the attenuations of the fundamental wave and second harmonic [21]

Hikata, et al. (1964) [21] confirmed that echoes displayed on the oscilloscope screen were the second harmonic generated by the specimen. The echoes were proved to be caused in the specimen by checking the second power law and the echo pattern of the second harmonic. The second harmonic is expected to be proportional to the square of the amplitude of the fundamental wave, as long as the attenuation change due to the generation of the higher harmonics is considered negligible. Thus the amplitude change of the second harmonic was measured as a function of the fundamental wave amplitude. Tests were conducted for single-crystal specimens of various orientations and for polycrystal specimens of aluminium alloys 2S and 11S. Furthermore an attempt to determine the ratio between the amplitudes of the second and the fundamental wave was completed. It was found that measurements indicated that the amplitude of the second harmonic generated in the specimen when compared with the fundamental wave, agreed well with predictions made.

It was important to distinguish the second harmonic among the other echoes that were displayed on the oscilloscope screen; this was done by representing the amplitude of the second harmonic as a function of distance travelled. This helped determine whether or not the maximum amplitude occurred after the full length of the specimen or before; thus allowing for the placement of the maximum amplitude. Ultimately the results showed that the observed wave was the second harmonic generated in the specimen and not leakage of the signal from the electronic equipment.

Hikata, et al. (1964) [21] experiment also looked at determining the dislocation contribution to the generation of the second harmonic, thus the effect of bias stress was investigation. The amplitude was dependent on bias stress due to oscillatory dislocation displacements rather than due to lattice anharmonicity. Hikata, et al. (1964) [21] expected that the higher-order coefficient of the strain recorded (in the absence of dislocation displacement) should not change in value when there is applied stress. When stress was applied there was an increase in amplitude which can be explained by dislocation displacement (when the stress-strain relationship for dislocation strain is nonlinear). Thus it was found that the amplitude of the second harmonic starts decreasing as the bias stress becomes large enough to cause unpinning which results in a maximum in the amplitude-bias stress relation. The effect of plastic deformation was also explored by increasing the deformation in the specimen; it was also found that the amplitude of the second harmonic became more sensitive to the stress as the amount of deformation increased. Hikata, et al. (1964) [21] results showed that the nonlinearity of the stress-strain relation required to generate higher harmonics originates from two sources the anharmonicity of the lattice itself and the nonlinear relationship between the glide displacement of a dislocation and an applied stress.

Suzuki, et al. (1964) [20] following the work of Hikata, et al. (1964) [21] looked at the generation of the second harmonic of an ultrasonic stress or strain wave propagation due to glide motion dislocations. The second harmonic of a high-intensity ultrasonic wave passing through a crystal was studied using the string model of dislocation in the presence of a static bias stress. Suzuki, et al. (1964) [20] found that calculated results agreed semi quantitatively with the experiment by Hikata, et al. (1964) [21]. The amplitude of the second harmonic was found to be due to the dislocation damping effect which was associated with the anomalous velocity change due to unpinning (only when stress is sufficient to cause dislocation unpinning).

Suzuki, et al. (1964) [20] made several assumptions about the calculation of the attenuation, velocity of ultrasonic waves and the generation of higher harmonics in the crystal (which was under the influence of static stress and an ultrasonic stress wave). The assumptions were that dislocation in the absence of the applied stress take a straight-line form between pinning points, the increase of the potential energy of a dislocation due to bowing out is given by $U=C(l-l_0)$ (C is the tension of the dislocation, l_0 the distance between pinning points and l the length of the dislocation), the distance between the pinning points l_0 is the same for all dislocation segments, the interactions between different dislocation segments are neglected and unpinning is not taken into account in the calculations.

Suzuki, et al. (1964) [20] revealed that the dependence on the static bias stress deviates from linearity with increasing values of bias stress, if the distance between pinning joints (l_0) increases the amplitude of the second harmonic decreases and the magnitude of the deviation from the linear dependence of the second harmonic by increasing the bias static stress was found to be in fair agreement with the experimental data. However the increase of attenuation due to bowing out of

dislocations was believed to be caused by the unpinning mechanism and possibly by conversion of energy from the fundamental into higher harmonics.

This section establishes that although nonlinearity effects have been known for 50 years, it is only recently that the potential of these phenomena are being seriously considered as an improvement to classic NDT/E techniques. This is partly due to the greater understanding of materials and the propagation of sound in materials, but largely due to improvement in computing and equipment capabilities.

2.5.2. Relationship between damage precursors, fatigue and the nonlinear ultrasonic techniques

A large proportion of these thesis is dedicated to the assessment of the residual fatigue life, thus it is imperative to understand the potential of nonlinear ultrasound to evaluate cumulative fatigue damage. This section is devoted to understanding how nonlinear techniques can be used to evaluate the most common failure mechanism in metals, fatigue failure.

The concern over the ageing of the global commercial aircraft fleet has led to many studies such as Yost, et al. (1992) [94] who researches new methodologies and re-examines old techniques for non-destructive evaluation and characterisation of metal fatigue. Yost, et al. (1992) [111] explores the potential of using bulk acoustic nonlinearity measurements in the determination of metal fatigue, with an emphasis on: acoustic harmonic generation, variation of the acoustic nonlinearity parameter with increasing levels of fatigue and aluminium alloys (especially Al 2024-T4). Experimental evidence presented by Yost, et al. (1992) [94] suggested a strong nonlinear interaction of acoustic waves with dislocation dipoles in fatigued metals. Their study aimed at creating a model of the interaction of an acoustic wave with dislocation dipoles and dipole-array approximations to veins and persistent slip bands (PSBs) formed during fatigue. Yost, et al. (1992) [94] focus on dislocation dipoles is due to the fact that the most prominent microstructural changes associated with metal fatigue are identified with the generation of dislocations, which are formed by the cyclic stressing during fatigue. Cyclic stressing during fatigue also promotes more complex, multipole arrangements of dislocations such as those found in vein and persistent slip band substructures of fatigue metals.

Suzuki, et al. (1964) [20] predicted the second harmonic to be linearly dependent on the applied or residual stress in the solid and dependent on the dislocation loop length to the fourth power, while Hikata, et al. (1964) [21] verified the linear dependence of applied stress in high-purity single crystal aluminium. Although Yost, et al. (1992) [94] second harmonic generation experiments on aluminium alloys show no dependence within experimental error on applied tensile stresses up to 1.6 MPa, thus harmonic generation from individual dislocations or arrays of single dislocations is expected to be insensitive to the applied stress as long as the dislocations remain pinned. Experiments performed by Yost, et al. (1992) [94] were completed using aluminium alloy

2024-T4 in a similar technique as performed by Hikata, et al. (1964) [21]. However rather than applying an increasing tensile load to the sample as in Hikata, et al. (1964) [21] the stress amplitude of the acoustic driving wave was increased and both unfatigued samples and samples fatigued for 10 kcycles in stress-controlled loading from zero to 276 MPa were used. Details of experimental set-up, definition of the nonlinearity parameter β and method of measurement of β are highlighted by Cantrell, et al. (1991) [95] and Yost, et al. (1992) [96].

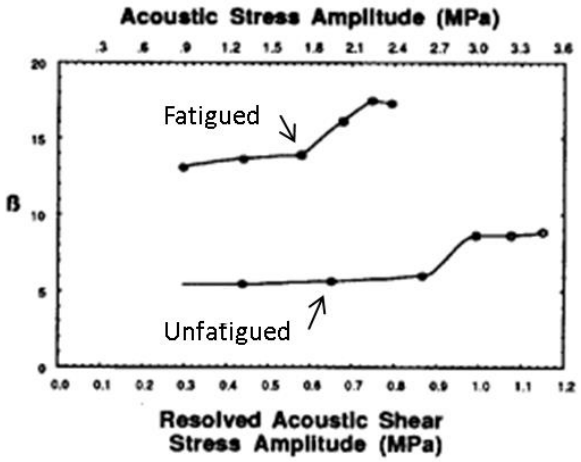

Figure 2.7: Acoustic nonlinearity parameters of unfatigued and fatigued samples of aluminium alloy 2024-T4 plotted as a function of the stress amplitude of the acoustic driving wave [94].

Figure 2.7 shows that the nonlinearity parameter is relatively constant over a large stress amplitude in both the fatigued and unfatigued sample, which is similar to results found by Hikata, et al. (1964) [21]. The increase in the nonlinearity parameter in the fatigued sample at lower acoustic stress amplitudes were assumed to be caused by the fact that the structures formed do not consist of isolated single dislocation monopoles but rather of complex arrangements of dislocation dipoles and multipoles [97].

Nazarov, et al. (1997) [98] examined the linear and nonlinear acoustic constants of a fractured medium. The model used was based on the assumption of uniform stress that is valid for low concentration of cracks. The crack behaviour used in the study assumed that the crack can be represented by an elastic contact of two rough surfaces, where these surfaces are pressed together by the surrounding internal stresses of the solid. Nazarov, et al. (1997) [98] found that negative values of the Poisson's ratio existed for their medium and that anomalously high values of the nonlinear constant existed. Other studies focusing on nonlinear acoustics and geophysics have shown that micro-inhomogeneous media exhibit high acoustic nonlinearity [99-101].

Nazarov, et al. (1997) [98] crack model made multiple assumptions about the crack interface. Each crack was modelled as the contact of two rough surfaces restricted to a circle of radius R (the latter being small compared to the radius of the rod with uniform spatial distribution of the cracks in the rod material and small concentration of cracks (i.e. the cracks do not interact with one another). Furthermore cracks were assumed to only change their volume under normal

stress to the crack surface (sliding motions of the crack surface were neglected and it was assumed that shear stresses do not influence cracks). The total strain of a medium with cracks was calculated as the strain for a perfectly homogenous medium plus the strain associated with cracks (stress was assumed uniform plus the value applied to any crack was assumed equal to that applied to the body as a whole) and the nonlinear properties of a medium with cracks are mainly determined by the nonlinearity of cracks. Finally the solid was considered linear and obeyed Hooke's law, while the nonlinear terms were considered small when compared with linear terms.

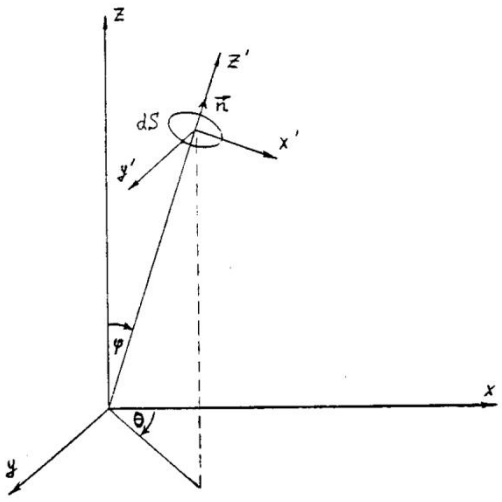

Figure 2.8: The coordinate system used to calculate the orientation of a single crack [98]

The following general equations were used by Nazarov, et al. (1997) [98] to determine the acoustic parameters of a cracked medium:

$$U_{zz} = \frac{\partial U_z}{\partial z} = \frac{\sigma_{zz}}{E}$$

Eq. (2.10)

$$U_{xx} = \frac{\partial U_x}{\partial x} = -\nu U_{zz}$$

Eq. (2.11)

$$U_{yy} = \frac{\partial U_y}{\partial y} = -\nu U_{zz}$$

Eq. (2.12)

$$\sigma_{nn} = \sigma \cos^2 \varphi$$

Eq. (2.13)

Where: E is the Young modulus, ν is the Poisson's ratio, U_x, U_y and U_z are components of the displacement vector in the Cartesian system coordinates (x, y, z), and σ_{nn} is the normal stress.

To obtain the elastic constants of a cracked medium a new coordinate system was used (x_i') and to find the additional strains dU_{xx}, dU_{yy} and dU_{zz} produced by those cracks [98]. The additional strain $dU'_{z'z'}$ which occurs along the z' axis was determined by:

$$dU'_{z'z'} = \Delta V(\varphi) N(\varphi,\theta) \sin\varphi d\varphi d\theta$$

Eq. (2.14)

Where: $N(\varphi,\theta)$ is a function of the crack distribution within the angles φ and θ, and $\Delta V(\varphi)$ is the volume variation of a single crack. The equation describing the longitudinal wave propagation in the rod was found using the Newton equation:

$$\rho U_z = \partial\sigma(\varepsilon)/\partial z$$

Eq. (2.15)

$$\varepsilon = U'_{zz}$$

Eq. (2.16)

Ultimately the nonlinear parameters for isotropically orientated cracks (G_1, G_2 and G_3) were determined [98] to be:

$$G_1 = (1 + \alpha N_0 / 5)^{-1}$$

Eq. (2.17)

$$G_2 = \beta N_0 G_1^2 / 7$$

Eq. (2.18)

$$G_3 = \gamma N_0 G_1^3 \left[1 - 27 G_1 \beta^2 N_0 / 49\gamma\right] / 9$$

Eq. (2.19)

$$\alpha = \pi h_s R^2 (E/\sigma_0)(1 + h_s/d_0)^{-1} > 0$$

Eq. (2.20)

$$\beta = \pi h_s R^2 (E/\sigma_0)^2 (1 + h_s/d_0)^{-3} > 0$$

Eq. (2.21)

$$\gamma = \pi h_s R^2 (E/\sigma_0)^3 (2 - h_s d_0)(1 + h_s/d_0)^{-4}$$

Eq. (2.22)

Where: α, β and γ are the linear and nonlinear (quadratic and cubic) coefficients of elasticity of the crack, d_0 is the distance between middle lines of the crack surface, $h_s = 2^{1/2}h_0$ (h_0 is the characteristic height of the rough surface irregularities), σ_0 is the compressive stress.

Nazarov, et al. (1997) [98] found that while the presence of cracks reduced the Young modulus and Poisson's ratio of the medium by about 1% the values of the nonlinearity parameters G_2 and G_3 achieved values of around 200 and 10^8 respectively. Therefore the presence of cracks caused the nonlinear parameter to increase by several orders of magnitude higher than the typical nonlinearity parameters of homogeneous solids, with quadratic and cubic nonlinear methods having a much higher sensitivity to the presence of cracks than conventional linear methods.

Cantrell, et al. (2001) [102] developed a quasi-isotropic model of the interaction of an acoustic wave with dislocation dipoles and dipole-array approximations to multipole substructures which lead to results that are different from those obtained by Suzuki, et al. (1964) [20] for pinned dislocation monopoles. This model predicted a substantial acoustic second harmonic generation that is independent of applied stresses or loop length, but strongly dependent on the particulars of the dislocation arrangements in the dislocation substructure.

Using this model the acoustic nonlinearity parameter of fatigued metals was written as:

$$\beta = \beta_{lat} + f_{dip}\beta_{dip} + f_{T-N}\beta_{T-N} + f_{pT-N}\beta_{pT-N}$$

Eq. (2.23)

$$\beta_{lat} = -\frac{A_3^H}{A_2^H}$$

Eq. (2.24)

Where: f_{dip}, $f_{T\text{-}N}$, and $f_{pT\text{-}N}$ are the volume fractions of material consisting of dipoles of density L (Taylor-Nabarro dislocation lattice structure of density $L_{T\text{-}N}$ and polarized Taylor-Nabarro dislocation lattice structure of density $L_{pT\text{-}N}$ respectively), β_{lat} is the contribution from the anharmonicity of the crystal lattice, and A_2^H and A_3^H are the second and third order Huang coefficients of the material [103].

Yost, et al. (1992) [94] revealed that the general agreement between theory and experiment provided strong evidence that dislocation dipole arrangements are significant to the generation of acoustic second harmonics. Both theory and experiment showed that the dislocation dipole contribution to the nonlinearity parameter was substantially larger than that due to the anharmonicity of the crystalline lattice when the dipole density is sufficiently large and isolated dipoles provided contribution to the acoustic nonlinearity that is independent of residual or applied stresses. Although, Yost, et al. (1992) [94] discovered that in more complicated cases dislocation arrangements can provide contribution to the acoustic nonlinearity parameter and theoretically acoustic nonlinearity is highly sensitive to the arrangement of the dislocation in the fatigue substructure and to volume fraction of each substructure.

It has consequently been found that damages formed during fatigue in materials produce substantial distortion of ultrasonic waves propagating through the fatigued material [13, 19-21, 23, 24, 29, 49, 53]. Cantrell, et al. (2001) [102] ascertained that it was possible to quantify wave distortion by means of a material nonlinearity parameter β. The nonlinearity parameter β has been observed to have a magnitude of up to around 300% larger in material (AA2024-T4) cyclically loaded for 100 kcycles in stress control at 276MPa than a virgin material [102]. This, due to the magnitude of the order, allows for a greater degree of accuracy when determining the damage of a material over linear techniques.

Cantrell (2009) [104] and others have discovered that the magnitude of the nonlinearity parameter is highly dependent on the crystalline structure of the solid and on the presence of defect structures [21, 23, 98]. Cantrell (2009) [104] also established that the magnitude of the nonlinearity parameter is dependent on symmetries associated with the modal direction in the solid, while qualitative explanation for the dependence of the acoustic nonlinearity parameters on modal direction was based on variations in crystal symmetry during loading along pure mode propagation directions of face centred cubic solids.

Cantrell, et al. (2001) [102] model described the interaction of ultrasonic waves with dislocation dipoles. It assumed that the total longitudinal strain ε was the sum of an elastic component ε_e and a plastic component ε_{pl} associated with the motion of dislocations in the dipole configuration. Thus:

$$\varepsilon = \varepsilon_e + \varepsilon_{pl}$$

Eq. (2.25)

The relation between the stress perturbation and elastic strain was written in nonlinear Hooke's law form as:

$$\sigma = A_2^e \varepsilon_e + A_3^e \varepsilon_e^2 + ...$$

Eq. (2.26)

Where: A_2^e and A_3^e are the Huang coefficients [103]. These equations and others were used to create the nonlinear acoustic wave equation and the total acoustic nonlinearity parameter of the material, which can be defined as follows:

$$\frac{\partial^2 \varepsilon}{\partial t^2} - c^2 \frac{\partial \varepsilon}{\partial a^2} = -c^2 \beta \left[\varepsilon \frac{\partial^2 \varepsilon}{\partial a^2} + \left(\frac{\partial \varepsilon}{\partial a} \right)^2 \right]$$

Eq. (2.27)

$$\beta = \beta_e + \beta_{dp}$$

Eq. (2.28)

$$\beta_e = -\frac{A_3^e}{A_2^e}$$

Eq. (2.29)

$$\beta_{dp} = -\frac{A_3^{dp}\left(A_2^e\right)^2}{\left(A_2^{dp}\right)^3} = \frac{16\pi^2 \Omega R^2 \Lambda_{dp} h^3 (1-\nu)^2 \left(A_2^e\right)^2}{G^2 b}$$

Eq. (2.30)

Where: a is the Lagrangian (material) coordinate, G is the shear modulus, b is Burgers vector, ν is Poisson's ratio, h is the dipole height ($y=h$), R is the Schmid factor, Ω is the conversion factor from the dislocation displacement in the slip plane to longitudinal displacement along an arbitrary direction, Λ is the dislocation dipole density, β_e is the elastic or lattice contribution to β, β_{dp} is the plastic contribution from the dislocation dipoles. Finally Eq. (2.30) can be solved assuming a purely sinusoidal input wave of the form $\varepsilon_0 \sin\omega t$ at $a=0$ where ε_0 is the wave amplitude, k the wavenumber and ω the angular frequency [105]:

$$\varepsilon = \varepsilon_0 \sin(\omega t - ka) - \frac{1}{4}\beta k \varepsilon_0^2 a \sin[2(\omega t - ka)]$$

Eq. (2.31)

Cantrell, et al. (2001) [102] used a standard 'dog bone' specimens of AA2024-T4 which was fatigued at a rate of 10Hz under uniaxial, stress controlled load at 276 MPa with a stress ratio of 0 (R=0). Four specimens were tested with each specimen being fatigued for a different number of cycles (3 cycles, 10 kcycles, 100kcycles and the last specimen was not fatigued). The process was followed by optical microscopical examination of the end surfaces which revealed that no cracks longer than 35-40 μm existed. Cracks of this length have been shown to be well below that needed to contribute measurably to the nonlinearity parameter [98]. Purely sinusoidal ultrasonic bulk waves of 5 MHz were used; this was done by using a 1.27cm diameter lithium niobate piezoelectric transducer (PZT) bonded to a flat end of the sample. The signal was received by an air gap capacitance transducer at the opposite end of the specimen. Measurements of the nonlinearity parameter was conducted by using the absolute amplitude measurements of the fundamental and second harmonic signals (a Fourier spectrum of the received distorted signal was calculated), this method has previously been used by Cantrell, et al. (1991) [95] and Yost, et al. (1992) [96].

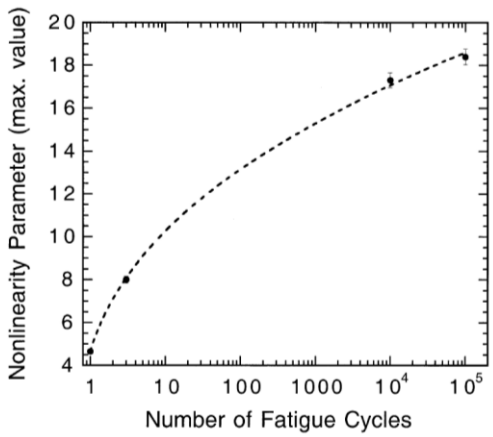

Figure 2.9:Graph of maximum measured value of nonlinearity parameter as function of number of fatigue cycles for aluminium alloy 2024-T4 [102].

Figure 2.9 demonstrates how the nonlinearity parameter increases monotonically with the increasing fatigue cycles, although the increase in the range from 10 to 100 kcycles is relatively smaller (assumed due to range dominated by the growth of persistent slip bands) [102]. The fact that the increase during this range is smaller may be due to the stress controlled loading of the aluminium producing slow but monotonic increase in the volume faction of persistent slip bands throughout the fatigue life; this was also found with single crystal and polycrystalline copper [106].

Increases in the nonlinearity parameter β due to an increase in number of fatigue cycles has additionally been observed for fatigued Ti-6Al-4V and in 410Cb stainless steel specimens [107]. Cantrell, et al. (2001) [102] established that there was good agreement between the value of the nonlinearity parameter measured at 100 kcycles of fatigue in AA2024-T4 and that predicted from the generic ultrasonic wave-dislocation dipole interaction model used. The origin of the increase in β is probably associated with the growth and transformation of dislocation dipole substructures formed in the material during fatigue and the large variation of β with measurement location in the material suggests that the relevant substructural changes are localised.

Cantrell (2006) [24] concentrated on quantifying the material nonlinearity parameter of microelastic-plastic nonlinearities that arise from the interaction of a stress perturbation with dislocation substructures and cracks that evolve during cyclic fatigue of wavy slip metals. Cantrell (2006) [24] uses the crack nonlinearity equation developed by Nazarov, et al. (1997) [98] along with the Paris law in order to determine whether there is an increase in the nonlinearity parameter due to the stage of fatigue life of an aluminium alloy 2024-T4. Cantrell (2006) [24] builds on the findings of Cantrell (2004) [108] in that self-organised substructural arrangements of dislocation formed in wavy slip metals during cyclic stress-induced fatigue produce substantial changes in the microelastic-plastic nonlinearity of the material, that can be quantified by a material nonlinearity parameter (experimentally determined from acoustic harmonic generation methods). The focus on fatigue life was due to the fact that no method had yet been able to provide an unambiguous assessment of accumulated damage at a given level of fatigue over the entire range (from the virgin

state to fracture). A pure metal and an alloy were used to evaluate the effect on the nonlinearity parameter (if any) due to material specification.

Cyclic stress-induced fatigue in metals and the nonlinear relationship that exists at each of the stages is very important in understanding the damaged state of the material. Cyclic stress-induced fatigue can be divided into five stages cyclic hardening/softening, strain localisation and microcrack nucleation, propagation or coalescence of microcracks to form macrocracks, macrocrack propagation and fracture. Multiple studies have revealed experimentally that each stage of the fatigue process can be characterised by a unique nonlinear relationship between an impressed stress perturbation (sound wave) and a microelastic-plastic straining of the material [23, 98, 102, 109, 110]. The nonlinearity parameters contribution at each stage is analytically described by Cantrell (2006) [24].

Cantrell (2006) [24] determined the relationship between an impressed longitudinal stress σ and the longitudinal elastic strain ε^e developed by Cantrell (2004) [108]:

$$\sigma = \sigma_0 + A_2^e \varepsilon^e + \frac{1}{2} A_3^e \left(\varepsilon^e\right)^2 + \cdots = \sigma_0 + A_2^e \varepsilon^e - \frac{1}{2} A_2^e \beta^e \left(\varepsilon^e\right)^2 + \cdots$$

Eq. (2.32)

The material elastic nonlinearity parameter defined was also used as well as equations developed by Cantrell (2004) [108] to describe the stress-strain relationship for dislocation monopoles and dipoles:

$$\sigma = \sigma_0 + A_2^{mp} \varepsilon^{mp} - \frac{1}{2} A_2^{mp} \beta^{mp} \left(\varepsilon^{mp}\right)^2 + \cdots$$

Eq. (2.33)

$$\sigma = \sigma_0 + A_2^{dp} \bar{\varepsilon}^{dp} - \frac{1}{2} A_2^{dp} \beta^{dp} \left(\bar{\varepsilon}^{dp}\right)^2 + \cdots$$

Eq. (2.34)

Where: superscript *mp* and *dp* represent dislocation monopoles and dipoles respectively. Therefore the Huang elastic coefficients and material elastic nonlinearity parameters for dislocation monopoles and dipoles are given as [24]:

$$A_2^{mp} = \frac{3G}{2\Omega\Lambda^{mp}L^2R}$$

Eq. (2.35)

$$A_2^{dp} = \frac{G}{4\pi\Omega R\Lambda^{dp}h^2(1-\nu)}$$

Eq. (2.36)

$$\beta^{mp} = \frac{24\Omega\Lambda^{mp}L^4R^3\left(A_2^e\right)^2}{5G^3b^2}|\sigma_0|$$

Eq. (2.37)

$$\beta^{dp} = \frac{16\pi^2\Omega R^2\Lambda^{dp}h^3(1-\nu)^2\left(A_2^e\right)^2}{G^2b}$$

Eq. (2.38)

Where: G is the shear elastic modulus, b is the amplitude of the Burger's vector, $|\sigma_0|$ is the magnitude of the initial (residual or internal) longitudinal stress in the material, L is half of the distance of the length of dislocation between the pinning points, Ω is the conversion factor from shear to longitudinal strain, R is Schmid or resolving factor, and h is dipole height, Λ^{dp} density of dislocation dipoles.

Cantrell (2006) [24] final solution of the nonlinearity parameter took into account not only the above equations relating to dislocation monopoles and dipoles, but built on those to create an effective microelastic-plastic nonlinearity parameter that was derived by solving an expression for the stress terms in terms of total strain. This nonlinearity parameter was further adapted to take into account substructural contributions of wavy slip metals; this took into account volume fractions of dislocation monopoles and dipoles that were contained within the substructure. Dislocation dipoles have a possible vein structure source and a possible persistent slip band (PSB) source depending on the state of fatigue, these fractions were estimated using values determined by a number of authors [97, 106, 111]. A factor of 1/8 was used as an estimate of the fraction of PSBs in the material that was found in the wall structure.

Finally, the effect of fatigue cracks on the nonlinearity parameter was taken into account by using the expression derived by Nazarov, et al. (1997) [98], which describes the contribution of non-interacting penny-shaped cracks in bulk material, thus giving:

$$\beta^{crk} \approx \frac{5.3x10^6C_{crk}R_{crk}^4}{\left(1+0.25C_{crk}R_{crk}^3\right)^2}$$

Eq. (2.39)

Where: C_{crk} is the concentration of cracks in the interior of the material, R_{crk} is the radius of the crack. In order to obtain the relationship between the nonlinearity parameter and crack growth

over the fatigue life of the material the Paris-Erdogan [112] equation was employed by Cantrell (2006) [24]. The Paris-Erdogan equation was developed in order to estimate the life of materials by assessing fatigue cracks. By plotting crack growth rate against a range of stress intensity factors, Paris, et al. (1963) [112] established that it gave straight lines on log-log scales; thus allowing quantitative predictions of residual life for a crack of a certain size. The Paris-Erdogan equation is defined as:

$$\frac{dR_{crk}}{dN} = A(\Delta K)^n$$

Eq. (2.40)

Where: N is the number of fatigue cycles, ΔK is the stress-intensity range, and A and n are material dependent constants. It was thus defined by Cantrell (2006) [24] the crack growth contribution β^{crk} to the total nonlinearity parameter β as a function of the fraction of total fatigue life f is given as:

$$\beta^{crk} = \frac{5.3x10^6 C_{crk}}{\left[a_1^{n-2} + a_2(1-f)\right]^{3/(n-2)}}\left[1 + \frac{0.25C_{crk}}{\left[a_1^{n-2} + a_2(1-f)\right]^{6/(n-2)}}\right]^{-2}$$

Eq. (2.41)

Where:

$$a_1 = \frac{B\sigma_{\max}}{K_{1c}}$$

Eq. (2.42)

$$a_2 = \frac{(n-2)}{2} N_{total} A(B\Delta\sigma)^n$$

Eq. (2.43)

Polycrystalline nickel and aluminium alloy 2024-T4 were tested by Cantrell (2006) [24] to determine the nonlinearity parameter versus percent fatigue life. Figure 2.10(a) shows that despite significant variations in loading stresses and volume fractions of veins and PSBs for the two cases, the model predicts similar variations of the nonlinearity parameters and both curves exhibit monotonically increasing values of β of roughly 300% over the fatigue life from substructural evolution alone. Figure 2.10(a) suggests that the nonlinearity parameter agrees to within 3% from 0.01% total life of fracture and the measurable contribution of crack growth begins roughly at 85% total fatigue life becoming the dominant contribution to the nonlinearity parameter as the crack increases in size until fracture. Figure 2.10(b) depicts similar results to that of Figure 2.10(a) although the contribution from crack growth begins at 80% of total fatigue life rather than 85% and contributions from substructural evolution alone produces an increase of more than 250%.

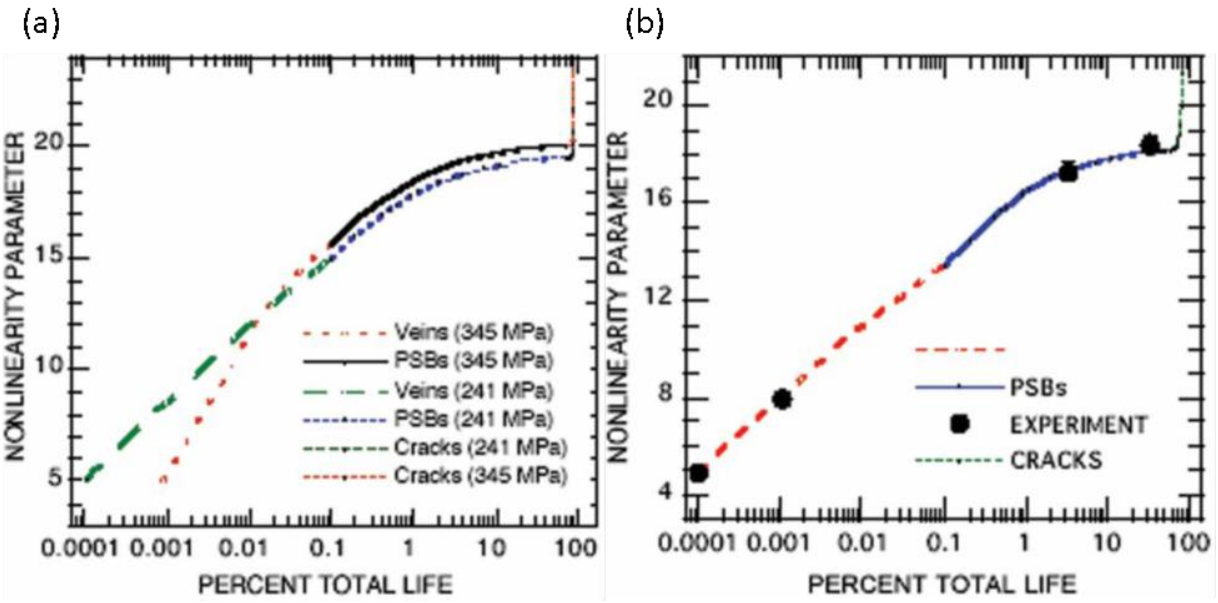

Figure 2.10: Graphs of nonlinearity parameter plotted as a function of per cent total fatigue life for polycrystalline nickel cyclically loaded in stress control at 345MPa and 241MPa (on the left: a) and aluminium allow 2024-T4 (on the right: b) [24].

Cantrell (2006) [24] established that the effects of crack growth on the nonlinearity parameters are dependent on well-known fracture mechanics concepts and material parameters. Cantrell's model predicted crack dimensions smaller than that of the Paris law (i.e. less than 250μm) make negligible contributions to the nonlinearity parameter. While cracks in the Paris law regime make significant contributions during the last 10-20% fatigue life inclusions, voids and cracks found in pure metals and alloys would produce monotonically increasing values of the nonlinearity parameter as a function of decreasing distance from the crack tip. Cantrell (2006) [24] also expects that the location of damages made little difference whether local or global for a pure metals or alloys and that the results may apply to all wavy slip metals subjected to similar loading conditions.

Kim, et al. (2006) [19] created a model to quantify the acoustic nonlinearity parameter due to elastic-plastic deformation applicable to general anisotropic elastic-plastic materials with existing microplasticity strains with monotonic or cyclic loading. Their work focused on a single crystal copper specimen that had been subjected to cyclic fatigue loading. They found that the acoustic nonlinearity parameter of this specimen increased monotonically with increasing fatigue cycles.

Kim, et al. (2006) [19] study built on some known scientific truths such as when elastic waves propagate through a nonlinear medium higher order harmonics are generated [18], the magnitude of one of these harmonics (the second order harmonic) gives a direct measure of the acoustic nonlinearity parameter (β), which is an absolute non-dimensional parameter that characterises the nonlinearity of the medium. Kim, et al. (2006) [19] measured good correlation between the fatigue damage and the acoustic nonlinearity parameter in metallic materials along with other authors [13, 20-22].

Although previous models created by Cantrell (2006) [24] had shown that aluminium alloy 2024-T4 under fatigue loading yields excellent agreement between theory and experiment, Kim, et al. (2006) [19] highlighted some difficulties that arose with these methods. Kim, et al. (2006) [19] suggested that although the dislocation-based model [24] provides a quantitative relationship between dislocation density and the acoustic nonlinearity parameter the model requires detailed information about the dislocation sub-structure (i.e. dislocation loop length and dipole height). Dislocation-based model [24] also required the evolution of statistical parameters such as the densities of dislocation monopoles and dipoles, volume fractions of veins and persistent slip bands during the fatigue. Most of the parameters required were not easily measured experimentally, nor could they be predicted with the then current modelling capabilities. Thus Kim, et al. (2006) [19] proposed an alternative approach which considered the continuum manifestation of dislocations with an emphasis on plastic deformation, instead of relating the acoustic nonlinearity parameter directly to the dislocation sub-structure.

Kim, et al. (2006) [19] study focused on the fact that the prediction of plastic strain and its accumulation during fatigue does not require detailed information on dislocation substructures. The research was based on the evolution of cumulative plastic strain for crystalline metals, which has been extensively studied using crystal-plasticity theories. The simplicity of the model is the ease at which plastic strain and its evolution can be simulated with sufficient accuracy and efficiency and the model being able to potentially predict the relationship between the acoustic nonlinearity parameter and the fatigue life of the component (due to the ability to relate the acoustic nonlinearity parameter to the cumulative plastic strain).

Kim, et al. (2006) [19] model defines three material states: the natural which describes the virgin state of the material when it is free from any deformation and stresses, the initial refers to the material state after microplasticity had occurred and the current configuration where ultrasonic wave-induced dynamic deformation was superimposed on the initial state of the material. Kim, et al. (2006) [19] model makes three main assumptions, the first is that deformation from the current to the initial states is assumed small, deformation from the natural state to the initial state can be finite and deformation from the natural state to the initial state is assumed known.

The outline of the model is shown in Figure 2.11 below:

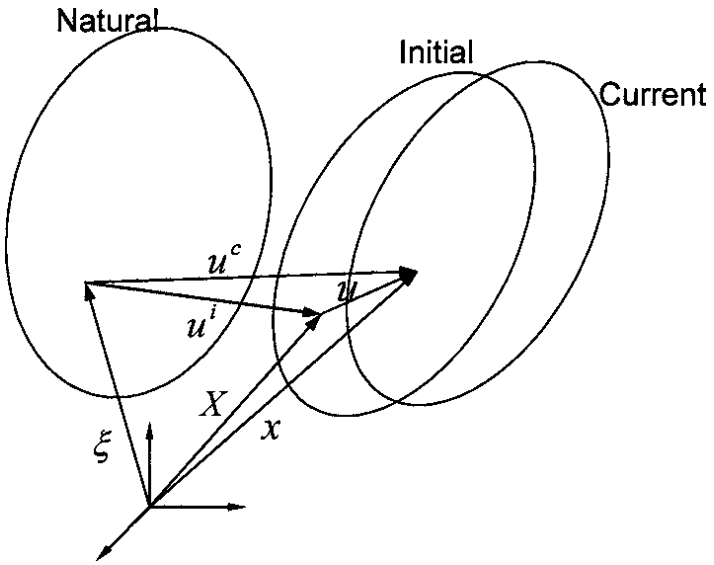

Figure 2.11: The three material configurations created by [19]

Kim, et al. (2006) [19] developed an equation for the nonlinearity parameter propagating in 1-direction (below).

$$\beta_I = -\frac{\Lambda_{(I)(I)(I)}}{\lambda_I}$$

Eq. (2.44)

Where: β_I is the nonlinearity parameter for wave mode I, $\Lambda_{(I)(I)(I)}$ are the diagonal terms, and λ_I are the eigenvalues. In the study by Kim, et al. (2006) [19] the longitudinal wave acoustic nonlinearity parameters of copper single crystal were measured as a function of the number of fatigue cycles. Two different plastic strain amplitudes were evaluated and increase monotonically by a significant amount (Figure 2.12). Three curves were drawn representing three different propagation directions of the longitudinal wave in X, Y and Z direction.

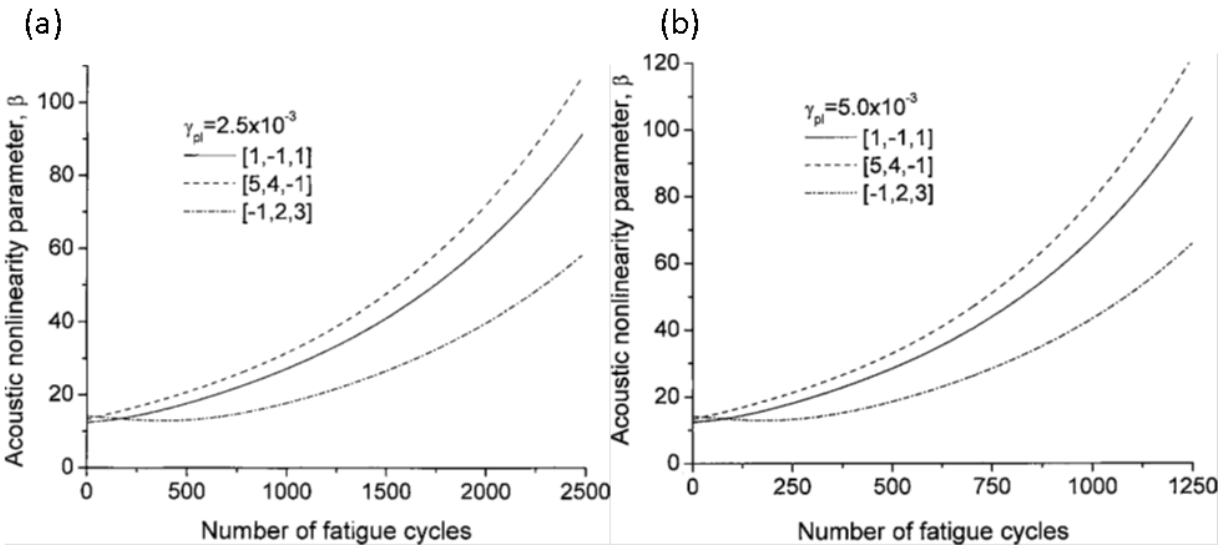

Figure 2.12: Acoustic nonlinearity parameter during fatigue for resolved plastic strain amplitude of $2.5x10^{-3}$ (a) and $5.0x10^{-3}$ (b) [19].

The increase in nonlinearity parameter was determined to be slightly more pronounced for higher plastic strain amplitudes. Results for the copper single crystals served as the upper bounds of the acoustic nonlinearity of polycrystalline coppers under similar fatigue conditions; as the plasticity induced acoustic nonlinearity in polycrystalline materials is expected to saturate with crack initiation.

The main findings by Kim, et al. (2006) [19] were that acoustic nonlinearity parameter of the entire specimen can be predicted using the applied resolved plastic shear strain amplitude (average plastic shear strain) as an input parameter and the predicted acoustic nonlinearity parameter may be close to those predicted by persistent slip bands. Kim, et al. (2006) [19] study proposes the need for a micromechanical averaging scheme to more accurately predict the overall nonlinearity parameter. The model provides a direct and quantitative link between the acoustic nonlinearity parameter and the cumulative plastic strain in the fatigued sample and due to the consideration of the contribution of residual microplasticity existing models for crystal plasticity experimental observations of fatigue damage can be utilised.

Recent research by Dutta, et al. (2009) [16] discussing the damage detection capabilities of nonlinear methods have focused on evaluating the high acoustic nonlinearity which manifests as harmonics in the power spectrum of the received signal and how harmonic components increase nonlinearity in magnitude with increasing amplitude of the input signal. The crack model used in this study, is one of the most popular models used to describe a crack, it is known as the ‘breathing crack model’ and assumes a crack closes during compression and opens during tension when ultrasonic waves propagate through a material. In addition to the crack model used, Dutta, et al. (2009) [16] uses a semi-analytic model to explain the phenomenon of harmonic generation and the crack is defined as a single infinitesimal element in the structure that exhibits bilinear stiffness [113-115]. The signal processing setup has changed drastically from early ultrasonic testing

methods observed in Hikata, et al. (1964) [21]. The modern setup used can be seen in Figure 2.13 below:

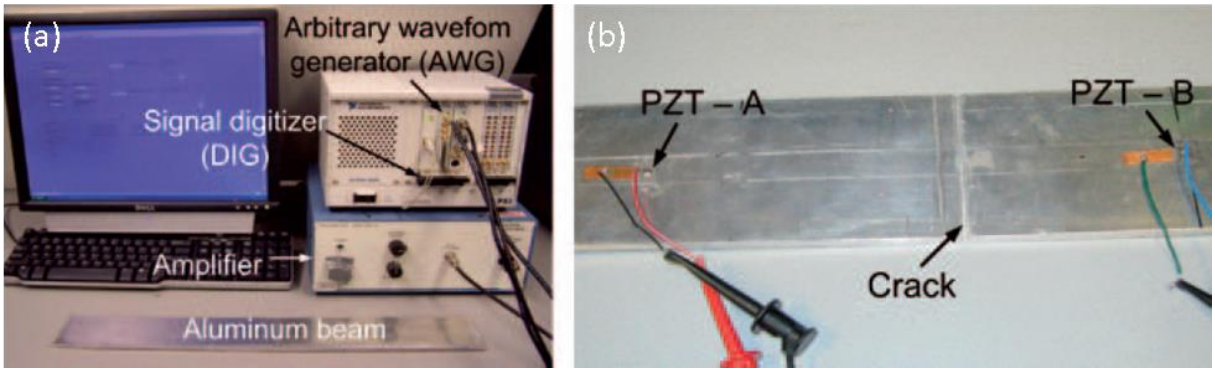

Figure 2.13: Experimental setup for detecting cracks on an aluminium beam: data acquisition system and the undamaged beam (a) and part of the beam that shows the crack and the PZT transducers (b) [16].

Dutta, et al. (2009) [16] experiment examined an aluminium and steel specimen. The excitation frequencies used were the same as the resonant frequency of the transducer-structure system, this was done to ensure the crack opening and closing happened to the fullest extent. The aluminium specimen was loaded until a visible crack appeared this was around 5000 cycles, whereas the steel specimen was loaded until 24000 cycles stopping at every few thousand cycles in order to collect data from the PZT transducers in the same manner as performed on the aluminium specimen.

Dutta, et al. (2009) [16] chose the driving frequency by evaluating the resonance frequency of the structure. This was achieved by determining the amplitude spectrum of the output signal for the transducer-structure system when the Gaussian white noise input applied to the actuator. Figure 2.14(a) shows that two resonance frequencies which were found, one at 250kHz and the other at 493kHz. The resonance frequency of 250kHz was chosen, as results for the resonance frequency of the structure did not vary significantly for the cracked and undamaged systems.

Dutta, et al. (2009) [16] measured the Fast Fourier Transform (FFT) of the response at PZT-B (Figure 2.13 (b)) and the absolute values of the FFT at the second and third harmonics of the driving frequency were taken. The process involved averaging 20 forwarding signals in the frequency domain; this was then repeated with the p-p excitation voltage varying from 2V to 40V with incremental steps of 2V. This was repeated for each state of the specimen; undamaged, notched and cracked. It ultimately exposed how the first, second and third harmonic amplitude (B, C, D in Figure 2.14 respectively) of the output signal varies with the excitation voltage for the three states of the material.

Dutta, et al. (2009) [16] revealed that the first harmonic amplitude of the output signal varies more or less linearly with the excitation voltage in the undamaged and notched cases as opposed to exhibiting nonlinear variance in the cracked case (Figure 2.14 (b)), the second and third harmonic

contents of the output signal are much more prominent in the cracked case than in the undamaged or notched cases (Figure 2.14 (c) and (d) respectively), variation of the harmonic amplitudes in the cracked specimen with increasing levels of excitation were found to be nonlinear and sources of harmonics in the undamaged and notched states was attributed to unknown sources of nonlinearity (such as circuit-nonlinearity). The experiments conducted were found to be replicable and thus results were found to be acceptable and with cracked state specimens distinguishable from undamaged and notched states by considering the amplitudes of the harmonic components and their variation with the excitation voltage.

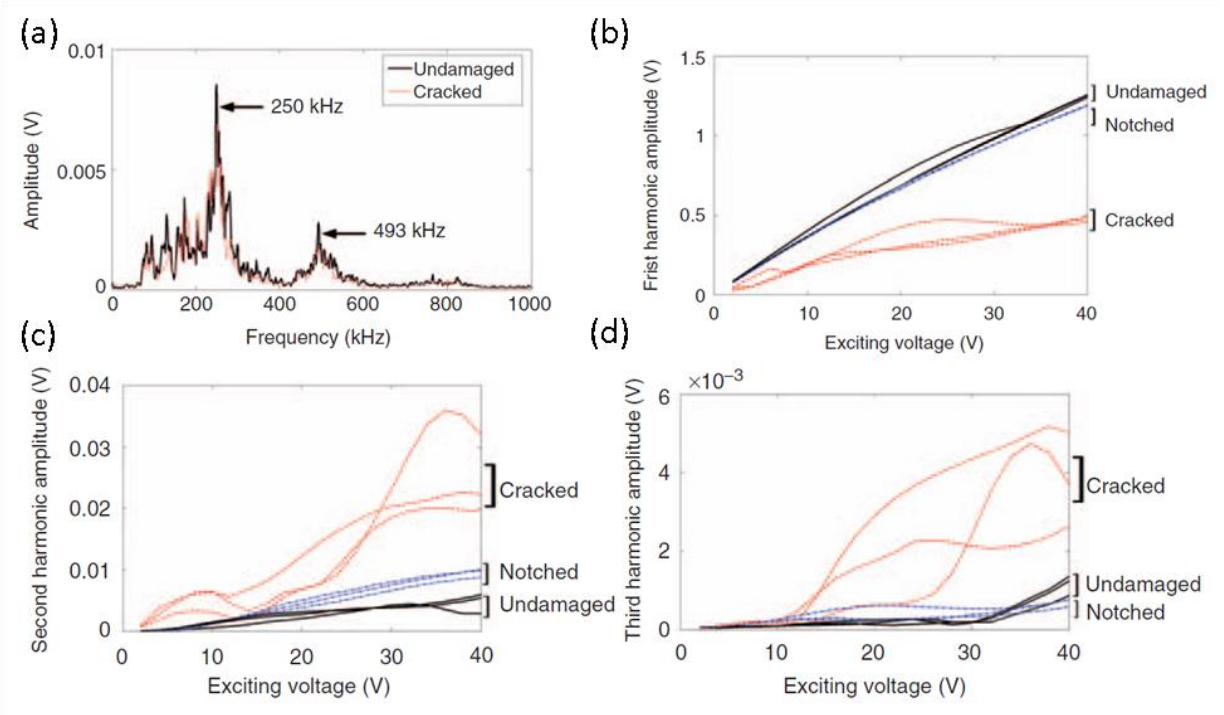

Figure 2.14: (a) is the amplitude spectrum of the output signal, (b) the variation of the first harmonic amplitude in the output signal for the aluminium specimen, with (c) and (d) the variation in the second and third harmonic amplitude respectively [16].

Dutta, et al. (2009) [16] when examining the steel specimen concluded that the first harmonic amplitude showed a general downward trend which was attributed to the reflection and scattering of acoustic waves from the crack interface (Figure 2.15(a)). The first harmonic amplitude dip around 10000 cycles was explained by energy shifting to the higher harmonics as there was an unusually high second harmonic amplitude around 10000 cycles (Figure 2.15(b)).

Nonlinearity effects became prominent at the inception of the crack although they became indiscernible after 14000 cycles. The effects after 14000 cycles have two possible explanations as the crack tip gets wider the opening and closing of the crack becomes insignificant and the crack tip moves away from the line of sight of the PZT actuator-sensor couple which results in an oblique incidence of the acoustic waves on the crack tip not strong enough to produce crack opening and closing.

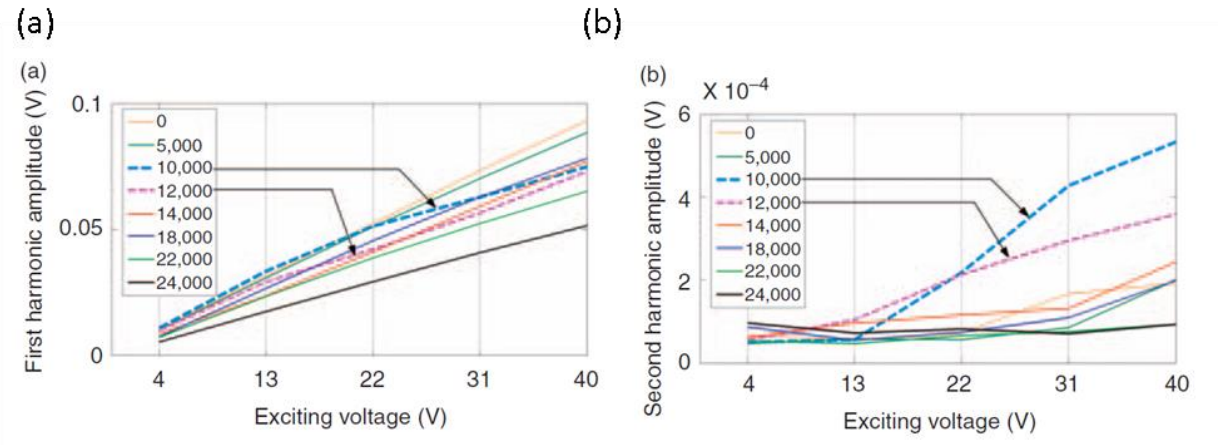

Figure 2.15: Variation of (a) first harmonic and (b) second harmonic amplitudes in the output signal with the increasing excitation voltage after given number of cycles of loading [16].

Dutta, et al. (2009) [16] when undertaking this experiment noted a number of concerns which were the distance between an actuator or a sensor from the crack and the orientation of the crack relative to the line of sight between the actuator and the sensor. Although it was found possible to identify cracks in a specimen by looking at the greater magnitude of the harmonics and higher amount of their variation with the excitation voltage as compared to those in the pristine state of the structure. From the above major litreture it has been shown that crack detection is possible using nonlinear ultrasonic techniques. The relative ease and speed at which such tests can be performed creates the current interest while highlighting the potential.

Dutta, et al. (2009) [16] experiments are built on in Chapter 3, which looks at the effect of voltage on the generation of various nonlinear parameters. The study does not directly confront the change in the fundamental and second harmonic but rather explores the ratio change of the two due to changes in voltage.

Pruell, et al. (2009) [25] undertook an experimental procedure for characterising fatigue damage in metallic plates using nonlinear guided waves. Their research evaluates the theoretical and practical considerations for the generation of higher order harmonics of guided waves in a dispersive medium. Pruell, et al. (2009) [25] discusses both phase and group velocity matching and whether they are essential for the practical generation of nonlinear guided elastic waves, while measuring the normalised acoustic nonlinearity of low cycle fatigue damaged aluminium specimens with Lamb waves. Pruell, et al. (2009) [25] study reveals whether the normalised acoustic nonlinearity is related to the measured cumulative plastic strain and ultimately evaluates Lamb waves as a quantitative assessment tool for plasticity driven fatigue damage using established higher harmonic generation techniques.

Pruell, et al. (2009) [25] investigation relies on previous research that has clearly shown that the amount of cumulative damage in metal due to either monotonic plastic deformation or cyclic fatigue is closely correlated with the nonlinearity parameter (β) measured with the second harmonic

[19, 102, 109]. Accurate experimental understanding of nonlinear Lamb waves has been found to be difficult due to their dispersive and multi-mode nature [44, 116-118].

Pruell, et al. (2009) [25] established certain conditions to ensure accuracy and validity of the results in terms of the nonlinear wave propagating in a dispersive medium. These conditions rely on the fundamental wavepacket being short while matching the phase velocity and the group velocity of the fundamental and second harmonic waves needs to be the same for the second harmonic wave to be cumulative (this ensures that the energy transferred from the fundamental frequency stays within the wavepacket thus accumulating). The generation of the cumulative second harmonic in a waveguide (elastic plate) has non-zero power flux from the primary mode to the second harmonic mode [44].

The reason for these conditions set out by Pruell, et al. (2009) [25] are that a pair of synchronous Lamb modes that either have matching group velocities or non-zero power flux between them have wave packets that may change as they propagate due to group velocity being different from phase velocity and they are not dispersive in that these two modes move in a single wave packet.

The figure below from Pruell, et al. (2009) [25] shows how mode pairs (s1, s2) satisfy both of the above conditions, while mode pairs (s2, s4) and (a2, a4) have very different group velocity. Therefore the second harmonic wave amplitude in this mode pair will saturate with propagation distance interrogation [25, 118]. Pruell, et al. (2009) [25] used mode pairs (s1, s2) as did other works [116, 117] as it is important to determine a mode pair that is best in both generating (modal excitability) and identifying the second harmonic wave amplitude. Selection of well-separated modes can avoid spurious contributions to the second harmonic amplitude calculation; as the mode (s2) propagates fastest in the wavepacket it can be detected without being significantly influenced by other non-synchronous second harmonic modes (which can potentially dominate the measured multi-mode signal).

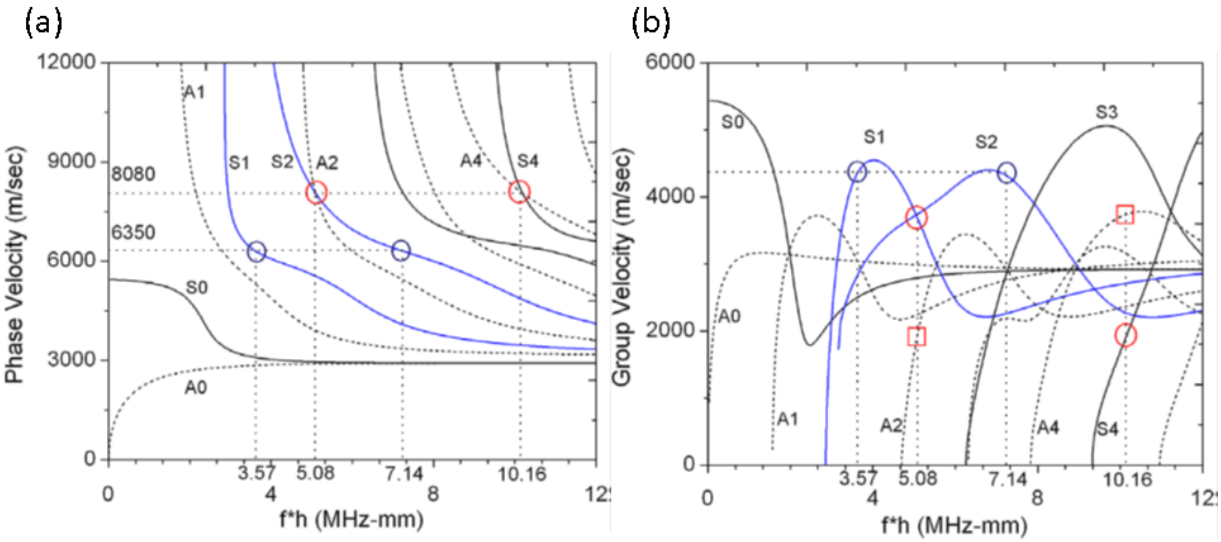

Figure 2.16: Normalised dispersion curves for an aluminium plate: (A) phase velocity and (B) group velocity versus normalised frequency [25].

Pruell, et al. (2009) [25] used methods described in various other works [19, 102, 108, 116, 119-122] to establish a normalised acoustic nonlinearity and unaltered acoustic nonlinearity. Pruell, et al. (2009) [25] generated a spectrogram of a measured time-domain signal (processed in the time-frequency domain with the short time Fourier transform) and measured the typical time-domain signal and sliced the fundamental and second harmonic frequencies as a function of time. Pruell, et al. (2009) [25] recorded the cumulative plastic strain versus fatigue cycle number, the normalised acoustic nonlinearity versus propagation distance, normalised acoustic nonlinearity versus per cent of fatigue life and the normalised acoustic nonlinearity versus plastic strain.

Pruell, et al. (2009) [25] discovered that the normalised acoustic nonlinearity measured was found to be the material nonlinearity (and not simply instrumentation nonlinearity, thus providing a direct measure of material nonlinearity) and that the increase in normalised acoustic nonlinearity is rapid during the initial stages of fatigue life and progresses more slowly towards the end (which is in agreement with findings of [102, 109, 119] (Figure 2.17 below). There was a clear relationship between normalised acoustic nonlinearity and plastic strain thus reinforcing the notion that Lamb waves can be used to quantitatively assess plasticity driven fatigue damage (qualitatively confirming theoretical approaches of [19, 108]).

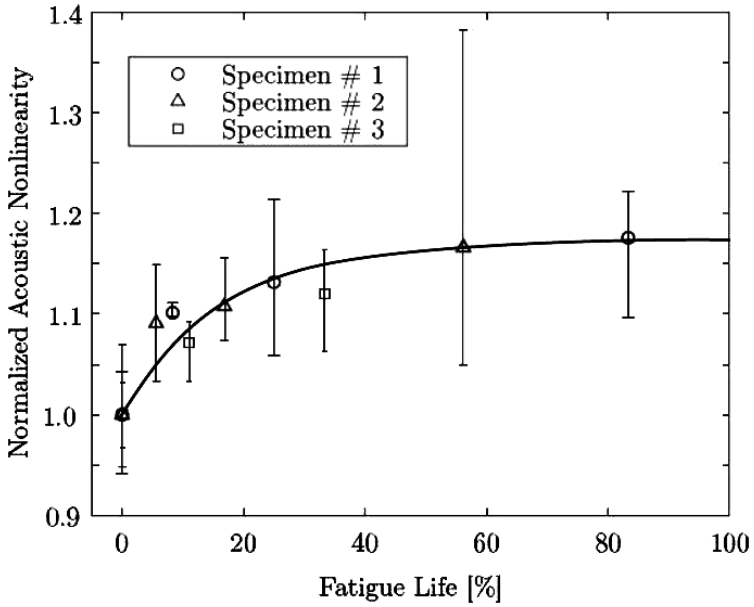

Figure 2.17: Normalised acoustic nonlinearity versus per cent of fatigue life (mean values, best fit and error bars) [25].

The experiments conducted by the author looks to establish relationships between the resonance frequencies of the structure, the excitation voltage and the generation and response of various nonlinear parameters (these nonlinear parameters will be discussed in great detail in Chapter 3.1.1 and 3.1.2). Various authors have discussed the use of the resonance frequency of the material when conducting their experiments (as it is perceived to generate larger harmonics). Although there has been no study that explicitly focuses on describing and quantifying the advantages of such an experimental procedure in terms of its effect on the generation of the nonlinearity parameters. Dutta, et al. (2009) [16] examines the response of the voltage vs. fundamental and second harmonic, but does not evaluate the nonlinear parameter vs. the voltage change. Thus the effects of resonance (and non-resonance) frequency testing are examined in great detail in Chapter 3.1.

Chapter 4.1 develops a theoretical model for residual fatigue life assessment using Nazarov, et al. (1997) [98] theoretical crack model. The theoretical model by Nazarov, et al. (1997) [98] provides great insight into the theoretical evaluation of further harmonic production by nonlinear ultrasound testing methods. This crack model is used to develop a residual fatigue life estimation framework for a dual frequency excitation technique. Dutta, et al. (2009) [16] and Pruell, et al. (2009) [25] also provide important information about fatigue assessment using nonlinear ultrasound. The following section evaluates a modulated nonlinear technique as a fatigue life assessment technique.

2.5.3. Nonlinear Ultrasound Modulation

Multiple frequency excitation methods result in further nonlinear effects being produced by damaged regions. These techniques provide various advantages and provide the basis for the experiment conducted in Chapter 4.1.

A nonlinear elastic wave modulation spectroscopy (NEWMS) method was employed by Straka, et al. (2008) [123] to assess the effects of two longitudinal elastic waves (low frequency and high frequency) and the production of second and third order intermodulation products over various fatigue cycles (up to 50000, measuring the signal by Fourier transform). Straka, et al. (2008) [123] evaluated the dependencies of the amplitudes of the intermodulation products on the number of fatigue cycles, the driving frequency and driving amplitude for various fatigue cycles. The research verified and demonstrated the suitability of the apparatus for evaluation of the damage of an aluminium alloy caused by fatigue loading.

NEWMS experiments use two elastic waves with frequencies f_1 and f_2 to excite the material. The fundamental frequencies have second order ($f_2 \pm f_1$) and third-order ($f_2 \pm 2f_1$) intermodulation frequencies which can attributed to nonlinear responses of damage [17, 124]. Straka, et al. (2008) [123] experimental setup for the aluminium specimen is shown in Figure 2.18(d) below.

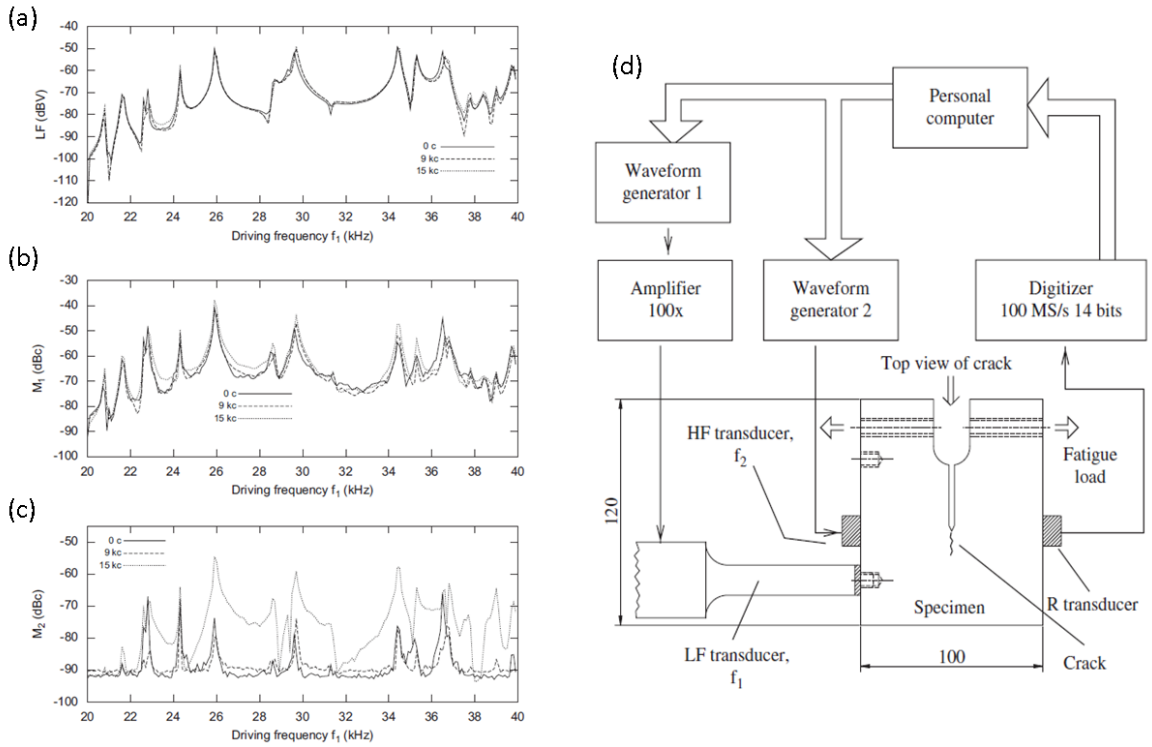

Figure 2.18: Low-frequency signal LF (a), second order intermodulation product M_1 (b), third-order intermodulation product M_2 as functions of driving frequency f_1 for the respective fatigue cycles (c), and experimental setup (d) [123].

Straka, et al. (2008) [123] evaluated various spectral components in order to determine the behaviour of the intermodulation response. These included the amplitude of the low frequency (LF) signal generated by the LF transducer at f_1 (from 20 to 40 kHz), the high frequency (HF) signal generated by the HF transducer at f_2 (at 4.8 MHz), the second order intermodulation products M_1^+ and M_1^- at $f_2 \pm f_1$ frequencies and the third-order intermodulation products M_2^+ and M_2^- at $f_2 \pm 2f_1$ frequencies. Where:

$$M_1 = \frac{M_1^+ + M_1^-}{2}$$

Eq. (2.45)

$$M_2 = \frac{M_2^+ + M_2^-}{2}$$

Eq. (2.46)

Where: M_1^+, M_1^-, M_2^+ and M_2^- are determined from the spectra as the average height of the spectral lines at $f_1 + f_2$, $f_1 - f_2$, $f_1 + 2f_2$ and $f_1 - 2f_2$ respectively, and M_1 and M_2 are the second and third-order intermodulation products respectively.

The spectra were obtained for specimens before and after the fatigue testing (up to 15000 cycles). Straka, et al. (2008) [123] recognised that for the low frequency tests the intermodulation products were considerably higher in the spectra measured after 15000 cycles, this leading to an increase of around 6 dB after 15000 fatigue cycles for the specimens tested (second harmonic) and the third harmonic resulted in an even greater increase of around 20dB (one order of magnitude).

Straka, et al. (2008) [123] also observed that the frequency dependences of the second and third-order intermodulation products ($M_2 f_1$ and $M_2 f_1$) did not change considerably after 9000 fatigue cycles, there was a slight increase in the second order intermodulation product after 15000 cycles and there was a significant increase in the third-order intermodulation product after 15000 cycles. A similar measurement was performed on another specimen from 0 to 36000 fatigue cycles it showed a much larger increase in magnitude of the second order and the third-order intermodulation products, this increase existed in almost the whole measured frequency range and the larger magnitudes of intermodulation products were related to greater damage in the specimen due to the higher number of fatigue cycles.

Straka, et al. (2008) [123] also tested a gradual increase in fatigue cycles; this again established a gradual increase in both the second and third-order intermodulation products with number of fatigue cycles up to 50000 cycles. Straka, et al. (2008) [123] assessed the dependence of the intermodulation products on the driving amplitude for all the specimens tested. The M_1 (A_1) dependencies were found to be approximately linear for all specimens and for all the fatigue cycles studied, while the slight curvatures observed on the dependencies were attributed to the slight nonlinearity of the LF transducer. Therefore Straka, et al. (2008) [123] suggested that the second

order intermodulation product M_1 depends approximately linearly on the low frequency driving LF regardless of the damage of the specimen and M_2 (A_1) dependences exhibited less linear behaviour as a consequence of the driving frequency and the number of fatigue cycles.

Straka, et al. (2008) [123] conducted SEM observations to confirm that cracks of considerable length existed in all specimens as well as evaluate the sensitivity of the method. These tests established that a 3dB change in the second-order intermodulation product can be reliably detected and cracks about 0.1mm were detectable with the length detectable being around 10 times shorter than the wavelength used (proving the high sensitivity of the nonlinear method used).

To conclude Straka, et al. (2008) [123] proved that there is a large monotonical increase in the magnitude of the intermodulation products with increasing number of fatigue cycles and these changes were consistent with appearance and growth of cracks in the specimens. The large sensitivity of the NEWMS method and suitability of the proposed apparatus for the investigation of fatigue damage in aluminium alloy was verified, although the microdamage accumulation (increase in dislocation density) before crack formation was not detected by the apparatus.

Considering the ability of nonlinear ultrasound modulation to detect accumulated fatigue damage, a novel baseline free modulated nonlinear technique was developed for the assessment of the residual fatigue life (Chapter 4.1).

2.5.4. Creep, Hardening, Thermal Ageing and Corrosion assessment using nonlinear ultrasonic techniques

Creep can be defined as the tendency for a solid material to slowly move or deform permanently under the influence of stresses. It is usually found in materials which have long term exposure to high levels of stress that are below the yield strength of the material and are subjected to heat for long periods of time (near melting point) [125]. The rate of deformation depends on material properties, exposure time and applied structural load.

Jeong, et al. (2003) [126] develops a non-destructive method for estimating the fracture toughness of steels used as the rotor material of steam turbines in power plants. Materials exposed to high temperatures for long periods of time can suffer from deterioration of the materials toughness due to embrittlement of the grain boundaries by the segregation of impurity elements present. Various non-destructive methods to test the actual rotor toughness were considered by Jeong, et al. (2003) [126]. Verification of the non-destructive testing methods included methods based on phosphorous content, small punch testing, electrochemical technique, eddy current examination and electrical resistivity measurements. Jeong, et al. (2003) [126] used an ultrasonic nonlinearity parameter which was correlated with the fracture toughness (results were also normalised), the expression used is shown below.

$$\beta' = \frac{\beta k^2 x}{8} = \frac{A_2}{A_1^2}$$

Eq. (2.47)

Where: β' is the normalised nonlinearity parameter, k and x are constants, A_1 and A_2 are the amplitudes of second order harmonic waves.

Jeong, et al. (2003) [126] experiments assessed the dependence of the FATT (fracture appearance transition temperature) and the nonlinearity parameter on ageing time. The correlations between the nonlinearity parameter and the FATT were also investigated (Figure 2.19 below). Jeong, et al. (2003) [136] found significant change in the nonlinearity parameter over time, although beyond around $75x10^3$ h the response was less sensitive (similar to the dependence of FATT on ageing time). The large growth of the nonlinearity in the early stages of the process can be explained as a result of the increase in the grain boundary segregation of impurity elements present in steel, while the reduction of the growth of the nonlinear response after $75x10^3$ h is a result of saturation of the grain boundary segregation (this also explains the effects of exposure time on the FATT) [127].

From the correlation between the nonlinearity parameter and the FATT the fracture toughness can be more reliably estimated from the ultrasonic nonlinearity measurement when the rotor samples are in the early stage of property degradation [127].

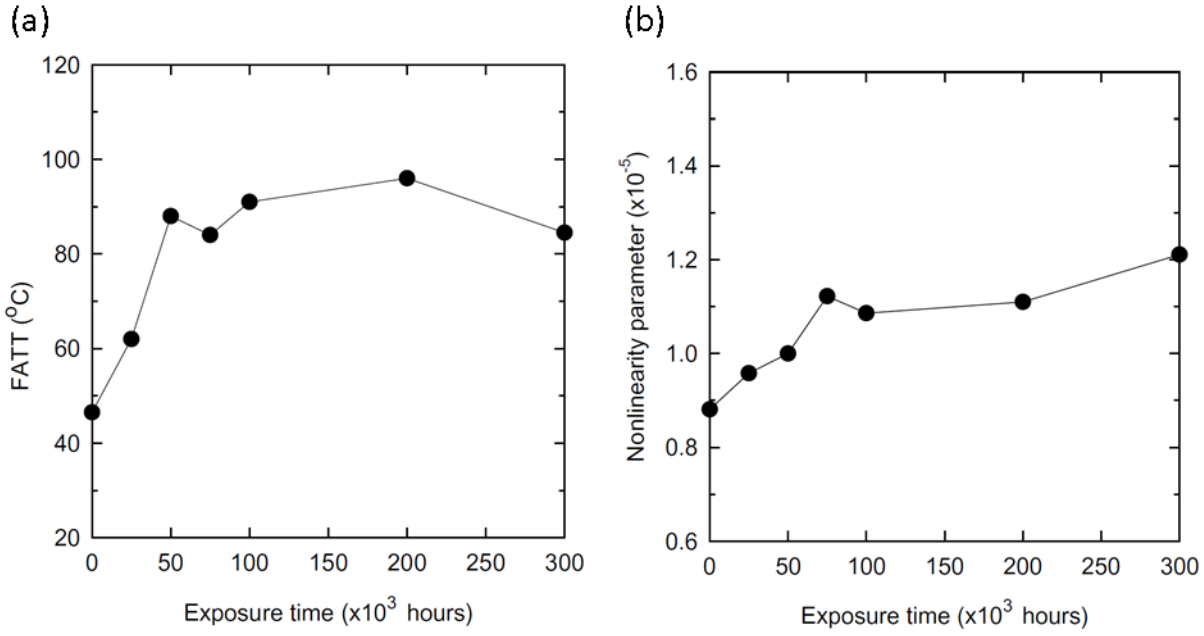

Figure 2.19: Dependence of FATT on ageing time (left) and dependence of ultrasonic nonlinearity parameter on ageing time (right) [126].

Although most nonlinear ultrasonic studies have focused on plastic deformation and fatigue damage, numerous investigations have focused on the evaluation of creep damage. Kang, et al. (2004) [128] observed a strong and unique correlation between the third order harmonic of the transmitted wave and the spent creep life fraction of a directionally solidified nickel base superalloy and also showed a strong correlation between plastic deformation accumulated during monotonic loading and the second harmonic nonlinear parameter of the transmitted wave (although they found no correlation between plastic strain and the third order harmonic nonlinear parameter). Ohtani, et al. (2007) [129] evaluated creep damage accumulation in steel welds using the second harmonic nonlinear ultrasonic methods and microstructural behaviour and found increased amplitudes of harmonics around the heat-affected areas, which corresponded to regions of high creep void density. Baby, et al. (2008) [130] studied the nonlinear response of creep damage in a titanium alloy and found that the nonlinear parameter is more sensitive to damage accumulation during creep deformation when compared with linear ultrasonic longitudinal velocity measurements.

Valluri, et al. (2010) [131] conducted tests on 99.98% pure copper, which included monitoring creep damage progression by conducting continuous and interrupted mode creep tests and nonlinear ultrasonic measurements (NLU) after fracture at different locations along the gage length. Valluri, et al. (2010) [131] also conducted NLU measurements at different creep life fractions for interrupted tests and investigated three nonlinear measurements (static displacement, second harmonic and third harmonic using theory set out by Kang, et al. (2004) [128]). The research found evidence of a relationship between the second harmonic amplitude and the square of the fundamental amplitude.

Valluri, et al. (2010) [131] tests concluded that fracture occurred where both the NLU parameters and the void content were the maximum and at fracture points the linear ultrasonic velocity was found to be a minimum. It was also determined that throughout the study that NLU parameters were found to have their highest values at locations where voids were at a maximum and final fracture in most cases occurred at these locations. The linear velocity was lower at void locations and the percentage change in the linear measurement was significantly smaller when compared to the nonlinear measurements, and it was suggested that further evidence was required to confirm these conclusions.

Valluri, et al. (2010) [141] tests conducted on creep damage evaluation through interrupted loading of specimens found that the NLU parameters showed a ‘hump’ at the lower creep life fraction value (0.3-0.4) followed by a more significant increase as the sample approached failure (0.7 and above) and observations found were consistent with earlier findings for the various materials tested [129, 130, 132].

Valluri, et al. (2010) [141] revealed that the third harmonic based nonlinear parameter displayed the highest sensitivity when compared with the second harmonic nonlinear parameters. The experiments found large nonlinear ultrasonic response increases (25-45%) with increasing

creep life after which it stayed more or less constant until rapidly increasing close to fracture. The nonlinear response increased with increasing time of exposure while the creep life decreased with increasing stress.

Valluri, et al. (2010) [131] acknowledge a number of limitations of their very promising contributions. These limitations include issues of replicability, issues of surface roughness and issues concerning their small sample size. They assert that these limitations need to be overcome before their technique is ready for field application.

Other failure mechanisms have been studied to determine the effect on the nonlinear ultrasonic parameter such as hardening, thermal ageing and corrosion [133-136]. Similar to fatigue damage tests using ultrasonic techniques, it has been found that the nonlinear parameter varied with final ageing treatment. The nonlinear parameter has also been shown to increase with increase of strain [133] and that there is a relative change in the magnitude of the nonlinear parameter as ageing time increases (which can be demonstrated by using the fundamental amplitude [134, 136]). These works highlight the extensive ability that lies within nonlinear ultrasonic techniques and the potential that one testing system could potentially provide solutions for many of the problems that relate to material degradation.

Most studies up to this point have focused on nonlinear methods for the detection, evaluation and localisation of damage in metallic structures. The following section discusses the potential of nonlinear techniques for damage detection in composite materials.

2.6. Composite Materials

In order to discuss the nonlinear ultrasound techniques with composite materials it is important to define them. Although composite materials are considered a mixture of two or more distinct constituents or phases, this definition is inadequate, for a greater understanding. First both constituents have to be present in reasonable proportions (greater than 5%), constituent phases need to have different properties (hence composite material has noticeably different properties than its constituents) and a man-made composite is usually produced by mixing and combining the constituents by various means [137]. Thus materials such as plastics and alloys are not normally classified as a composite material.

Non-destructive evaluation of fatigue damage in composite materials are an important requirement for structural applications and thus it is important that testing methods (whether ultrasonic methods or not) produce reliable and repeatable characterisations of the types, dimensions and locations of fatigue damage and are accurate in evaluation of changes to the mechanical properties (such as stiffness etc.) due to fatigue damage [138].

2.6.1. Damage Progression of Composite Materials

Estimating the fatigue life and damage of materials is difficult, even more so for composite materials as there are many failure modes and mechanisms which act differently to the accumulation of damage. Stress distribution can be several orders of magnitude different in different directions in composites even though strains are of the same order (exhibit strong anisotropy) and generalised stress measures to predict fatigue life are difficult (like von Mises stress in metals) [139].

When using a material safely and with confidence, its fatigue characteristics are essential in order to estimate the durability of the material within its structural application. There are various theories on how to predict the fatigue life of a material. One of them, the stress life approach, can be broken down into three main expectations about the stress levels applied to a material over its life. The three stages of the stress life approach are: low cycle fatigue which assumes high maximum stress level in the load cycle and low number of cycles to failure, high cycle fatigue where the maximum stress in the load cycle is well within the elastic regime and endurance limit which assumes that the fatigue stress levels are below a certain value and thus no failure will occur no matter the number of cycles (see Figure 2.20) [139].

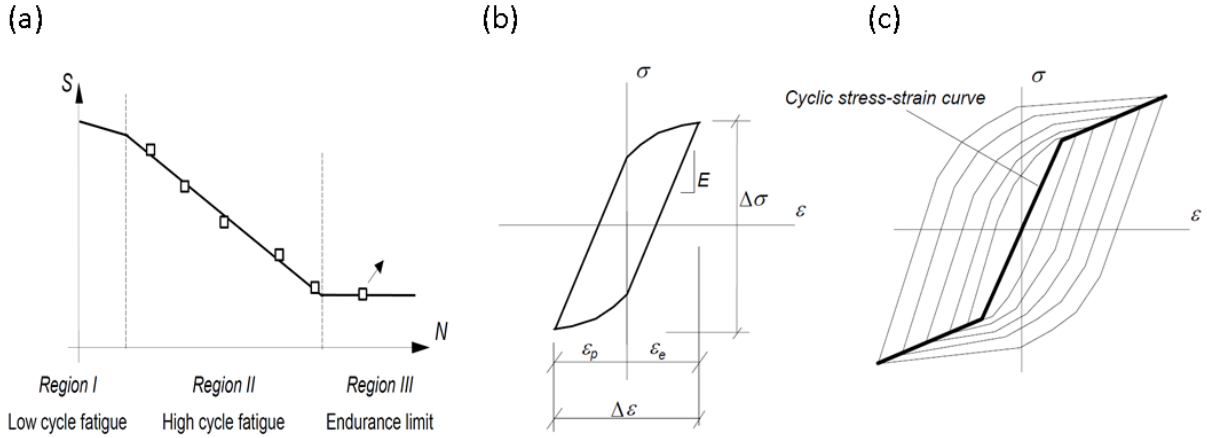

Figure 2.20: Typical S/N diagram with the line showing a piece-wise linear representation of the fatigue function (a), schematic representation of the stable stress-strain hysteresis (b) and cyclic stress-strain curve drawn through the tips of the stable loops (c) [139].

The prediction of the fatigue life of a composite material relies on various other factors such as the mean stress effect which is the relationship between the mean stress and the stress amplitude[139]. Another important factor is material degradation due to fatigue loading which takes into account cyclic softening or hardening of the material and is accompanied by an increase or decrease in strain amplitude at constant stress amplitudes. Crack growth which can simply be broken down into three phases initiation, stable crack growth and unstable crack growth.

Early work completed by Talreja (1987) [140] outlines the fatigue process of composite materials. Due to the composition of composite materials (fibre volume fractions and direction of fibres), it is more logical to use strain versus number of cycles than stress. Thus the way a composite behaves at various loads (high, intermediate and low) have very different effects on the composite materials fatigue life.

For high loads near the static strength of the fibres, the process of fatigue starts with some fibres failing after the first load (as each fibre has a slightly different strength which may vary along its length), then some fibres will fail after the second loading as the stress state will have changed and finally once the number of total fibre failure becomes large enough in a local area due to the stress concentration cracks will form and grow very fast for the next load cycles until eventual failure [139]. Low loading of composite materials does not result in fibre failure after the first loading and thus there is no active failure mechanism. Whereas intermediate loading for crack growth; stress and strain in the material needs to change, if there is no change, no energy is dissipated and thus no growth [139]. If the composite matrix is subject to strain controlled fatigue and the strains exceed the fatigue (strain) limit for the matrix, matrix cracks will occur. If the strain level is low, matrix cracks stop at the fibre interface but if strain is high the cracks will continue to grow and thus material degradation will occur. Finally if the strain level is high the stress intensity at the crack tip might exceed the fracture stress of the fibre and lead to fibre failure. A general model of the development of damage can be seen in Figure 2.21 below.

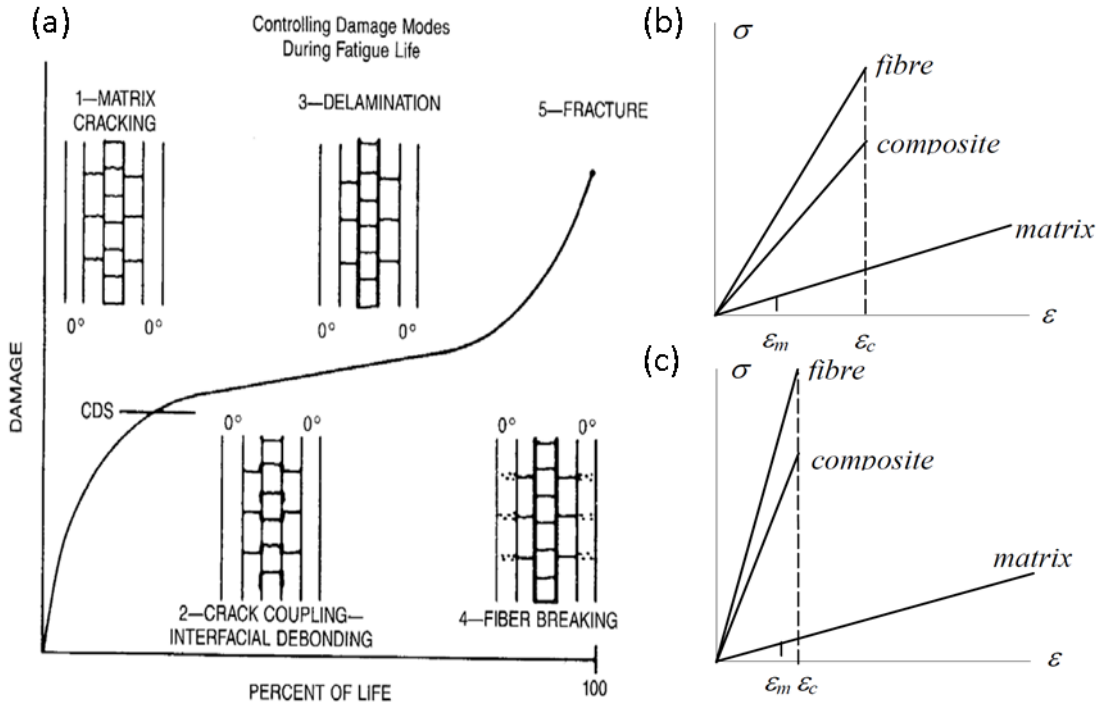

Figure 2.21: Development of damage in composite laminates under fatigue (a), stress-strain relation for low stiffness fibres (b) and high stiffness fibres (c) [140].

The effect of composite stiffness on fatigue performance limits the strength of a composite to the lower of its matrix strain to failure or the fibre strain to failure (Figure 2.21 above). Other areas not covered that may also affect the fatigue life of a composite material are: off-axis loading, modelling of angle-plied laminates, cross-ply laminates and other laminate configurations. Along with the difficulties involved in using nonlinear ultrasonic techniques, it becomes extremely difficult to create models that can reliably estimate the stage of fatigue life using these techniques. The complex composite failure modes which make fatigue life assessment extremely difficult have led to a focus of composite damage detection in this thesis.

2.6.2. Recent Studies and Findings

Experimental work by the author (Chapters 3.2) evaluates kissing bonds (for a composite-composite joint) and delamination of a compressed composite structure using a novel nonlinear ultrasound acoustic moments method. Thus it is important to understand whether nonlinear effects respond in a similar manner in composite materials as they do in metals. Furthermore a novel thermosonic method was developed to evaluate impact damage (Chapters 5) of a composite plate this method relies on the ability of nonlinear ultrasound to detect impact damage. The following sections assess the ability of nonlinear ultrasound methods to detect damage in composite structures.

Oskouei, et al. (2010) [141] highlights various studies evaluating delamination and other failure modes of composite materials, these studies include:

(i) Considerable amount of research has focused on delamination (due to the potential danger of this damage mode) where fracture mechanics approaches tend to dominate [142-144],

(ii) Mode I fracture (which has received the greatest consideration) where various standards have been developed for the double cantilever beam test [145],

(iii) Surface energies of Mode I fracture using propagation effects [146, 147]

(iv) Microscopic behaviour of fiber-matrix interface microdamage (due to its evaluation difficulties) [148, 149],

(v) Fiber breakage, interface decohesion and matrix cracking in composite materials has been evaluated using acoustic emission [150-156]. One of the major problems facing AE methods is the evaluation of the damage stages due to the difficulties with interpretation of the signals [141].

2.6.3. Damage detection and delamination

Meo, et al. (2008) [5] shows promising results for damage detection of carbon fibre reinforced plastic (CRFP) using nonlinear elastic wave spectroscopy (NEWS) methods. NEWS methods monitor the integrity of structures by evaluating the material nonlinear elastic behaviour caused by the presence of damage and as discussed before these nonlinear methods provide an advantage of linear acoustic parameters.

Meo, et al. (2008) [5] evaluates two separate techniques; a nonlinear resonant ultrasound spectroscopy (NRUS) and nonlinear wave modulation spectroscopy (NWMS). NRUS involves observing the hysteretic behaviour of a material as it is excited by a sine wave with different amplitudes (A_1 and A_2) and establishing the stress strain curve which can be described as a loop having an average modulus (K_1 for and amplitude of A_1 and K_2 for and amplitude of A_2) along with the amount of energy dissipated. Meo, et al. (2008) [5] describes a NRUS technique which used resonance methods to analyse the dependence of the resonance frequency on the strain amplitude while exciting the sample at relatively low amplitudes. A schematic representation can be seen in the Figure 2.22 below:

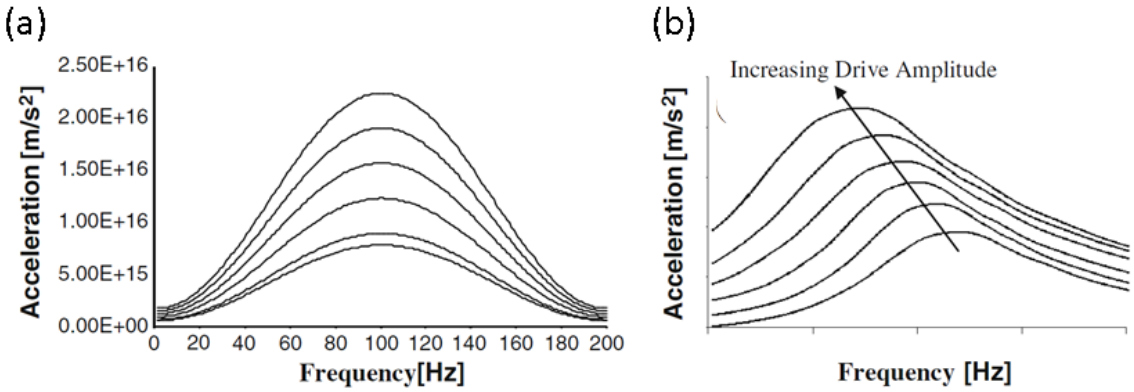

Figure 2.22: Resonance frequency versus drive amplitude: intact specimen (a) and damaged specimen (b) [5].

The NWMS method developed by Meo, et al. (2008) [5] involved applying two continuous waves of different frequencies (one low f_1 and one high f_2). It was expected that in a damaged material the amplitude of the high-frequency wave will be modulated with the low frequency thus in the frequency domain the wave spectrum acquires sidebands and new frequencies are created. If nonlinearities are strong enough additional sidebands can appear forming a complex modulation spectrum (Figure 2.23, below).

The NWMS method investigated by Meo, et al. (2008) [5] revealed that amplitudes of sidebands and harmonics increase with the increase of the amplitude of the fundamental frequencies. The results clearly showed that impact damage introduced material non-classical nonlinear hysteretical behaviour and presence of the harmonics and sidebands were a clear

indication of fibre breakage, matrix cracking and delamination. When using the NRUS method the samples exhibited a significant shift of resonance frequency with an increase of the external drive amplitude. The behaviour of nonlinear parameter was also clearly found to be strongly dependent on the damage severity (the higher the nonlinear parameter the higher the delamination area) and the nonlinear parameter was highly sensitive to the damage magnitude. Meo, et al. (2008) [5] suggested that the method could be used to assess progressive fatigue damage or cyclic compression damage after a low velocity impact. Further studies are needed to link the magnitude of nonlinear parameters to the entity of damage.

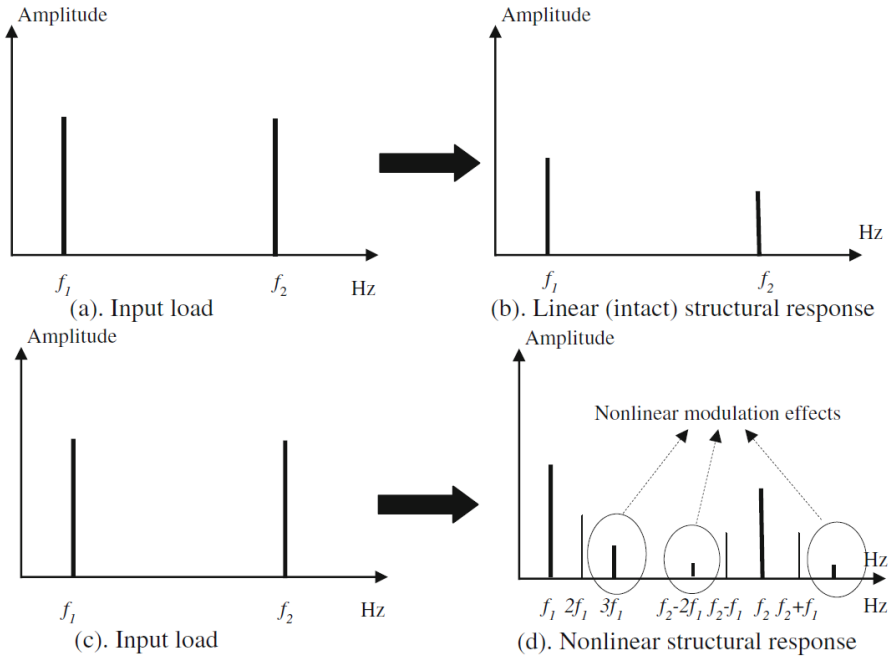

Figure 2.23: Linear and nonlinear modulation effects: excitation frequencies (a), response of a linear undamaged (b), excitation frequencies (c) and nonlinear response of a hysteretic damaged material [5].

Meo, et al. (2008) [5] findings provide important insight into the ability of the NWMS procedure to excite damage regions in composite structures. The novel thermosonics method developed by the author (Chapters 5) uses this excitation ability to heat damaged regions, in order to view them using an infrared camera (this will be discussed in detail in the prescribed chapter).

A transient nonlinear elastic wave spectroscopy (TNEWS) method was used by Zumpano, et al. (2008) [157] in order to detect and localise a scatter zone (damage) in a composite plate. The TNEWS method analysed the uncorrelations between two structural dynamic responses generated by two different pulse excitation amplitudes by using a time-frequency coherence function. Damage detection using the NEWS method relies on analysing the materials nonlinear elastic behaviour; it has been shown that the classical nonlinear models [158] cannot explain the nonlinear behaviour generated by local nonlinear forces due to damage presence [17, 159-164], the equations below were used to demonstrate this behaviour.

$$\sigma = \int E(\varepsilon, \dot{\varepsilon}) d\varepsilon$$

Eq. (2.48)

$$E(\varepsilon, \dot{\varepsilon}) = E_0 \left\{1 - \beta\varepsilon - \delta\varepsilon^2 - \alpha\left[\Delta\varepsilon + \varepsilon(t) sign(\dot{\varepsilon}) + \cdots\right]\right\}$$

Eq. (2.49)

Where: E in the nonlinear and hysteretic modulus, E_0 is the linear modulus, $\Delta\varepsilon$ is the strain amplitude change over the last period, β and δ are classical nonlinear coefficients, and α a material hysteresis measure.

Zumpano, et al. (2008) [157] describes the non-classical nonlinear elastic material on the Preisach and Mayergoyz (PM) space [165, 166]. The macroscopic behaviour of damaged materials was described by the contribution of a number of mesoscopic material cells composed by a statistical collection of microscopic units with varying properties defining their stress-strain relation. The strain of these microscopic units was a combination of a classical nonlinear state relation (elastic component contribution) and a non-classical addition due to hysteretic effects (interface binding contribution). While the strain component of hysteretic mesoscopic elastic unity (HMEU) is described as the strain of a microcrack when subjected to an external pressure that produces its closing and opening and the pressure-displacement of microcracks is characterised by a rectangular look defined by two couples of parameters (pair of two equilibrium lengths and a pair of pressures).

Zumpano, et al. (2008) [157] established that damage was identified by analysing the time-frequency coherence, with a drop in coherence associated with frequency content shaped around the third harmonic of the pulse central excitation frequency (which was in line with non-classical nonlinearity prediction [165, 166]). Damage was plotted as a function of the frequency and could be localised with the change of the frequency within the tolerance of the methodology due to the piezoelectric patch finite dimension. The non-classical nonlinear elastic material behaviour was found to increased with the excitation pulse amplitude. Improved accuracy of damage localisation of the TNEWS method could be found by adjusting A_2 and ΔA which lead to a threshold for damage localisation. TNEWS accuracy was affected marginally as the error of the predicted damage location was comparable with that of the least accurate A_1 and A_2 combinations. Ultimately, the TNEWS technique clearly identified the faulted zone displaying its robustness to detect and locate nonlinear sources in the presence of multilayer material.

Oskouei, et al. (2010) [141] studied mode I interlaminar fracture of glass/polyester composites using acoustic emission (AE) to analyse the damage evolution and evaluate the interlaminar performance of polymeric composites. The process was simulated with a double cantilever beam in opening mode (Mode I) while using an AE technique (Figure 2.24, below), with microscopic observation (scanning electron microscopy) being used to determine the correlation between different fracture mechanisms and the corresponding AE signal frequency content.

Considerable efforts have been made to characterise the delamination process where fracture mechanics approaches tend to dominate due to the danger of delamination [142-144].

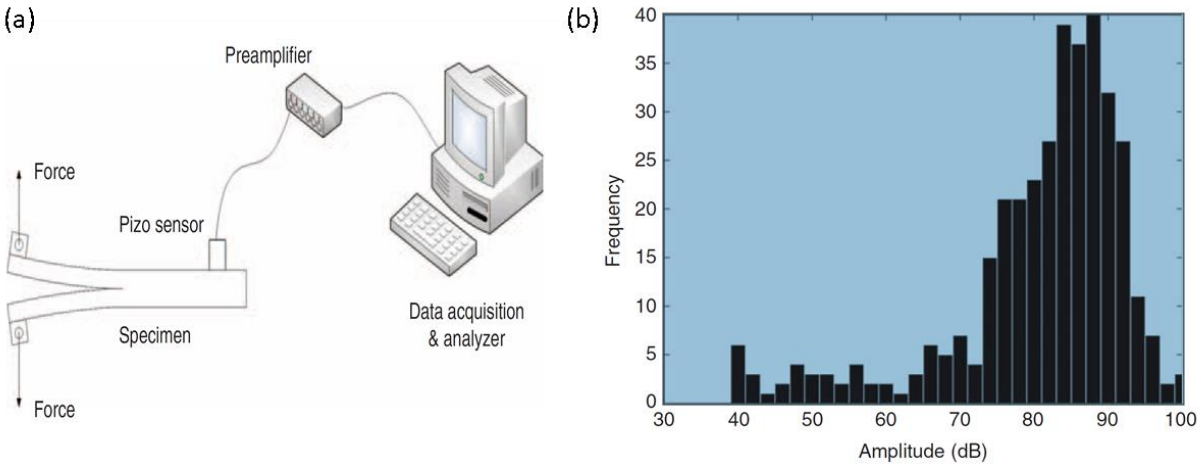

Figure 2.24: AE testing configuration with the sensor clamped to the test specimen (a), and amplitude distribution for bundle with 70mm gage length (b) [141].

Oskouei, et al. (2010) [141] established various distributions of AE amplitudes due to fiber breakage and friction between the filaments. Amplitudes of 80-95 dB were attributed to fiber breaks while other distributions (40-70 dB) were related to friction between fibers [155]. Statistical results show that a bimodal strength distribution in a fiber bundle causes fiber failure at different stress levels [155, 167], while the dominant frequency range of signals are at a lower level than the dominant frequency range of fiber bundle breakage. Intrinsic frequencies and elastic acoustic velocities of the relaxation processes differ in the fiber and matrix because of their correlation with the relaxation time, elastic module and densities [167].

Oskouei, et al. (2010) [141] evaluates delamination initiation and propagation by dividing the load-displacement plot into four stages: before nonlinearity (NL, point A), after NL point but before maximum load, a sudden load decrease and constant load (Figure 2.25, below). Oskouei, et al. (2010) [141] suggested that variations in AE event energy reflect different damage mechanisms (no events were recorded before point A). The onset of the macroscopic delamination growth was revealed to be the point of deviation from linearity on the load-displacement plot (point A) and before the newly defined maximum load point. Thus AE characterises the kinetics of progressive delamination propagation.

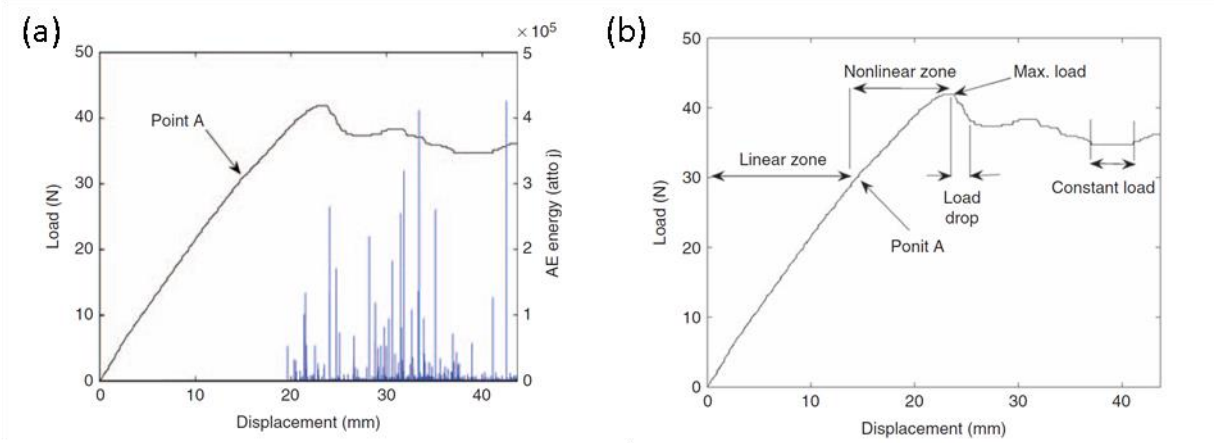

Figure 2.25: Delamination force and AE signal energy vs. displacement (left), force vs. vertical displacement showing delamination stages for signal processing (right) [141].

Oskouei, et al. (2010) [141] investigate the correlation between AE energy and mechanical energy (due to the importance of event energy) and describes a linear correlation between the AE energy and the mechanical energy release rate of microscopic damage processes and correlation can be used for similar composite materials to determine the damage tolerance of specimens by using AE signal energy as a damage criterion. Ultimately Oskouei, et al. (2010) [141] demonstrates that the AE method coupled with signal processing techniques can be used to monitor the damage evolution and interface damage contribution to the overall failure process of a composite material (microscopic (SEM) observations of the fracture surface showed that the frequency spectra are related to the microscopic damages). The next section focuses on the use of thermosonic methods for the detection and localisation of damage in composite.

2.6.4. Thermosonics and Nonlinear Ultrasound

Thermosonics forms part of optical non-destructive testing (NDT) methods which include other methods such as thermography, holography, electronic speckle pattern interferometry (ESPI), Moire' techniques and shearography. Due to the ever wider use of composite materials across many engineering disciplines it has become increasingly important to determine the presence of defects or damage. Complicated methods of manufacturing composites as well as inherent material susceptibility to various damages (impact damage), has resulted in evaluation of damage in these materials both after manufacturing and during the service life of the component. There is no debate of the importance of NDT methods (product safety, in-line diagnostics, quality control, health monitoring, etc.) but rather on accuracy, time and cost related factors relating to the multitude of methods available today.

Thermosonics relies on the excitation of a medium using a piezoelectric transducer (PZT) or welding horn [168]. The excitation of the medium results in heat generation through the dissipation of mechanical energy at the crack interfaces by vibration. The outcome is the visibility of defects

due to the local generation of heat caused by friction and/or stress concentration and visualisation of the temperature rise around the defect is possible using a high-sensitivity infrared imaging camera. Traditional systems use an ultrasonic welding horn to excite components which results in large disadvantages in the process. Which include the ability to control and reproduce the excitation is extremely difficult due to; the nonlinearity in the coupling between the horn and component, damage of the component can occur due to the large energy output of the horn and from decoupling between the tip of the horn and component (chattering). Current methods have moved to using PZTs as they provide many advantages, such as the excitation can be accurately repeated, controlled and altered, and they do not necessarily cause damage to the component (due to lower energy requirements).

Thermosonics has potential to provide important information about the damaged state of components and has been subject to numerous investigations [169-177]. Although one of the major disadvantages of such methods is the acoustic excitation process employed as this can be a complex and time consuming process. There remains a need for a simple 'excitation adequacy' indicator to promote wide adoption of this potentially powerful and attractive damage detection technique [169].

Polimeno, et al. (2010) [92] focused on creating an image to determine the presence of low velocity impact damage using nonlinear ultrasonic methods. The research investigated the nonlinear response of damaged carbon/epoxy composite samples and the sensitivity of second harmonic imaging technique (SEHIT) based on material nonlinear elastic effect known as second harmonic generation (SHG). The SEHIT method was validated using two conventional techniques; pulse thermography and thermosonics. The base theory of the report focused on the assumption of nonlinear stress-strain relations in flawed materials, which have been extensively researched [5, 17, 157, 178-182].

Nonlinear damage localisation of the composite used by Polimeno, et al. (2010) [92] was completed by monitoring the source of harmonics and their amplitudes to create an image. The experimental set up can be seen in Figure 2.26 (below), the measurements were carried out by positioning the microphone at various points in an area enclosing the barely visible impact damage (BVID) and analysing the spectral response by extracting the harmonic response at each point.

Polimeno, et al. (2010) [92] establish that the spatial distribution was not correlated with location of damage or defects although the strongest contribution came from modal shape and by plotting the harmonic amplitude scaled with the fundamental amplitude it was possible to obtain a clear indication of damage location. Ultimately the new thermosonic technique succeeded in localising the damage and the results were in good agreement with the defect position evaluated with the nonlinear image technique while the well-established pulsed thermography technique failed to detect the BVID damage.

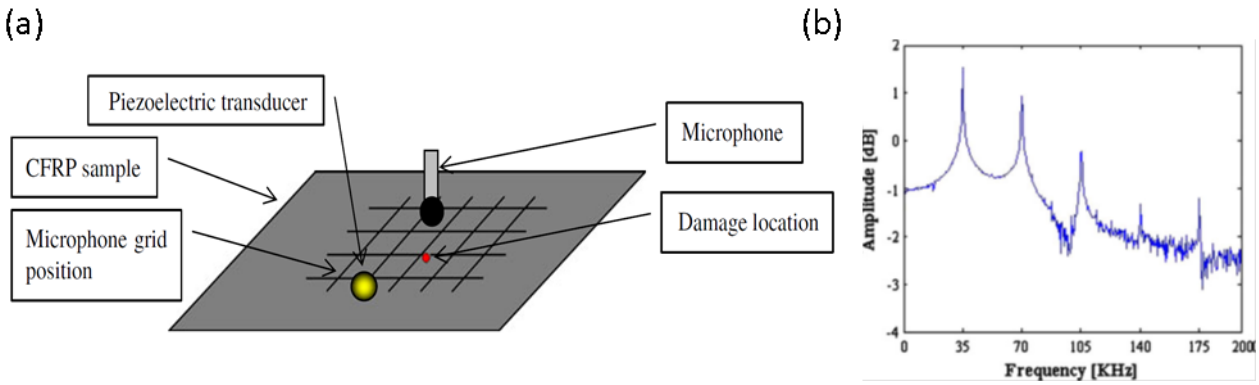

Figure 2.26: Schematic view of the sample front face, grid points correspond to positions of the microphone (a), and frequency content of sample response acquired close to the damage position (b) [92].

Chapter 5 looks at the development of a dual frequency damage-specific resonance frequency thermosonic excitation method, where the excitation frequency is determined by using nonlinear ultrasound principles. Nonlinear ultrasound methods provides benefits in the determination of excitation frequencies that specifically excite damage regions generating larger heat differentials and increases the probability of damage detection due to the dual frequency excitation method. This method has great potential for rapid damage detection compared with other optical and NDT/E techniques.

2.7. Summary of Literature Review

This review of ultrasonic techniques used in determining damage in various materials outlines the early development of such techniques while highlighting their growth and potential. Various areas were focused on in order to show the progression of these techniques, such as:

(i) linear ultrasonic methods [7, 9, 11, 46, 55-83],

(ii) nonlinear ultrasonic methods focusing on micro-damage detection and plastic deformation in metals [16, 20, 21, 98-101, 113-115]

(iii) nonlinear ultrasonic methods focusing on damage precursors and fatigue life in metals [13, 18, 19, 22, 24, 72, 94-97, 102-112, 116-124]

(iv) nonlinear ultrasonic methods focusing on creep in metals [125-131, 183]

(v) nonlinear ultrasonic methods applied to composite materials [5, 17, 141, 150-164]

(vi) other ultrasonic methods [92, 133-136, 164, 178-182].

Due to the vast research that has been completed on these methods it is clear that they can be used to determine micro-cracks, crack propagation, fatigue life, creep, and various other mechanical failure modes of materials. There has been extensive work determining the applications of linear and nonlinear ultrasonic techniques with regard to metals and the results have shown a lot of promise; although research into the effects of nonlinear techniques regarding composite materials are fairly undeveloped. Providing the ever increasing importance of non-destructive testing of materials it is evident that such methods play an important role in material defect discovery and will have an even greater role to play in the future.

3. EXPERIMENTAL STUDIES: KISSING BONDS, ACOUSTIC MOMENTS AND BOLTED JOINTS

This chapter will discuss various nonlinear ultrasound techniques such as; the second and third order nonlinearity parameter (G_{2E} and G_{3E}, Section 3.1.1), the sum-frequency (β_S) and the difference-frequency (β_D, Section 3.1.2), the second harmonic moment ratio ($R_{f2/f1}$), third harmonic moment ratio ($R_{f3/f1}$) and the second and third harmonic moment ratio ($R_{(f2+f3)/f1}$, Section 3.2.1).

Chapter 3.1 evaluates the accuracy of various nonlinear ultrasound methods to assess a simulated kissing bond joint (and cracked region), with the aim of highlighting key factors affecting results such as hysteresis and resonance frequency testing. Chapter 3.2 investigates an acoustic moments method, again to assess a simulated kissing bond joint (and loaded joint), for both an aluminium-aluminium and composite-composite adhesive joint. While Chapter 3.3 uses all the nonlinear methods and some linear techniques (damping curve measurement and response signal energy) to establish the bolt loosened state of a tension joint.

3.1. Dual-Frequency, Hysteresis, Modelling Techniques, and Resonance Frequency Testing

This thesis develops a new novel resonance frequency nonlinear ultrasound testing method as well as explores other methods such as modal analysis for the improvement of test results. The main aim is to use a novel resonance frequency testing method to improve the accuracy of nonlinear responses due to damage. A rig was designed to simulate the presence of kissing bonds and cracked regions in order to explore the robustness of the method as a damage detection tool. Two circular aluminium plates (single interface system) were used to replicate the behaviour of a kissing bond (cracked region), which allowed for practical evaluation of the testing methodologies.

Two types of signal setups were used, the first, a transmission system (single and dual-frequency) where the signal was passed through the object and received on the other side and the second a reflection system (single frequency only) where the signal was reflected off the damaged area (crack, kissing bond) and was captured on the same side that the excitation signal was made.

The effectiveness of the resonance frequency method was assessed by comparing the amplitudes of the nonlinear responses, the variation of responses and the hysteretic response. Early work by Solodov, et al. (2001) [184] reveals how the dynamic characteristics of the second and third harmonics were affected by the input voltage and the hysteretic effect of the input voltage on the second and third harmonics of a fundamental signal. This study evaluates these effects with regard to the nonlinearity parameters.

The nonlinear ultrasound responses were measured using the second order nonlinearity parameter (G_{2E}) (Section 3.1.1, Eq. (3.1)), the third order nonlinearity parameter (G_{3E}) (Section

3.1.1, Eq. (3.2)), the sum-frequency (β_S) (Section 3.1.2, Eq. (3.20)) and the difference-frequency (β_D) (Section 3.1.2 Eq. (3.20)). The variation of the nonlinearity parameters allowed conclusions to be drawn on the effectiveness of the different methods (transmission, reflection, single and dual frequency excitation).

Hysteresis was assessed for single and dual-frequency nonlinear ultrasound methods to determine whether variance in defect hysteresis can be alleviated by using the resonance frequency testing technique. By exploring the nonlinear hysteretic response at resonance and non-resonance frequencies, as well as taking into account modal analysis results, it was found that results may be greatly improved using the new method developed.

Modal analysis using Ansys FEA software was examined in order to determine areas on the sample where maxima out-of plane displacements occur (areas where 'clapping' effects are maximised), these locations were used for sensor location. Modal analysis showed good correlation to experimentally derived resonance frequencies and locations of sensors maximised nonlinear responses. Resonance frequency testing of the structure produced more consistent and larger nonlinear responses, due primarily to an increase in excitation of damaged regions, as well as resulting in less variance in the hysteretic behaviour.

The nonlinear response of compression loaded crack interfaces were also evaluated in order to measure any differences in the results of *in-situ* and free structures, while assessing the practical applicability of the method. Compression loading of the structure showed that nonlinear responses are highly sensitive to loading (due to the restriction of the crack interface) and thus can be used in the assessment of *in-situ* compression loaded structures.

This chapter investigates whether or not the second and third nonlinearity parameters (G_{2E} and G_{3E}) exhibit a hysteretic pattern when subjected to a change in input voltage, whether this hysteretic pattern was evident in the modulated response (sum-frequency and difference-frequency) of a dual-frequency signal (β_S and β_D) and the effect of structural loading on the nonlinear parameters.

3.1.1. Experimental Second and Third Order Nonlinearity Parameters

Non-linear ultrasound techniques and methods centre on the theory of the 'clapping/rubbing mechanism', which include cracks and debonded surfaces. When an ultrasonic signal passes through a crack the propagation of the wave forces the crack to open and close, this opening and closing gives rise to further harmonics in the response signal. These further harmonics are known as the second harmonic, third harmonic and so forth. Nonlinear ultrasound uses these extra harmonics to determine the extent of defects in a material. Dual-frequency ultrasonic excitation uses this theory of the 'clapping mechanism', which give rise to even more additional harmonic responses in the output signal, known as the sum-frequency and difference-frequency.

Figure 3.1 below shows the further harmonics that are produced for single-frequency and dual-frequency signals. Figure 3.1(b) highlights the second (2*f1*) and third (3*f1*) harmonics produced from a single frequency (*f1*) signal, whereas Figure 3.1(d) displays the modulated response for a dual-frequency signal. Where; (*f2-f1*) is the difference-frequency modulated response, and (*f1+f2*) is the sum-frequency modulated response with *f1* being the lower and *f2* being the higher of the dual-frequencies. Modulation in a dual-frequency system gives rise to second and third harmonics of the two individual frequencies (as well as the sum and difference-frequency responses), which results in a large array of further harmonics which do not exist in a single frequency system.

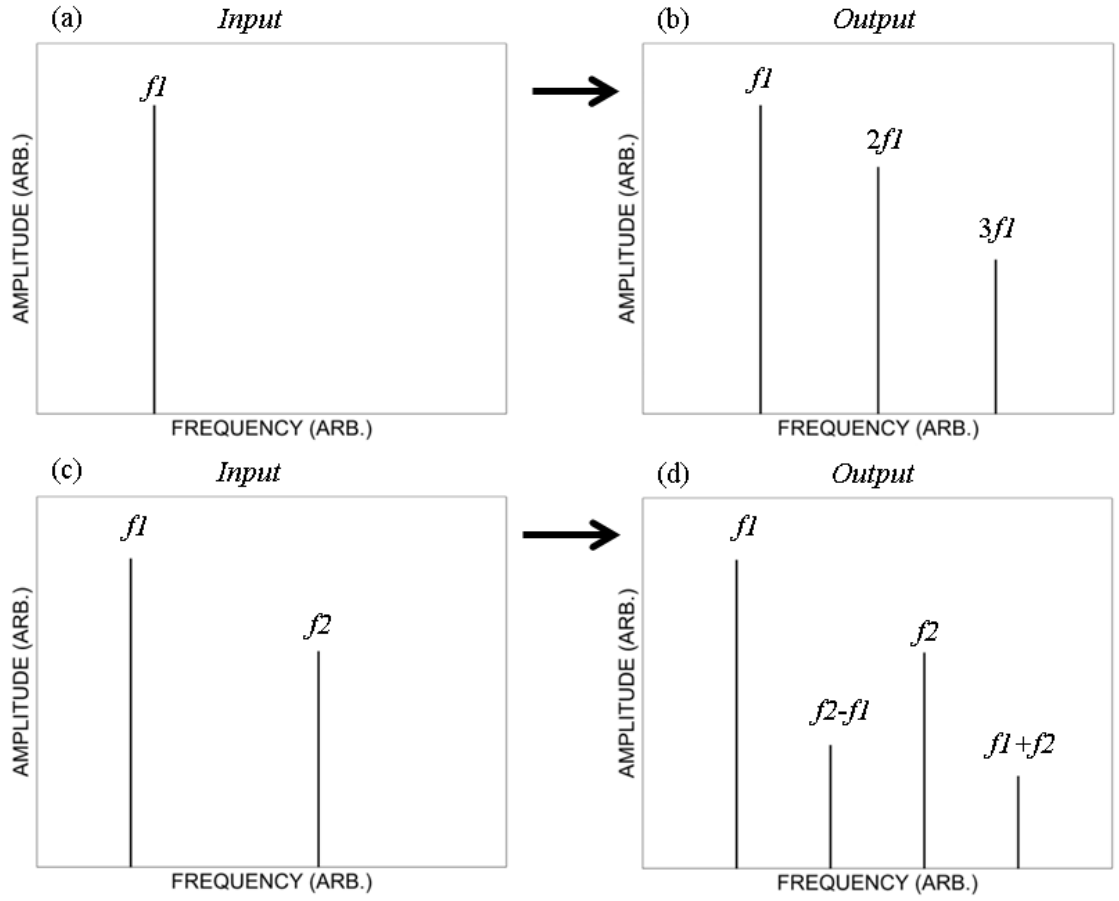

Figure 3.1: Plot (a) and (c) show the input signal for a single frequency and dual-frequency signal, plot (b) and (d) show the output signals for a single frequency and dual-frequency signal, respectively.

The development of the theory behind nonlinear ultrasonic methods has been well documented and tested. The fundamental equations used and developed in order to determine the further harmonics (second and third order nonlinearity parameters) are highlighted below. These equations provide essential information that allow for these harmonics to be quantified and analysed.

The second order nonlinearity parameters can be described by the equation below. [185]:

$$G_{2E} = \frac{8A_2}{A_1^2 k^2 a_1}$$

Eq. (3.1)

Where: A_1 and A_2 are the respective frequency amplitudes of the first and second harmonics of the recorded time domain waveforms, k is the wavenumber, and a_1 is the propagation distance. The second and third order nonlinearity parameter allows for experimental evaluation of the respective nonlinear parameter, the third order parameter is shown below [186]:

$$G_{3E} \approx \frac{A_3}{A_1} \frac{48}{k^3 a_1}$$

Eq. (3.2)

Where: A_3 is the frequency amplitude of the third harmonic of the recorded time domain waveform. The derivation of the sum and difference frequency (modulated nonlinearity parameters) for a dual frequency excitation system are discussed in section 3.1.2 below.

3.1.2. Derivation of the Experimental Modulated Nonlinearity Parameters

The experiment used theory and builds on work completed by Meo, et al. (2010) [186] and Nazarov and Sutin [98]. A dual frequency wave is considered in order to calculate the modulated nonlinear response by using a perturbation analysis. Chapter 4.1 uses the experimental modulated nonlinear parameters derived here to assess its correlation with a theoretical nonlinear material parameter (derived by Meo, et al. (2010) [186], section 4.1.1), in order to estimate the residual fatigue life of a component. While this Chapter focuses on its use to assess kissing bonds, the presence of cracks and damage detection capabilities under load.

The fundamental equations used were Nonlinear Hooke's Law (Eq. (3.3)), the Nonlinear Wave equation (Eq. (3.4)) and the dual frequency wave equation (Eq. (3.9)). By combining and substituting between these equations using a perturbation method it is possible to determine the sum-frequency (β_S) and difference-frequency (β_D) (Eq. (3.20)).

The Nonlinear Hooke's Law response of a dual-frequency system can be described as:

$$\sigma = E\varepsilon + \frac{E\beta}{2}\varepsilon^2 + \frac{E\gamma}{6}\varepsilon^3$$

Eq. (3.3)

The Nonlinear Wave equation:

$$\rho \frac{d^2u}{dt^2} = \frac{d\sigma}{dx}$$

Eq. (3.4)

where:

$$\varepsilon = \frac{du}{dx}$$

Eq. (3.5)

$$c^2 = \frac{E}{\rho}$$

Eq. (3.6)

Where: ε is the strain, c the wave speed, E is Young's Modulus, and ρ the material density. Substituting Eq. (3.5) and Eq. (3.6) into Eq. (3.3), and then Eq. (3.3) into Eq. (3.4) leads to:

$$\frac{d^2u}{dt^2} - c^2 \frac{d^2u}{dx^2} = c^2 \left(\beta \frac{du}{dx} \frac{d^2u}{dx^2} + \gamma \left(\frac{du}{dx} \right)^2 \frac{d^2u}{dx^2} \right)$$

Eq. (3.7)

Eq. (3.7) can be solved using the perturbation method that has the general solution:

$$u = u^{(1)} + u^{(2)} + u^{(3)} + ...$$

Eq. (3.8)

The Dual frequency wave can be defined as:

$$u^{(1)} = A_1 \sin\left[k_{f1}(x - ct)\right] + A_2 \cos\left[k_{f2}(x - ct)\right]$$

Eq. (3.9)

Where: A_1 and A_2 are the respective frequency amplitudes for frequencies f_1 and f_2. Substituting Eq. (3.9) into the left hand side (Linear Part) of Eq. (3.7):

$$\frac{d^2u}{dt^2} - c^2 \frac{d^2u}{dx^2} =$$

$$\begin{aligned} &- A_1\omega_1^2 \sin\left[k_1(x - ct)\right] - A_2\omega_2^2 \sin\left[k_2(x - ct)\right] \\ &+ A_1\omega_1^2 \sin\left[k_1(x - ct)\right] + A_2\omega_2^2 \sin\left[k_2(x - ct)\right] = 0 \end{aligned}$$

Eq. (3.10)

Substituting Eq. (3.9) into the right hand side (Nonlinear Part) of Eq. (3.7) we obtain:

$$c^2\beta\frac{du}{dx}\frac{d^2u}{dx^2}=$$

$$c^2\beta(-A_1^2k_1^3\sin[k_1(x-ct)]\cos[k_1(x-ct)]+A_2^2k_2^3\sin[k_2(x-ct)]\cos[k_2(x-ct)]$$
$$-A_1A_2k_1k_2^2\sin[k_1(x-ct)]\cos[k_2(x-ct)]+A_1A_2k_2k_1^2\sin[k_2(x-ct)]\cos[k_1(x-ct)])$$

Eq. (3.11)

By using Double angle formula, Eq. (3.11) can be shown as:

$$\frac{c^2\beta}{2}(-A_1^2k_1^3\sin[k_1(x-ct)]\cos[k_1(x-ct)]+A_2^2k_2^3\sin[k_2(x-ct)]\cos[k_2(x-ct)]$$
$$-A_1A_2k_1k_2^2[\cos((k_1+k_2)(x-ct))+\cos((k_1-k_2)(x-ct))]$$
$$+A_1A_2k_2k_1^2[\cos((k_1-k_2)(x-ct))-\cos((k_1+k_2)(x-ct))])$$

Eq. (3.12)

The solution to Eq. (3.10) is obtained by assuming the general solution:

$$u^{(2)}=$$
$$f(x)\sin[2k_1(x-ct)]+g(x)\cos[2k_1(x-ct)]+h(x)\sin[2k_2(x-ct)]$$
$$+m(x)\cos[2k_2(x-ct)]+n(x)\sin[(k_1+k_2)(x-ct)]+p(x)\cos[(k_1+k_2)(x-ct)]$$
$$+q(x)\sin[(k_1-k_2)(x-ct)]+r(x)\sin[(k_1-k_2)(x-ct)]$$

Eq. (3.13)

Substituting Eq. (3.13) into Eq. (3.14) provides the solution of Eq. (3.15), below:

$$\frac{d^2u^{(2)}}{dt^2}-c^2\frac{d^2u^{(2)}}{dx^2}$$

Eq. (3.14)

Solution of Eq. (3.14):

$$
\begin{aligned}
&-(f''(x)\sin[2k_1(x-ct)]+4k_1 f'(x)\cos[2k_1(x-ct)]+h''(x)\sin[2k_2(x-ct)]\\
&+4k_2 h'(x)\cos[2k_{21}(x-ct)]+g''(x)\cos[2k_1(x-ct)]-4k_1 g'(x)\sin[2k_1(x-ct)]\\
&+m''(x)\cos[2k_2(x-ct)]-4k_2 m'(x)\cos[2k_2(x-ct)]+n''(x)\sin[(k_1+k_2)(x-ct)]\\
&+2(k_1+k_2)n'(x)\cos[(k_1+k_2)(x-ct)]+p''(x)\cos[(k_1+k_2)(x-ct)]\\
&-2(k_1+k_2)n'(x)\cos[(k_1+k_2)(x-ct)]+q''(x)\sin[(k_1-k_2)(x-ct)]\\
&+2(k_1-k_2)q'(x)\cos[(k_1-k_2)(x-ct)]+r''(x)\cos[(k_1-k_2)(x-ct)]\\
&-2(k_1-k_2)n'(x)\sin[(k_1-k_2)(x-ct)]
\end{aligned}
$$

Eq. (3.15)

Equating Eq. (3.15) and Eq. (3.12), while removing similar terms and making the below assumptions (Eq. (3.16), the solution Eq. (3.17) was determined:

$$
\begin{aligned}
&g''(x)=0 \therefore f'(x)=0, f''(x)=0, f(x)=0\\
&m''(x)=0 \therefore h'(x)=0, h''(x)=0\\
&n''(x)=0 \therefore p'(x)=0, p''(x)=0\\
&q''(x)=0 \therefore r'(x)=0, r''(x)=0\\
&g'(x)=-\beta\frac{A_1^2k_1^2}{8}, m'(x)=\beta\frac{A_2^2k_2^2}{8}, n'(x)=\beta\frac{A_1A_2k_1k_2}{4}\\
&q'(x)=-\beta\frac{A_1A_2k_1k_2}{4}, g(x)=-\beta\frac{A_1^2k_1^2}{8}x, m(x)=\beta\frac{A_2^2k_2^2}{8}x\\
&n(x)=\beta\frac{A_1A_2k_1k_2}{4}x, q(x)=-\beta\frac{A_1A_2k_1k_2}{4}x
\end{aligned}
$$

Eq. (3.16)

The general Modulated response solution:

$$
\begin{aligned}
&u^{(2)}=\\
&-\beta\frac{A_1^2k_1^2}{8}x\cos[2k_1(x-ct)]+\beta\frac{A_2^2k_2^2}{8}x\cos[2k_2(x-ct)]\\
&+\beta\frac{A_1A_2k_1k_2}{4}x\sin[(k_1+k_2)(x-ct)]-\beta\frac{A_1A_2k_1k_2}{4}x\sin[(k_1-k_2)(x-ct)]
\end{aligned}
$$

Eq. (3.17)

The second harmonics of the dual frequency incident wave was determined as:

$$
=-\beta\frac{A_{f1}^2k_{f1}^2}{8}x\cos[2k_{f1}(x-ct)]+\beta\frac{A_{f2}^2k_{f2}^2}{4}x\cos[2k_{f2}(x-ct)]
$$

Eq. (3.18)

By replacing β (Eq. 3.17, lower line, term on the left) which relates to the sum-frequency term with β_S and the term (Eq. 3.17, lower line, term on the right) which relates to the difference-frequency with β_D, it was possible to distinguish the individual terms. While the modulated response, for sum-frequency and difference-frequency of the excitation frequencies can now be shown as:

$$= \frac{\beta_S A_{f1} A_{f2} k_{f2} k_{f1}}{4} x \sin\left[\left(k_{f1} + k_{f2}\right)\left(x - ct\right)\right] - \frac{\beta_D A_{f1} A_{f2} k_{f1} k_{f2}}{4} x \sin\left[\left(k_{f1} - k_{f2}\right)\left(x - ct\right)\right]$$

Eq. (3.19)

By separating the terms determined in Eq. (3.19) above, into sum and difference-frequency components and relating them to the amplitude of the respective nonlinear parts A_S (amplitudes of the sum-frequency ($f_1 + f_2$)) and A_D (amplitude of the difference-frequency ($f_2 - f_1$)), the experimental β parameter for the individual modulated sidebands can be derived. The sum-frequency (β_S) and difference-frequency (β_D) (modulated responses) are highlighted below:

$$\beta_D \approx \frac{4A_D}{A_{f1} A_{f2} k_{f1} k_{f2} x}$$

$$\beta_S \approx \frac{4A_S}{A_{f1} A_{f2} k_{f1} k_{f2} x}$$

Eq. (3.20)

Where: A_{f1} and A_{f2} are the respective frequency amplitudes for frequencies f_1 and f_2. The above modulated responses are related to the linear fundamental frequency responses, and thus serve as a comparison between the nonlinear and linear results.

β_D and β_S describe the experimental modulated material nonlinearity parameters when excited by a dual frequency excitation. All the terms highlighted in Eq. (3.20) can be determined from the frequencies used or the FFT of the time-domain data recorded during ultrasound testing. The hypothesis of the above theory is that as cracks form and grow over a specimens fatigue life it is expected that the fundamental frequencies (f_1 and f_2) amplitudes will decrease as damage increases (this is a linear effect and is subsequently used in linear ultrasound methods to detect cracks). Along with the decrease in the fundamental frequencies the amplitudes of the modulated responses (sidebands/harmonics, A_D and A_S) should increase as damage escalates due to the growth in 'clapping/rubbing' generated from the cracks. Cracks or other damages are expected to generate larger harmonics as damage increases this relationship has been demonstrated in several studies. The dual effect of the described reduction in the fundamental frequencies amplitudes and the rise in the harmonics produced by the cracks result in nonlinear parameters that should increase as damage grows.

3.1.3. Experimental Setup

The experiment conducted explores the use of the resonance frequencies of the material to excite the cracked area and the effect on the production of nonlinear responses. It is expected that the energy transfer at resonance frequencies of the material is far greater than arbitrarily selected frequencies resulting in larger stress exerted on crack locations and thus improved harmonic generation. Resonance frequency testing should also improve the consistency of energy transfer through the specimen providing greater accuracy in the assessment and behaviour of crack hysteresis.

By assessing the change of these nonlinear ultrasound parameters (at both resonance and non-resonance frequencies) it is possible to determine the hysteresis effect. Crack hysteresis is believed to be due to thermally induced microstrain, caused by the small stresses exerted by ultrasound waves on damage locations.

In a single frequency nonlinear ultrasound system the second (*2f1*) and third (*3f1*) harmonics are produced from a single frequency (*f1*) excitation, whereas in a dual-frequency system; modulation is expected to occur at *f2-f1* (β_D) and *f1+f2* (β_S) where *f1* is the lower of the two fundamental frequencies. One of the main proponents for the use of dual-frequency nonlinear ultrasound systems is the removal of harmonics produced by equipment.

In order to establish which frequencies would be used for the tests, the resonance frequencies of the material were determined. This was evaluated using the sweep function of the arbitrary waveform generator (100MHz Arbitrary Waveform Generator TGA12104, Thurlby-Thandar Instruments Ltd.) between 1kHz and 100kHz. Figure 3.2 shows the results of the sweep, the resonance frequencies can clearly be seen as the peaks.

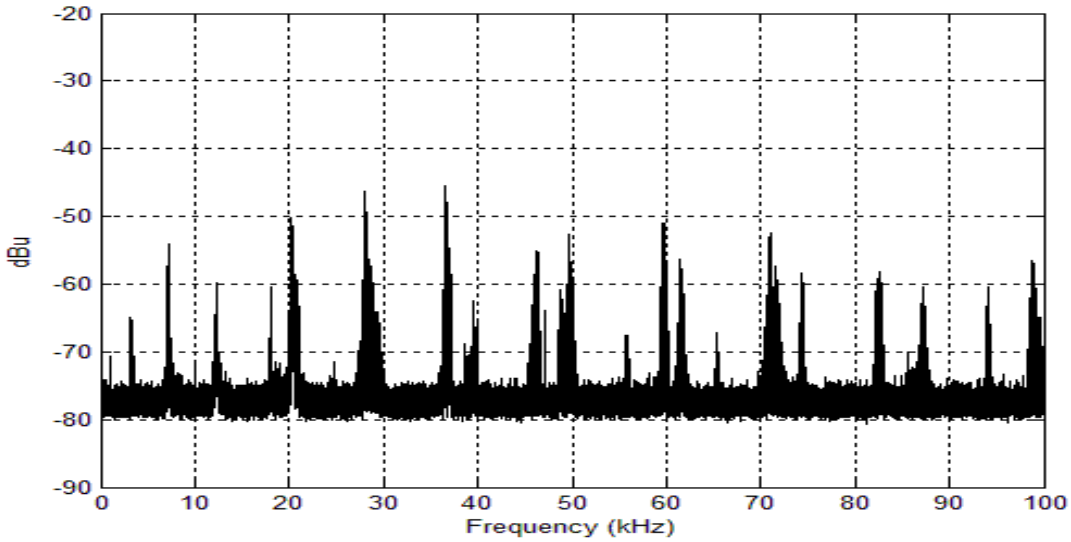

Figure 3.2: Resonance Frequencies

Table 3.1 and Table 3.2 below shows the determined resonance frequencies and the excitation frequencies used for the experiment. The effect of the voltage on the various test parameters was completed sequentially in one continuous test, i.e. input voltage was increase at specified increments over a range from low to a maximum of 20V (pk-pk) and then the process was repeated from the maximum voltage to the low voltage. Generally a large input voltage adjustment was 2V from a minimum of 1V to the maximum 20V (the final step required an increase of 1V from 19V to 20V). A small input voltage adjustment used steps of 0.2V.

Large Input Voltage Adjustment:			**Small Input Voltage Adjustment:**	
Transmission:	***Reflection:***	***Dual Frequency:***	***Transmission:***	***Dual Frequency:***
7.190	28.100	12.222 & 28.100	28.100	28.100 & 36.700
12.222	36.700	28.100 & 82.226	70.898	70.898 & 82.226
28.100		36.700 & 49.770		
36.700		61.500 & 70.898		
55.492				
59.584				
70.898				
82.226				

Table 3.1: Frequencies (kHz) investigated for the various tests preformed

Resonance (Excitation) Frequency (kHz)	**Second Harmonic (kHz)**	**Third Harmonic (kHz)**
3.595	7.190	10.785
7.190	14.380	21.570
12.222	24.444	36.666
18.140	26.280	54.420
20.330	40.660	60.990
28.100	56.200	84.300
36.700	73.400	110.100
45.960	91.920	137.880
49.770	99.540	149.310
55.492	110.984	166.476
59.584	119.168	178.752
61.500	123.000	184.500
65.881	131.762	197.643
70.898	141.796	212.694
82.226	164.452	246.678

Table 3.2: Plates Resonance Frequencies

Four piezoelectric transducers (PZTs) were bonded to two thin cylindrical aluminium plates (Material A refer to Appendix 1, 90mm diameter, 3mm thickness, AA2024) which were used to replicate crack formations and a kissing bond of a debonded adhesive joint (Figure 3.3, below). P1 (850WFB D-008 Piezoelectric disc, APC International Ltd) and P2 represent the PZTs that were bonded to the top plate where the input signals were delivered, and P3 and P4 are the PZTs that were bonded to the bottom plate where output signals were received. The PZTs were bonded to the aluminium surfaces using M-Bond 200 two-part cyanoacrylate adhesive. For the transmission tests the input signal used PZT P1 and the output signal was received by PZT P3. The reflection tests used PZT P1 to send the input signal and PZT P2 to receive the signal.

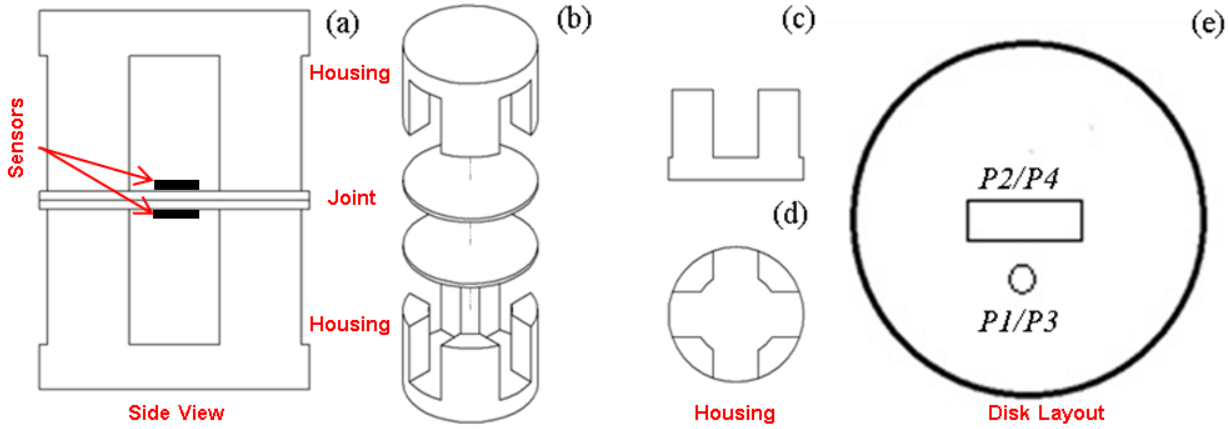

Figure 3.3: Experimental setup: side view of rig (a), exploded view of rig (b), side view of housing (c), top view of housing (d), and positioning of PZTs (e).

The signal output of the PZT receiver was measured using an oscilloscope (PicoScope 4424, Pico Technology). Raw data captured using Picoscope Software 6 was then formatted using MATLAB (R2012b, The MathWorks, Inc., Natick, Massachusetts, United States.), which was used to measure the second and third-order nonlinearity parameters (G_{2E} and G_{3E}), quantify the modulated response (β_S and β_D) of the dual-frequency excitation and plot important figures in order to assess if any relationships exist between key factors.

3.1.4. Results: Transmission, Reflection and Dual Frequency

Transmission tests were performed by sending and receiving signals on either side of the two plates (PZT P1 and P3). The results found that G_{2E} increased as input voltage increased for all the tested frequencies, G_{2E} increased at an increasing rate for most frequencies and that the magnitude increase over the voltage range was large. For frequencies 36.7 kHz, 59.584 kHz and 70.898 kHz there was a significant increase in the value over the voltage range.

Results found that G_{3E} increased as input voltage increased for all the tested frequencies, the increase was at an increasing rate for most of the tests (like G_{2E}) and that the magnitude increase over the voltage range was large. For frequencies 36.7 kHz, 59.584 kHz and 70.898 kHz there was a significant increase in the value of G_{3E} over the voltage range. The results are considerably higher than that found for G_{2E} and suggest that G_{3E} is more sensitive to changes in input voltage. Figure 3.4 shows clearly that both G_{2E} and G_{3E} increase as signal amplitude increases, G_{3E} increased at a greater rate than G_{2E} and an increase in signal amplitude results in a hysteresis in G_{2E} and G_{3E}. Figure 3.4 also illustrates that hysteresis is more visible when smaller amplitude changes were made.

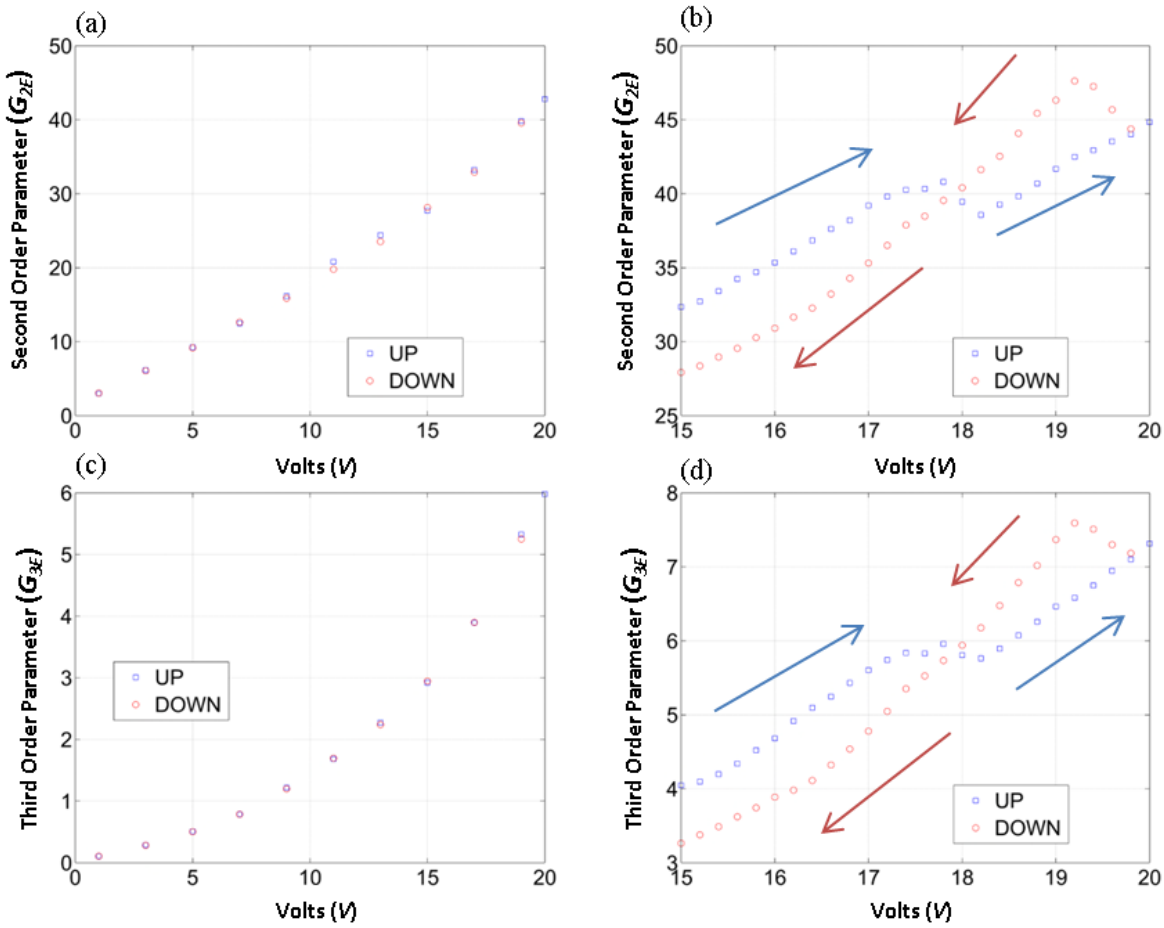

Figure 3.4: G_{2E} results vs. Frequency (a) and (b), and G_{3E} results vs. Frequency (c) and (d). (Frequency equals 28.1kHz, Transmission)

In Figure 3.4 there is a difference between the magnitudes of G_{2E} and G_{3E} for the large voltage changes (plot (a) and (c)) versus the small input voltage changes (plot (b) and (d)). The discrepancies in the magnitudes of the nonlinear parameters are due to contact between the plates changing during equipment setup. The change in the orientation of the plates leads to different conditions for the production of nonlinear responses and thus the variation in the magnitudes of G_{2E} and G_{3E}.

Reflection tests were performed by sending and receiving signals from the same surface. This was possible by using both input and output PZTs that were attached to the same surface of the prescribed aluminium plates (PZT P1 & P3). Figure 3.5 show the G_{2E} and G_{3E} results found for reflection from the results of G_{2E} and G_{3E} it is clear that both results increase as the input voltage increases, G_{3E} results are more sensitive than G_{2E} results to increases in input voltage, both exhibit hysteretic patterns and are less sensitive to changes in voltage input for reflection than transmission.

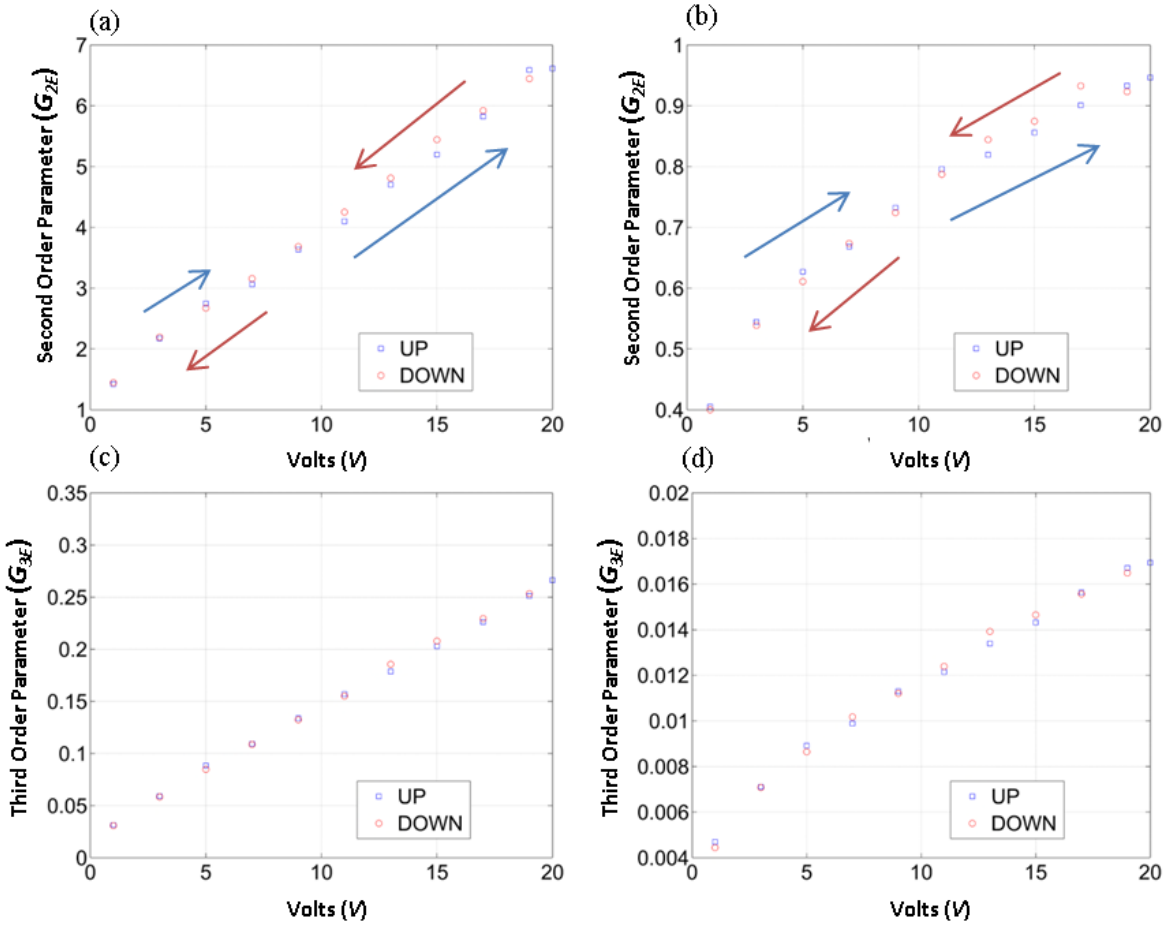

Figure 3.5: G_{2E} results vs. Frequency (a) and (b), and G_{3E} results vs. Frequency (c) and (d). ((a) and (c) Frequency equals 28.1kHz, (b) and (d) Frequency equals 36.7kHz, Reflection)

The nonlinear dual-frequency response was investigated to confirm whether measurable and unique harmonics in the response signal were produced. The sidebands (modulation, β_S and β_D) were investigated to determine whether they behave like G_{2E} and G_{3E}, their suitability for defect detection, and sensitivity to changes in the input voltage.

Figure 3.6 (below) shows a summary of G_{2E} and G_{3E} for the dual-frequencies tests. Results reveal that G_{2E} and G_{3E} exhibited an exponential (most cases) increase as input voltage increased for all the tested frequencies. When comparing 28.1kHz for the two dual frequency pairs that it has been used in (12.222kHz & 28.1kHz and 28.1kHz & 82.226kHz) the results are similar in terms of

G_{2E} and G_{3E} graph shapes and magnitude increase over the input range. Although, the amplitude of G_{2E} and G_{3E} vary significantly when compared to single frequency results, this can be due to a difference in the conversion of the energy of different dual-frequency pairs into respective nonlinear harmonics, generation of the sidebands reducing the energy converted into second and third order harmonics, and dissipation of energy into other further harmonics.

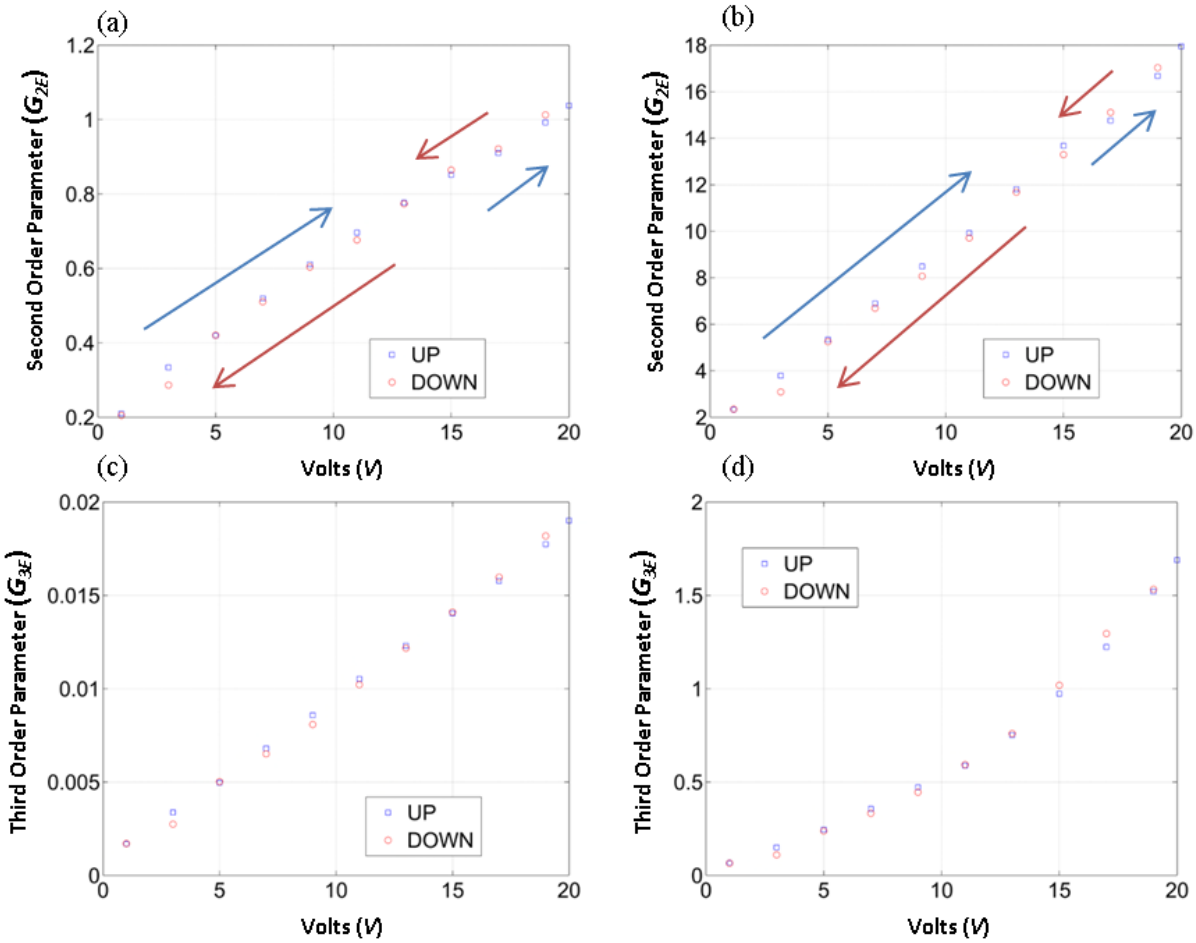

Figure 3.6: G_{2E} and G_{3E} of High Frequency 82.226kHz vs. Input Voltage ((a) and (c), respectively), G_{2E} and G_{3E} of Low Frequency 28.1kHz vs. Input Voltage ((b) and (d), respectively). 28.1kHz & 82.226kHz pair.

When comparing the G_{2E} and G_{3E} results of single frequency transmission with the results of the dual frequency it was found that in terms of magnitude increase due to an increase in input voltage the dual frequency results are less sensitive to increases in voltage, and certain frequencies (such as 70.898kHz) have a greater response to increases in input voltage whether part of a dual-frequency or not.

3.1.5. Results: Dual Frequency-Resonance Frequency

In order to determine whether a benefit of more accurate nonlinear results could be gained by using the resonance frequencies of the material, tests were conducted at both resonance (Figure 3.7) and non-resonance (Figure 3.8) frequencies for G_{2E}, G_{3E}, β_S and β_D. Only results for β_S and β_D are discussed.

For the additional harmonics (β_S and β_D) produced by a dual-frequency it was found that (Figure 3.7, below): (i) β_S results were more consistent than β_D results, (ii) generally both increased in magnitude as input voltage increases, (iii) the magnitude increase of β_S is low compared with G_{3E} results and equivalent to some G_{2E} results, (iv) the magnitude of β_D for consistent results were far greater than that of β_S and G_{2E} but equivalent to various G_{3E} results, (v) for inconsistent results, β_D was generally lower than β_S, G_{2E} and G_{3E} results in terms of magnitude increase, and (vi) both showed a hysteretic response.

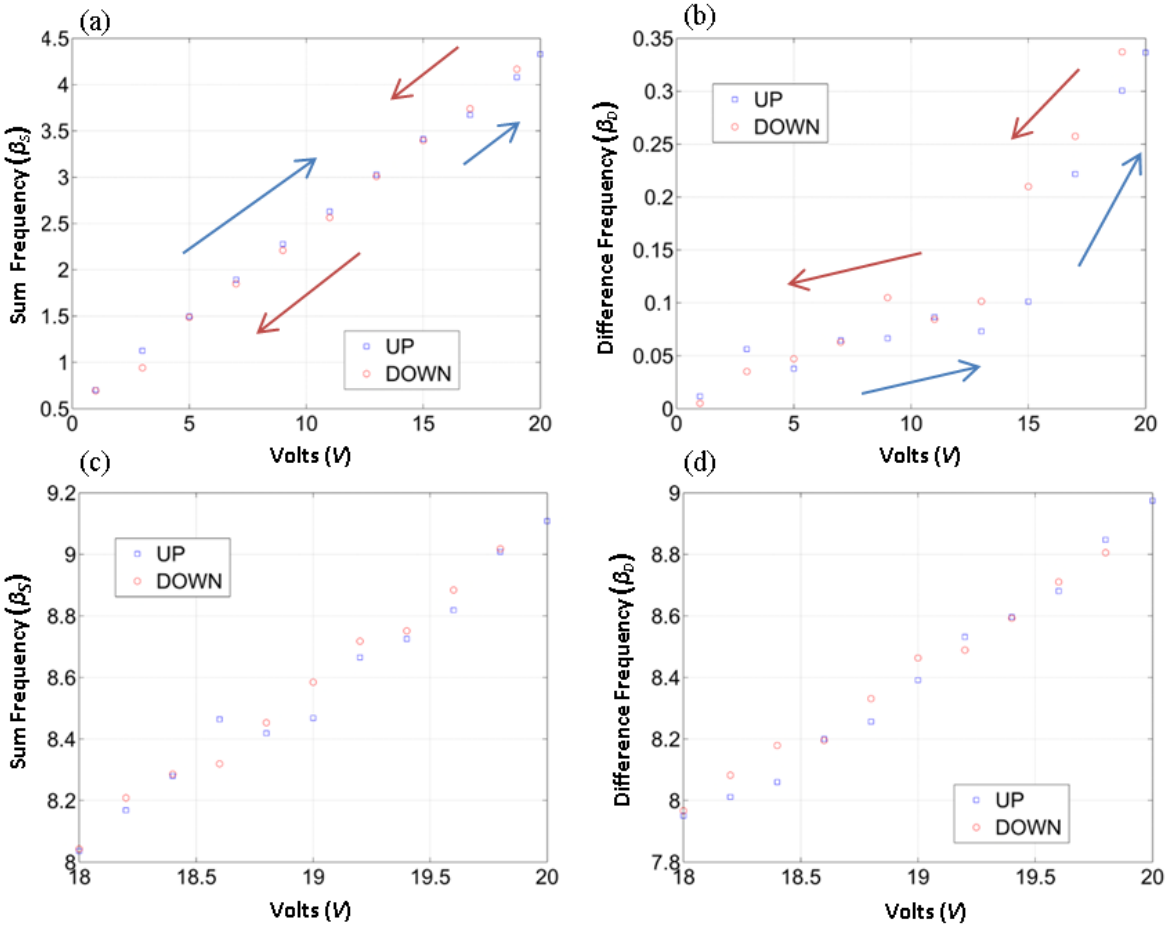

Figure 3.7: β_S (a) and β_D (b) vs. Input Voltage, 28.1kHz and 82.226kHz pair. β_S (c) and β_D (d) vs. Input Voltage, 28.1kHz and 36.7kHz pair.

3.1.6. Results: Non-Resonance Frequency

The effect of the resonance frequency testing method was assessed by investigating the same nonlinear parameters for random frequencies (non-resonance frequencies). By comparing Figure 3.7 and Figure 3.8 it is clear that β_S results have a lower increase in amplitude with non-resonance frequency pairs, the β_D results are more consistent at resonance frequencies and the β_S results show clear signs of hysteresis. Figure 3.7 and Figure 3.8 also underline the signs of hysteresis of β_D at large input voltage adjustments although at smaller voltage adjustments hysteresis is not evident due to the large scattering of results. It is clear from the results that the outcome of resonance frequency pairs maximize nonlinear responses and are more consistent. Non-resonance frequency results found a decrease of between 3 to 5 orders of magnitude over resonance frequency tests for β_S and β_D (similar results were determined for G_{2E} and G_{3E}).

The β_D outcome for both the resonance and non-resonance frequency pairs have been poor relative to the β_S (with inferior non-resonance frequency results) this implies that crack detection and analysis using this method may not be as accurate as a β_S method. One issue that may affect the modulated results is whether the sideband falls close to or on a resonance frequency; this may be the case with β_S and β_D results, in that the sideband (*f2-f1*) of β_D falls further from a resonance frequency than that of β_S.

These results demonstrate that excitation at the resonance frequencies of a structure in order to determine and maximise nonlinearities has a great advantage over arbitrary frequency selection, there is a reduction in hysteretic and nonlinear parameter scattering at resonance frequencies and excitation of clapping/rubbing mechanisms at the correct frequencies (i.e. resonance frequencies of the material) provide better results.

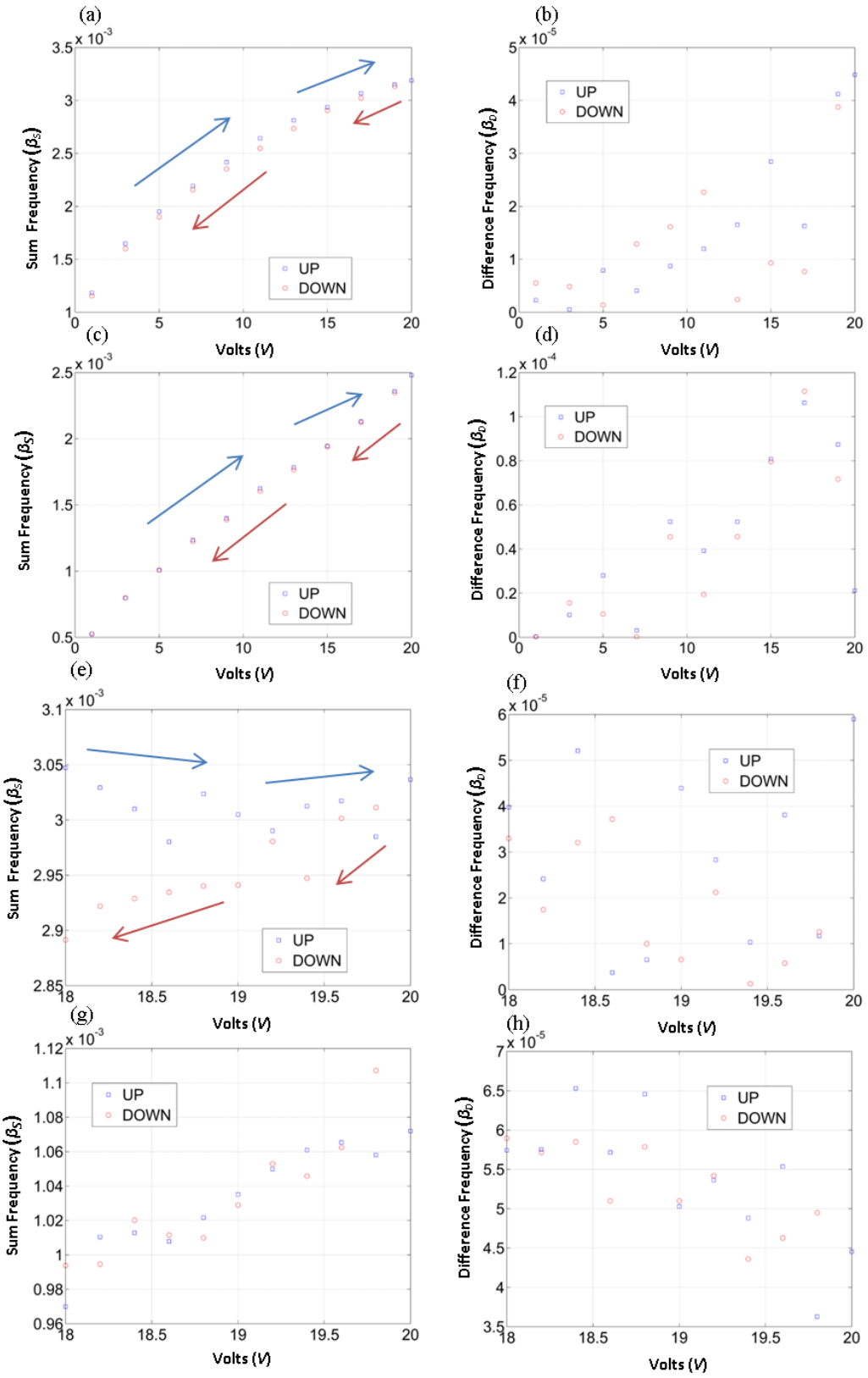

Figure 3.8: β_S (a) and β_D (b) vs. Input Voltage, 24kHz and 33kHz pair. β_S (c) and β_D (d) vs. Input Voltage, 40kHz and 68kHz pair. β_S (e) and β_D (f) vs. Input Voltage, 24kHz and 33kHz pair. β_S (g) and β_D (h) vs. Input Voltage, 40kHz and 68kHz pair.

3.1.7. Results: Modelling

A modal analysis of the cylindrical disks used in the test was performed using ANSYS finite element analysis software. A modal analysis was completed to evaluate mode shapes and resonance (natural) frequencies of the structure this allowed for the selection of key frequencies (resonance) while drawing attention to the differences between the modelled and experimental resonance frequencies. The modal analysis used the same geometric dimensions as the actual test pieces. It was possible to identify high displacement regions on the disk which may magnify the 'clapping phenomena' thus helping to determine the placement of the PZTs. The ANSYS Block Lanczos method to determining vibration characteristics of finite element models was used, which is a built in iterative algorithm that computes eigenvalues and eigenvectors of matrices.

The modal analysis was conducted from 0 Hz to 100000 Hz, the solution provided many resonance frequencies that were close to actual values measured during the experimental tests. The boundary conditions of the disk were fixed in four areas in order to replicate the housing which would hold the disk down. Other than these four areas the disk was free to move. There was generally good correlation between the actual resonance frequencies and those determined using ANSYS even though a simple model was used. Some of the variances between the experimental and computational modal are a consequence of the simplified boundary conditions of the model as they did not take into account the bottom disk and the clamping of the bottom housing part. The placement of the PZTs and size of the mesh may also have adversely affected the results.

Figure 3.9 below emphasizes the modeled deformation of the disk for the ANSYS resonance frequency solution of 27680 Hz. The figure also displays the general areas where displacement (vibration) is likely to occur and highlights the mesh used to generate the solution. The mesh was chosen by taking into account the minimum wavelength of the simulation (found at 100kHz) which has a length of around 5.5cm in the given material (A). At an element size of 1mm this means that there are over 50 points per wavelength, generally speaking 15 points per wavelength is usually sufficient to provide accurate results that will not benefit greatly from a reduction in the elements size. The value found using the modal analysis is very close to the actual value of 28100 Hz, therefore the solution gives a good approximation of were modal displacement is likely to occur. Modal displacement is essential to produce the 'clapping mechanism' and thus frequencies that have large modal displacements are likely to give better results.

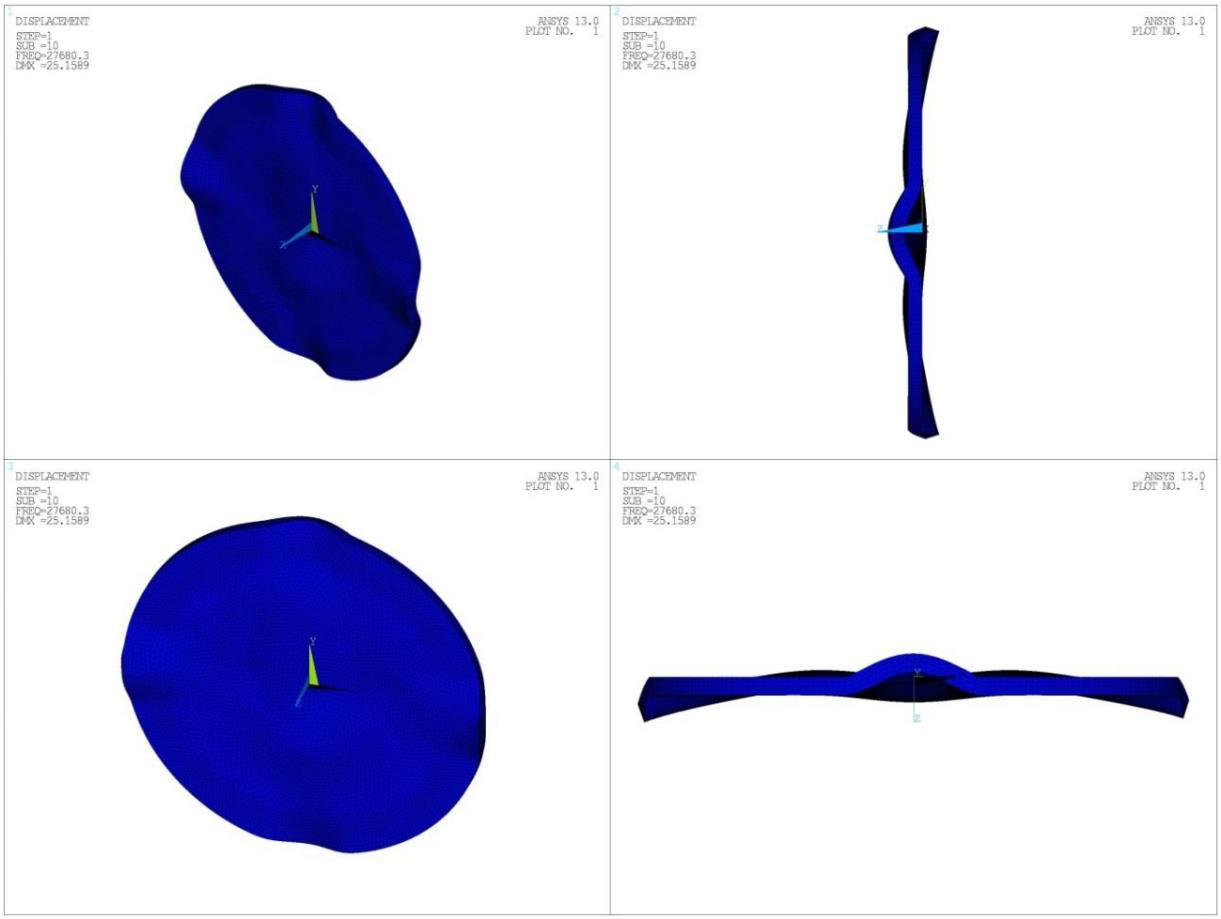

Figure 3.9: Mode Deformation of cylindrical disk (Frequency: 27680)

Figure 3.10 demonstrates the contour plots of mode displacement for 27680 Hz ((a) and (b)) and 82632 Hz ((c) and (d)), which was close to the actual value of 82.226. The bright green areas represented in Figure 3.10(b) and (d) are the areas where boundary conditions were applied to simulate the clamping of the housing. The dark blue and grey areas ((a) and (b)) and yellow areas ((c) and (d)) display areas where large displacement is likely to take place. The figure conveys clearly that there is large out-of-plane displacement for the modelled frequency, from nonlinear 'clapping/rubbing' theory it is expected that these regions should give rise to larger nonlinear responses than areas where the out-of-plane displacement is less.

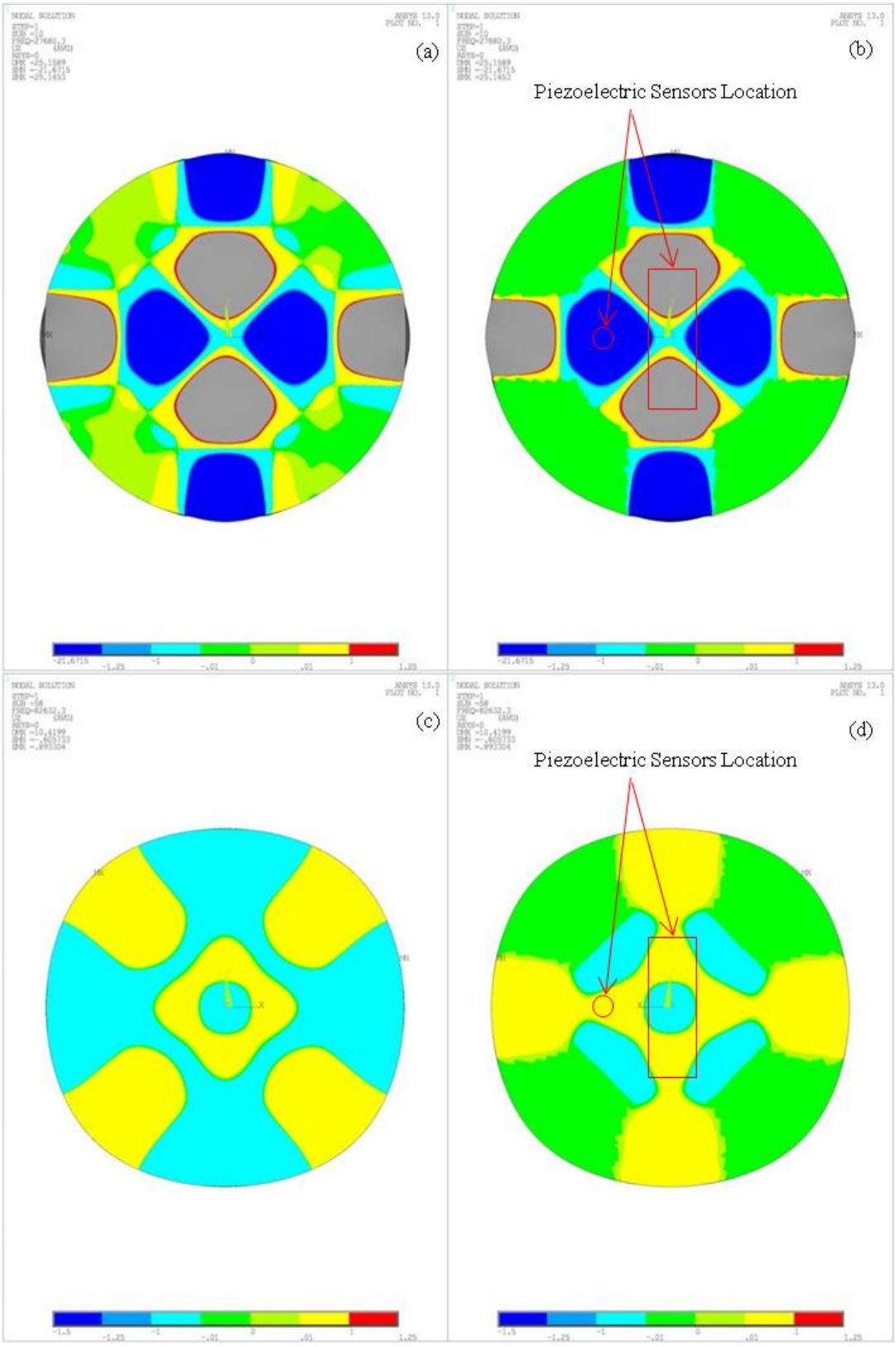

Figure 3.10: Contour plot of modal displacement of cylindrical disk, Frequency 27680Hz (a) and (b), and 82632Hz (c) and (d), ((a) and (c)-Bottom Surface, (b) and (d) –Top Surface)

3.1.8. Results: Pressure effects on the Nonlinear Parameters

Further test were completed on the outlined rig to test the effects of pressure on simulated kissing bond. The test involved increasing the pressure between the two thin aluminum plates in order to determine the response of the nonlinear parameters (G_{2E}, G_{3E}, β_S and β_D) as pressure increased and whether voltage (signal amplitude) had an effect on the nonlinear parameters as pressure increased or decreased. The theory of nonlinear ultrasound suggests that if the opening and closing mechanism that is stimulated by an ultrasound wave (small-stress) is constrained in the out-of–plane direction (compression) the ability of this mechanism to open and close under the same small stress will be reduced, resulting in lower nonlinear responses.

The area of interest is whether these diminishing harmonics can be amplified or alleviated by increases in the amplitude of the fundamental frequencies. This is particularly important for conducting *in-situ* tests where inherent pressures may exist and reduce defect detection using such a method. Another important area is determining debonding in adhesive joints. The tests were conducted by applying six different pressures to the rig outlined earlier:

Pressure (Pa):
1. 80 (thin plate only)
2. 780 (thin plate + housing)
3. 4975
4. 9171
5. 13366
6. 16163

Table 3.3: Pressures applied to rig

Figure 3.11 below shows the results for the various nonlinear parameters investigated. Four input voltages were selected, and are highlighted as individual points across the pressure range, while a best fit plot curve was determined to assess the general trend as pressure increases.

The results indicate that the nonlinear parameters decrease as pressure increases, there is a higher response at low pressures as input voltage increases and as the pressure increases the response of the nonlinear parameters decrease to a point where they are indistinguishable regardless of initial input voltage. The tested input voltage range reveals there is no substantial gain when the pressure exceeds 5000 Pa and the results advocate that a much larger input voltage would be required in order to determine whether ‘clapping mechanisms’ can be excited. Although it is important to note that at higher pressures the effectiveness of the increases in magnitude reduces, due to an increase in energy transferred (as pressure increases) and in the transmission of the fundamental frequency. There is also less dissipation of energy due to cracked region and relatively (to the fundamental) small increases in the second and third harmonic amplitudes.

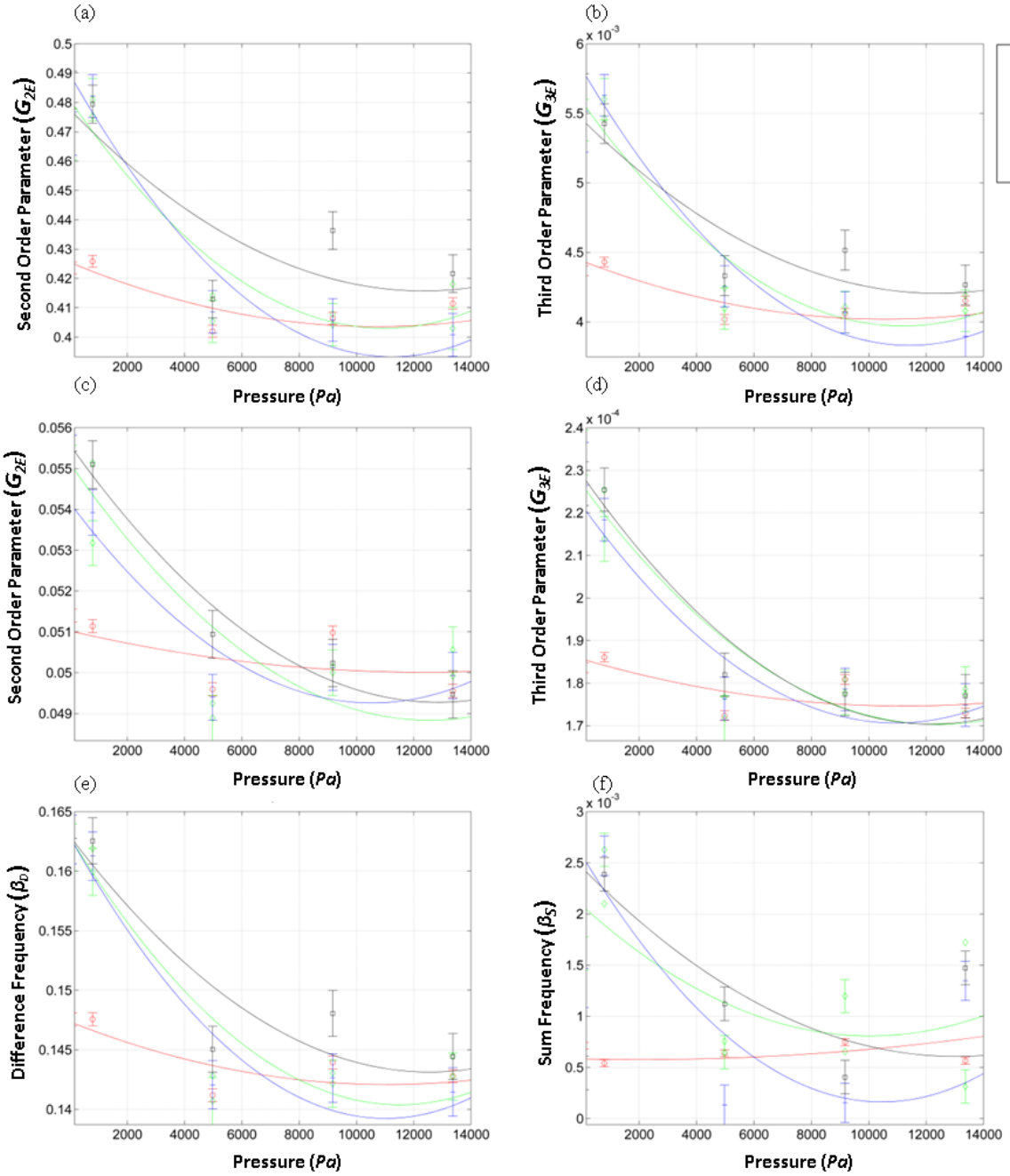

Figure 3.11: Plots show various harmonic responses vs. pressure and input signal amplitude ((a) and (b) refer to the fundamental input 28.1kHz for G_{2E} and G_{3E}, (c) and (d) refer to a fundamental frequency of 82.226kHz for G_{2E} and G_{3E}, and (e) and (f) refer to the β_S and β_D respectively).

3.1.9. Conclusion

The main aim of this work was to determine what relationship exists between the β_S and β_D nonlinearity parameters and resonance frequency excitation. The work also investigated whether these prospective relationships have a hysteretic response and implications of sidebands (β_S and β_D) created when conducting dual-frequency tests.

Two ultrasound methods were used transmission and reflection. The transmission tests were split into two distinct tests the first explored a single frequency ultrasound signal, investigating second and third-order nonlinearity parameters and their responses to changes in input voltage. The second explored a dual-frequency ultrasound signal, which along with second and third-order nonlinearity parameters investigated β_S and β_D responses. The reflection tests only investigated single frequency ultrasound signals and their subsequent responses. The general results from all the tests showed that G_{2E} increased as frequency amplitude (input voltage) increased, G_{3E} increased as frequency amplitude increased and β_S and β_D increased as frequency amplitude increased.

Transmission results discovered that G_{2E} increased at exponential rate (for most frequencies) as input voltage increased for all the tested frequencies and that the magnitude increase over the voltage range was large. G_{3E} results displayed similarities to those of G_{2E} in that they also increased exponentially in most cases and that the magnitude increase over the voltage range was large. It is clear to see form the results that the magnitude increase for G_{3E} is considerably larger than that found for G_{2E}. Reflection results found that both G_{2E} and G_{3E} increase as the input voltage increases, G_{3E} results were more sensitive than G_{2E} results to increases in input voltage and both G_{2E} and G_{3E} exhibit hysteretic patterns. Generally G_{2E} and G_{3E} were found to be less sensitive to changes in input voltage for reflection than transmission.

The results for dual-frequency found that G_{2E}: increased as input voltage increased for all the tested frequencies, the increase was found to be at a linear or exponential rate for most frequencies and that the magnitude increase over the voltage range was large. G_{3E} results found that G_{3E} increased exponentially (for most tests) as input voltage increased for all the tested frequencies and that the magnitude increase over the voltage range was large. The G_{3E} results are considerably higher than that found for G_{2E} and suggest that the third-order nonlinearity parameter (G_{3E}) is more sensitive to changes in input voltage, this was found for both single and dual frequency experiments.

Resonance frequency tests outperformed non-resonance frequency tests, highlighting the expected result that more ‘clapping’ occurs at the resonance frequencies and that these frequencies are desired.

The results of the dual-frequency tests when compared with results from the single frequency transmission tests suggested that the magnitude increase of β_S and β_D as voltage increased is less than G_{2E} and G_{3E} and certain frequencies (such as 70.898Hz) have a greater nonlinear response regardless of method used. The β_S and β_D results revealed that β_S results were generally more

consistent than those of β_D and both generally increased with voltage. The magnitude increase of β_S is low compared with G_{3E} results and equivalent to some G_{2E} results while the magnitude of the β_D (low scattering results) is far greater than that of β_S and G_{2E} but equivalent to various G_{3E} results. If there is large scattering of results the β_D parameter is generally lower than the β_S, G_{2E} and G_{3E} results in terms of magnitude increase and additional tests are required in order to determine the true effect of the input voltage on the β_D.

The modal analysis undertaken revealed resonance frequencies results close to experimental results and this allowed for the assessment of the optimum PZTs located by taking into account the maximum modal displacement regions. Ultimately the modal analysis provided a quick and accurate method to predict important information about the structure before conducting the experiment.

The assessment of the effect pressure has on the 'clapping mechanism' and nonlinear parameters, revealed that there was a decrease in these parameters as pressure increased. These results were expected as clamping together a defect reduces the production of further harmonics by reducing movement ('clapping') of the defect. An increase in voltage of the fundamental signal as pressure increased showed that the effect of pressure on the 'clapping mechanisms' could be reduced and thus increase further harmonic generation only up to low pressure values of around 5000 Pa. Further studies of the effect of larger input voltage values need to be considered to fully explore the effect of pressure on these nonlinear parameters.

This study establishes the advantages of using a resonance frequency testing method and reconfirms that the further harmonics found in response signals of a dual-frequency can be used as a crack detection method for materials. It suggests that the β_S parameter method may be more accurate and have less limitations than a β_D method.

3.2. Nonlinear Acoustic Moment evaluation of Aluminium and Composite Materials

A nonlinear acoustic moment method was explored experimentally for structures that are under high pressures and thus probability of defect discovery is reduced. Previous studies using acoustic moments have focused mainly on the health of adhesive joints and bonds. This work focuses on developing a methodology that uses both the linear and nonlinear acoustic moments of a given signal to help determine the damage present in a compression loaded specimen. A rig was used that allowed the adjustment of the pressure between two flat plates (Aluminium (Material A) and CFRP (Material B – refer to Appendix 1), while the contact between the two plates was used to simulate metallic and composite joints. Two PZTs were used to send and receive the input and output signals. The acoustic moment was based on the integral of the Power Spectral Density (PSD) function and preliminary tests were conducted in three steps: (i) initially the first, second and third harmonics of the output PSD function were located, (ii) then they were isolated by filtering out other noise and responses thus leaving the peaks of the respective harmonics, and (iii) finally the respective harmonics were evaluated using integration, giving the respective acoustic moments. The results reveal that nonlinear acoustic moments (second and third harmonic responses) responded adversely to increases in pressure than that of the linear acoustic moment (fundamental frequency). The work provides a solid platform for the proposed acoustic moment method suggested, and it is believed that the link between the linear and nonlinear acoustic moments can provide useful information about damage in compression loaded systems.

Compression loaded structures increase the difficulty for damage detection due to the physical behaviour of ultrasound waves passing through such components. In a loaded structure as the wave passes through the defected area, less energy is lost to the surrounding area which can result in an underestimate of the size of the defect. In structures where there is variable loading, energy dissipation of the wave will vary depending on the load and sensitivity of the testing technique becomes an important factor as loading increases. Nonlinear ultrasound techniques have been found to be sensitive to small defects and therefore in the case of a loaded structure the sensitivity of the methods may be extremely advantages in damage detection. Although linear techniques have been around for many years and have been proven to be accurate for a wide range of industrial applications, the complexity of the problem and the benefits of nonlinear ultrasound methods provide an interesting research opportunity.

This method looks at determining a nonlinear acoustic moment for a compression loaded structure and comparing this to the linear acoustic moment at different structural loading levels. The theoretical expectation is that as loading increases the linear acoustic moment should increase (less energy loss to defected regions), while the nonlinear acoustic moment should decrease (also due to less energy loss). Nonlinear ultrasound methods rely on the production of further harmonics,

these further harmonics are produced by the 'clapping/rubbing' of defected areas, if load increases this phenomena should decrease.

The proposed nonlinear acoustic moment method relies on the determination of the PSD function which evaluates the power (V^2/Hz) of a signal over a specific frequency range, this is then integrated to determine the energy (V^2s/Hz) of signal in terms of time. The inverse relationship between the linear acoustic moment and the nonlinear acoustic moments should allow for a good contrast in behaviour and thus good sensitivity in terms of structural loading changes.

3.2.1. Related Theory and derivation of Nonlinear Acoustic Moment

The acoustic moment can be simply measured as the integral of the PSD function. The PSD was used to evaluate the power of the signal at each predetermined load (calculated from the FFT of the time domain signal), it was then integrated across the selected frequency bands to assess the acoustic moment for the specified frequencies and harmonics. Integration took place between two frequencies, *fl* (lower) and *fh* (higher), with the maximum peak at *f* falling between the two (refer to Figure 3.13 below). Frequencies, *fl* and *fh*, were found by calculating the *Q*-factor of the signal, which determines the frequencies by applying a 3dB drop on either side of *f*. Due to the good quality of the signal, high *Q*-factors were observed. The fundamental frequency is the initial driving frequency and the second and third harmonic are 2 and 3 times the fundamental frequency, respectively. Figure 3.12 below, shows the the excitation of the system (a), the loaded interface which are the two cylindrical disks (b) and the expected response of the system (c) in the frequency domain.

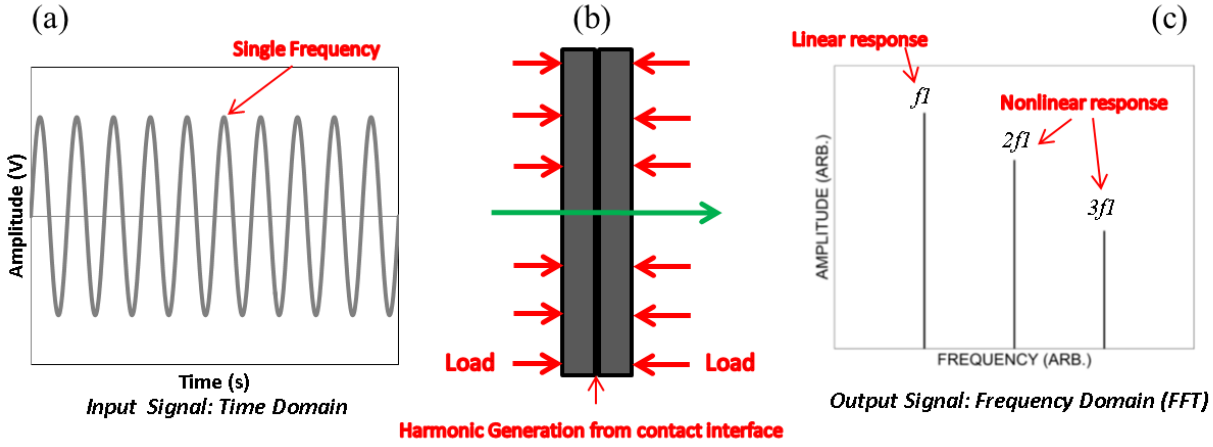

Figure 3.12: Single frequency excitation of the system (a), loaded interface-cylindrical disks (b), and the expected response of the system (c).

The experiment layout was the same as was used in Chapter 3.1.3 (page 70), the rig used is highlighted in Figure 3.3 and the load applied to the housing shown in Figure 3.14 (below).

The acoustic moment method used in this thesis assesses structurally loaded systems (metal and composites) for debonding of joints (kissing bonds) and damage. Acoustic moment methods rely on determining the signal energy and how this energy is affected by damage or load.

The nonlinear acoustic moment of an output signal in the frequency domain is measured by evaluating the power spectral density (PSD) or the power of the signal. The nonlinear acoustic moment requires that the energy of each frequency response be calculated. This was achieved by filtering out any noise before and after the identified frequencies. For example, before and after the fundamental, second and third harmonics of the response signal. The fundamental frequency is the initial driving frequency and the second and third harmonics are two and three times the fundamental frequency, respectively. The Power Spectral Density and Acoustic Moment can be defined as [187]:

$$W(f) = Y.conj(Y)/L$$

Eq. (3.21)

$$M_n = \int_0^{f_N} W(f) f^n df$$

Eq. (3.22)

Where: W(*f*) is the Power Spectral Density (PSD) function, *Y* is the Fast Fourier transform (FFT) of the time domain series, *L* is the length of the time domain series, *f* is the frequency variable, f_N is the Nyquist frequency.

The zeroth moment or M_0 means the signal energy calculated as the area under the spectral density curve, and can be analytically related to the mean square of voltage signals [187]. The M_0 mode is described by the following function:

$$M_0 = \int_0^{f_N} W(f) df$$

Eq. (3.23)

The acoustic moment for the individual frequency band (i.e. 20kHz) can be described as:

$$M_f = \int_{fl}^{fh} W(f) df$$

Eq. (3.24)

Where: *f* is the frequency assessed, *fh* is a point just after the frequency band, and *fl* is a point just before the frequency band.

The individual frequency spikes (in the frequency domain) were examined and the individual acoustic moments were assessed. For example, Figure 3.13 below shows the selection of the frequency band (highlighted in red) that would be used to determine the acoustic moment. Any noise below *fl* and above *fh* is filtered out, thus by integrating between *fh* and *fl* it is possible to measure the acoustic moment for that particular frequency (this can be applied to the fundamental frequency as well as the further harmonics second and third). This method allows for direct comparison between the linear acoustic moment (calculated from the fundamental frequency, i.e. 10kHz) and the nonlinear acoustic moments (calculated from the second and third harmonics generated by defects, i.e. 20kHz and 30kHz respectively).

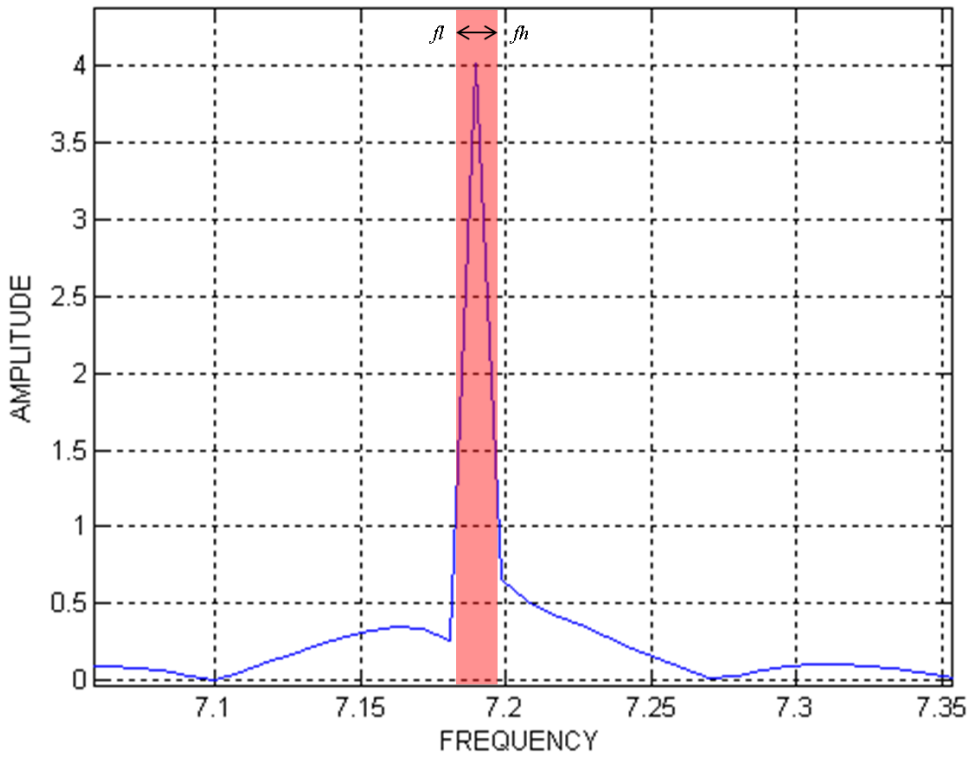

Figure 3.13: Acoustic Moment Band Selection (7.19kHz)

The damage of a loaded structure was assessed by determining the relationship of the nonlinear acoustic moments and the linear acoustic moment. The nonlinear acoustic moments refer to moments of the second and third harmonic, while the linear acoustic moment refers to the moment of the fundamental frequency. The results were evaluated by examining the ratio of the nonlinear moments over the linear moment. Remembering that the specific frequency bands were individually selected and the acoustic moment determined for each band, the follow ratios were used to evaluate the effect loading had on damaged structure and are described below.

The Second Harmonic Acoustic Moment Ratio:

$$R_{f2/f1} = \frac{M_{f2}}{M_{f1}}$$

Eq. (3.25)

Third Harmonic Acoustic Moment Ratio

$$R_{f3/f1} = \frac{M_{f3}}{M_{f1}}$$

Eq. (3.26)

Second and Third Harmonic Acoustic Moment Ratio

$$R_{(f2+f3)/f1} = \frac{M_{f2+f3}}{M_{f1}}$$

Eq. (3.27)

Where: M_{f2+f3} was the moment of the second harmonic plus the moment of the third harmonic, M_{f2} was the moment of the second harmonic, M_{f3} the moment of the third harmonic, M_{f1} was the moment of the fundamental frequency, R was the ratio of the respective moments. These ratios were used to evaluate the structure at different loads and at the above described frequencies.

3.2.2. Experimental Setup

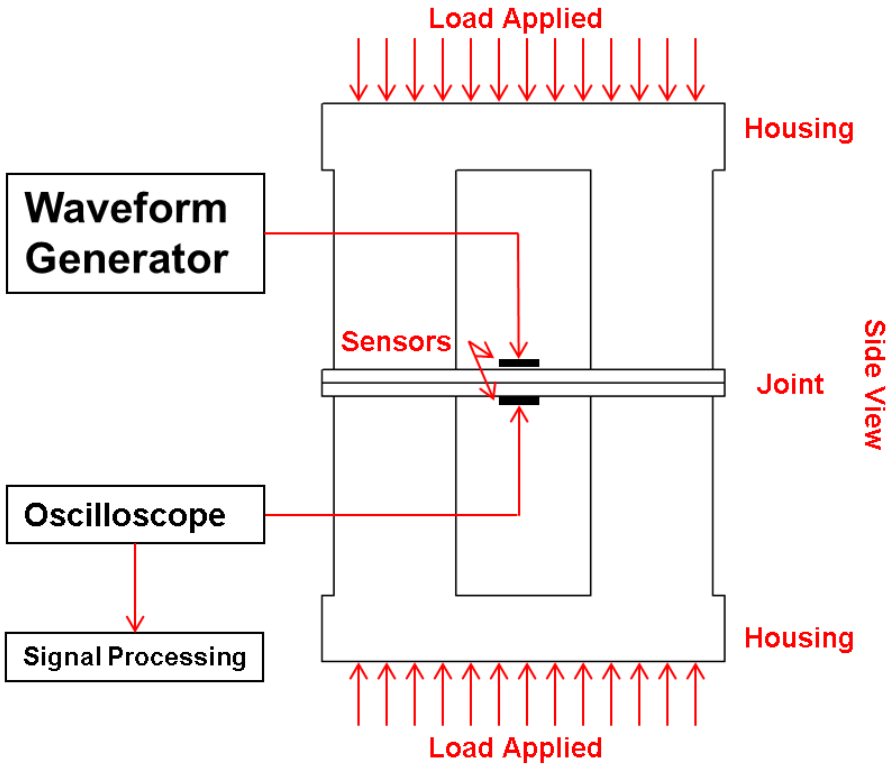

Figure 3.14: Rig and Load Setup

The experiment investigated a transmission test through the thickness of the cylindrical disks (Aluminium (AA2024) and Composite (CFRP) – fibre orientation [0°/90°/90°/0°]) in order to measure the fundamental frequency response (linear response) and the second and third harmonic responses (nonlinear response) of a known defected region. The Power Spectral Density (PSD) function was calculated for the frequency ranges investigated, in order to establish the acoustic moment for the entire frequency range, the acoustic moments for the individual frequencies investigated (i.e. fundamental frequency, second and third harmonic) and evaluate if a relationship between the linear and nonlinear acoustic moment responses can be used as a defect detection method for loaded structures.

The materials resonance frequencies (Aluminium and Composite) were used as the fundamental excitation frequency for the experimental tests. The sweep function of the arbitrary wave form generator was used and the output was recorded using the PicoScope 6 software. The sweep ran from 1kHz to 100kHz over a period of 100 seconds and the software recorded over 130000 points. Figure 3.2 (Chapter 3.1.3, page 70) shows the results of the sweep for the Aluminium Structure, the resonance frequencies can be clearly seen as the peaks and are displayed in Table 3.2 (Chapter 3.1.3, page 70).

Table 3.4 below lists the excitation frequencies used for the experiment and voltage. The voltage of the signal was carefully determined by assessing frequency responses with and without a

signal amplifier. The response signal was amplified, and it was found in this case that the amplified signal was clear. The maximum input voltage was adjusted and carefully selected for each of the frequencies in order to ensure that the response signal was accurate and not impeded by the amplifier.

Frequencies Tested: Aluminium Disks	
Transmission:	***Input Voltage***
7.190	5V *pk-pk*
28.100	1V *pk-pk*
45.960	2V *pk-pk*
2.226	1V *pk-pk*
Frequencies Tested: Composite Disks	
Transmission:	***Input Voltage***
13.400	20V *pk-pk*
19.540	20V *pk-pk*
44.890	20V *pk-pk*
73.090	20V *pk-pk*

Table 3.4: Frequencies (kHz) investigated for the various tests preformed

Raw data captured using Picoscope Software 6 was formatted using MATLAB which was used to compute the Fast Fourier Transform (FFT) of the output signal, measure the Power Spectral Density of the signal, filter and analysis the moments at the tested frequencies and harmonics, and establish whether any relationships existed between the tested data. The experiments were conducted three times for both the aluminium and composite disks at the various frequencies and loading conditions, these tests are recorded in Figure 3.15 and Figure 3.18 (plots (a) and (b)).

3.2.3. Results: Aluminium Disks

By determining the acoustic moments of the individual frequencies (first, second and third harmonic) and relating them to one another the relationship between the harmonics can be used to evaluate whether damage exists.

With an increase in the fundamental frequencies response and a decrease in the nonlinear harmonic responses as load increases; a factor (nonlinear moment/fundamental frequency moment) can be established and used to determine whether damage has occurred.

Damage in a loaded component can be evaluated by the suggested method by making a few assumptions: that is loaded, for example:

(i) In a clean undamaged specimen the nonlinear moment ratio will be very low (due to low or no nonlinear harmonic generation).
(ii) As damage increases this ratio will increase (nonlinear harmonic generation increases).
(iii) The magnitude of the ratio can be related to the extent of damage for many different loading conditions.
(iv) The tests could be simple/fast and have a wide range of applications.

A few of the resonance frequencies determined were used to evaluate the effect of load on the rig. Figure 3.15, Figure 3.16 and Figure 3.17 display the results for two frequencies tested as load increased.

Figure 3.15 shows how the second order nonlinear moment decreases as the load increases for the two frequencies tested. Three tests were conducted at each load, and it can be seen that at a frequency of 28kHz the variability in the second order nonlinear moment is very low, at 7kHz the variability is much larger (before pressure is added to the system) and at low levels of pressure (0 kN/m^2 and 2 kN/m^2) larger variability between results occurs. The general trend discovered was a decrease in the nonlinear acoustic moment as the load increased.

The reason for the variability of the results at low force levels is due to the design of the rig and the fundamental theory of harmonic generation. At low levels of force contact between the two disks may vary due to the fact that they do not have dimensions that fit perfectly, therefore: as pressure changes (at low levels) better or worse contact between the two plates arises, as this contact changes the generation of the harmonics change and good and consistent contact between the plate occurs around $8kN/m^2$ of pressure as there is a large decline in the second harmonic moment (almost to zero). It should be noted that this is an experimental anomaly and that this is unlikely to occur in an actual structure due to the fact that the resolution of the fit between the crack/defect and structure will be a lot finer, the defect will have grown from the structure itself rather than pressing two individually manufactured plates together and results are likely to improve on actual components due to the before mentioned reasons. For adhesively bonded structure these

assertions should hold true as a well bonded structure will have good contact between the specific layers (component/adhesive/component),

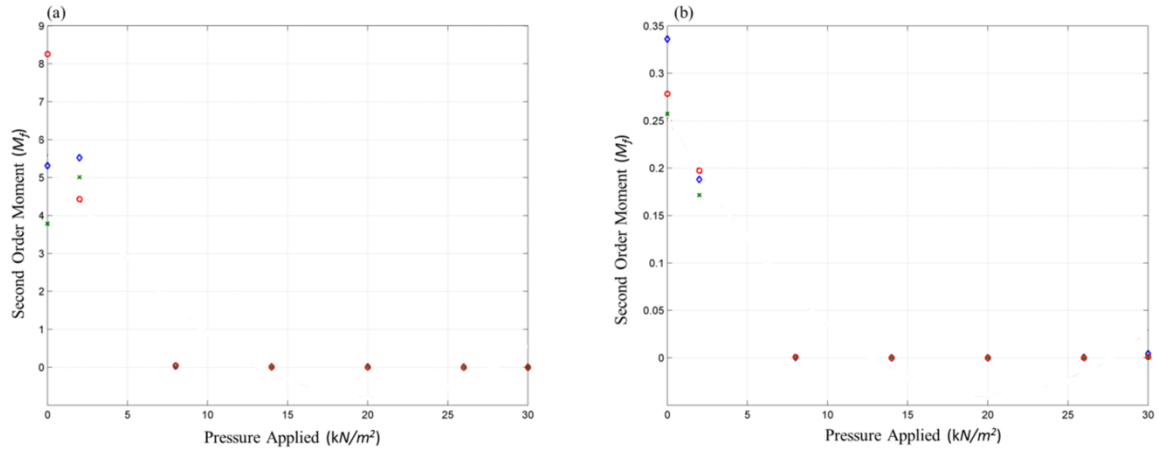

Figure 3.15: Second Order Nonlinear Moment (7190Hz (a), 28100Hz (b))

Figure 3.16 below shows the ratio between the second order nonlinearity moment and the fundamental frequency moment. It can clearly be seen that the second order nonlinearity moment decreases relative to the fundamental frequency moment as the load increases. One of the other interesting observations is that at 7kHz, the initial problems with the signal output due to the contact between the plates disappears and consequently there is a clear decreasing trend. This decreasing trend is likely due to the response of both the fundamental and second order moments which were affected by the contact between the two plates, the ratio between the two moments reflecting the loading of the structure.

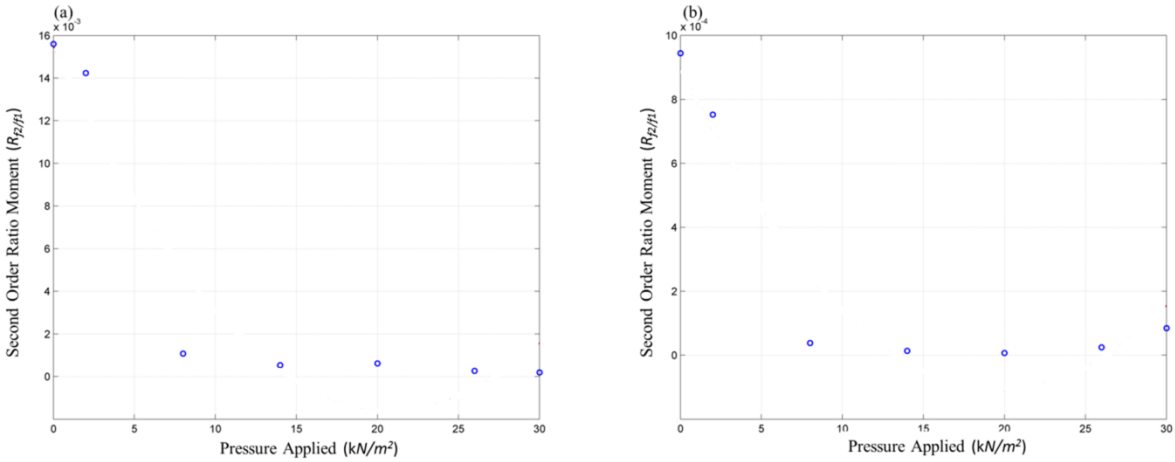

Figure 3.16: Second Order Nonlinear Moment over the Fundamental Frequency (7190Hz (a), 28100Hz (b))

Figure 3.17 below highlights the ratio of the second and third order nonlinearity moments over the fundamental frequency moment. The figure examines the same frequencies as the previous figures, and it can be observed that the third order nonlinearity moment has no real effect on the outcome outlined in Figure 3.16. The third order moment is very small compared with the moment produced by the second order nonlinearity and the fundamental frequency consequently having little effect on the results. Due to the small magnitude of the third order moment Figure 3.15 and Figure 3.16 appear to be identical, this is not the case, and there is a small variation between them. These experimental results suggests that the second order moment is sufficient in determining a good relationship between the nonlinear acoustic moment and loading of the structure.

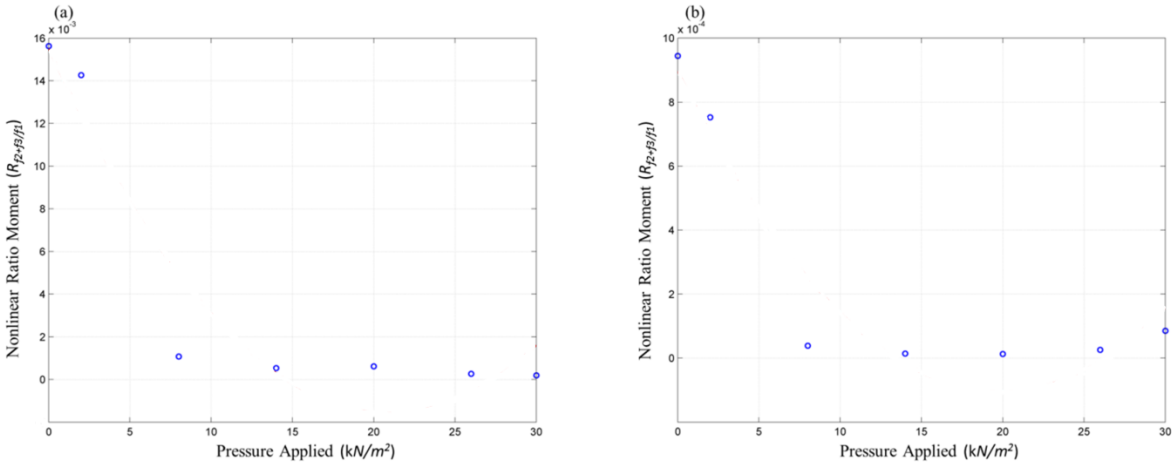

Figure 3.17: Second and Third Order Nonlinear Moment over the Fundamental Frequency (7190Hz (a), 28100Hz (b))

3.2.4. Results: Composite Disks

After observing the results of the Aluminium disks the same test was conducted on two cylindrical CFRP disks with similar dimensions and PZT location as the aluminium disk setup. This setup simulated composite joints and compressively loaded structures (e.g. aircraft wing joints/components, helicopter/wind turbine blades, and sail masts) as there has been a large increase in composite structural use in engineering disciplines. Although there are large benefits of using composites such as weight to strength ratio, composite joints have increased risk due to brittleness (less stress relief around a bolted joint), anisotropy (higher stress concentration factors), low transverse strength, delamination, and complex failure modes among others.

The author noticed during the aluminium tests, that the nonlinear response is dampened at very low levels of pressure (around 8kN/m^2), thus the voltage for the composite disks tests were increased (refer to Chapter 3.2.1, Table 3.4, page 87) in order to determine whether a better trend between the nonlinear moments and the increase in pressure could be obtained.

Figure 3.18 below shows the results for the second order moment (M_f), second order ratio moment $R_{f2/f1}$ and the nonlinear ratio moment ($R_{(f2+f3)/f1}$) for 44kHz and 73kHz. The trend is much

clearer than that found with the aluminium plates due to the increase in voltage. The dampening effect of the pressure on the clapping/rubbing mechanism (contact area of two disks) can be alleviated by increasing the fundamental signals voltage. This increase in voltage results in an increase in the small internal stress caused by the wave and results in excitation of the contact area of the two disks (damage regions).

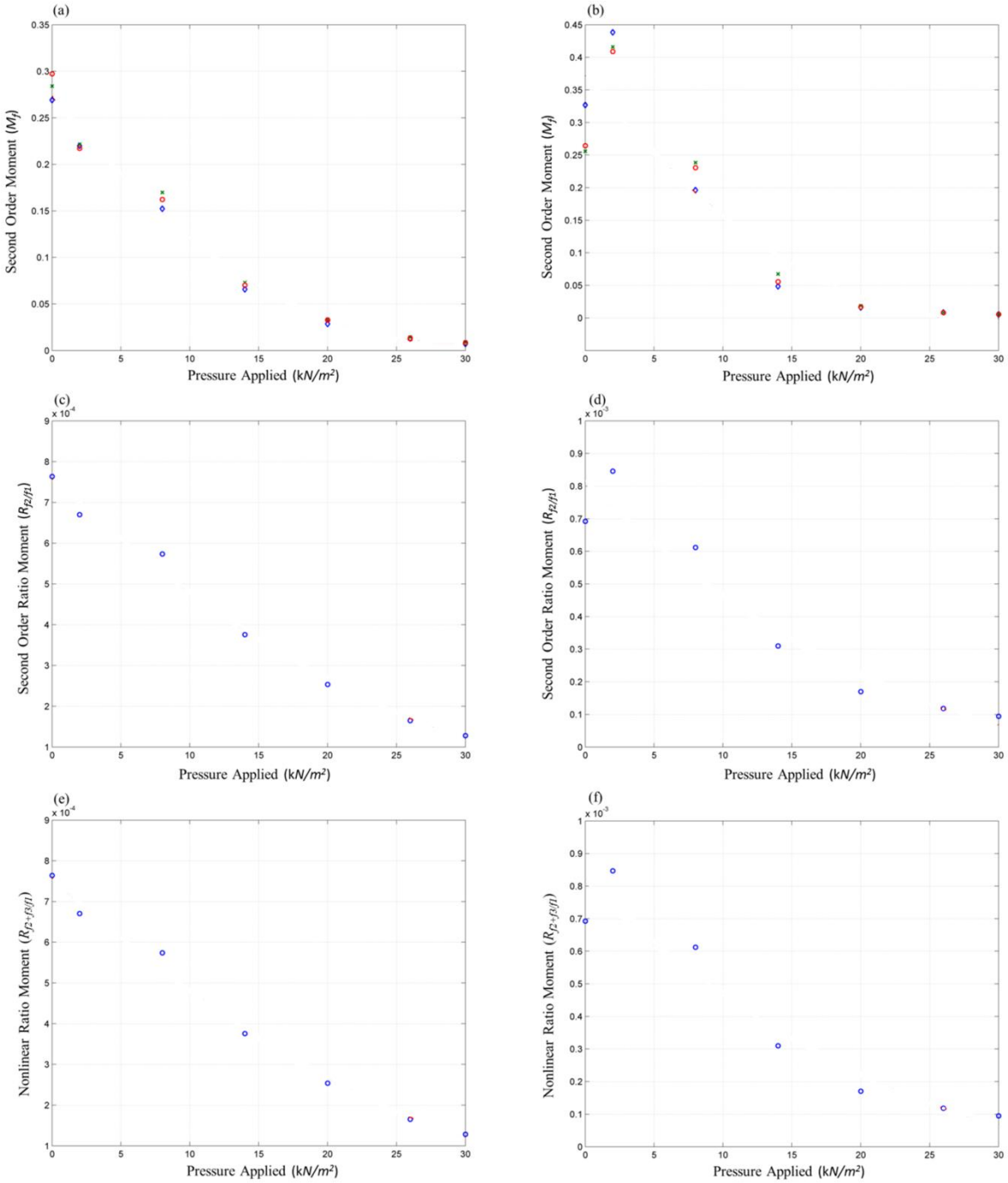

Figure 3.18: Second Order Nonlinear Moment (a) and (b), Second Order Nonlinear Moment over the Fundamental Frequency (c) and (d), Second and Third Order Nonlinear Moment over the Fundamental Frequency (e) and (f) (44.890Hz (a),(c) and (e), 73.090Hz (b), (d) and (f))

The effect of the third nonlinear moment on the change in magnitude as pressure increases is barely visible when comparing Figure 3.18 (c) with (e) and Figure 3.18 (d) with (f) (this was also found for the aluminium disks, Figure 3.16 and Figure 3.17). The downward trend is unaffected by the third nonlinear moment, due to its small magnitude.

Figure 3.18 (b), (d) and (f) show that the initial recordings at 0kN/m^2 are lower than at 2kN/m^2, which is contrary to the expected outcome (results should be lower at 2kN/m^2), this is due to surface roughness of the two disks, which results in areas that are not in contact at low levels of load and lower harmonic production leading to lower levels of the key factors at 0kN/m^2 (Figure 3.19 (a) and (b)). As load increases the contact between the two plates increases resulting in greater harmonic production and higher levels of the nonlinear acoustic moments at 2kN/m^2 and as load increases the contact between the two plates will increase to a maximum level (highest nonlinear response), after which the dampening effects will reduce the nonlinear response. In terms of fastened and bolted joints as loosening occurs the pressure applied to the contact surfaces reduces, suggesting this technique can also provide useful information about these joints. It has been shown that a reduction in pressure can be evaluated using the nonlinear acoustic moment method developed and thus the health of the joint can be assessed by the second order ratio moment ($R_{f2/f1}$).

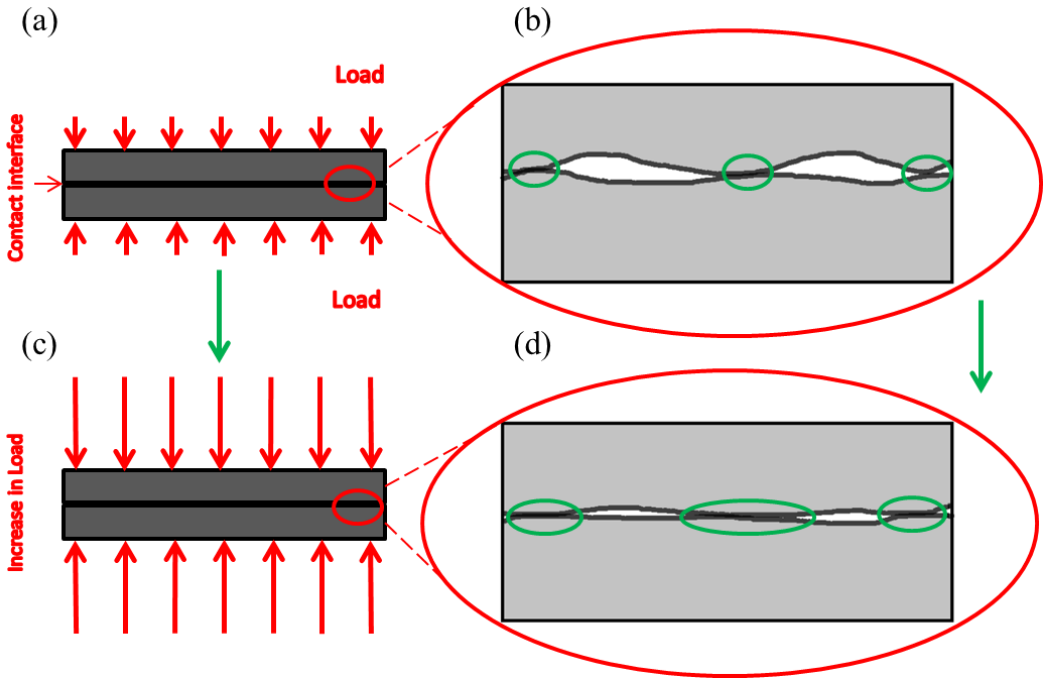

Figure 3.19: Low load levels for disks (a), contact areas associated with low load level (b), higher load levels (c), and contact areas associated with high load levels (d)

3.2.5. Conclusion

The experiment shows conclusively that the relationship between the further harmonic moments (second and third) and the fundamental frequency decreases as load increases. It also builds a framework for damage detection using this methodology for constant compression loaded structures, variable compression loaded structures and kissing bond and joint evaluation. The experiment establishes that a decrease in load can be determined by an increase in the ratio of the nonlinear moment and fundamental frequency moment. The experiment conducted also reveals the potential for this relationship to be applied to a system where testing may take place in conditions where there is variable loading.

Some of the drawbacks of the described method are for both constant and variably loaded structures the load was known, this may not be the case in a real world environment and the level of damage cannot be determined (without a baseline test), only whether damage has increased.

Other than the above mentioned limitations of the method it is quick, simple and easy to setup and regulate. It can be carried out on many components in many engineering fields as preliminary results suggest that high accuracy can be achieved through further development of the methodology and testing, and the simplicity of the technique is one of its main driving factors. Further work is needed to increase the scope and determine the accuracy of acoustic moments over the lifetime of a component.

3.3. Bolted Structure Assessment using various Nonlinear Ultrasound Methods

After exploring the benefits of various testing techniques in Chapters 3.1 (resonance frequency testing and second and third order nonlinearity parameters, page 62) and 3.2 (Nonlinear Acoustic Moments method, page 86) an experiment was set up to test the accuracy of these techniques on a real world structure. A section of a wind turbine was obtained which can simply be described as a steel bolted structure consisting of four bolts. The structure was a simple tension joint (consisting of two identical parts, Material C – refer to Appendix 1) found on large wind turbines; primarily used to attach the wind turbine rotor blades to the rotor hub. The main aim of the experiment was to assess the loosened state of each of the four bolts using various nonlinear and other techniques, while only using two ultrasound PZTs.

The Global Wind Energy Council and Greenpeace International presented the fourth edition of the Global Wind Energy Outlook (2012) which outlined some of the main issues facing wind energy as well as growth areas. The industry has seen growth of around 28% for the 15 years prior to 2012, with over 240GW installed. It is expected that installed wind power will exceed 750GW by 2020, thus showing the potential of the market and the large amount of maintenance that would be needed for the hundreds of wind farms. The cost of maintenance and catastrophic failure mechanisms present in wind turbines highlight the importance of reliable *in-situ* structural health monitoring systems (SHM). Some of these costs have been discussed by Ciang, et al. (2008) [188] and include difficulties to perform inspection and maintenance work due to the ever growing sizes of wind turbines, human costs such as fatal accidents, locations of wind turbines (usually remote and difficult to get to), difficulties in setting up equipment, due to location or terrain and the increase in wind turbine sizes and price.

Hameed, et al. (2009) [189] discusses some of the main SHM advantages for wind turbines which include early warning (which avoids breakdown and repair costs), problem identification (allows for the right service at the right time ultimately reducing the maintenance costs) and continuous monitoring (providing constant information that the system is working). Due to the complexity of wind turbines there are multiple possible failure mechanisms from generators and electrical system failures to mechanical failures of rotor blades and hubs. Germanischer (2007) [190] identifies that these failures can be attributed to many different defects within the system such as: surface damages, cracks, structural discontinuities, damage to lightning protection systems, leakages, corrosion, wear, fastenings, and dirt to name a few.

The structure investigated preforms the primary task of joining the turbine blade to the hub. The gigantic size of modern wind turbines (diameters of between 40m and 90m) emphasise the importance of the joint, as failure would be catastrophic. Khan, et al. (2005) [191] suggests that bolt failure and reliability to be the fourth worst after blade tip breaking, yaw bearing failure and blade failures. There is a multitude of different techniques available to assess the structural integrity of wind turbines although most of the methods used to date focus on blade and tower

failure. The various testing techniques employed have been summarised by Ciang, et al. (2008) [188], they are shown in the table below.

Wind Turbine Damage Detection Techniques:	Damage Detected
Acoustic emission methods which focus on broad spectral responses due to cracking.	Deformation, debonding, delamination, impacts, crushing and other processes.
Thermal imaging methods mainly used for observing temperature differences on turbine blades.	Thermoelastic stress analysis is used for fatigue test of wind turbine blade, and indicates stress concentrations and sub-surface damage before visible surface damage occurs
Ultrasonic methods for composite structures (commonly for blades).	Reveals cracks, delaminations, impact damage, voids and porosity.
Modal approaches, which use embedded shakers, external actuators, strain gauges, piezoceramics and accelerometers to monitor structural dynamic responses.	Detects reductions in stiffness resulting from the onset of cracks or loosening of a connection.
Fiber and plastic optical methods.	Measure loads of wind turbine (attached to blades), grids of fibers can be used to detect traverse crack evolution and impact damage.
Laser doppler vibrometers (LDV).	Detects changes of operation deflection shapes to indicate and possibly locate damage.
Electrical resistant and X-radioscopy methods among others.	Detects fatigue damage as structure stiffness reduces and electrical resistance increases. X-rays are capable of detecting missing glue between laminates, cracks and voids.

Table 3.5: Wind Turbine damage detection techniques

The bolts were fastened to the structure at predetermined levels of torque (clamping force) using a torque wrench. This tightening of the bolt follows a defined sequence of events and causes predictable results in the fastener. If the nut and head of the bolt are firmly seated against non-compressible materials the torsional action of tightening the assembly stretches the bolts, thus creating tension in the bolt. Preloading in most cases is required to make the fastening and the build-up of tension can be controlled by the torque applied. This tensile pre-stress (equivalent to the compressive stress introduced in the joint material) which is determined by the levels of torque the bolts are tightened with have large implications on the behaviour and life of the joint. Some of the issues that can affect tension joints over time are if the bolts are clamped with too little force loosening may occur. Whereas if the bolts are clamped with too much force (the proof load of the

bolt may be exceeded) leading to failure, warping, advancement of hydrogen embrittlement and stress corrosion cracking.

Due to the uncertainty in wind conditions and thus the tensional load applied to the joint if the proof load is exceeded the bolt may plastically deform resulting in a reduction in clamping force. Likewise if the load results in a reduction in the clamping force the bolts energy may be released causing loosening or failure of the bolt.

Considering the applications of nonlinear methods it is expected that as the clamping force increases for the joint the load or pressure (over the area) between the two connected surfaces of the joint increases and the load or pressure between the bolt head/nut, washer and top surface increases. This increase in pressure has the same effect on the production of the nonlinear parameters (G_{2E}, G_{3E}, $R_{f2/f1}$, $R_{f3/f1}$ and $R_{(f2+f3)/f1}$) discussed in Chapters 3.1 (page 62) and 3.2 (page 86), which is that there should be a decrease in these parameters as torque is applied to the system. The modal displacements of the structure at various resonance frequencies were determined in order to evaluate whether individual bolts could be excited by specific frequencies. The modal displacement method aims at discovering the loosened state of individual bolts and would provide an important step forward in the assessment of bolted joints.

3.3.1. Related Theory and Experimental Setup

Similarly as in the previous chapters the experiment looks to evaluate the nonlinear ultrasound responses when load is applied to two surfaces. Although in this case, the structure is preloaded by tightening bolts to various torque values rather than applying a load directly to the top and bottom surface of the structure as done previously. The structure also has six contact loaded surfaces instead of one, between: the bolt head and washer, washer and front surface, between steel blocks, back surface and washer, washer and bolt nut, and bolt shank and thread and internal hole surface.

The structure consists of two identical rectangular blocks (345mm x 200mm, with a depth of 100mm) fastened by four bolts with a diameter of 25mm (Figure 3.20, Figure 3.21), and used eight washers. The bolts were located central in terms of the vertical plane (100mm up), and 60mm from either side with 75mm between each bolt. A TTi 50MHz Function Generator (Arbitrary and Pulse) TG5011 was used to generate the output signal, while a Falco Systems DC-5MHz High Voltage Amplifier WMA-300 was used to amplifier the output signal. A Picoscope 4424 was used as the oscilloscope to capture and process the output signal on a laptop. Four PZTs were used to evaluate the specimen: PZT 1 was a Panametrics NDT X1020 100kHz 515345 actuator, PZT 2 was a Panametrics V101 0.5MHz 707718 and used to capture the output signal, while PZT 3 and PZT 4 were both APC International PZTs (Diameter 6.35mm, Thickness 0.25mm, Type 850 WFB). PZT 1 and 2 were located in two different locations L1 (top surface on opposite corners) (Figure 3.20

and Figure 3.21) and L2 (middle of the two blocks on the front and back surface Figure 3.21) which allowed for a transmission test through the thickness.

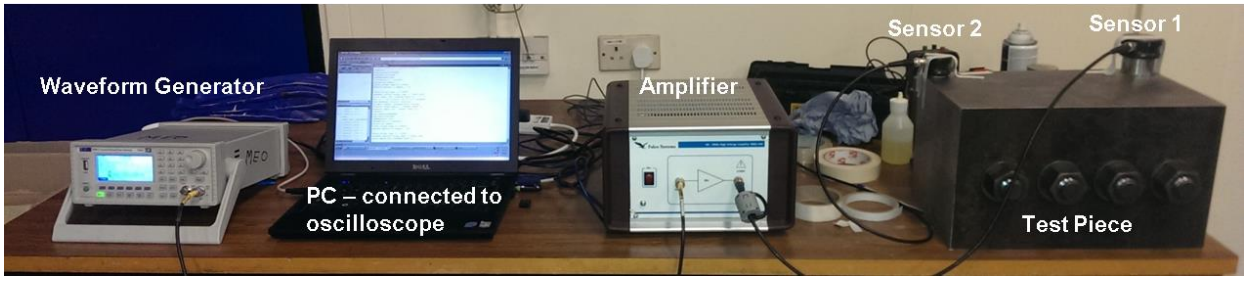

Figure 3.20: Experiment Setup

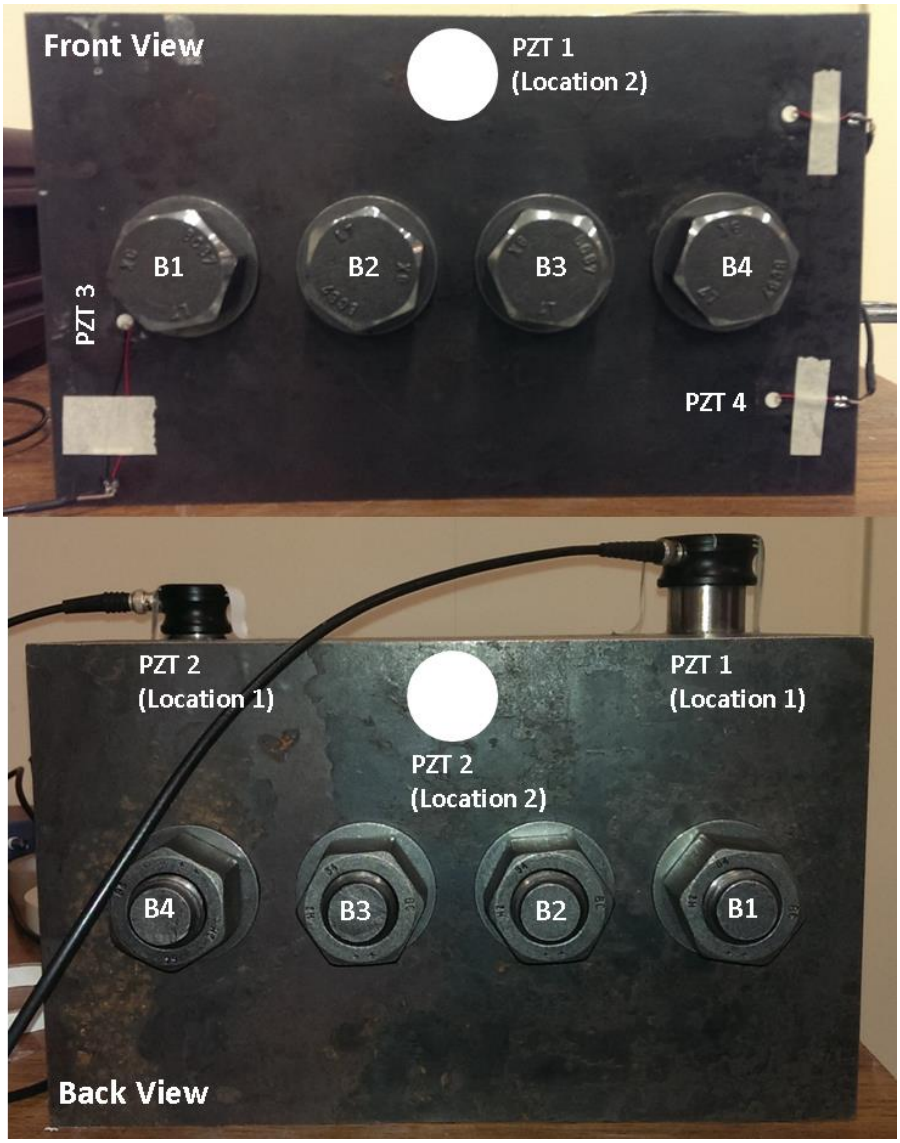

Figure 3.21: Test Piece: PZTs and Bolt Locations

The difficulty of NDT/E of the structure lies in determining which bolt has loosened rather than a general solution where any bolt may have loosened. A great advantage in terms of the speed and frequency of maintenance can be gained by the ability of determining individual bolt conditions. Other issue that compounds the problem is the large size of the structure and material

properties of steel, which require large amplitude excitation signals in order to capture accurate responses of the system. Five cases were used to evaluate the looseness of the bolts, shown below in Table 3.6 and Table 3.7.

Figure 3.22 (b) and (d) displays the side view of the structure at two loading conditions, determined by increasing preloading (tightening) of the bolts. It is expected that as load increases the nonlinear responses (G_{2E}, G_{3E}, $R_{f2/f1}$, $R_{f3/f1}$ and $R_{(f2+f3)/f1}$) should decrease (Figure 3.22 (e)) according to the earlier results found. The excitation method used a single frequency wave to excite the structure determined by evaluating the resonance frequencies of the bolted structure.

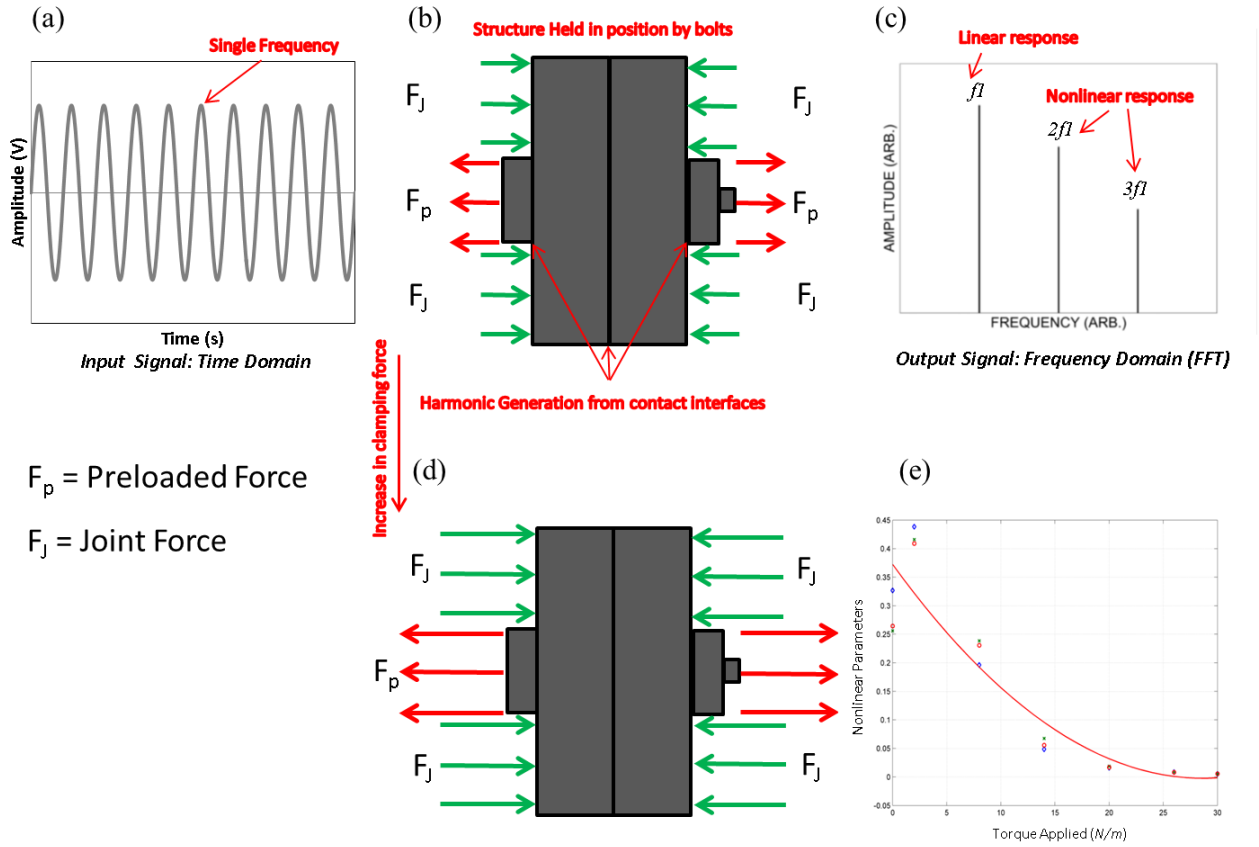

Figure 3.22: Single frequency input signal (a), force diagram of bolted structure (b), nonlinear responses (c), increase in clamping force of bolted structure (d), and expected nonlinear response of system vs. torque (e).

Different fastening cases	
CASE 0 (C0)	All bolts (B1, B2, B3, B4) are fastened.
CASE 1 (C1)	B1 is gradually unfastened, while B2, B3, B4 remain fastened.
CASE 2 (C2)	B2 is gradually unfastened, while B1, B3, B4 remain fastened.
CASE 3 (C3)	B3 is gradually unfastened, while B1, B2, B4 remain fastened.
CASE 4 (C4)	B4 is gradually unfastened, while B1, B2, B3 remain fastened.
CASE 5 (C5)	All bolts are unfastened gradually by the same amount.

Table 3.6: Different fastening cases.

	Applied torque for bolts- PZT 1 & 2 (L1)	Applied torque for bolts- PZT 1 & 2 (L2)	Applied torque for bolts- PZT 3 & 4
C0	350Nm	250Nm	350Nm
C1	B2, B3, B4 = 350Nm B1 reduced: 350, 300, 250, 200, 150	B2, B3, B4 = 250Nm B1 reduced: 250, 200 150, 100, 50, 0	B2, B3, B4 = 350Nm B1 reduced: 350, 250, 150, 0
C2	B1, B3, B4 = 350Nm B2 reduced: 350, 300, 250, 200, 150	B1, B3, B4 = 250Nm B2 reduced: 250, 200 150, 100, 50, 0	B1, B3, B4 = 350Nm B2 reduced: 350, 250, 150, 0
C3	B1, B2, B4 = 350Nm B3 reduced: 350, 300, 250, 200, 150	B1, B2, B4 = 250Nm B3 reduced: 250, 200 150, 100, 50, 0	B1, B2, B4 = 350Nm B3 reduced: 350, 250, 150, 0
C4	B1, B2, B3 = 350Nm B4 reduced: 350, 300, 250, 200, 150	B1, B2, B3 = 250Nm B4 reduced: 250, 200 150, 100, 50, 0	B1, B2, B3 = 350Nm B4 reduced: 350, 250, 150, 0
C5	350, 250, 150, 0		350, 250, 150, 0

Table 3.7: Torque Strategies

The structure was excited using a sweep function of a waveform generator in order to determine the resonance frequencies of the structure, observed as the peaks (Figure 3.23, below). The FFT data recorded was as an average of 25 samples. After which a Laser Vibrometer was used to measure surface and bolt modal displacements. After examining the modal displacements, by assessing which frequency corresponds to each of the four bolt locations testing could begin.

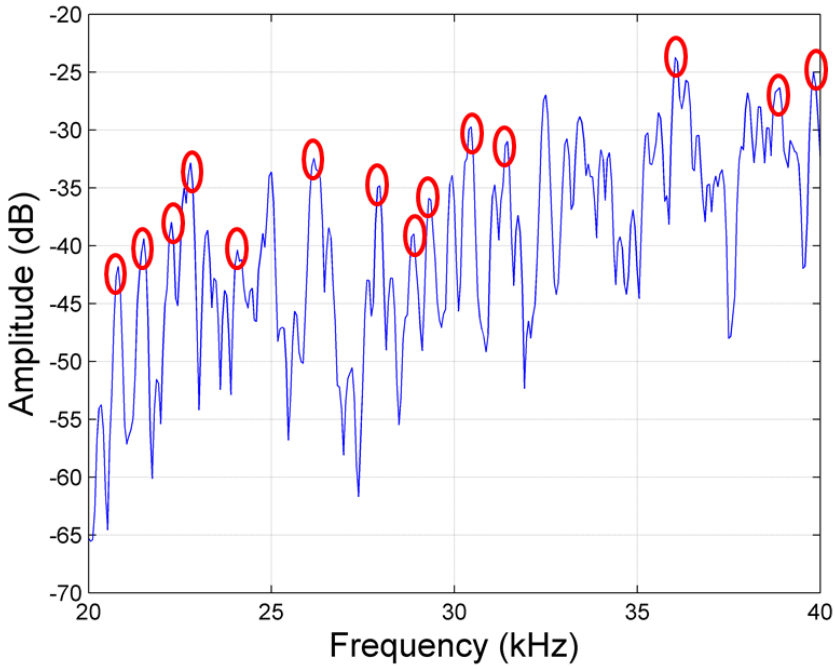

Figure 3.23: Frequency Sweep between 20kHz and 40kHz

Resonance Frequencies (kHz)
5.300, 6.900,7.800, 9.090, 10.500, 10.640, 11.300, 11.600, 12.700, 13.250, 14.550, 15.200, 16.040, 17.550, 17.750, 18.100, 18.700, 19.500, 20.800, 21.500, 22.260, 22.800, 24.000, 26.160, 27.900, 28.900, 29.300, 30.450, 32.500, 36.050, 38.000, 39.850

Table 3.8: Resonance Frequencies

3.3.2. Modal Analysis and Results (G_{2E} for PZTs 1 & 2 (L1))

A modal analysis method was investigated in order to evaluate its potential to determine which bolt had loosened. The structure was excited at the various resonance frequencies and the modal response of the individual bolts as well as the surface of the structure was measured using a Laser Vibrometer (LV). By assessing which bolt/surface modal displacements were greatest at the various bolt locations and for the various frequencies tested, it was assumed that for a bolt in position 1 where modal displacements are maximised in that area alone at a given frequency the response should be the greatest for that bolt location. As torque decreases the nonlinear response for that bolt location should increase, while when decreases occur at different bolt locations at the same frequency nothing specific should be observed. Thus by determining these individual bolt location frequencies it should be possible to pinpoint the loosened location. Nonlinear responses refer to second and third order nonlinear parameters as well as the nonlinear acoustic moments of the system.

A grid was setup using the LV to capture the out-of-plane movement of the surface and bolt heads of the structure for numerous points. Once the individual points had been evaluated an image was created using the LV software, which showed either the displacement (in terms of a fast Fourier transform (FFT)) or velocity of the points at the various frequencies.

Four frequencies were tested to evaluate whether a bolt specific frequency could be determined, the frequencies tested were 21.5 kHz (B1 and C1), 20.8 kHz (B2 and C2), 24 kHz (B3 and C3) and 5.3 kHz (B4 and C4). It is expected that when the structure is excited at 21.5 kHz and all the various cases (1-4) are tested (as shown in Table 3.7 earlier) bolt 1 (B1) will give the greatest nonlinear parameter response as it is loosened.

As can be seen in Figure 3.24 below the displacement of B1 is far greater than those exhibited by the other bolts, suggesting: that at 21.5kHz it is possible to excite B1 to a greater extent than the other bolts. The hypothesis is that as the B1 becomes looser this movement relative to the other bolts will result in a greater generation of nonlinear responses due to the larger clapping mechanisms and by evaluating multiple frequencies it should be possible to determine frequencies that relate to individual bolt clapping mechanisms, ultimately allowing for individual bolt analysis of a structure.

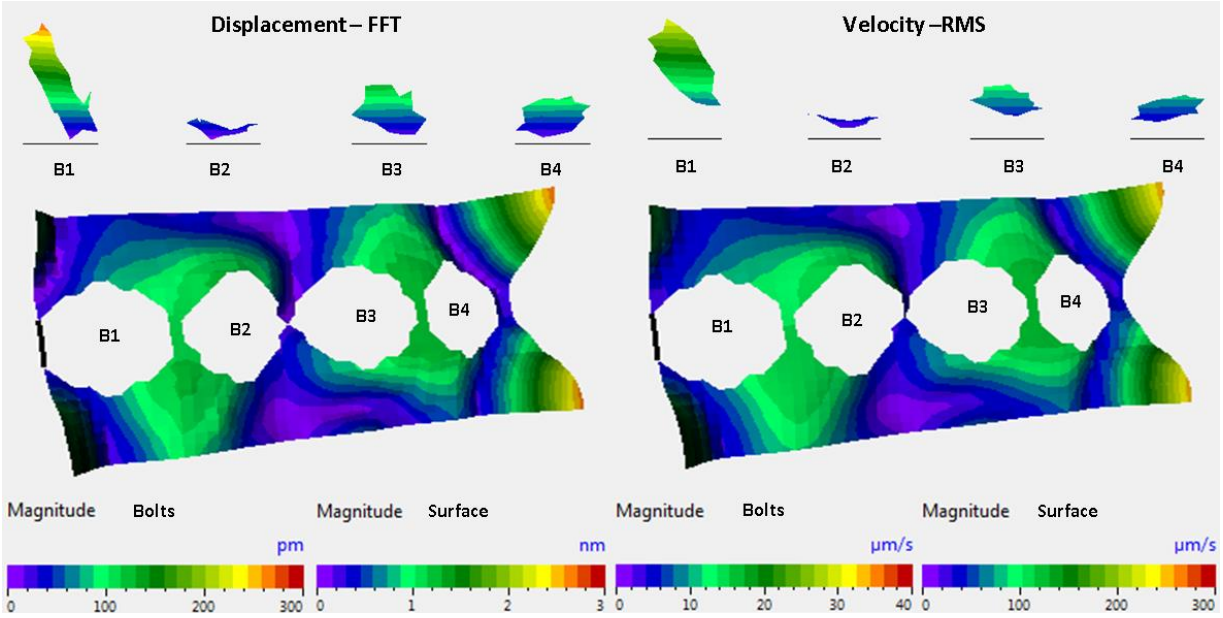

Figure 3.24: Out-of-plane displacement (left) and velocity for the surface and bolts (21.5kHz).

The second-order nonlinearity parameter (G_{2E}) was evaluated for 4 different bolt cases (C1, C2, C3 and C4, as described in Table 3.6 and Table 3.7 above), and it can clearly be seen that the nonlinear response for C1 (Figure 3.25 (a)) increases as torque is reduced (reduction in clamping load at B1). The response for the other three cases (C2, B2 loosened only, C3, B3 loosened only and C4, B4 loosened only) show inconsistent behaviour either increasing or decreasing regardless of torque applied. The final magnitude for C1 (at 150 Nm torque) is three times that of the next closest case and the nonlinear parameter G_{2E} only exhibits a clear increasing trend when B1 is loosened and the structure excited at 21.5 kHz.. The same approach was conducted for the other three cases and the results have been highlighted in Figure 3.26 to Figure 3.30.

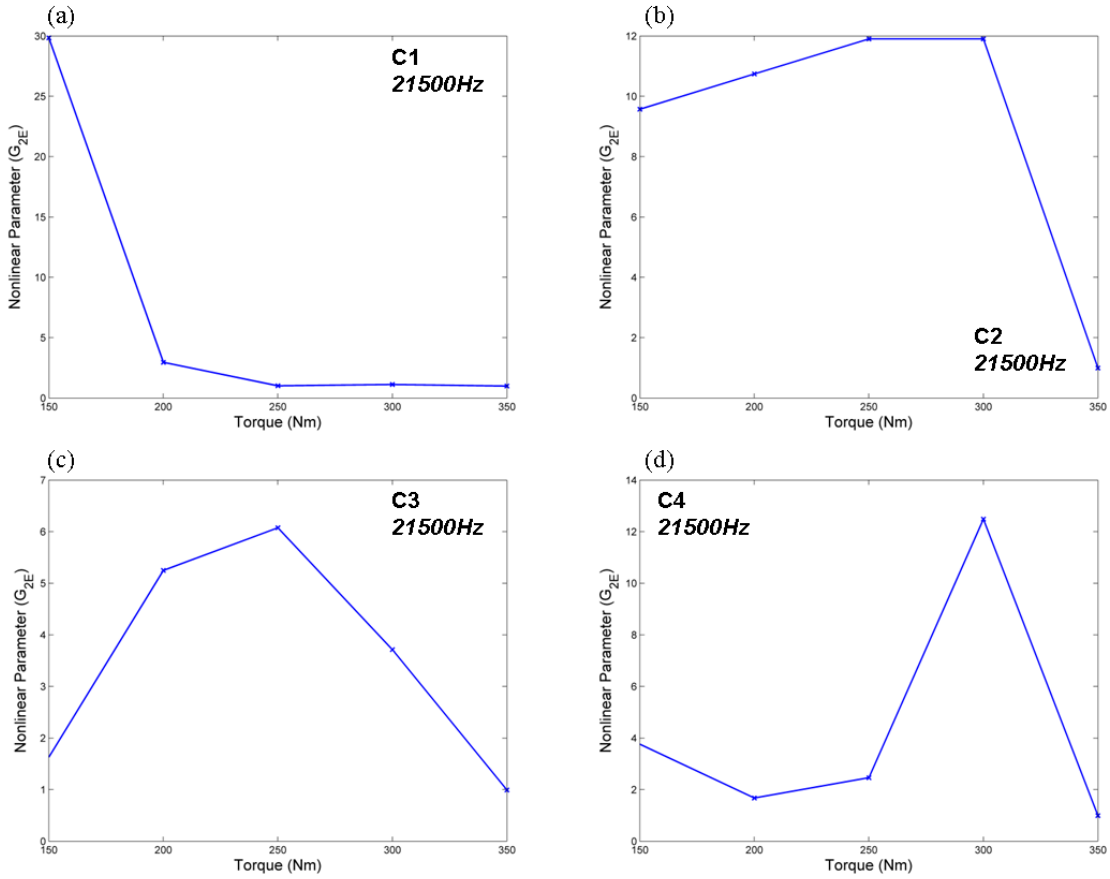

Figure 3.25: Second order nonlinear response (G_{2E}) for four cases explored (21.5kHz, PZTs 1 & 2)

Figure 3.26 and Figure 3.27 show the modal and nonlinear results for 20.8kHz for the four investigated cases. The importance of the interaction of the bolts and surface to create clapping is underlined in this case as the displacements of the bolts suggest that C1 should give the best results due to movement of B1. Although the surface displacements do not coincide with the bolts movements, with high displacement areas starting from the right side of B1 to the right side of B4, suggesting that B2, B3 and B4 should result in the greatest clapping regions. Good positive results are generated for C2 and C4, which are considered to be due to the larger magnitudes of surface displacements when compared to bolt displacements (Figure 3.27 (b) and (d)).

C1 and C3 exhibited no general trends and low G_{2E} magnitudes corresponding to results of C2, C3 and C4 for 21.5kHz were found. Displacements from the surface plot point towards B2 resulting in the best nonlinear responses, this was confirmed by comparing the magnitudes of the G_{2E} results for C2 and C4.

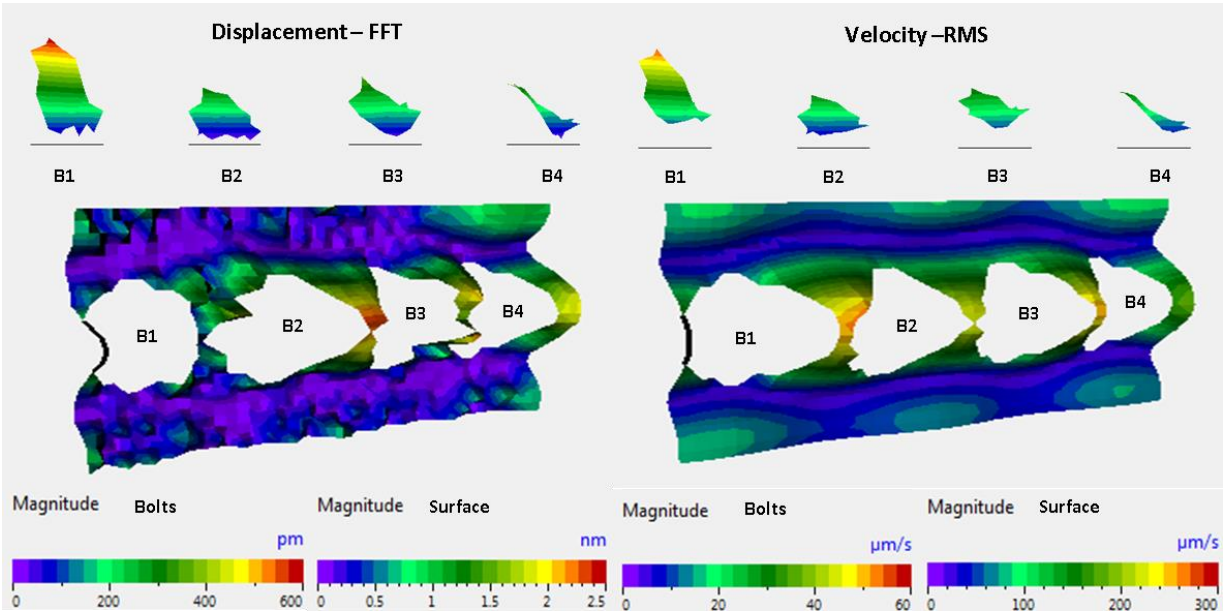

Figure 3.26: Out-of-plane displacement (left) and velocity for the surface and bolts (20.8kHz).

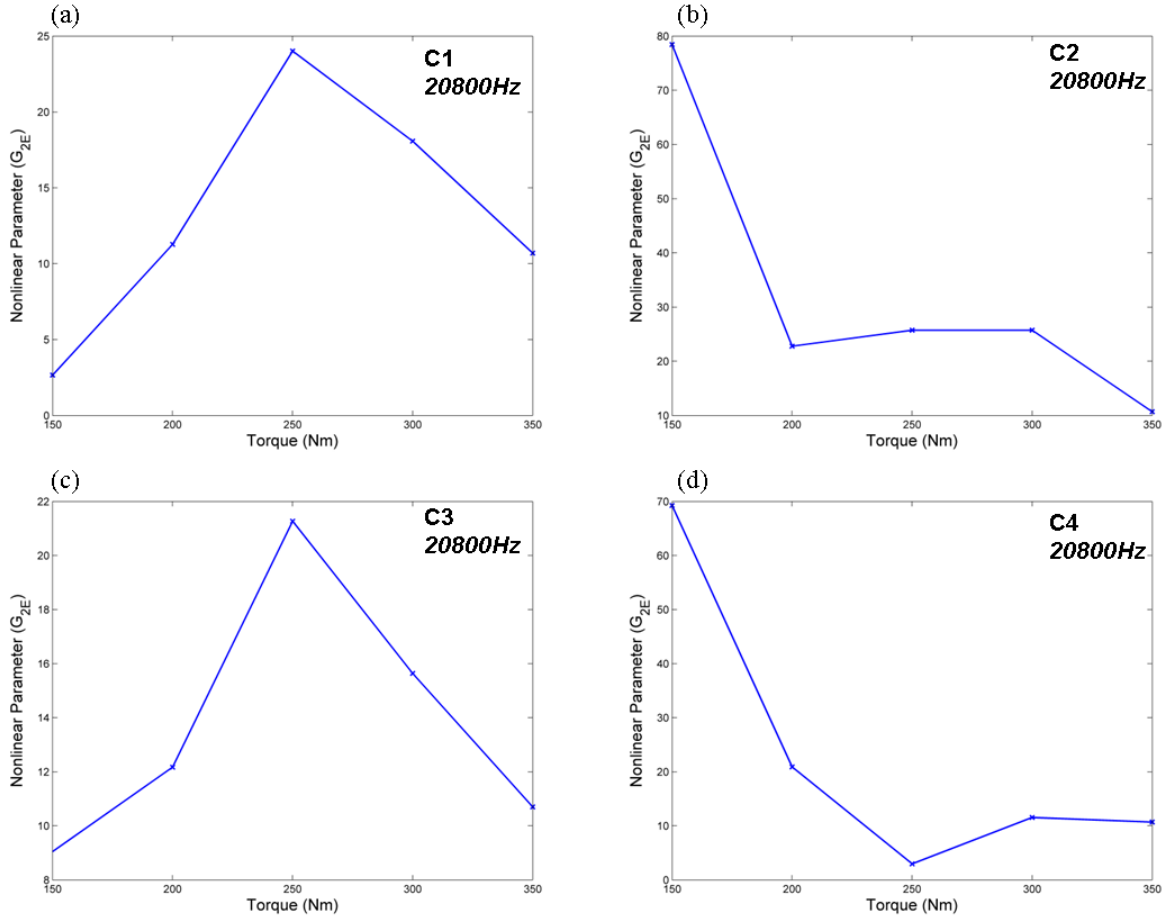

Figure 3.27:Second order nonlinear response (G_{2E}) for four cases explored (20.8kHz, PZT 1 & 2)

Figure 3.28 and Figure 3.29 follow on from results found at 20.8kHz which suggest that surface displacements may be the main contributing factor to the generation of further harmonics due to the larger magnitude exhibited over the bolts in these cases. Bolt displacements suggest B1 should result in the best nonlinear response although B3 has the second greatest displacement and there are more areas of movement around B3 (on the surface: north east, south east and west) than compared with B1 (fewer areas and smaller).

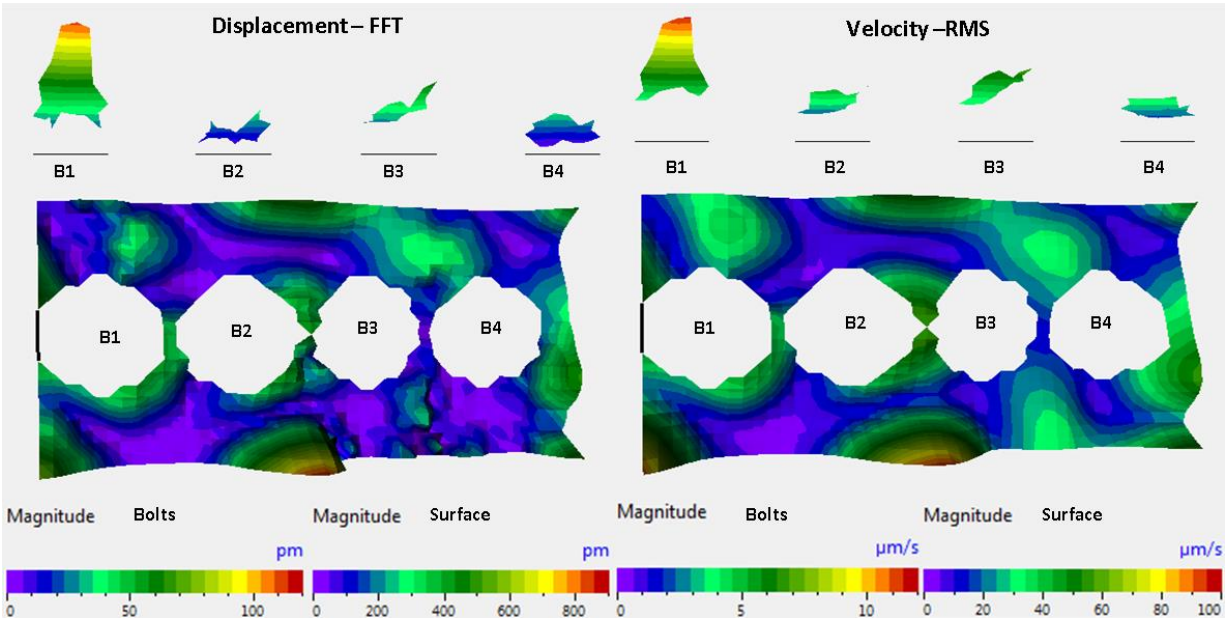

Figure 3.28: Out-of-plane displacement (left) and velocity for the surface and bolts (24kHz).

Comparing the different cases (Figure 3.29, below) it was found that C3 had a clear trend and its final G_{2E} magnitude was far greater than for the other cases. Surprisingly results for C1 were poor, possibly due to surface displacements.

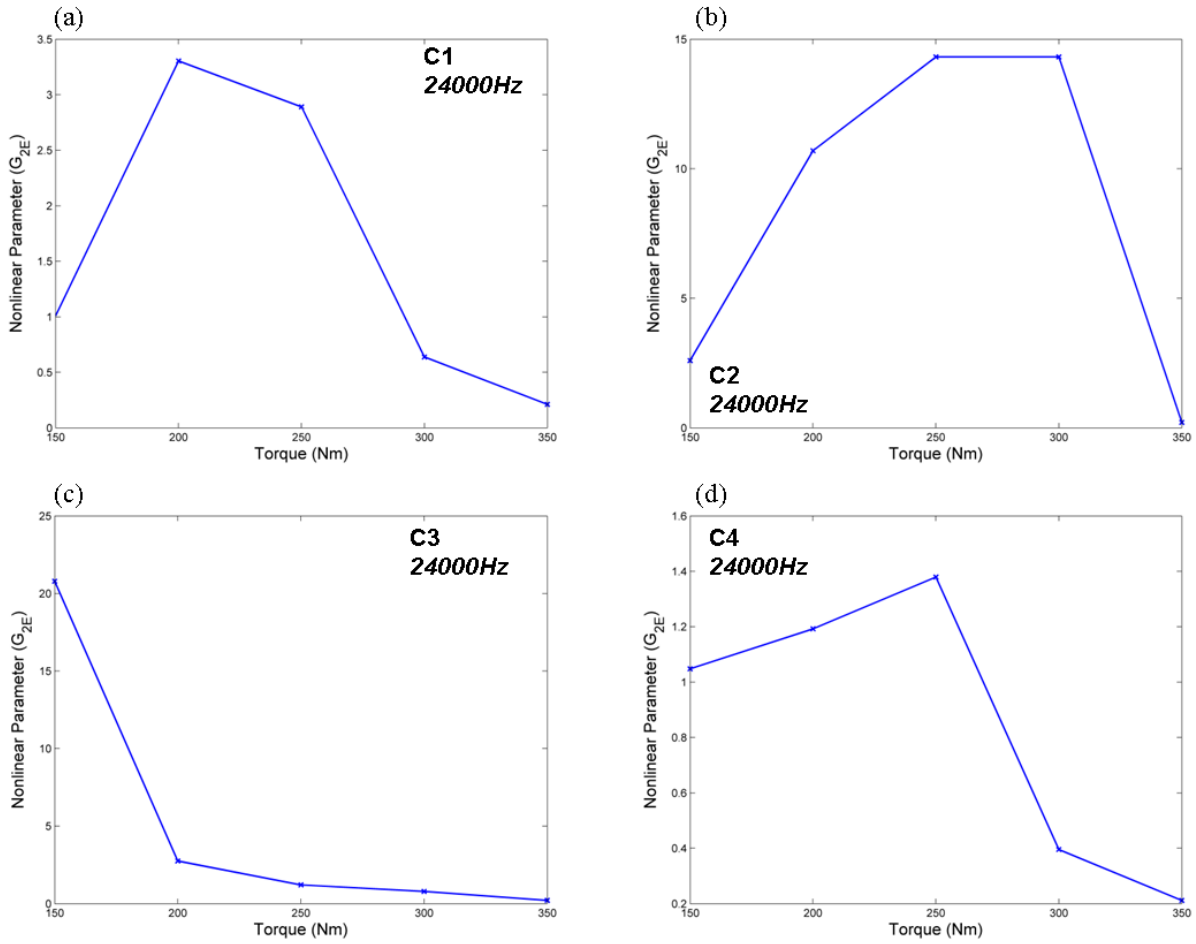

Figure 3.29: Second order nonlinear response (G_{2E}) for four cases explored (24kHz, PZTs 1 & 2)

Finally, Figure 3.30 and Figure 3.31 show the results for 5.3kHz, although in this case the difference in surface and bolt displacements are much lower than those found in the other cases. C4 exhibits a clear trend like in the other cases relating to other bolts. From the four frequencies selected and according to the interaction between the bolts and surface it is possible to determine which bolt has loosened when considering the nonlinear parameter G_{2E}. There is a definitive correlation between the inherent clapping mechanisms within the structure, the torque applied and the modal displacement of the structure. After conducting these tests it suggests that a particular threshold magnitude of G_{2E} may exists for each bolt position relative to a resonance frequency. In the case of maintenance it suggests that once a critical G_{2E} value (linked to a loosened state of a bolt) was exceeded for the predefined frequency, maintenance would be carried out. Multiple frequencies could be used to evaluate many different bolt conditions and accumulation of all the resultant information could determine the maintenance decision.

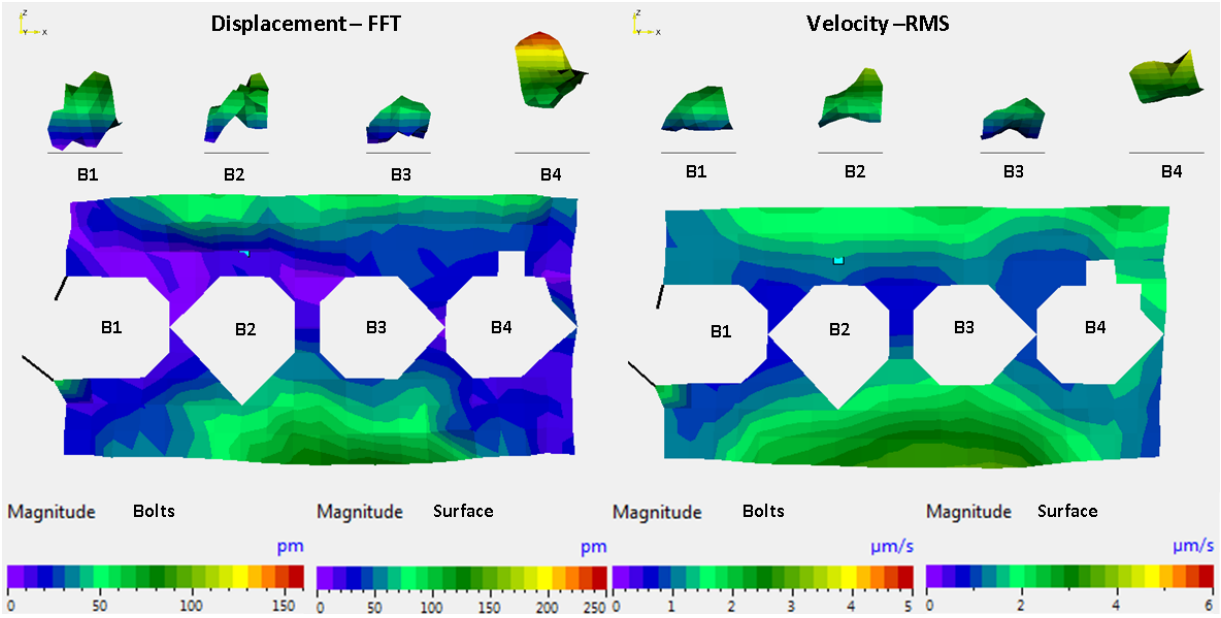

Figure 3.30: Out-of-plane displacement (left) and velocity for the surface and bolts (5.3kHz).

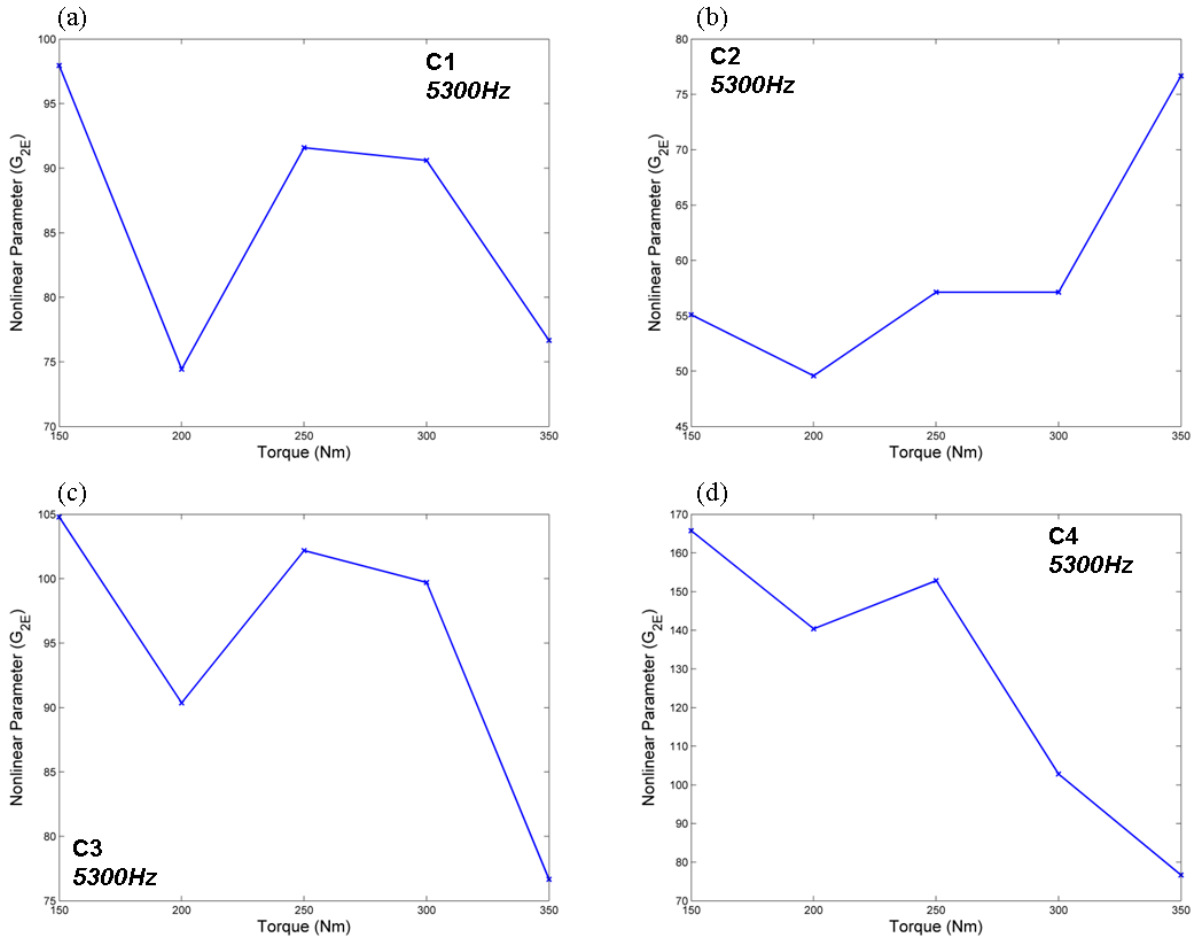

Figure 3.31: Second order nonlinear response (G_{2E}) for four cases explored (5.3kHz, PZTs 1 & 2)

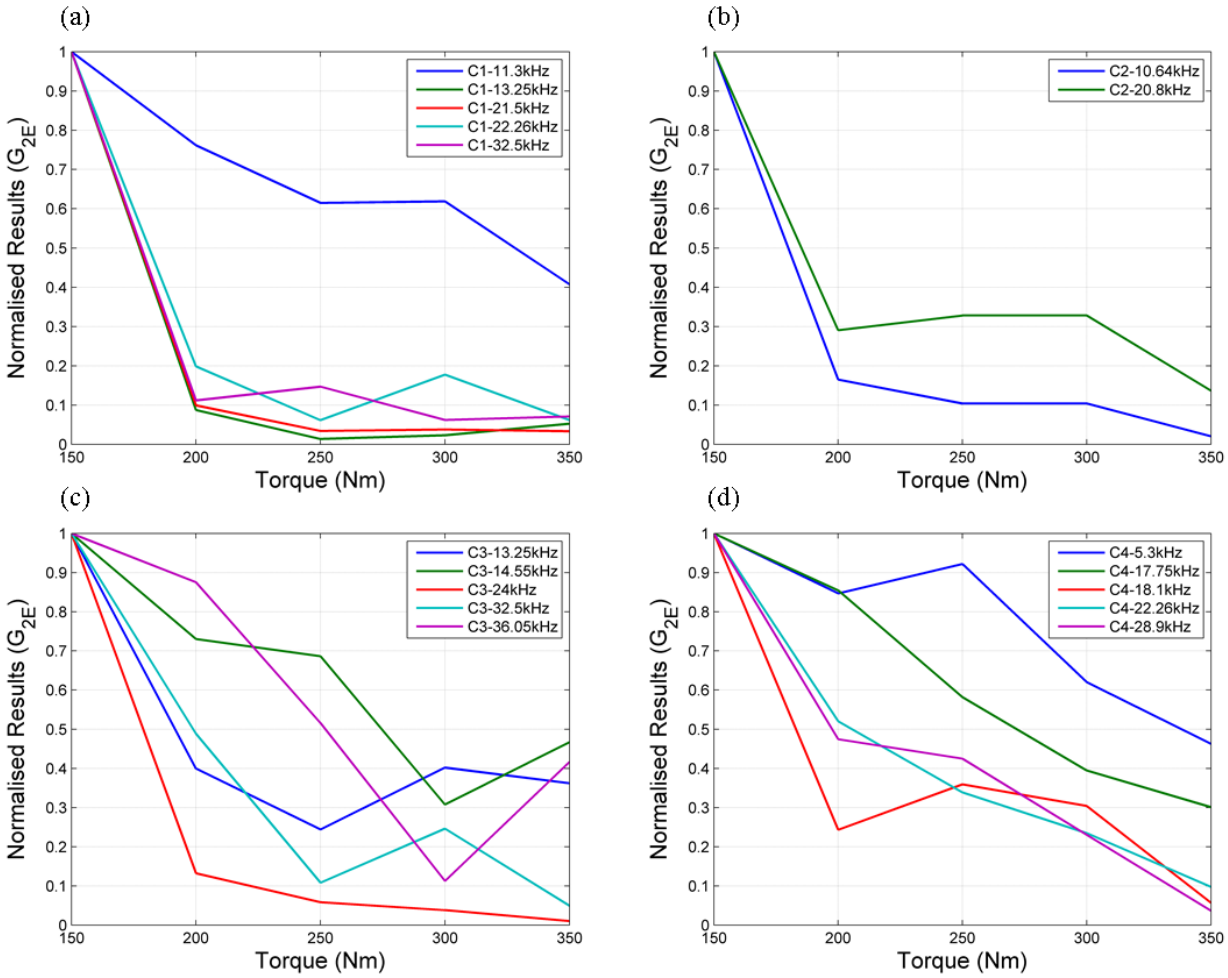

Figure 3.32: Normalised results for various frequencies

3.3.3. Results: G_{3E}, $R_{f2/f1}$ and $R_{(f2+f3)/f1}$ for PZTs 1 & 2 (L1 and L2), G_{2E} and G_{3E} for PZTs 3 & 4

The third order nonlinearity parameter (G_{3E}) and the nonlinear acoustic moments ($R_{f2/f1}$ and $R_{(f2+f3)/f1}$) were also assessed for the PZTs 1 and 2 (Figure 3.33 and Figure 3.35), and the second order and third order nonlinearity parameters (G_{2E} and G_{3E}) for PZTs 3 and 4 (Figure 3.34).

Generally, G_{3E}, $R_{f2/f1}$ and $R_{(f2+f3)/f1}$ follow the same trends as were found in the previous section, with increasing nonlinear parameters as torque was decreased for each of the bolt specific frequencies. It is expected that the G_{3E} figures should be similar to G_{2E} as the governing nonlinear responses should generate a third harmonic as long as it is large enough. In this case G_{2E} was much greater than G_{3E} (by a factor of 10^{-3}) and due to the low relative response of the third harmonics it may be more affected by changes in the conditions of the experiment, as may be the case with Figure 3.33(g). $R_{(f2+f3)/f1}$ is a function of the amplitude of the second and third harmonics, in that the higher the amplitude the greater the energy of the individual frequency, therefore the results fall in line with what was expected. Out of all the frequencies that were tested which gave favourable

results, the results of G_{3E} and $R_{(f2+f3)/f1}$ followed those of G_{2E} in terms of increasing nonlinear parameter versus decrease in torque.

Examining results from PZTs 3 & 4 (Figure 3.34) showed that similar trends were found in terms of bolt specific frequencies. Although after examining all the results not all the bolt frequency combinations found for PZTs 1 & 2 aligned with those found for the different PZTs and locations. Although 21.5kHz (B1, C1) and 5.3kHz (B4, C4) produced good results, B2 and B3 responded well to different frequencies (32.5kHz and 29.3kHz), but both G_{2E} and G_{3E} parameters exhibited the same trends found in the results of PZT 1 and 2. It is evident that the positioning of the PZT has an effect on the response of the system; although this may be the case, if the setup is calibrated for a particular PZT location the individual bolt loosening cases should still be able to be determined. Other important factors that are difficult to predict or quantify are which contact surface generates the greatest level of harmonics (contact between the bolted surfaces or between washer bolt head and surfaces) and does the areas of production of these harmonics change as the bolts become looser. PZT 1 and 2, location 2, explored the effects of the contact surface of the two steel blocks by conducting a transmission test through the specimen (similar to experiments in Chapters 3.1 and 3.2). The results (Figure 3.35 and Figure 3.36) did show an increase in the nonlinear parameters as was expected although there were fewer frequencies found that exhibited the desired behaviour a decrease in nonlinear parameter vs. torque increases. The findings suggest that the contact condition between the two surfaces may not be greatly affected by the loosening of one bolt and the majority of clapping may in fact be attributed to the surface, washer and bolt. Another issue is the energy required to excite both the front and back surfaces of the bolted structure, which may lead to the results determined by PZT in L2. Figure 3.36 shows the normalised results found by PZT 1 and 2 in location 2.

Another area that was considered to have an effect on the production of further harmonics and nonlinear outputs was the bolt fit within the structure. During testing it was noted that various bolts were looser, not in terms of torque applied, but in terms of fit within the holes of the structure. Taking into account the principles of nonlinear behaviour, a bolt that is too tight or too loose would result in a reduction in the clapping mechanism and lead to poor results. B1 and B4 were assessed to have the best fit (tightest) and B2 and B3 the loosest fit, but after reviewing the results it is assumed that the tolerances between the bolts and holes were not significantly different that they affected results.

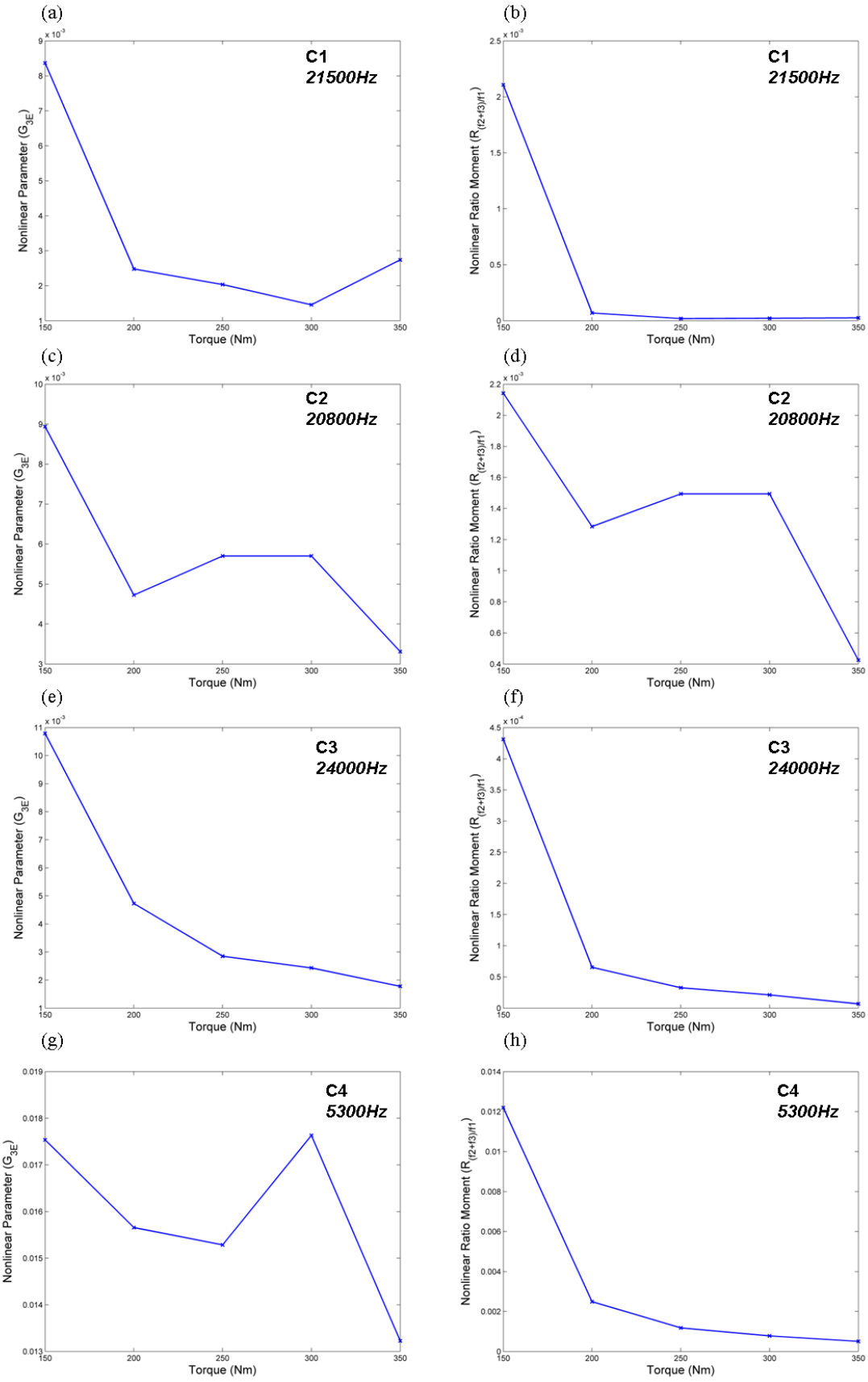

Figure 3.33: G_{3E} and $R_{(f2+f3)/f1}$ results for C1 to C4 (PZTs 1 & 2, L1)

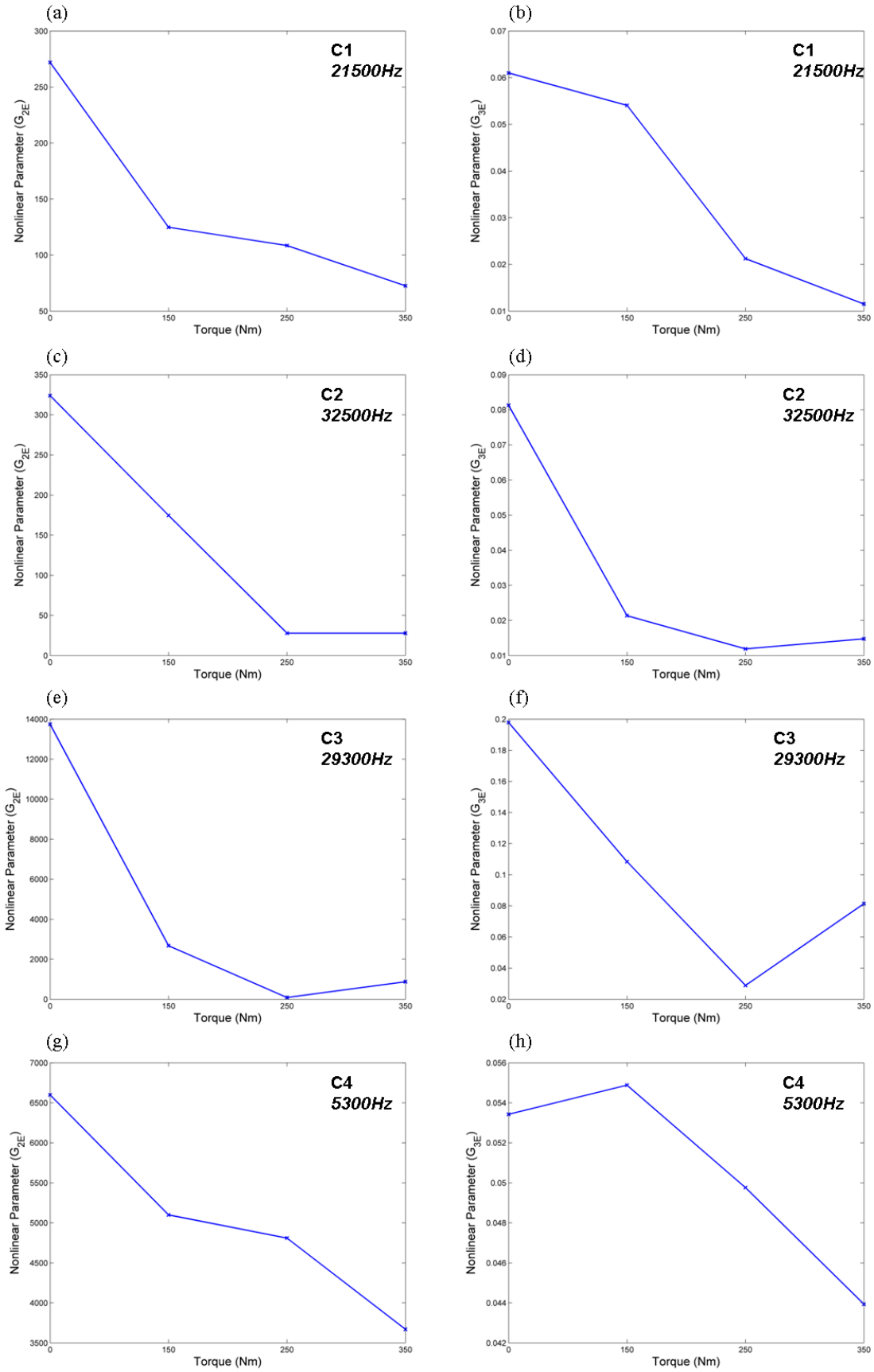

Figure 3.34: G_{2E} and G_{3E} for C1 to C4 (PZTs 3 & 4)

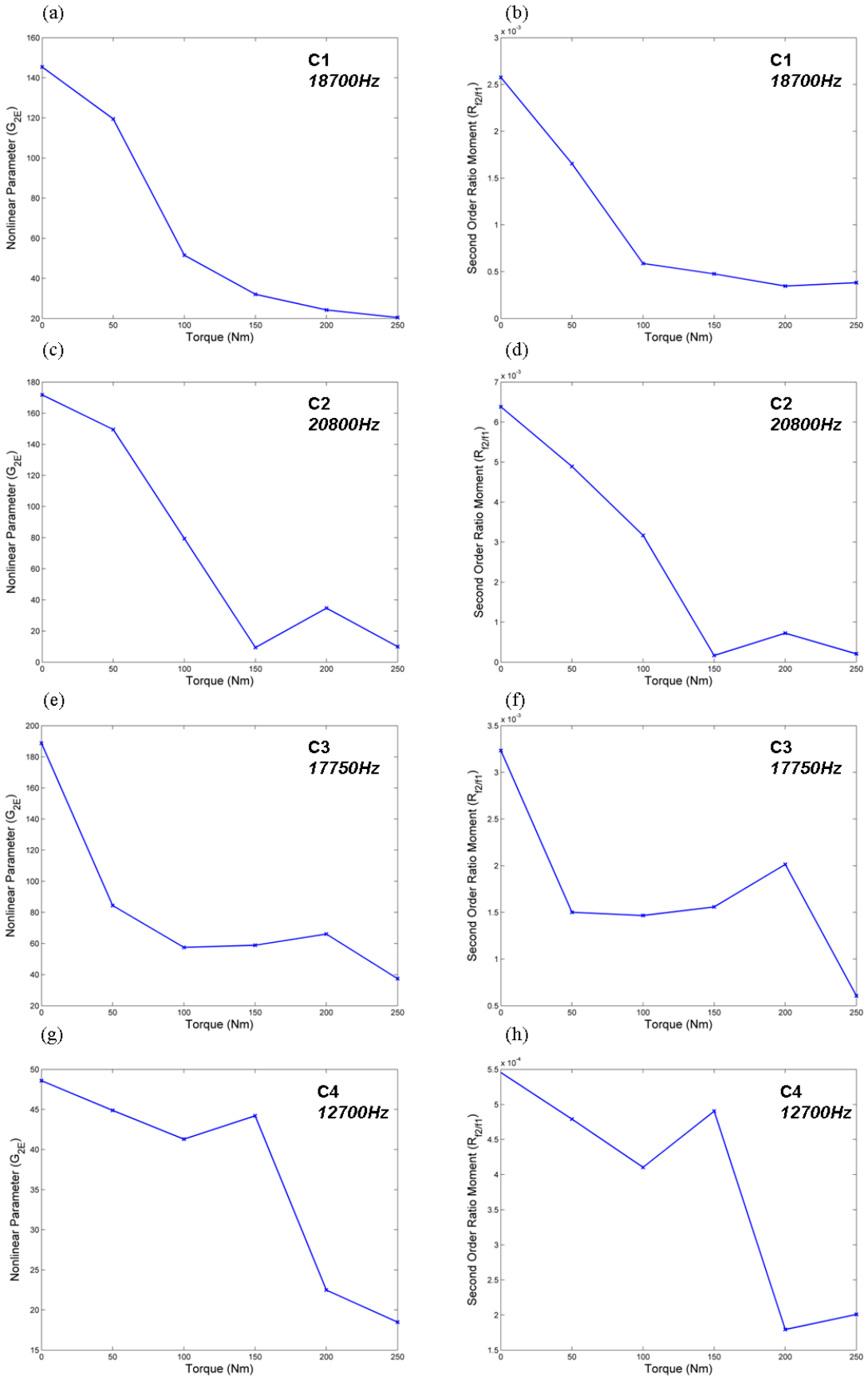

Figure 3.35: G_{2E} and $R_{f2/f1}$ results for C1 to C4 (Sensors 1 & 2, L2)

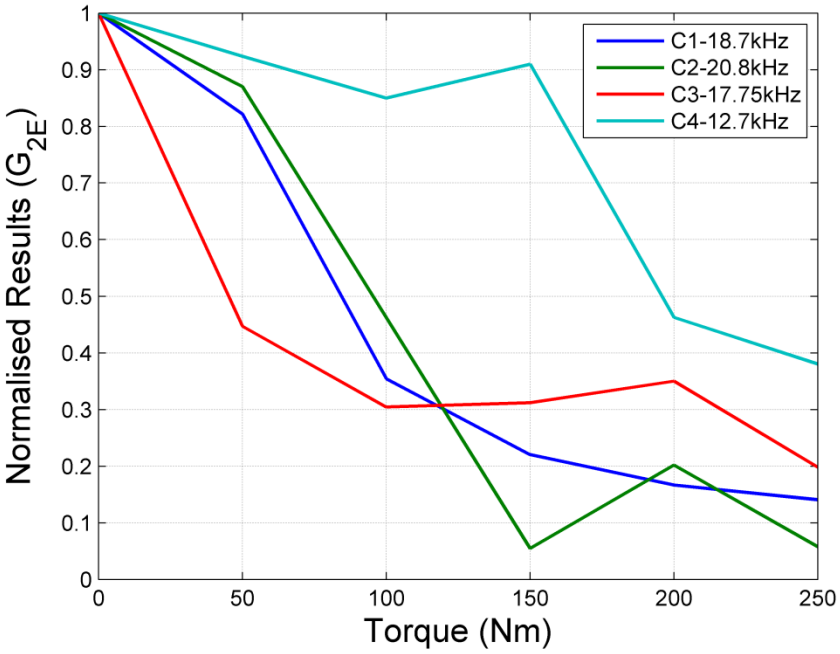

Figure 3.36: Normalised Results for PZTs 1 and 2 (L2)

3.3.4. Other Methods: Damping Curve Method

The damping coefficient can be described as the rate of decay of a signal as time passes. A pulse burst function (PBF) was generated using the above specified waveform generator and setup with sensors 1 and 2 (L1 position). A PBF with an output of 6 V was generated using the waveform generator and then amplified to 300 V. The PBF had a delay of 10μs, band width of 15μs, and a rise and fall of 10ns. The waveform generated required the selection of a general frequency for the generation of the function and thus seven resonance frequencies were used (10.5 kHz, 12.7 kHz, 18.1 kHz, 18.7 kHz, 21.5 kHz, 32.5 kHz, 36.05 kHz). The testing procedure is shown below:

	Applied torque for bolts-Sensors 1 & 2 (L1)
C0	350Nm
C1	B2, B3, B4 = 350Nm B1 reduced: 350, 250, 150, 0
C2	B1, B3, B4 = 350Nm B2 reduced: 350, 250, 150, 0
C3	B1, B2, B4 = 350Nm B3 reduced: 350, 250, 150, 0
C4	B1, B2, B3 = 350Nm B4 reduced: 350, 250, 150, 0
C5	350, 250, 150, 0

Table 3.9: Testing Procedure

The capture of the output signal was triggered using Picoscope 6.0 software, and for each test 32 PBF responses were captured. A damped sine wave can be described as:

$$x(t) = Ae^{-\delta t}\sin(\omega t + \phi)$$

Eq. (3.28)

Where: δ damping coefficient and A is the amplitude. Figure 3.37 (a) shows the PBF generated and used to excite the structure (forced excitation), while Figure 3.37 (b) displays the response and damping of the system for two cases (all bolts tight at 350Nm in red, and all bolts loose in blue). It is clear to see that there is a decrease in amplitude (attenuation) of the response signal as the bolts are tightened. The envelope or damping coefficient of the response of the signal can be determined to evaluate the dampened response of the system. Remembering that the bolts within the structure act as springs when they are preloaded, damping the response of the structure. It is expected that as the bolts are loosened, due to the reduction in preloading and thus the

damping force applied on the structure, damping should be reduced and result in an increase in amplitude in the response of the forced vibration (PBF) resulting in a shift of the damping curve (Figure 3.37 (c)). The damping of the structure (related to torque of bolts) should not be confused with damping caused by the material (expected to remain constant), thus a parallel shift in the damping curve is expected.

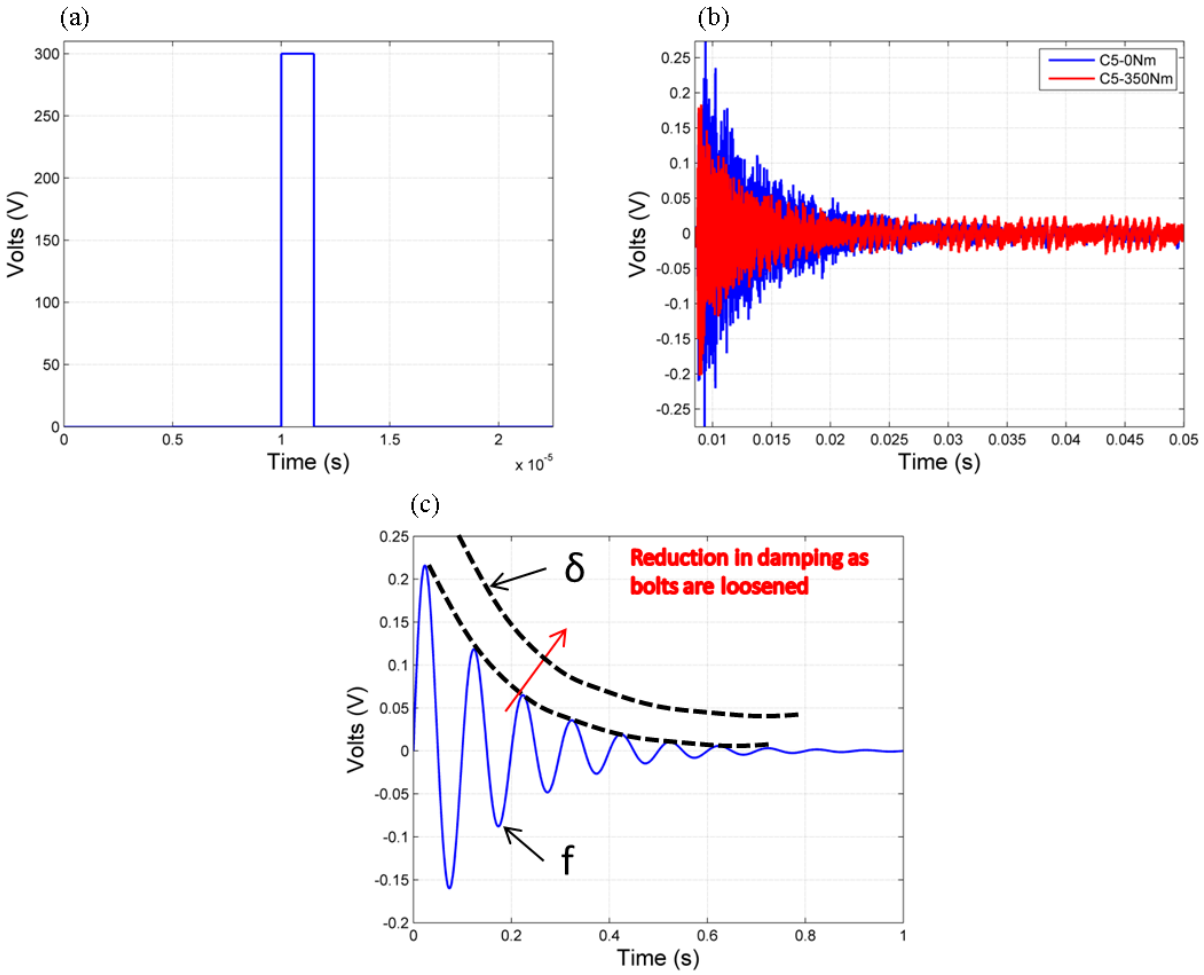

Figure 3.37: Pulse Burst Function (PBF) (a), damping response (b), damping curve calculation (c)

Figure 3.38 shows the results for the individual four bolt cases (C1, C2, C3 and C4) as the bolts are loosened. Generally, the final bolt case, when torque equals zero (light blue line), is greater than the initial bolt case (where torque equals 350Nm, dark blue line), although this trend is not generally followed by the middle torque cases of 150Nm and 250Nm. It is expected that all the curves should shift up as load is reduced on the individual bolt (all others remain at 350Nm), but this is not the case, and although preloading has reduced on one bolt this results in a very small change in the dampening condition of the structure. Due to the magnitude of the change in dampening it may be influenced by external factors such as noise. Another possible issue is that the required amplification of the excitation signal is not great enough to generate a large enough output signal that can be accurately evaluated and are less prone to errors.

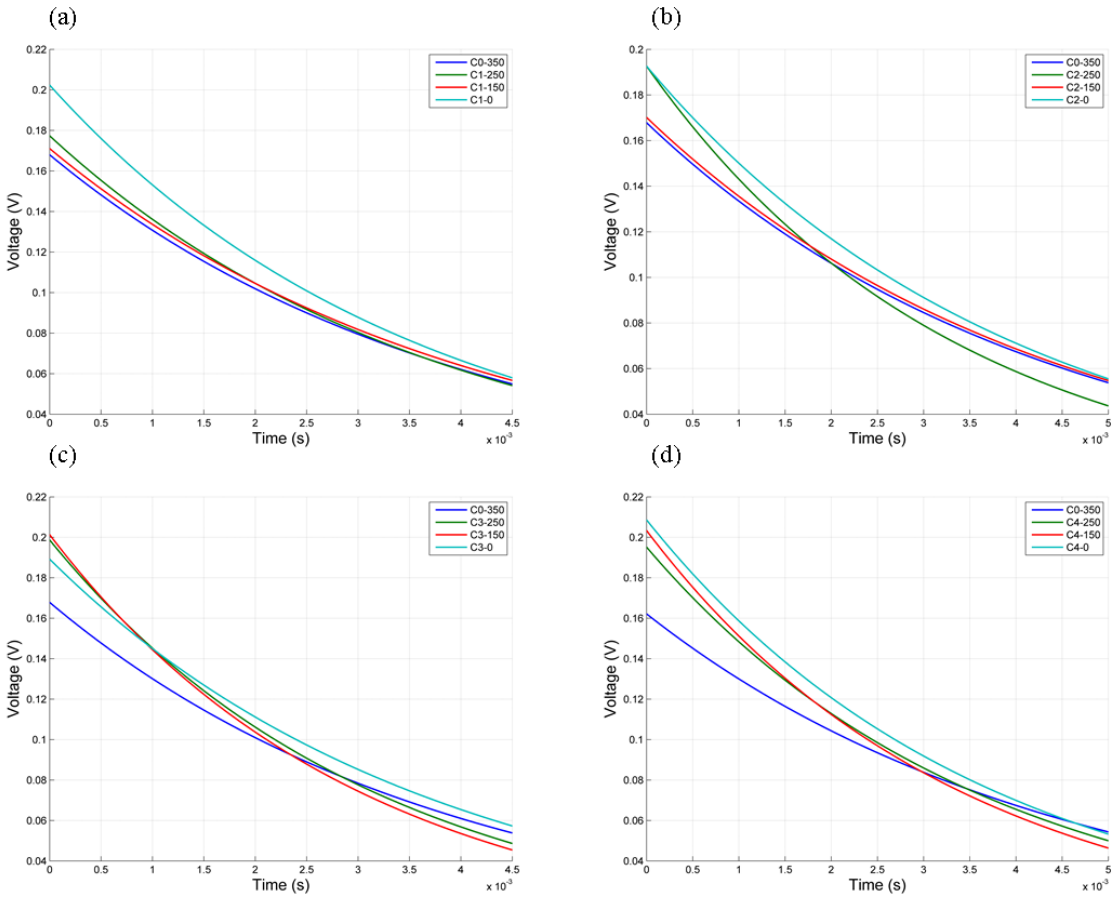

Figure 3.38: Damping curves for individual bolt loosening cases

After evaluating the individual bolt cases, a final case where all bolts were reduced equally and at the same time was explored. Figure 3.39 shows that for C5 there is a clear increase in the damping curve as the bolts are loosened. There is a large increase between 150Nm and 0Nm torque, suggesting that at 150Nm the structure was still significantly dampened. The individual bolt results imply that it is very difficult to assess individual bolt conditions using the damping curve for this structure. A general solution when all bolts are loose can be accurately achieved and can provide general information about the condition of the structure. If the results are compared to the findings of the nonlinear methods evaluated the magnitude of change from case to case is significantly smaller, thus the dampening curve method is more sensitive to errors. Another advantage of the nonlinear methods is that they can provide accurate individual bolt assessment and reduced the excitation voltage requirements significantly (100V nonlinear rather than 300V damping curve).

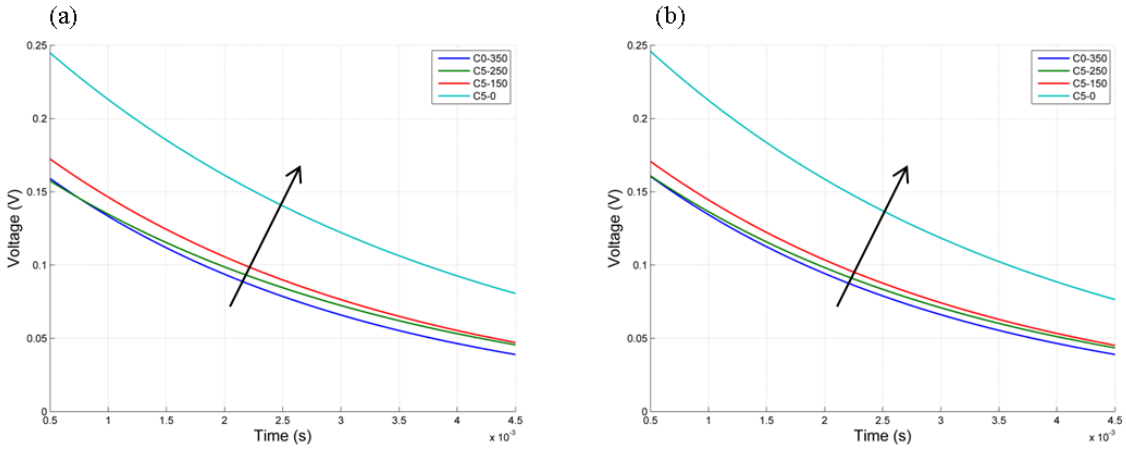

Figure 3.39: Damping curves for bolt loosening case (C5)

3.3.5. Other Methods: Response Signal Energy

The last method used to try and measure the loosened state of the bolts was a response signal energy method. Where the energy of the time domain response was calculated by the equation below:

$$E_s = \int_{-\infty}^{\infty} |x(t)|^2 \, dt$$

Eq. (3.29)

From Figure 3.37(b) it can be seen that the length of the response signal from the PBF is just over 0.01s. The energy of the response signal was calculated for each of the five experimental cases (Figure 3.40, below) by taking into account the first 0.01s of the response. This allowed for the majority of the energy of the response to be determined and assessed. It can be seen in Figure 3.40 that as preloading is reduced there is a release of energy for each of the cases, due to the reduction in dampening.

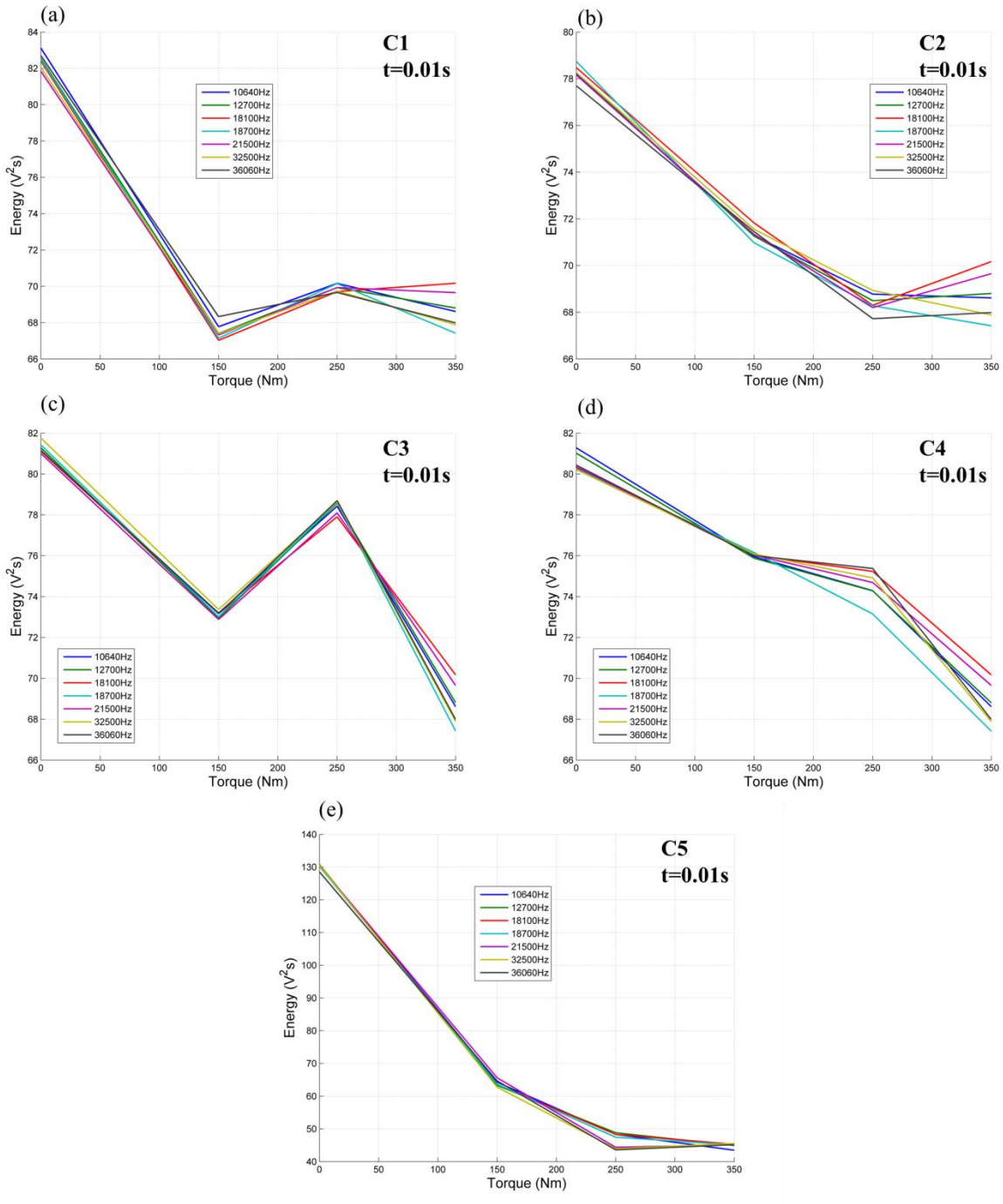

Figure 3.40: Energy vs. Torque for the five cases tested

The energy curves agree well with the damping curve results in that it can be assumed that a higher damping curve will produce a higher energy response. By comparing Figure 3.39 with Figure 3.40 (e) this is clear that as the dampening curve shifts up (a result of loosening) the energy increases. For C1 (Figure 3.38(a) and Figure 3.40(a)) the damping curve was higher at 250Nm than that at 150Nm and so was the energy of the signal, similar correlations between the damping curve positions for different torque values and energy of the response signal are evident for the other cases. Figure 3.40 suggests that when the energy of the response signal exceeds roughly $80V^2s$ at least one bolt is loose, although it is not possible to determine which bolt the energy gain is

attributed to. The gain in energy as one bolt is loosened is also equivalent regardless of which bolt is loosened. Figure 3.40(e) shows that the loosened state of all the bolts result in a dramatic energy gain in the system. There is the potential for a threshold method which could ultimately give observations of the state of the joint as a whole. For example: if the energy of the system was above $80V^2s$ (Figure 3.40(e)) this would imply that there is general loosening of a combination of bolts or an individual bolt is loose, likewise if the signal energy rose above $100V^2s$ this would suggest significant loosening on numerous bolts and energy levels above $115V^2s$ would suggest a critical level of loosening. This method can be used as a quick general testing method, for cases were individual bolt states are not required.

3.3.6. Conclusion

A broad range of testing techniques were conducted on the structure which provided good results (some better than others), they consisted of: linear (damping curve responses and time domain signal response energy) and nonlinear techniques (G_{2E}, G_{3E}, $R_{f2/f1}$ and $R_{(f2+f3)/f1}$), continuous (nonlinear testing) and discrete excitation signals (PBF). Testing also used two different types of PZTs and incorporated multiple PZT locations.

The advantages of the nonlinear results over the linear techniques used were that there were larger magnitude changes due to torque which provides greater certainty that responses were in fact due to the loosening of the bolts. Nonlinear techniques were also able to assess the individual bolt loosened state and provided multiple evaluation techniques. The signal response energy method provided good consistent results for general assessment of the joint, but was unable to distinguish individual bolt loosening.

The small increases of the damping curve relative to all bolts being loosened fell in line with the assumptions made during the through thickness tests (PZTs 1 and 2, in location 2), in that, the preloading of the structure is still high even though one bolt is loose, this makes it difficult to excite the contact region between the two structures, albeit positive results were still possible. The findings imply that clapping and generation of further harmonics are likely to come from surface interactions with the washers, bolt head and nut. The ability of the nonlinear methods to predict which bolt has loosened is far greater than that of the other techniques tested.

This experiment provides and important step in terms of possible SHM systems that can be employed *in-situ* on large scale wind turbines (and other structures). The fact that only two sensors are needed to monitor the state of four bolts is a great improvement to current techniques that are available today, and would provide large cost savings if such a system were to be implemented.

4. NONLINEAR ULTRASOUND METHODS FOR THE EVAULATION OF FATIGUED STRUCTURES

This chapter evaluates nonlinear ultrasound methods for fatigue assessment. Both single and dual frequency methods are utilised. Chapter 4.1 develops a modulated nonlinear elastic wave spectroscopy (NEWS) method for the evaluation of fatigue in a metallic structural component. A baseline-free estimation method is assessed, by comparing the amplitudes of theoretical and experimental nonlinear parameters. Furthermore a dual frequency ultrasound testing technique is used.

Finally, Chapter 4.2 evaluates the accuracy of a developed computational FEA model to generate nonlinear responses, which is validated using experimentally derived results of a fatigued dogbone coupon.

4.1. Baseline-free Estimation of the Residual Fatigue Life using a Modulated Nonlinear Ultrasound Method

Predicting the residual fatigue life of a material is not a simple task and requires the development and association of many variables that as individual tasks can be difficult to measure. This experiment develops a modulated nonlinear elastic wave spectroscopy (NEWS) method for the evaluation of a metallic components residual fatigue life. An aluminium specimen (Material D - AA6082-T6 – refer to Appendix 1) was tested at predetermined fatigue stages throughout its fatigue life using a dual-frequency ultrasound method. A modulated nonlinear parameter was derived, which described the relationship between the generation of modulated (sideband) responses of a dual frequency signal and the linear response. The sideband generation from the dual frequency (two signal output system) increased as the residual fatigue life decreased and can be used to show an increase in a materials damage. A baseline-free method was developed by linking a theoretical model, obtained by combining the Paris law and the Nazarov-Sutin crack equation, to experimental nonlinear modulation measurements. The results found good correlation between the derived theoretical model and the modulated nonlinear parameter, allowing for baseline-free material residual fatigue life estimation.

Predicting the residual fatigue life of a material has broad implications across a wide range of engineering disciplines, such as utilising components until the end of their useful life, avoiding catastrophic and unexpected failures that may lead to the loss of life, and reducing component maintenance and replacement costs. The objective of this research was to develop a new technology, based on the principles of nonlinear elastic wave spectroscopy (NEWS) for accurate detection of accumulated fatigue damage and baseline-free residual fatigue life estimation in metals.

Early work by Yost, et al. (1992) [94] aimed at the development of new methodologies as well as the re-examining of old techniques for non-destructive evaluation and characterisation of metal fatigue; due to the concern over the ageing of the global commercial aircraft fleet. Their focus was to explore the potential of using bulk acoustic nonlinearity measurements in the determination of metal fatigue, with emphasis on: (i) acoustic harmonic generation, (ii) variation of the acoustic nonlinearity parameter with increasing levels of fatigue, and (iii) aluminium alloys (especially Al 2024-T4). Experimental evidence revealed by Yost, et al. (1992) [94] suggests a strong nonlinear interaction of acoustic waves with dislocation dipoles in fatigued metals. It has been widely shown that damages formed during fatigue in materials produce substantial distortion of ultrasonic waves propagating through the fatigued material [13, 19-21, 23, 24, 29, 49, 53]. It is expected that the distortion of ultrasonic waves can be quantified and evaluated in order to assess the residual fatigue life of a structure.

Meo, et al. (2010) [186] published empirical evidence predicting the residual fatigue life of a metallic material using nonlinear guided waves. Meo, et al. (2010) [186] also found a relationship between the second and third order nonlinearity parameters and the fatigue life of a metallic component without the need for a baseline and derived a quadratic nonlinearity parameter by combining the Paris Law with the Nazarov-Sutin nonlinearity equation for cracks that evolve during fatigue mechanisms in metals [186, 192]. These studies establish a robust relationship between the nonlinear parameters and the fatigue life of a metallic component, the work focused on a single frequency output signal.

One of the potential drawbacks of a single frequency sinusoidal excitation is the nonlinear effects generated by the instrumentation itself, to minimize these effects a nonlinear wave modulation technique is proposed in this work.

Straka, et al. (2008) [123] employed a nonlinear elastic wave modulation spectroscopy (NEWMS) method to establish the effects of two longitudinal elastic waves (low frequency and high frequency) and the second and third order intermodulation products over various fatigue cycles (up to 50000) measuring the signal by Fourier transform. Straka, et al. (2008) [123] also explored the dependence of the amplitudes of the intermodulation products on the number of fatigue cycles and the dependencies of the intermodulation products on the driving frequency and driving amplitude for various fatigue cycles. The NEWMS experiments used two elastic waves with frequencies f_1 and f_2 to the material, which have second-order ($f_2 \pm f_1$) and third-order ($f_2 \pm 2f_1$) intermodulation frequencies [17, 124], it was found that there is a large monotonical increase in the magnitude of the intermodulation products with increasing number of fatigue cycles, changes are consistent with appearance and growth of cracks in the specimens and the large sensitivity of the NEWMS method and suitability of the proposed apparatus for the investigation of fatigue damage in aluminium alloy was verified.

The proposed nonlinear wave modulation technique focuses on additional sidebands (modulation) that are produced when two different frequency signals pass over a cracked region. It

should be noted that along with the modulated response (sum and difference-frequencies) in a dual-frequency excitation, harmonics of the two individual frequencies exist (f_2, f_1) , and additional sidebands such as f_2-$2f_1$ or f_2+$2f_1$ exist, which give rise to a large array of further components which do not exist in a single frequency system.

These additional sidebands are then related to the fatigue life of the material and compared to a "theoretical model" constructed by measuring the crack size at different fatigue cycles. The results indicate that there is a good correlation between these modulated responses (sidebands), the fatigue life and the crack growth which leads the way to baseline-free fatigue estimation.

4.1.1. Derivation of the Theoretical Modulated Nonlinearity Parameter as a Function of Crack Size

Crack behaviour can be simulated using a model developed by Nazarov and Sutin [98] where the crack is represented as an elastic contact of two rough surfaces, pressed one to the other under the action of internal stresses in the surrounding solid. This theoretical model relates the small internal stresses, produced by the passing wave (ultrasound propagation through a medium), to the nonlinear parameters. The model describes how a crack behaves when an internal stress passes through the medium, and it takes into account the dimensions of the crack (height of crack surface irregularities, crack radius, distance between middle lines of crack surfaces) and the propagating internal stress through the medium. This model allows for the theoretical estimation of the nonlinear parameter passing through a described damaged medium. By combining the Paris-Erdogan and Nazarov-Sutin models, the magnitude of the nonlinear parameter can be evaluated throughout the fatigue life of the medium. The Paris-Erdogan equation is used to relate the crack propagation to the fatigue life of the material. These factors allow for the creation of the fatigue life estimation equation by relating the fatigue percentage of the specimen to the appropriately estimated nonlinear parameter β_D and β_S values. Ideally the theoretic nonlinear parameter G_{2T} is expected to be equal to the measured modulated nonlinear parameters β_D and β_S described in Eq. (3.20). The development of the fatigue life percentage as a function of the nonlinearity parameters (G_{2T}) is discussed in equations Eq. (4.1) to Eq. (4.8).

The fatigue life prediction equation was derived by combining both Nazarov-Sutin and Paris-Erdogan theories of crack behaviour and crack growth [186, 192]. The linear (G_1) and theoretical quadratic (G_{2T}) nonlinearity parameters of non-interacting penny-shaped cracks in bulk material was shown to be by Nazarov, et al. (1997) [98]:

$$G_1 = \left(1 + \frac{\alpha N_0}{5}\right)^{-1}$$

Eq. (4.1)

$$G_{2T} = \frac{\beta N_0 G_1^2}{7}$$

Eq. (4.2)

where:

$$\alpha = \pi h_s R^2 \left(\frac{E}{\sigma_0}\right)\left(1 + \frac{h_s}{d_0}\right)^{-1}$$

Eq. (4.3)

$$\beta = \pi h_s R^2 \left(\frac{E}{\sigma_0}\right)^2 \left(1 + \frac{h_s}{d_0}\right)^{-3}$$

Eq. (4.4)

Where: N_0 is the crack concentration, α and β are the linear and nonlinear elastic constants of the crack, h_s is the characteristic height of the crack surface irregularities, R is the crack radius, E is the Young modulus, σ_0 is the internal stress (equal in amplitude but opposite in sign to the external stress), d_0 is the distance between the middle lines of the crack surfaces.

To derive the nonlinearity parameter as a function of crack growth during the fatigue process, the Paris–Erdogan equation was used, where the variation in the crack size R is expressed as a function of percent fatigue life to final fracture:

$$\frac{dR}{dn} = C\Delta K^m$$

Eq. (4.5)

Where: the material dependent constants C and m are the crack growth intercept and the crack growth exponent, n is the number of fatigue cycles and ΔK is the stress intensity range defined by:

$$\Delta K = \sigma_0 F(R)\sqrt{\pi R}$$

Eq. (4.6)

Where F(R) is the shape factor and it was assumed as a constant in the fatigue stable propagation phase. The derivation of the shape factor F, also known as geometry factor, for a circular hole in a plate can be found, where it is reported how the geometry factor changes when

the crack size increases from a circular hole. In detail, for stable crack propagation phase, that behaviour is almost constant: for a crack size 5 mm < a< 20 mm, F varies between 1 and 0,8.

This justifies the assumption of a constant F.The fatigue life percentage has been determined by Meo, et al. (2008) [5]:

$$f = \frac{n}{n_{tot}} = \frac{\left(R^{1-\frac{m}{2}} - R_0^{1-\frac{m}{2}} \right)}{\left(R_f^{1-\frac{m}{2}} - R_0^{1-\frac{m}{2}} \right)}$$

Eq. (4.7)

While the crack size as a function of fatigue life was also determined [5]:

$$R = \left[f\left(R_f^{1-\frac{m}{2}} - R_0^{1-\frac{m}{2}} \right) + R_0^{1-\frac{m}{2}} \right]^{\left(1-\frac{m}{2}\right)^{-1}}$$

Eq. (4.8)

Where: R_f is the final crack length, R_0 is the initial crack size, f is the fatigue life percentage, m is the crack growth exponent.

Finally, substituting Eq. (4.8) into Eq. (4.4) (β) and then into Eq. (4.2), allows for the evaluation of the modulated nonlinearity parameter as a function of crack size. Substituting different crack lengths (from zero to the maximum) into Eq. (4.8), allows for different theoretical G_{2T} parameters at various fatigue life percentages to be evaluated. Thus by adjusting the crack length in the theoretical model a fatigue life percentage curve that relates to the modulated responses (sum and difference-frequency) can be generated. This curve relates the fatigue life of the specimen in number of cycles to the nonlinearity parameter. The fatigue life percentage can be assumed to be the point at which the modulated response recorded by ultrasound tests equals a specific value on the prediction curve (Eq. (4.2)). Thus by superimposing the experimental modulated response values over the prediction curve an estimation of the residual fatigue life of the material can be determined.

4.1.2. Residual life estimation procedure

The experimental nonlinearity parameters determine the response of the sidebands ($f_2 + f_1$ relates to β_S the sum-frequency and $f_2 - f_1$ relates to β_D the difference-frequency parameters) is compared with the expected level the theoretical nonlinearity parameter which is calculated by taking into account the crack size and various other material properties.

Figure 4.1 shows how the experimental model will be assessed against the fatigue life prediction curve, constructed by applying crack sizes from R_0 to R_f into the theoretical model (Chapter 4.1.1, Eq. (4.8), page 128). The black dot represents the experimental nonlinearity parameter derived from Eq. (3.20) (β_D and β_S), while the red curve is developed using Eq. (4.2) ($G_{2T,}$ for various crack lengths, which relate to the fatigue life percentage). The procedure to estimate the residual life of a metallic structure is as follows:

(i) estimate type of fatigue loading of component (stress ratio),

(ii) determine the crack size as a function of fatigue life percentage,

(iii) compute the theoretical modulated nonlinearity curve (as a function of crack size and fatigue life),

(iv) measure experimentally the nonlinearity parameters, and

(v) finally by overlaying the experimental value onto the theoretical curve the estimation of the residual fatigue life can be determined.

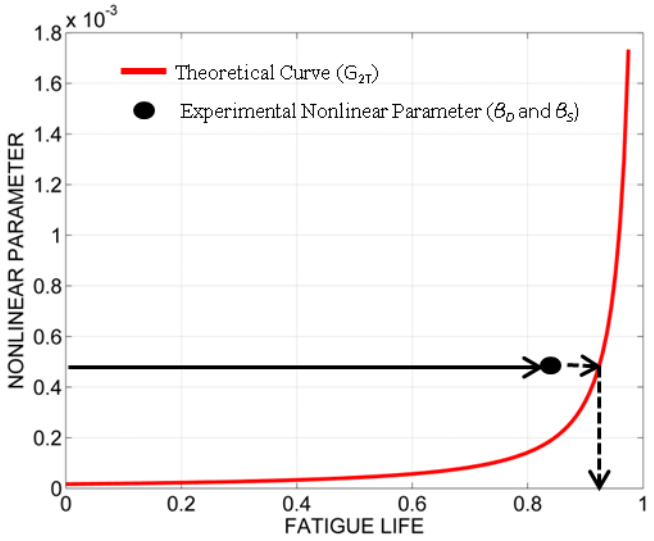

Figure 4.1: Residual Life estimation procedure

4.1.3. Experimental Setup

This experiment used a coupon that had been designed to allow for fatigue and crack growth. The samples geometry was representative of a rib of a military aircraft. This geometry was used because the rib experiences fatigue cracks at certain locations (around the rivet holes). Demonstration of the capability of the proposed techniques to estimate fatigue life on a reduced geometry of a real structure was analyzed. The coupon was made from high grade Aluminum 6082-T6, with a length of 245mm, thickness of 8mm, breadth of 50mm, and had four 5mm diameter holes through the thickness (details of hole positions and coupon setup are highlighted in Figure 4.2).

The design of the coupon ensured that high stress concentration areas existed, fatiguing of the sample focused on the initial crack region and crack propagation occurred. The piezoelectric sensors used were glued in place (15mm either side of the inserted holes and centered) and thus were attached to the coupon during the fatigue testing. This allowed evaluation of permanently installed PZTs (APC International-Diameter 6.35mm, Thickness 0.25mm, Type 850 WFB) and evaluation of the proposed techniques in real-life conditions.

The actuating piezoelectric sensor was driven directly by an Arbitrary Waveform Generator, and the receiving sensor was not amplified. The frequencies used were carefully selected. The frequency pairs were found by determining the resonance frequencies of the sample. The Arbitrary Waveform Generator was used to conduct a sweep of the frequencies between several frequency ranges. Figure 4.3 shows the frequency sweep for 0 to 100kHz, the frequencies that peak are the resonance frequencies of the material. Linear resonance frequencies were examined at each stage of crack growth and no significant difference or frequency shift were found (outside of instrumentation errors). Five frequencies were selected 24509 Hz, 34466 Hz, 94760 Hz, 405750 Hz, and 585327 Hz. Four frequency pairs were constructed using these five resonance frequencies which were 24kHz & 585kHz, 34kHz &585kHz, 34kHz & 405kHz, and 94kHz &405kHz.

The frequency pairs were tested at amplitudes of 20V pk-pk. The high frequencies found were paired with lower frequencies in order to ensure there was no mixing or overlapping of frequency bands and the nonlinear modulated responses (sidebands) would result at high frequencies, this ensured that the wavelengths of the captured data were very small relative to the coupon. These four frequency pairs were tested on three samples, as outlined in table 1.

The three samples tested were fatigued using an Instron Fatigue Testing machine and nonlinear parameters were measured using experimental layout (below) at the same fatigue cycle intervals: 0, 4000, 8000, 12000, 13000 (including 14000, 15000, and 16000 for samples that broke later). The samples were cyclic fatigued between 0 and 70kN at 5Hz.

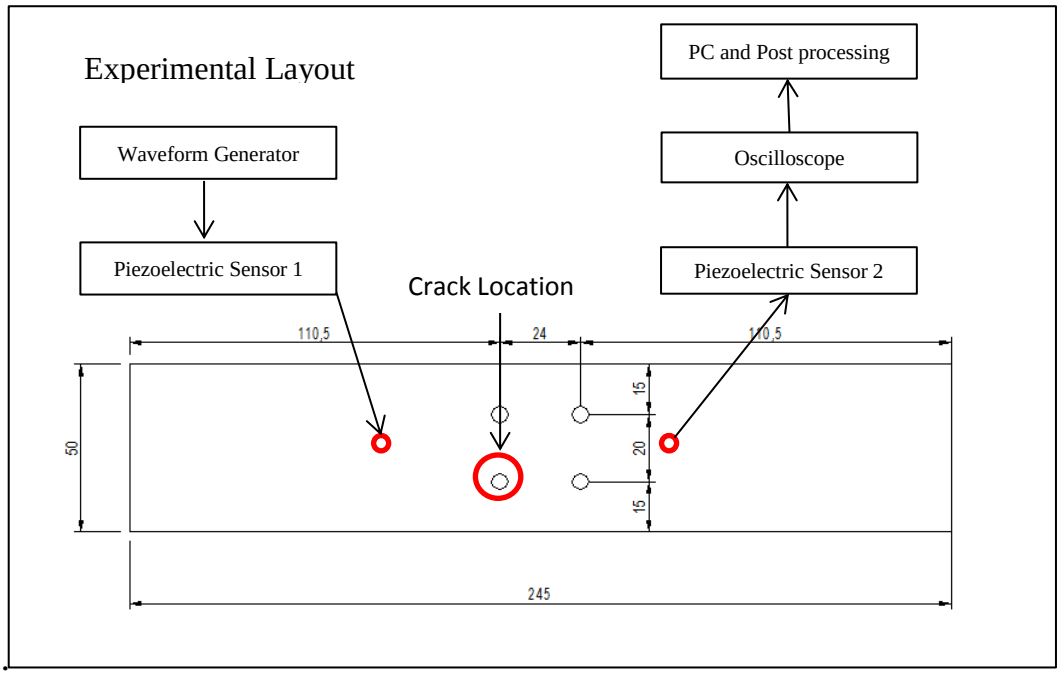

Figure 4.2: Optimised Experimental Layout.

	Frequencies Investigated	Amplitudes of Signal Investigated
	Top of plate: 1 Point Tested	**Voltage (Amplitude)**
SAMPLE 1-3	24kHz & 585kHz	20
	34kHz &585kHz	20
	34kHz & 405kHz	20
	94kHz &405kHz	20

Table 4.1: Optimised Testing Frequencies and Amplitude.

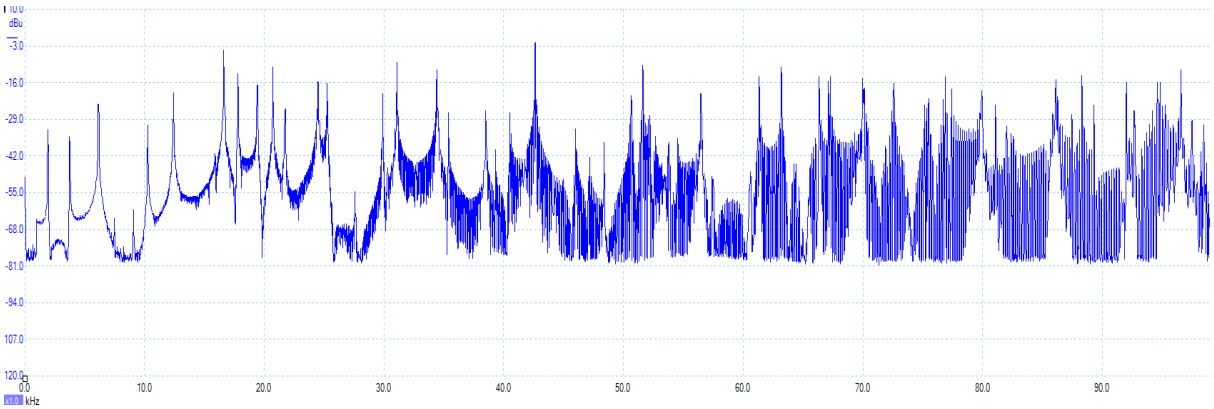

Figure 4.3: Frequency Sweep Results 0-100kHz.

4.1.4. Modal Analysis

A modal analysis of the coupon and the selected frequencies were performed using ANSYS Workbench R14.0, in order to determine the mode shapes and resonance frequencies of the structure in order to assess the likelihood of crack interface excitation (clapping/rubbing mechanism) and the differences between modeling and experimental resonance frequencies. Areas that displayed large deformation or high strain regions near the potential areas of crack propagation should result in greater nonlinear frequency responses. The generation of the nonlinear responses is due to shear excitation of the crack resulting in rubbing, in-plane excitation (perpendicular to crack surface) which would result in clapping and a combination of the two. Modal analysis was conducted over various frequency bands that contained the selected frequencies identified through experimentation, i.e. between 20kHz and 30kHz for the frequency of 24509Hz. The modal results showed good correlation to the experimentally measured resonance frequencies.

Figure 4.4 and Figure 4.5 below was constructed in ANSYS Workbench using the same geometric dimensions as the test sample and had a mesh of: (i) 21620 elements and 102734 nodes for frequencies 24kHz, 34kHz, 94kHz and 405kHz (element lengths were set to allow for at least 8 points per wavelength, 1.7mm element lengths), and (ii) 54726 elements and 248287 nodes with an element length of 1.25mm for a frequency of 585kHz The fundamental frequencies modal deformation responses are shown in Figure 4.4 and Figure 4.5 below.

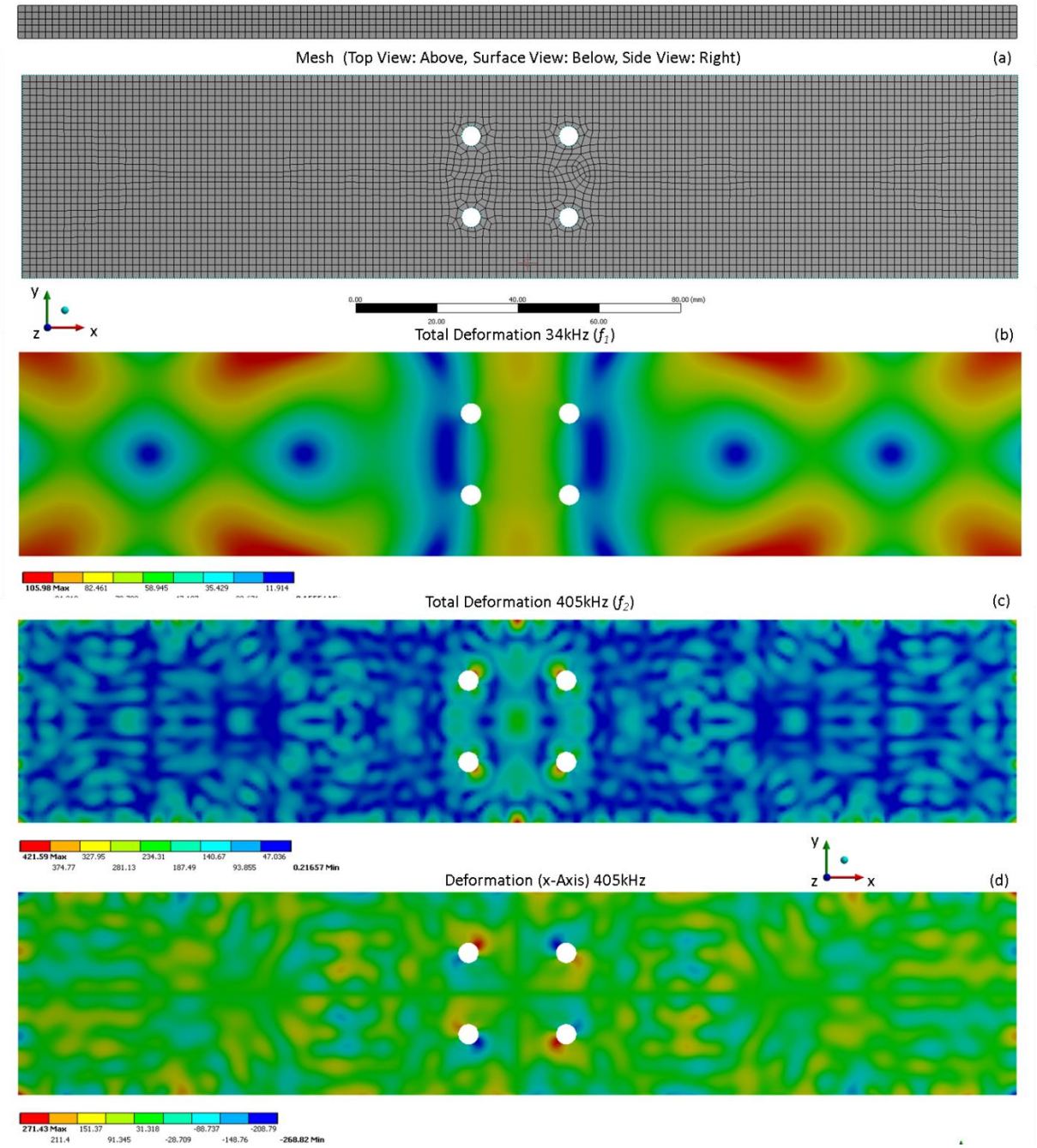

Figure 4.4: Mesh layout (a) and Modal Deformation of Coupon for fundamental frequencies (b) and (c) and for x-Axis (d).

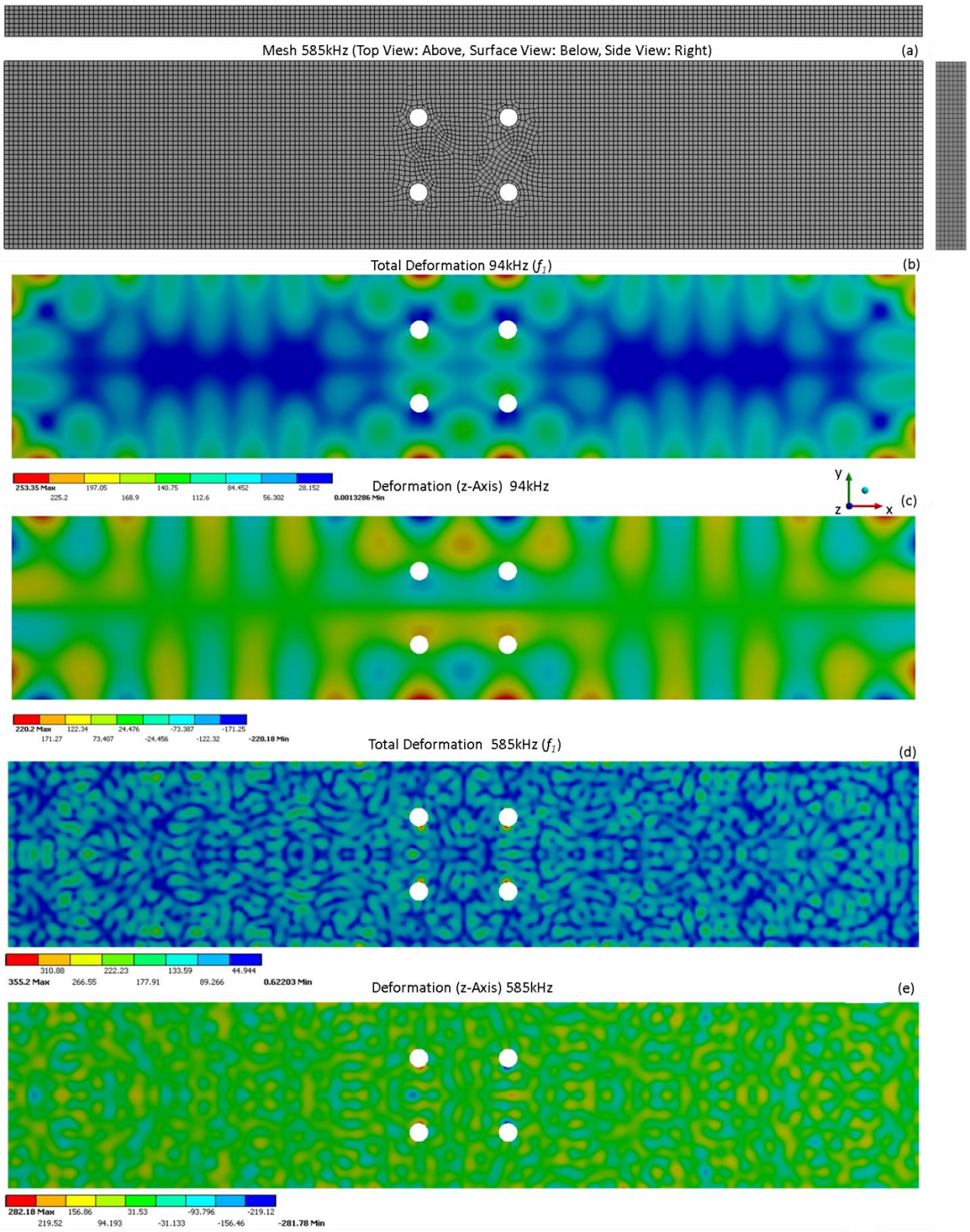

Figure 4.5: Mesh layout for 585kHz (a) and Modal Deformation of Coupon for fundamental frequencies (b) and (d) and for z-Axis (c) and (e).

Figure 4.4 and Figure 4.5 reveals that the regions between the holes result in large deformations, the movement of a crack propagating between the holes as the structure is excited would be expected to result in rubbing or clapping. By investigating the x plane deformations, it is clear to see that the crack will propagate through areas that will result in high excitation resulting in nonlinear frequency responses (f_2-f_1 and $f1$+f_2). While the correlation between experimentally derived resonance frequencies and modelled resonance frequencies for the 34kHz and 405kHz frequency pair are shown in Table 4.2 below.

Table 4.2: Comparison of experimental and computational frequencies determined

Frequencies Investigated		
Experimentally Determined Frequency (Hz)	**ANSYS Modal analysis (Hz)**	**ANSYS Analysis Info**
24509	24806	21620 elements & 102734 nodes, element length 1.7mm
34466	34480	21620 elements and 102734 nodes, element length 1.7mm
94760	94804	21620 elements and 102734 nodes, element length 1.7mm
405750	405710	21620 elements and 102734 nodes, element length 1.7mm
585327	585300	54726 elements and 248287 nodes, element length 1.25mm

Figure 4.6 below shows the results of a mesh sensitivity analysis for the coupon for the resonance frequency of 24509 Hz. The figure shows that at an element length of around 2.5mm there is little change in the results, highlighting the convergence of the model and justifying the chosen element lengths.

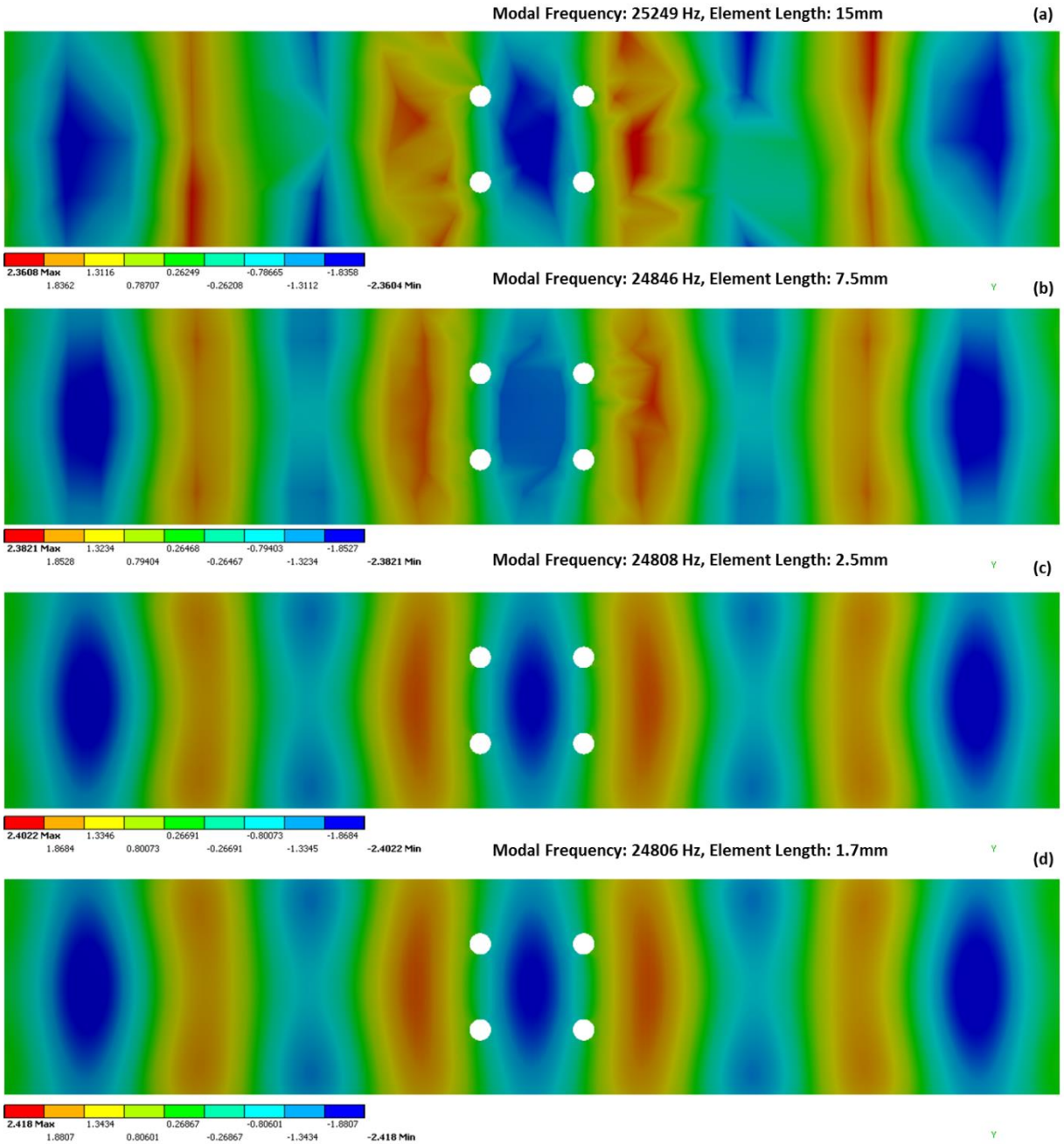

Figure 4.6: Mesh Sensitivity Analysis Results

4.1.5. Experimental Validation

Sample one failed at 13300 cycles, Figure 4.7 (a, b, c and d) below shows the crack propagation for sample 1, it was found that at 13000 cycles the crack length of sample one was much shorter than in other samples at the same fatigue life (which failed at 16000 cycles). This highlights that at the same number of cycles the crack size was different for different samples. It was found that crack growth and propagation varied significantly between samples.

Sample 2 appeared to have no crack growth up to 12000 cycles microcracks would have started forming, increasing the levels of the modulated response and the original incisions which were made on both the top and bottom surface of the coupon would have connected forming a crack through the thickness of the coupon. The main advantages of the testing procedure used were that:

(i) The sensors were glued to the test piece, this ensured that their position remained constant and that initial contact was good,

(ii) No amplifiers were used which removed the uncertainty of unwanted mixing of the further harmonics by equipment,

(iii) A frequency sweep was performed to determine the resonance frequencies of the material, it was found that frequencies lower than 1MHz responded better than higher frequencies.

(iv) The frequency pairs chosen had a large differential (i.e. 24kHz and 585kHz), this was done to ensure that if unwanted harmonics were produced they would not interfere with the measurements.

Figure 4.7 (e) and (h) show the modal results for 34kHz, 405kHz, 94kHz and 585kHz with the crack position and length overlaid to confirm the expectation that movement of the crack should result in nonlinear harmonic production. Figure 4.7 (d) to (h) refer to the same geometric areas and thus use the same scale.

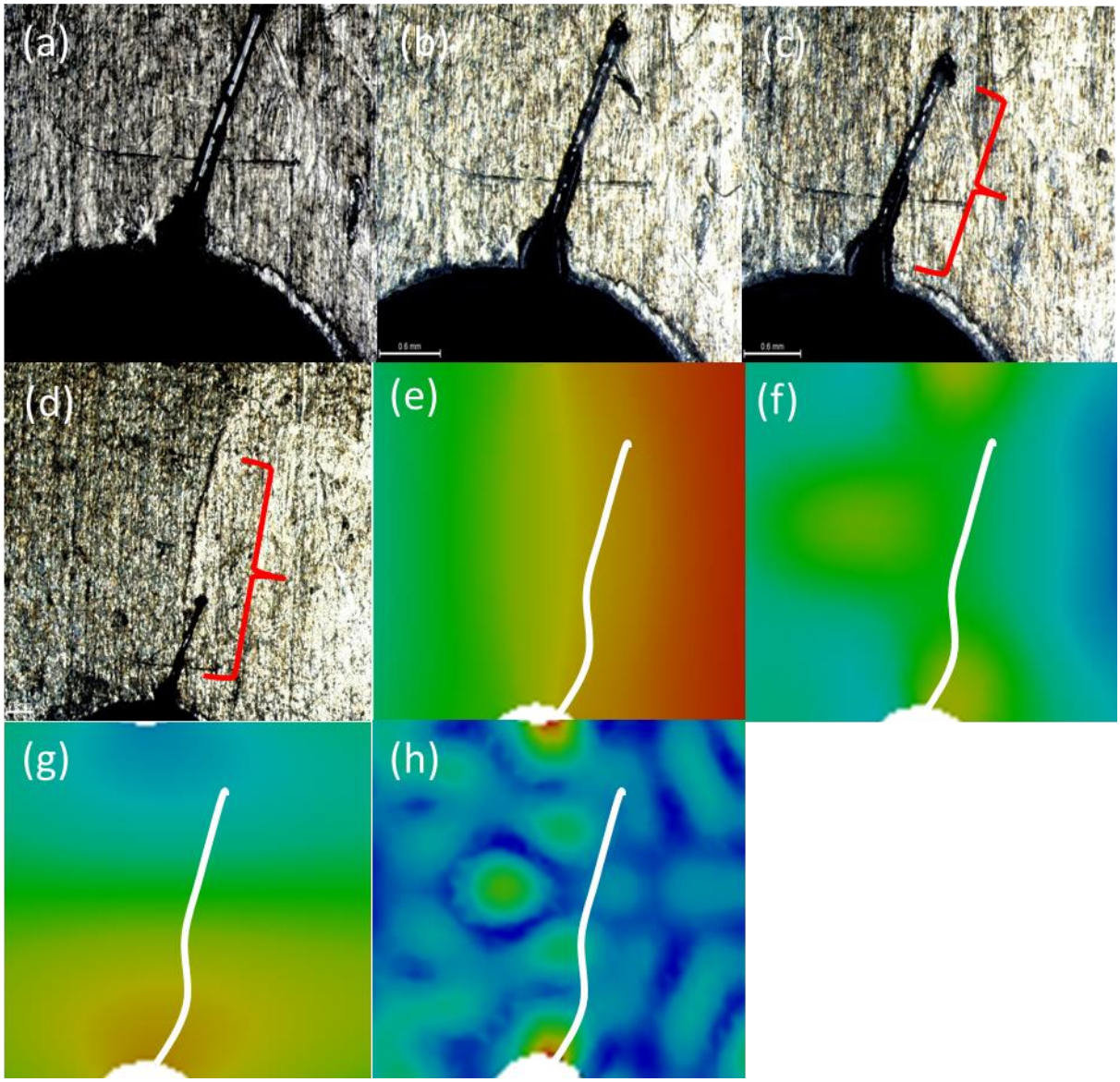

Figure 4.7: Crack Propagation (Sample 1): (a) Initial Crack, (b) 8000 cycles, (c) 12000 cycles, (d) 13000 cycles, (e) to (h) superposition of crack over modal deformation regions for 34kHz, 405kHz, 94kHz and 585kHz respectively.

Figure 4.8 and Figure 4.9 show the change in the FFT for the 94kHz and 405kHz pair as the number of cycles increase. The tests displayed good correlation with the general theory, in that the amplitude of the fundamental frequencies (f_1 and f_2) decreased as crack growth and number of cycles increased (Figure 4.8 (a) to (c)). The modulated responses (sum-frequency (f_2+f_1) and difference frequency (f_2-f_1)) increased with crack growth and number of cycles and results were clear and accurate.

Figure 4.8 (a) to (c) emphasise the decrease in the two fundamental frequencies from 0 to 12000 cycles, initially f_2 decreases from 0 to 8000 cycles and then f_1 decreases from 8000 cycles to 12000 cycles. The figures show a good alignment with the theoretical model and linear ultrasound techniques which use the reduction in the amplitude of the fundamental frequencies to determine damage. There is no apparent generation of the modulated responses from 0 to 12000 cycles.

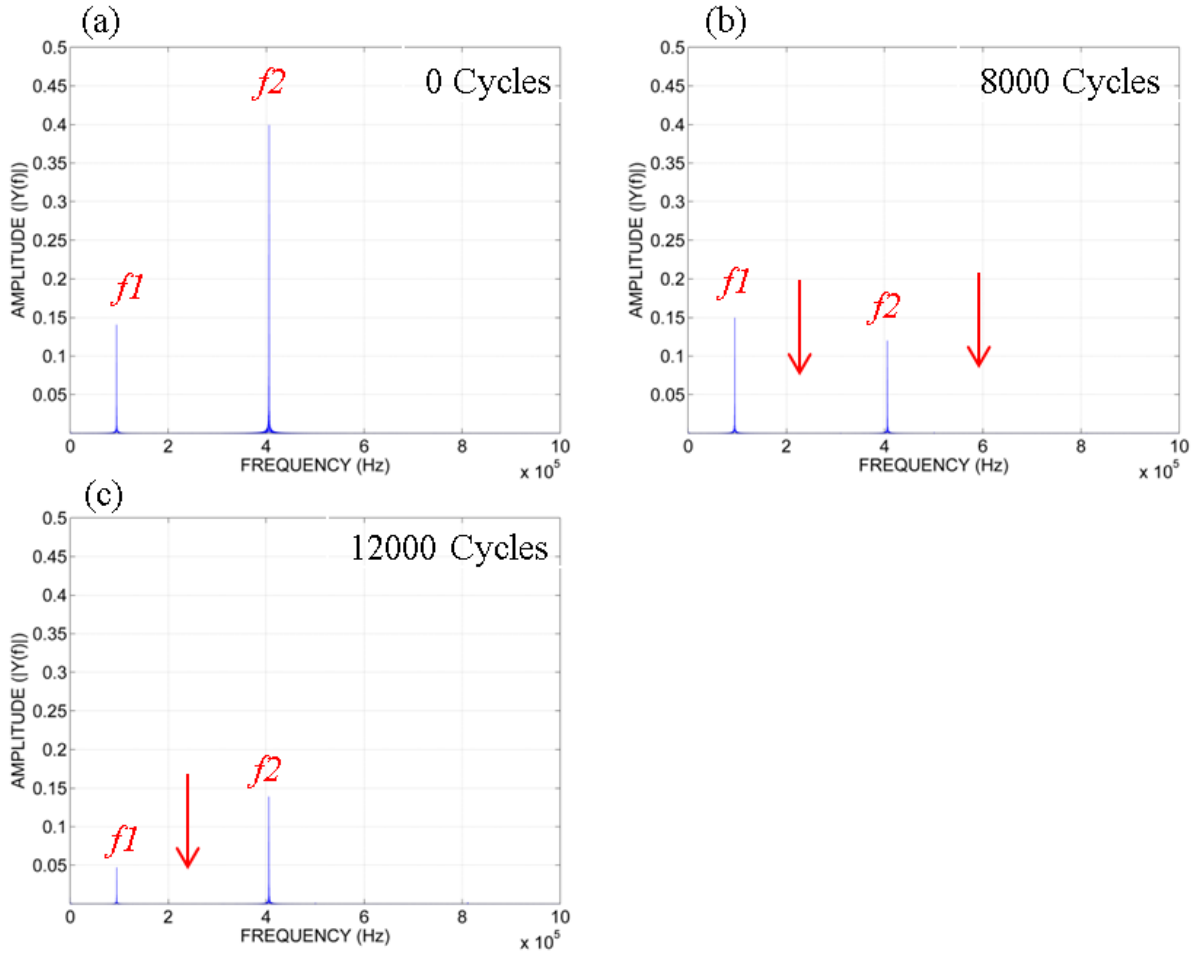

Figure 4.8. Part 1:FFT progression for 94 and 405 kHz pair (Plot 5(a)-(c): Full Spectrum, Plot 5(d)-(g): Focused Spectrum (300kHz-510kHz).

Figure 4.9 (d) to (g) show a focused view around the higher fundamental frequency (f_2) between 300kHz and 510kHz (sidebands are within this range). It can be observed that between 0 and 4000 cycles there is no harmonic generation. Harmonic generation occurs at 8000 cycles with the appearance of the sum-frequency and the difference-frequency components. Borh the sum and different frequency increase from 12000 to 13000 cycles and when comparing Figure 4.9 with Figure 4.7 it is clear to see that the harmonic generation coincides with crack growth (although it cannot be clearly seen in Figure 4.9 f_2 is decreasing). From the setup it is clear that the large difference in the fundamental frequencies (f_1 and f_2) has resulted in a much clearer signal that does not exhibit problems of harmonic mixing and the results showed good alignment to the expected theoretical outcome.

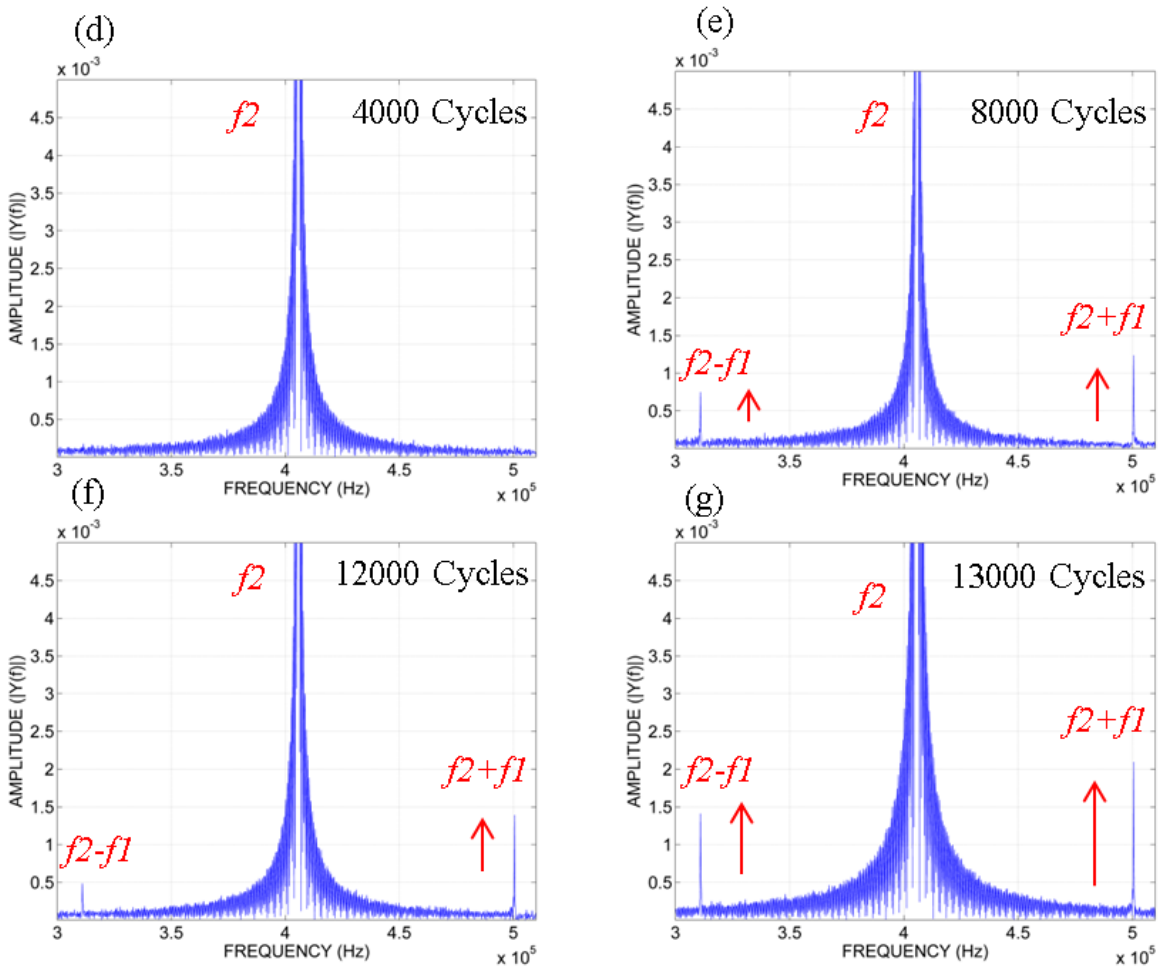

Figure 4.9. Part 2:FFT progression for 94 and 405 kHz pair (Plot 5(a)-(c): Full Spectrum, Plot 5(d)-(g): Focused Spectrum (300kHz-510kHz).

4.1.6. Residual Fatigue Life Estimation

The residual life fatigue estimation was carried out by comparing the experimental and the theoretical results. G_{2T} (Eq. (4.2)) was used to draw the theoretical curve, while the experimental results (β_S and β_D) are displayed on the same set of axis. Figure 4.11 shows the theoretical vs. the experimental results for the four frequency pairs for the 3 samples investigated.

The general values used in the theoretical equation were $R_f = 0.015$ m, $R_0 = 5\text{x}10^{-4}$ m, m = 5, $h_s = 1\text{x}10^{-6}$ m, $d_0 = 3\text{x}10^{-5}$, $E=76.5\text{x}10^{7}$, $N_0 = 2.6\text{x}10^{-1}$, $\sigma_0 = 3\text{x}10^{4}$, where: R_f is the final crack length (length at failure), R_0 is the initial crack length, m is the crack growth rate, h_s is the surface roughness, d_0 is the diameter of the crack, E is the Young Modulus of the material, N_0 is the starting number of cycles, σ_0 is the internal stress of the material.

Eq. (3.20) (Chapter 3.1.2, page 69) was used to evaluate the nonlinearity parameters for the sum (β_S) and difference (β_D) frequencies for the pairs 34kHz & 405kHz, 94kHz & 405kHz, 34kHz & 585kHz and 24kHz and 585kHz (shown in Figure 4.11). A best fit curve was used to determine the general trend of the results, and the results were plotted against number of cycles.

Figure 4.11 demonstrates that the nonlinear parameters for all the tested frequency pairs increase. The increase in the nonlinear parameters are due to a decrease in the fundamental frequencies (f_1 and f_2, Figure 4.8) and increase in the modulated responses ((f_2-f_1) & (f_2+f_1), Figure 4.9). The nonlinear parameters increase as damage increases and the magnitude of the different frequency pairs are fairly similar which suggests that a broad range of frequencies can give similar results. Discrepancies between frequency pairs may be a consequence of varying test conditions and higher material resonance at different frequencies.

Figure 4.10 shows the general trend as of the nonlinear parameters over the fatigue life of the sample, a clear increasing trend can be observed. The nonlinear values exhibit a definitive increase over the fatigue life of the materials and this increase is due to the dual effect of a decrease in the fundamental frequencies and increase in the harmonic response, only considering the linear response would result in smaller changes as the crack grew.

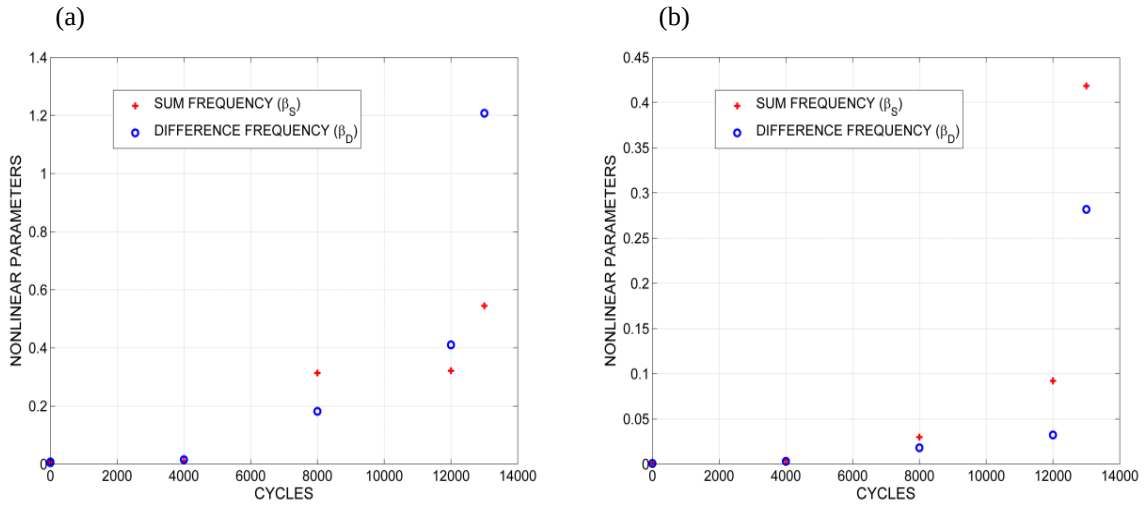

Figure 4.10: Modulated Results Sample 1 (MOD1=Sum-Frequency (β_S), MOD2=Difference-Frequency (β_D)).

Figure 4.11(a) shows good correlation for the difference frequency results and the curve. Figure 4.11 (b) also displays good correlation for the difference frequency results and better correlation for the sum frequency results. Figure 4.11(c) has good correlation between the theoretical and difference frequency results, with the sum frequency results less accurate. Figure 4.11(d) results found a marked decrease in the experimental results compared with the theoretical results. Figure 4.11 (a) to (c) exhibit larger sum and difference frequency results at 60% fatigue life and the difference frequency results have higher correlation to the theoretical curve.

Figure 4.11 (e) shows the average of all the results for sample 1. The average was calculated using both the difference frequency and sum frequency results for each fatigue life point. The averaged results produce a good correlation with the theoretical curve at high and low fatigue life percentages, although the experimental value at 60% fatigue life was larger than the theoretical. The close results of the averaged experimental results to the theoretical results provide an

alternative method, which would include conducting a large number of dual-frequency pair observations on the test sample and averaging the results. This method could potentially ensure that any outliers are removed from the test sample results.

Figure 4.11 (f) shows the averaged results and how the Nonlinear Wave Modulation Spectroscopy (NWMS) method works. Three points have been highlighted A which relates to a fatigue life percentage of 98%, B (90%) and C (60%). Using the NWMS method to determine the fatigue life percentage of the specimen the recorded values of A and B would under predict the actual fatigue life percentage by around 5% each and point C would over predict the fatigue life percentage by around 20%. The accuracy of the method at high and low levels of fatigue is reasonably consistent, although a large increase in the nonlinear parameters occurred at around 60% of the fatigue life. The model provides realistic insight into the fatigue life of the material at high levels of damage and the large distortion in results between point C and the theoretical curve could be due to the growth of other microcracks.

The nonlinear parameters determined though the ultrasound testing increase moderately before point C, where there is a large increase. The microscope images found that there was only visual confirmation of crack growth after the fatigue life had exceeded 50% (for this sample around 6500-7500 cycles). This implies that there is potentially a critical crack length that results in a large increase in the nonlinear response. Another factor that may affect results is that the theoretical model assumes a constant crack growth rate whereas the actual crack growth rate varies throughout the fatigue life of the material. Improvements can be made to crack size detection of the method by increasing the frequencies which result in higher resolution.

There are many factors that affect the experimental results, such as temperature changes that may affect the piezoelectric sensor and/or material, positioning of sensors, the type of sensors used, fatigue machine accuracy, resonance frequencies may be slightly different from sample to sample, amplification, hidden defects in samples, crack growth variation between samples, lab conditions may change daily, and piezoelectric sensor bonding and fatiguing. Considering the number of variables the results are encouraging.

Fixing the position of the sensors allowed for clearer and more consistent results than those found using a gel coupled sensor. The advantages of fixed sensors are that the position of the sensors remained constant throughout the fatigue life of the coupon and the initial contact between the two surfaces was more consistent. However, fixing the sensors to the specimen did have some disadvantages; fatigue loading can results in sensor damage and fatigue could results in a reduction in the bonding of the sensor and specimen. Thus sensors were located in low stress concentration areas relative to the high stress concentration areas (holes).

Sensors were removed when the sample was near failure, and replaced with new sensors exhibiting new bond conditions. There was no significant change in the sensors bond condition for the samples tested. Some of the highlighted factors could clearly generate nonlinear effects disguising the real nonlinear signature of the fatigue process, however, carrying out the experiments in the above mentioned procedure would simulate a real situation where PZTs would be permanently attached to a structure for structural health monitoring, while allowing for bonding condition evaluation.

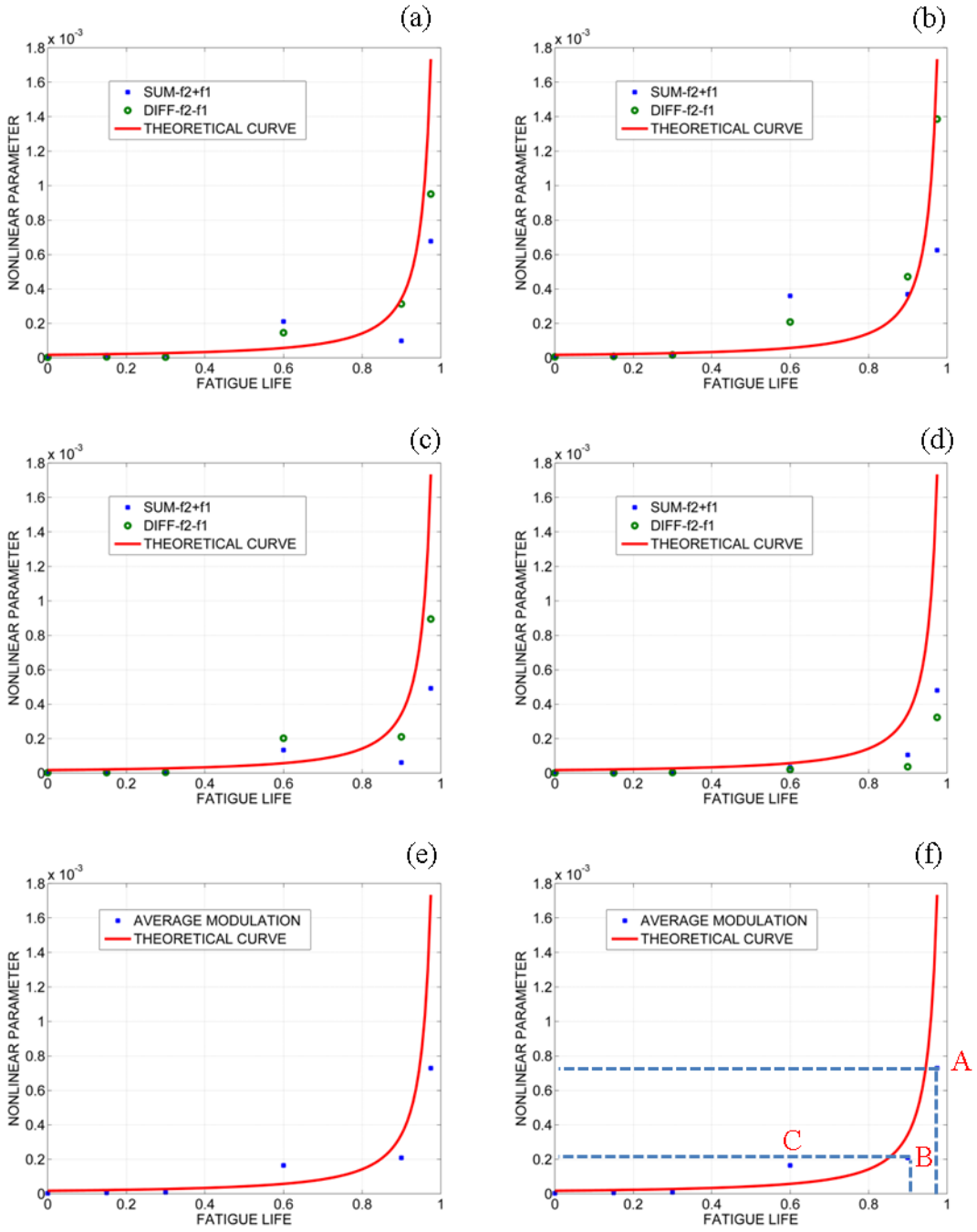

Figure 4.11. Experimental vs Theoretical Results against fatigue life percentage Sample 1. (Plot (a): 24 & 585 kHz, Plot (b): 34 & 405 kHz, Plot (c): 34 & 585 kHz, Plot (d)4: 94 & 405 kHz, Plot (e): Average of all results, Plot (f): Application of NWMS method).

4.1.7. Conclusion

The objective of this research was to develop a new technology, based on the principles of nonlinear elastic wave spectroscopy (NEWS) for accurate detection of accumulated fatigue damage and residual fatigue life estimation of an aircraft structure. A novel nonlinear wave modulation technique was developed, where an ultrasonic probe signal was generated by modulating two optimised waves coupled to analytical models to find the relationship between nonlinear parameters and the residual fatigue life.

The theoretical and experimental data demonstrate that the estimation of residual fatigue damage could be obtained using the proposed nonlinear wave modulation spectroscopy method. The results found good correlation between the experimental data and the theoretical model. In terms of the usability and affordability requirements, the suggested method has great potential to be scaled-up to industrial level, although further work is needed to develop the algorithms further.

Transfer of the method and algorithms onto portable c-scan and phased array equipment is possible and given accurate detection (through further development) of fatigue accumulated damage the price/performance ratio could be highly advantageous for military applications and would result in a reduction of unforeseen in-service failures. This research demonstrated the feasibility of the proposed nonlinear techniques and supporting models to detect widespread fatigue damage and predict residual fatigue life. The technology can be used during field maintenance of military aircraft and other structures that are subject to fatigue damage.

4.2. Modelling and Validation of Nonlinear Elastic Behaviour in Fatigued Structures

There is still a lack of numerical models available in commercial finite element analysis (FEA) tools that are able to simulate the interaction of elastic waves with the nonlinear behaviour of the material. In this study, a nonlinear constitutive material model was developed to predict the structural response under continuous harmonic excitation of a fatigued isotropic sample that showed anharmonic effects. This section provides a brief summary of the experiment and results, the full paper submitted to the Journal of Sound and Vibration (awaiting review) can be viewed in Appendix 2.

This work involved collaboration between many researchers at the University of Bath, and in recognition of the many hard hours spent special thanks goes to: (i) Dr. Francesco Ciampa for development of the Numerical and Nonlinear Finite Element Theory, (ii) Dmitri Ginzburg for implementation and simulation of the Nonlinear FEA model in LS-DYNA, and (iii) Efe Onder for experimental work which included fatigue and ultrasound testing. The contribution of the author included the development of the ultrasound and fatigue testing methodology as well as the collation of the various contributions by the other researchers. The work completed in Section 4.1 provided vital information about the determination of PZT locations, excitation frequencies and general testing procedure as well as the compilation of the various theoretical and experimental results.

An aluminum (Material D – refer to Appendix 1) dogbone structure was fatigued to failure, at multiple points throughout the fatigue process ultrasound testing was conducted in order to evaluate the experimental second order nonlinearity parameter (G_{2E}). G_{2E} saw an increase as the size of the fatigue crack grew and the residual fatigue life reduced. This was expected as further harmonics (second and third) can be directly related to damage or the increase in damage [193-195]. It has also been found in other studies that the second order nonlinearity parameter G_{2E}, determined by relating the fundamental frequency and nonlinear second harmonic response, increases as crack propagation increases over the fatigue life of a component [196]. The experimental design and setup was used to validate further harmonic generation, the magnitude of G_{2E}, the crack size and the fatigue life percentage of the component. This was confirmed during the study and is highlighted in Appendix 2.

The development and implementation of the finite element model within LS-DYNA (Dr. Francesco Ciampa and Dmitri Ginzburg) allowed for the assessment of the numerical model to predict the generation of the second harmonic produced by a given crack size. Landau's theory and Kelvin tensorial representation used by the developed model provided an understanding of the elastic nonlinear phenomena in this case the second harmonic generation in 3D media. This numeric model was then applied to a nonlinear response area (NRA) which was a 3D area used to simulate the cracked region. This process required the insertion of the experimental nonlinear parameter (G_{2E}) within the numerical model. By adjusting the size of the NRA (modelled cracked

region) within the FEA model it was possible to assess whether the crack lengths used in the model agreed to experimental crack measurements (determined using microscopic evaluation of the dogbone specimens at various points throughout its fatigue process).

The results revealed that the modelling of the nonlinear elastic effect using the determined model correlated well to experimental results. Therefore the model developed provides the first step in potential FEA methods which will allow: the incorporation of nonlinear ultrasound effects in modeling, the assessment of the generation and dispersion of nonlinearities due to damage in complex structures, the generation of more complex and realistic models and estimation of residual fatigue life of components without baseline tests.

5. NOVEL THERMOSONIC EVALUATION OF A COMPOSITE STRUCTURE

This chapter assesses the ability of a novel thermosonic method to evaluate barely visible impact damage (BVID) in composite materials. The ever increasing use of CFRP composite materials across a wide range of engineering fields has led to greater focus on the determination of the presence and location of defects and/or damage in these materials. The assessment of such materials becomes difficult under low impact damage as there may be very little surface damage but beneath the surface delaminations occur which can significantly reduce the materials strength. This type of damage is generally referred to as BVID and can be caused during manufacturing as well as in service. Due to the hidden nature of BVID composite materials must be regularly inspected, thus inspection should ideally be quick and cover large areas.

The method developed relies on the dual frequency excitation of damaged regions, where the excitation frequencies are determined by using fundamental principles of nonlinear ultrasound testing techniques. The excitation frequencies are considered to be damage-specific resonance frequencies which excite and heat the damaged regions. The novelty of the process lies in its ability to identify the damage specific excitation frequencies and the dual frequency excitation method which should result in defects (cracks, delaminations) clapping/rubbing together thus generating heat that can be observed using an IR camera. Other advantages of thermosonics include: less sensitive to noise (as excitation of sample can be controlled) and have good potential for automation.

Thermosonics falls under thermographic NDT/E techniques which have the potential to provide quick evaluation of damage in materials. Other methods and their associated disadvantages include pulsed laser spot thermography, which can only be used for surface crack evaluation (2mm long, 1 mm deep, and 1μm opening), with inspection confined to comparatively small areas. Pulsed eddy current thermography has a restricted inspection area due to the non-uniformity of the eddy current distribution induced by the excitation coil.

Techniques such as lock-in and transient thermography are only capable of detecting BVID close to the sample surface, up to 2mm, this limitation means that only thin composite components or situations where damage lies on the surface are applicable. Other methods such as vibration excitation shearography (or speckle pattern shearing interferometry) measure the out-of-plane displacement gradient of a sample's surface, relying on defects altering the material response to an applied stress (such as vibration excitation using a piezoelectric transducer). Disadvantages of these methods are the lengthy time taken to determine the excitation frequencies and plate modes can hide damaged regions.

Active traditional thermography (heating or cooling methods) suffer from inadequate sensitivity to small defects, due manufacturing processes and safety standard requirements these

methods are becoming less effective. Another factor with these techniques is that the methods tend to be subjective and do not provide easy adaptation to an automated defect detection process. Contrast-based methods which focus on subtracting reference pixels or pixel groups from time history of each pixel in the image in order to determine a contrast of the temperature time history of the area, require the identification of defect free areas to provide a reference point, which is not always possible. Other general limitations such as requiring low signal to noise ratios, large dynamic ranges (pulses of energy used to heat sample), high processing powers (computer), storage space and memory make these applications difficult for in field work and automation.

New promising techniques such as pulse phase and thermographic signal reconstruction look to evaluate subsurface conditions by the examination of the time history of pixels independently, while traditional techniques focus on visual or numerical identification of changes in surface temperature contrasts, these methods have provided some benefits in terms of the measurement of size of defects and effects of noise on detection limits [214].

Thermographic techniques have been estimated to be up to 30 times quicker than underwater ultrasonic c-scan techniques, illustrating the ability to rapidly inspect large areas of composite materials [197]. Thermal NDT/E relies on the generation of thermal waves in the sample which allow transient thermal images of the sample to be captured [197], the theory of heat conductivity including differential equations on the propagation of thermal waves has been extensively discussed by Almond, et al. (1996) [198].

The method developed uses a nonlinear ultrasound method to determine the damage-specific resonance frequencies (DSRF) in order to evaluate BVID in composite materials. Given that the production of further harmonics can be related to damaged regions, the second harmonic (twice the excitation frequency) was measured over a range of frequencies for the given test pieces in order to assess which frequencies gave rise to the largest second harmonic amplitudes. This found which excitation (fundamental) frequency gave the highest levels of clapping/rubbing of the damaged region, and thus heating. By using a dual frequency DSRF method it is expected that the ability to excite defect and damage regions will be amplified. This study provides a preliminary testing technique that has shown some great advantages over other techniques.

5.1. Equipment

A waveform generator (TTi-TGA12104) was connected to an amplifier (Piezoshaker-Amplifier HVA-DB100, includes vacuum pump) and piezoelectric transducer (Piezoshaker PS-X-03-6/1000) in order to provide vibration excitation ranging from 0 to 100kHz. A vacuum pump and sucker attachment was used to attach the transducer to the test samples. The infrared camera used was a mid-wavelength infrared device (CEDIP Jade 3 MWIR 3-5 μm) that uses an electrically cooled indium antimonide detector and has a frame rate of up to 150 Hz, a resolution of 320 x 256 pixels (vertical x horizontal) average NeDT of 30mK. A dual frequency sinusoidal continuous wave form was generated and used to excite the defect while thermal images were recorded by the camera. Two piezoelectric sensors were used to determine the DSRF, the excitation sensor was located at position A (PZT-Panametrics NDT X1020 100kHz 515345) while the signal was captured at position B (PZT-Panametrics V101 0.5MHz 707718, refer to Figure 5.1(b)). The waveform generator was used to generate the output signal sweep from sensor A, while sensor B was connected to a Picoscope oscilloscope and PC.

5.2. Test Sample

Two rectangular samples of CFRP were tested. Both samples (Sample 1: A22, Sample 2: A31, Material E – refer to Appendix 1) consist of 24 layers of prepreg with quasi-isotropic orientations $[0°/45°/90°/-45°/0°/45°/90°/-45°/0°/45°/90°/-45°]_s$ (A22) and $[0°/15°/30/°/45°/60°/75°/90°/-75°/-60°/-45°/-30°/-15°]_s$ (A31). They were subjected to low velocity impact damage (8-10 Joules). The damage caused a small perturbation on the bottom surface and a dent at the point of impact on the top surface, thus classified as BVID.

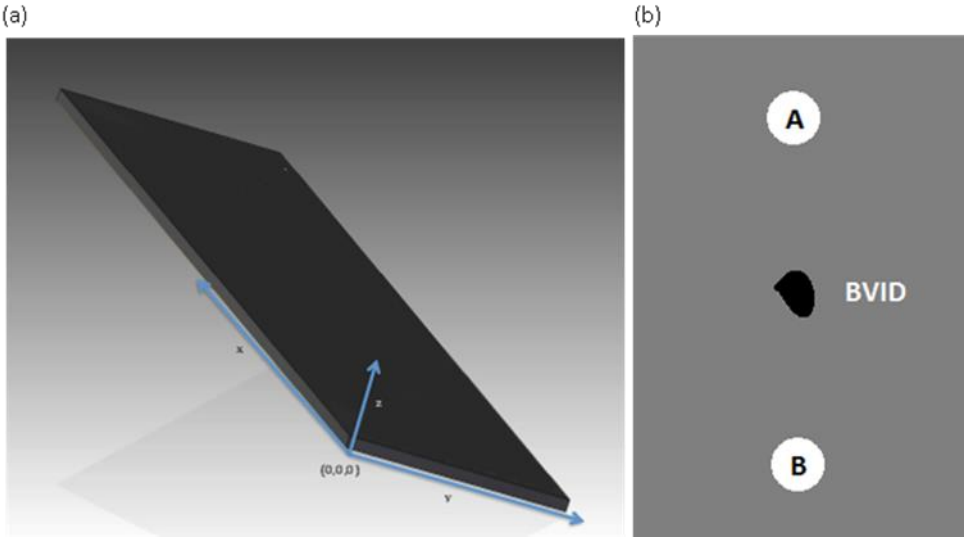

Figure 5.1: CFRP Structure (a) and PZT locations (b)

5.3. Thermosonic Testing using DSRF

A frequency sweep was conducted using frequency bands of 20kHz from 20kHz up to 100kHz in order to determine the DSRF, which were evaluated by using the fundamental frequency of the highest second harmonic response. The DSRF were used when conducting the thermosonic tests, by pairing two frequencies together. The test samples were painted with black paint to increase their emissivity/absorptivity and to reduce their reflectivity before being tested using thermosonics. The images captured using the infra-red camera were processed off-line using a commercial software package (MATLAB R2013b, The MathWorks Inc., Natick, MA, US, 2013), a background subtraction method was used and images were averaged over period of 1s (12 frames). Figure 5.2 to Figure 5.5 display the results from Sample 1 (A22) for various frequency pairs and excitation times.

Figure 5.4 shows the results for Sample 2 (A31). It is clear to see from Figure 5.2(a) and (b) (A22) that the impact damage has resulted in two areas of damage on either side of the impact point, and only one damage region located at the impact point in Figure 5.4(a) and (b) (A31). Regions A and B highlighted in Figure 5.2(a) (and in the other figures) relate to damage, whereas region C relates to heat generated by the piezoelectric transducer (PZT) (attached to the back surface). The PZT generated heating in the area in which it was attached. As this heating would hide any damage located directly below it, the sensor was placed to the side of the specimen away from the centrally located damage. The tests were initially run for long time periods in order to: (i) assess the amount of time needed to accurately find the damaged regions, and (ii) whether longer testing periods would increase the accuracy of the results. Figure 5.2(a) and (b), show the temperature evolution of the damaged region over time, Figure 5.2(c) and (d) establish the temperature change for the areas that contain damage and Figure 5.2(e) examines the change in temperature due to heating from the PZT. Figure 5.2(c) and (d) highlight that there is a large change in temperature in the damaged zones after a very short period of time (highlighted zones in figure), which shows the effectiveness of the method to quickly determine damage. After the initial large increase in heat at the damaged areas the temperature increases linearly, therefore suggesting that there are no advantages gained from longer testing periods for a given excitation power. Figure 5.2(e) shows that the temperature in position C is due to the externally applied heat from the PZT as the temperature rises linearly from the beginning of the testing period.

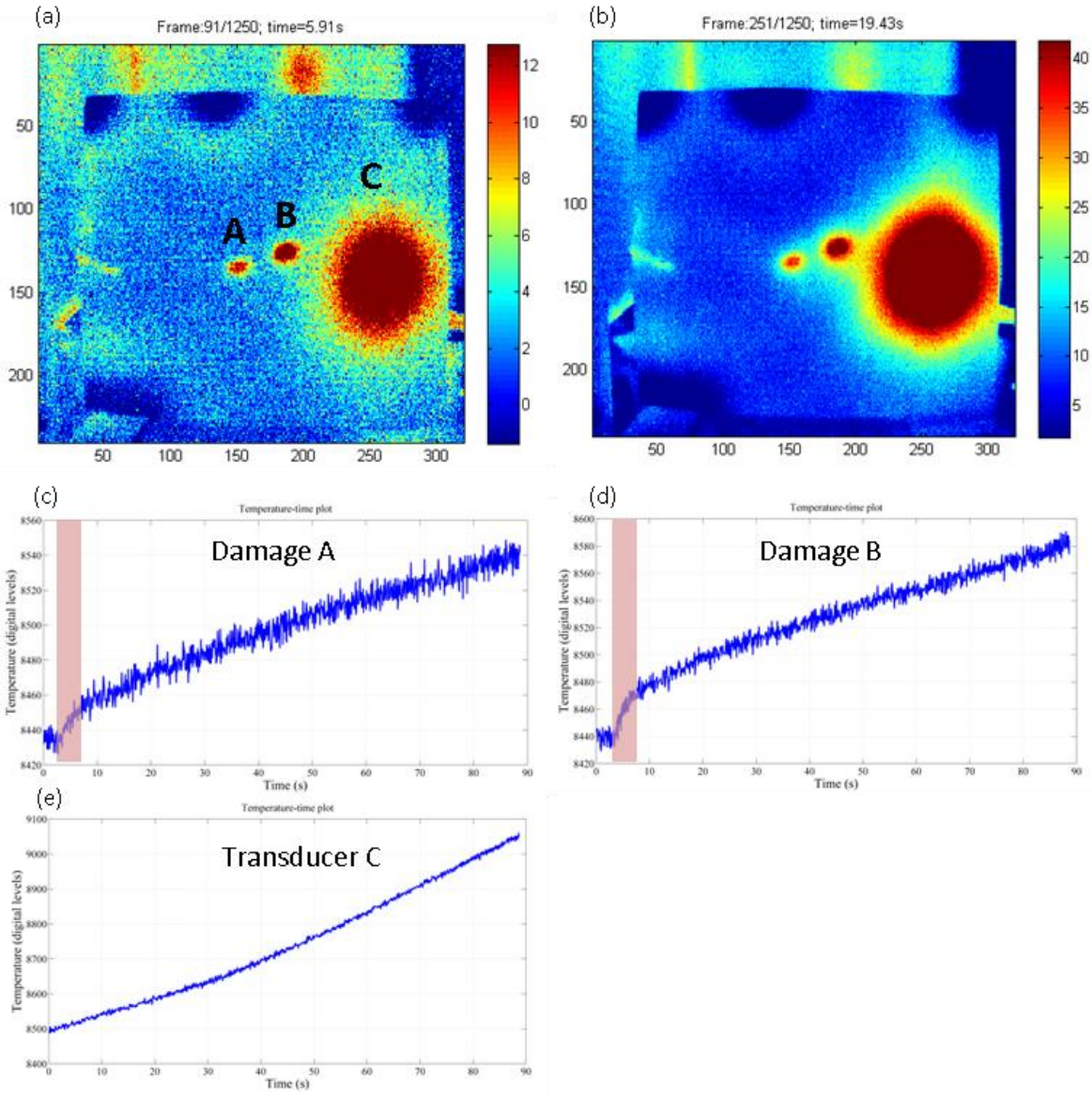

Figure 5.2: Dual Frequency 26kHz and 67kHz pair (Sample 1 (A22)): (a) time = 5.91s, (b) time = 19.43s, (c) change in temperature vs. time for damage area A, (d) change in temperature vs. time for damage B, (e) change in temperature vs. time for area heated by PZT.

Figure 5.3 shows the relative temperature change (in digital levels) for damaged areas A and B, across a 2-D plane. Two planes are highlighted for each damaged area (X and Y), and it is clear to see that there is a large resultant temperature change across the damage region relative to undamaged regions. The change due to the transducer is clearly visible located between 200 to 300 pixels in the X-plane. The effectiveness of the method to locate the damaged regions is clearly highlighted in Figure 5.3(e) and (f), which exclude the heat produced by the transducer as they show y-profiles.

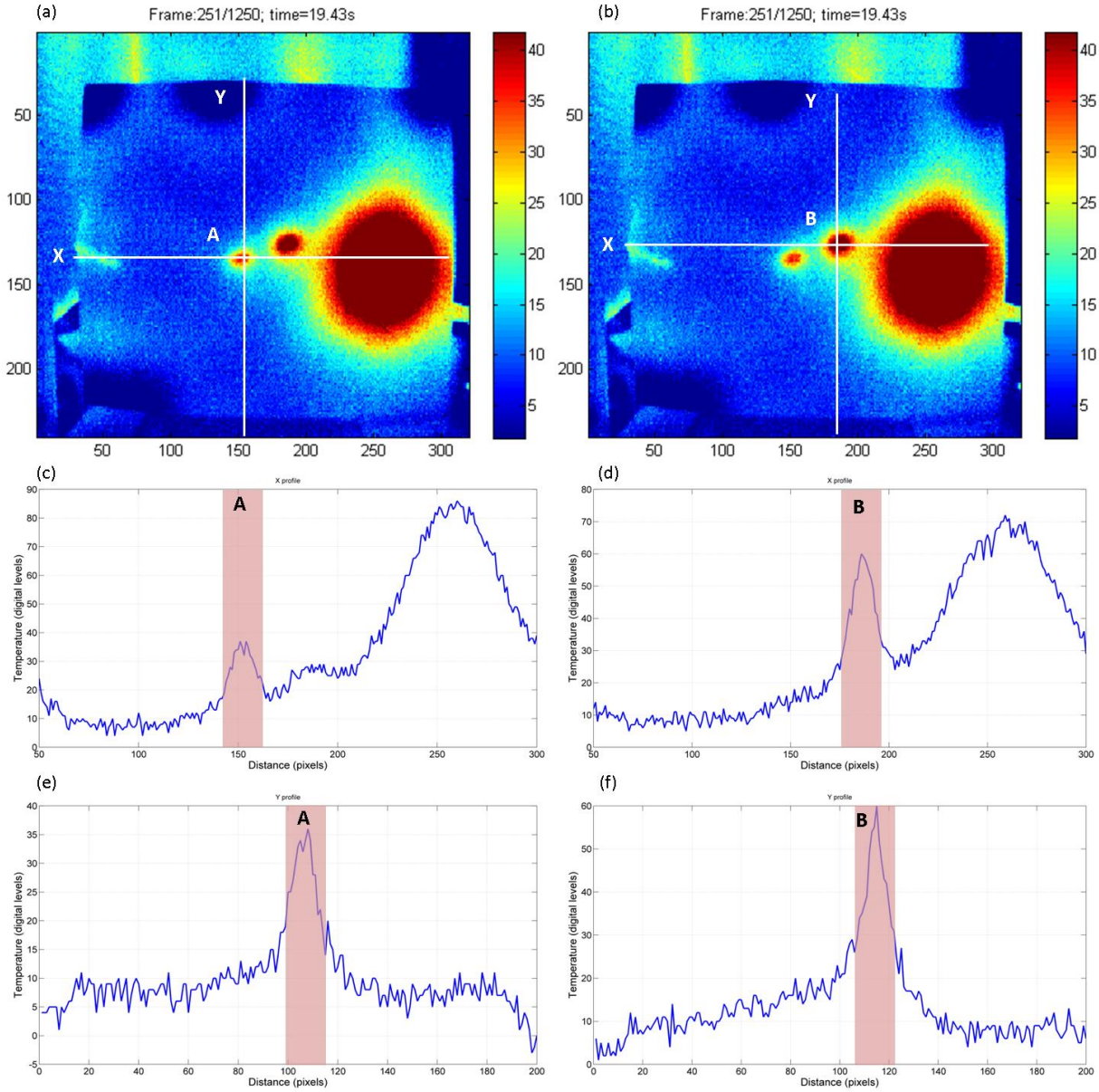

Figure 5.3: Relative temperature variation: (a) X and Y planes for damage A, (b) X and Y planes for damage B, (c) X plane temperature profile for damage A, (d) X plane temperature profile for damage B, (e) y plane temperature profile for damage A, (d) y plane temperature profile for damage B.

Figure 5.5 (below) highlights the difficulties of damage detection, and the advantages of using the novel dual-frequency DSRF method. Figure 5.5 confirms that both damage regions were found with the 50kHz and 70kHz frequency pair (Figure 5.5(a)) and the 67kHz and 70kHz (Figure 5.5(c)) frequency pair, although the 50kHz and 67kHz (Figure 5.5(b)) pair only illuminated one damaged region. These results show the importance of accurately determining the DSRF, as damage regions respond differently to different excitation frequencies.

By combining 67kHz and 70kHz, both damaged regions are clearly indicated (Figure 5.5(c)), this suggest that the initially determined DSRF of 50kHz may be invalid. There are a number of possible reasons why heating does not occur at 50kHz. One reason is that the amplitude of the second harmonic response at 50kHz was lower than other harmonic responses found (i.e. at 26kHz

and 67kHz), thus leading to reduced excitation of the damaged region and ultimately insignificant conversion of energy to generate heat. Also, the determined frequency could be a false DSRF and does not excite the damaged area (due to equipment errors and response of material). This draws attention to the difficulties in determining which harmonic responses are actually true DSRFs.

Figure 5.4 shows the results for Sample 2 (A31) for two different frequency pairs. The BVID resulted in one main damage region which was easily located using the dual frequency method.

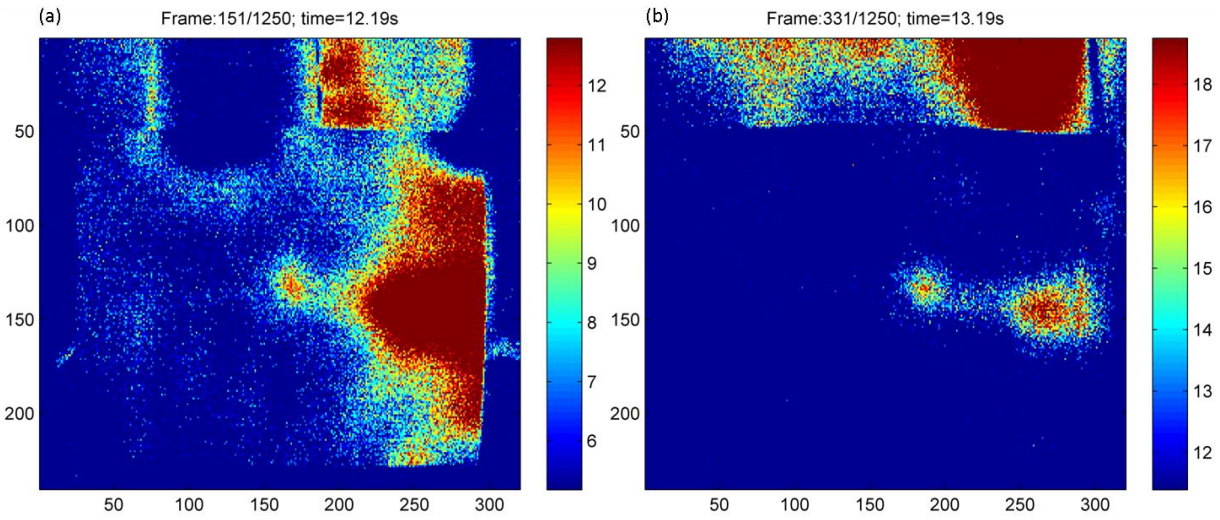

Figure 5.4: Dual Frequency: (a) 35kHz and 81kHz pair Sample 2 (A31), (b) 28kHz and 81kHz pair Sample 2 (A31).

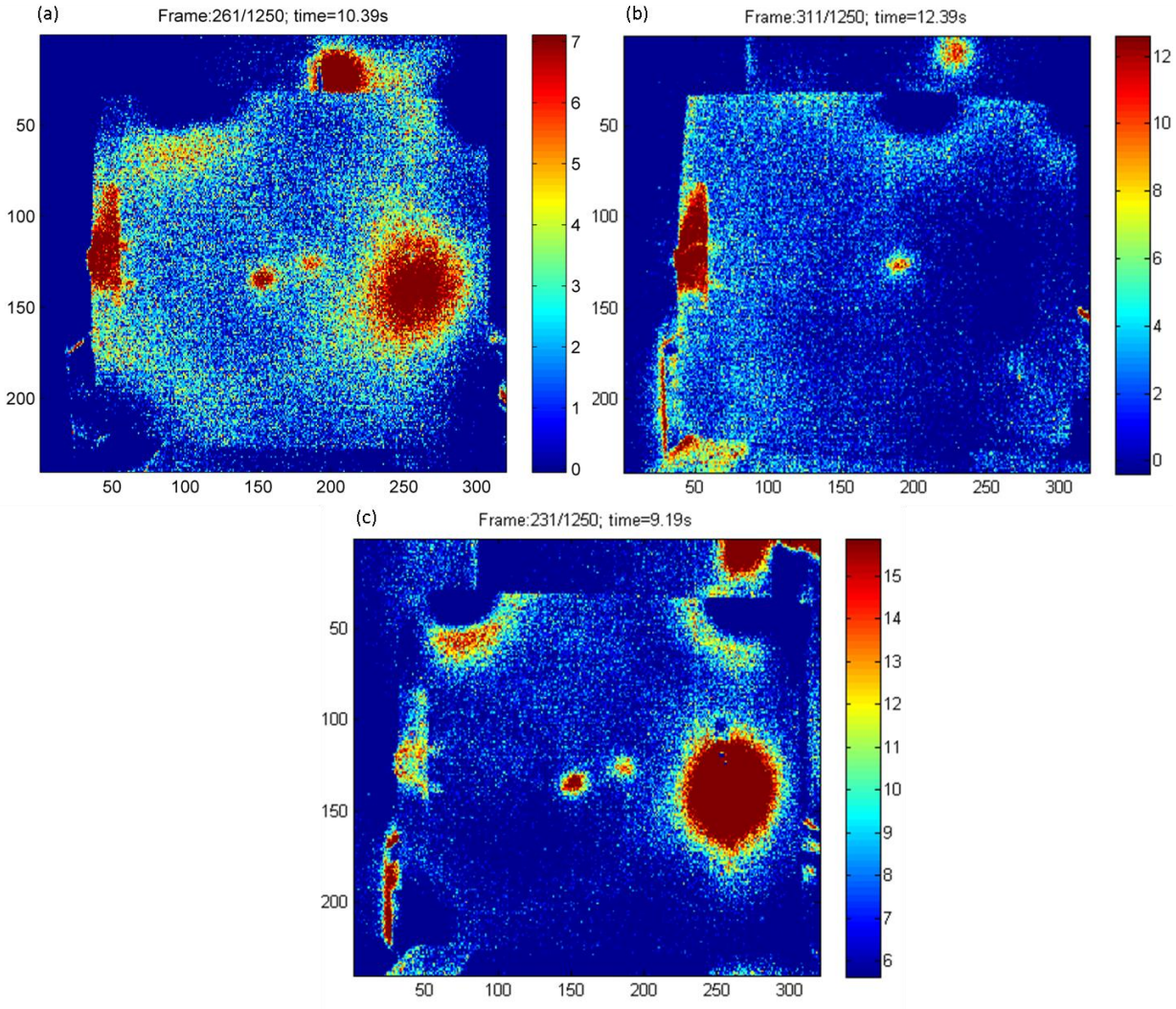

Figure 5.5: Dual Frequency: (a) 50kHz and 70kHz pair Sample 1 (A22), (b) 50kHz and 67kHz pair Sample 1 (A22), (c) 67kHz and 70kHz pair Sample 1 (A22)

5.4. Conclusion

The method proposed provides a quick and accurate technique to locate BVID in CFRP structures. The work highlights a novel nonlinear dual-frequency thermosonic method for the detection and location of damage. It requires the detection of damage-specific resonance frequencies (DSRF) in the specimen (produced by the nonlinear harmonic response of damage regions) and employs a dual-frequency excitation method. The method relies on the principles of nonlinear ultrasound testing techniques, where excitation of a damaged region by a fundamental frequency gives rise to further harmonics. By assessing the production of these further harmonics, which are a result of clapping/rubbing mechanisms (damage), it is possible to determine the DSRF. The excitation of the damage at the chosen DSRF results in heat generated by the clapping and rubbing of damage interfaces, these changes in temperature can then be assessed using an infra-red camera.

The method also provides some advantages over single frequency testing techniques as the discovery of damaged regions are more likely using the outlined nonlinear dual-frequency DSRF method than single frequency methods and dual frequency excitation improves the probability of damage detection while reducing the number of tests required. The method can also highlight hidden damages that single frequency methods may miss.

Other advantages include the quick determination of DSRFs and dual-frequency pairs which lead to quick application and damage finding. The potential to automate the process could result in faster testing when compared with other thermosonics methods and other optical methods such as shearography.

Further work should establish the minimum excitation power required to generate accurate results, sensitivity of damage detection relating to the distance between the PZT and damaged region and application of more than two (dual frequency) DSRFs concurrently. Other work should also focus on determining the size of damaged areas by comparing thermosonic results with size measurements from surface profilometry techniques.

6. CONCLUSIONS AND FUTURE WORK

6.1. Concluding Remarks

This thesis explores a broad range of nonlinear testing techniques from single to dual frequency excitation, to fatigue life and thermosonic evaluation of structures. The primary objective of the research was to develop new and innovative nonlinear ultrasound techniques that were both accurate and robust. Four main problem areas were focused on: the assessment of loaded structures (joints, kissing bond evaluation), evaluation of the health of a bolted structure (tension joint), nonlinear methods to assess the fatigue life of structures and incorporation of nonlinear principles into other NDT fields to yield better results.

These problem areas are found throughout many engineering disciplines and the adaptability and suitability of the nonlinear ultrasound techniques developed shows the great potential for this relatively new technique.

Primary analysis focused on developing a thorough understanding of the key factors affecting the response and accuracy of nonlinear techniques in order to do so multiple testing techniques (single and dual frequency excitation methods, transmission and reflection) and nonlinear parameters (second, third, modulated nonlinear parameters and nonlinear acoustic moments) were evaluated and tested using various experimental setups.

The results for all the aforementioned tests and techniques have provided very positive findings for the large range of applications, highlighting the flexibility of nonlinear ultrasound techniques to many engineering problems.

6.2. Key Factors Affecting Nonlinear Techniques and New Applications

Chapter 3 develops a new novel resonance frequency nonlinear ultrasound testing method as well as exploring other methods such as modal analysis for improvement of test results. With the main aim to improve accuracy in the measurement of nonlinear responses due to damage by exciting structures and damaged regions at their resonance frequencies. A rig was designed to explore the robustness of the method to determine the presence of kissing bonds and cracked regions. The effectiveness of the method was assessed by comparing amplitudes of nonlinear responses, variation of responses, and the hysteretic responses. Hysteresis was assessed for single and dual-frequency nonlinear ultrasound methods, in order to determine whether variance in defect hysteresis can be alleviated depending on testing techniques such as resonance frequency testing. By exploring the nonlinear hysteretic response at resonance and non-resonance frequencies as well as taking into account modal analysis results, it was shown that results could be greatly improved.

Furthermore, the effect loading has on the 'clapping mechanism' and nonlinear parameters were assessed and it was found that there was a decrease in these parameters as pressure increased. These results were expected as clamping together a defect reduces the production of further harmonics by reducing movement ('clapping'). An increase in the voltage of the fundamental signal as load increased showed that the effects of load on the 'clapping mechanisms' could be reduced.

A nonlinear acoustic moments method was developed to improve testing accuracy of loaded structures. It was shown conclusively that the relationship between the further harmonic moments (second and third) and the fundamental frequency decreases as load increases. It also built a simple framework for damage detection using this methodology for constant compression loaded structures, variable compression loaded structures, kissing bonds and joint evaluation. The study also established that an increase in damage can be determined by an increase in the ratio of the nonlinear moment and fundamental frequency moment at a selected load. Suggesting that this relationship can be applied to a component where testing may take place when different loading conditions exist. The main advantages of the method were that it is quick, simple and easy to setup and regulate. The method can be carried out on many components in many engineering fields, with preliminary results suggest that high accuracy can be achieved through further development of the methodology and testing. The simplicity of the method is one of its main driving factors.

The nonlinear methods were tested on both metallic and composite structures and provided good results regardless of the material. Composite materials have complex failure modes and are susceptible to damage from low velocity impact, this coupled with the fast adoption of these materials leaves a large capacity for adequate structural health monitoring systems. The tests conducted throughout this thesis suggest that nonlinear ultrasound techniques can be applied to a number of materials with substantially varying properties and still provide accurate results, as the nonlinear principles do not change.

Finally after evaluating the fundamental issues affecting nonlinear ultrasound techniques, the methods were used to evaluate a tension joint that fixes a wind turbine blade to the hub. In many engineering fields where bolts are used to fasten structures, loosening can lead to failure. A broad range of testing techniques were conducted on the bolted structure which provided good results.
The methods tested were:

(i) Linear, damping curve responses and time domain signal response energy.

(ii) Nonlinear techniques (G_{2E}, G_{3E}, $R_{f2/f1}$ and $R_{(f2+f3)/f1}$). There was a vast array of testing approaches, such as: (i) continuous (nonlinear testing) and discrete excitation signals (PBF).

(iii) Two different types of PZTs were used and multiple sensor locations were evaluated.

The advantages of the nonlinear methods results over the linear techniques were that they found larger magnitude changes as torque decreased (loosening of bolt), which provided greater certainty that responses were in fact due to the loosening of the bolts. It was also possible to assess the individual bolt loosened state and multiple nonlinear evaluation techniques provided good results.

This research provides and important step in terms of possible SHM systems that can be employed *in-situ* on large scale wind turbines (or any other bolted structure). The fact that only two sensors need to be used to monitor the state of four bolts provides great improvement to current techniques that are available today, and would provide large cost savings if such a system were to be implemented.

6.3. Fatigue Testing and Modelling of Nonlinear Ultrasound

Fatigue failure is a great threat to many engineering structures and possibly one of the most difficult failure mechanisms to predict accurately. Current methods simple replace structures/components that are likely to fatigue after a predetermined maximum number of cycles. This process leads to high costs associated with the maintenance and replacement of the parts, but more importantly in cases where failure occurs early the consequences can be catastrophic. A large proportion of the research focused on developing a baseline-free nonlinear ultrasound method, with the aim of predicting the residual fatigue life of a material. This study developed a modulated nonlinear elastic wave spectroscopy (NEWS) method for the evaluation of a metallic components residual fatigue life. An aluminium specimen (AA6082-T6) was tested at predetermined fatigue stages throughout its fatigue life using a dual-frequency ultrasound method. A modulated nonlinear parameter was derived, which described the relationship between the generation of modulated (sideband) responses of a dual frequency signal and the linear response. The sideband generation from the dual frequency (two signal output system) was found to increase as the residual fatigue life decreases, and as a standalone measurement method it can be used to show an increase in a materials damage. A baseline-free method is developed by linking a theoretical model, derived by combining the Paris law and the Nazarov-Sutin crack equation, to experimental nonlinear modulation measurements. The results found good correlation between the derived theoretical model and the modulated nonlinear parameter, allowing for baseline-free material residual fatigue life estimation.

After gaining a substantial understanding of fatigue assessment using nonlinear ultrasound techniques the following investigation focused on modelling the nonlinear response using a user defined material constitutive model and validating it through fatigue life experimentation. The developed nonlinear constitutive material model could predict the production of further harmonics directly related to the extent of damage within a material. The material constitutive model was developed in LS-DYNA that could replicate and relate the production of further harmonics to a

predefined nonlinear response area (NRA); this allowed for the estimation of the second harmonic when taking into account the experimental G_{2E} value and an estimation of damage progression related to the numeric generation of the second harmonic.

The direct correlation between the generation of the second harmonic, damage, and the ability of the model to calculate the second harmonic showed that it can provide useful information about the growth of damage within a component. The G_{2E} derived experimentally was used within the model in order to assign nonlinear characteristics to known high stress regions or damaged regions, this allowed for the estimation of the second harmonic for various sized NRA's. Good correlation between the numerical prediction and experimental results were found for the prediction of the second harmonic.

The results of this experiment suggest that it is possible to generate FEA models based on nonlinear ultrasound theory and material models that would be able to estimate damage without baseline tests of components. The robustness of the method relies on the comparison of the experimental and the numerical results, which showed good correlation.

6.4. Thermosonics

Finally, the general principles governing nonlinear ultrasound techniques were applied to a thermosonic testing setup in order to expedite and improve testing results. The investigation explored a novel thermosonic technique that used a dual-resonance frequency testing method for the evaluation of barely visible impact damage (BVID). The method initially determines the damage-specific resonance frequencies (DSRF) of a low impact damaged CFRP test specimen. The quick evaluation of the DSRF is one of the main advancements of this method. The test procedure then uses combinations of two of these resonance frequencies to determine the location of the impact damage by exciting the material using a PZT and capturing the change in surface temperature using an infrared camera. The damage-specific resonance frequencies are found by evaluating which fundamental frequency corresponds to the highest harmonic response.

The advantage of this developed technique is that the DSRFs can be assessed very quickly and excitation of the damage region by two frequencies increases the chance for damage detection. The dual frequency excitation method provides significant advantages over single frequency excitation as it is possible to miss damaged regions when only using a single frequency and thus dual frequency excitation increases the chances of damage detection. The repeatability and control offered by the method provides further benefit.

6.5. Future Work

There is a great potential for future work regarding the techniques developed and the areas explored by this thesis. Fatigue testing and more importantly a baseline free method, would provide a great leap forward in testing techniques. The current method provides a good base point but further testing and development is required, such as; the development of the algorithms, *in-situ* testing, increased complexity of the structure and application of other nonlinear techniques. The testing technique should also be broadened to include the assessment of a baseline free method that involves the use of Lamb waves, as this may provide more detailed and accurate results.

The last study involving thermosonics has great potential to provide quick, accurate and automated evaluation of damage in composites. The method can simply be extended by exciting the structures with three, four, or even eight fundamental frequencies rather than only two. By increasing the number of excitation frequencies it is expected that there will be an even greater possibility for damage detection. It should lead to more accurate and quicker testing with a reduction in the possibility of missing damaged regions. Further work should also establish minimum excitation power required to generate accurate results and sensitivity of damage detection relating to the distance between the PZT and damaged region. Other work should also focus on determining the size of damaged areas by comparing thermosonic results with size measurements from surface profilometry techniques.

7. REFERENCES

[1] C. Chen, *Ultrasonic and advanced methods for nondestructive testing and material characterization*: World Scientific Pub Co Inc, (*2007).*

[2] Y. Bar-Cohen, *In-Service NDE of Aerospace Structures–Emerging Technologies and Challenges at the end of the 2nd Millennium*. *NDT. net*, vol. **4(9)**, pp. 1–21, 1999.

[3] K. Tan, N. Guo, B. Wong and C. Tui, *Experimental evaluation of delaminations in composite plates by the use of Lamb waves*. *Composites Science and Technology*, vol. **53**, pp. 77-84, 1995.

[4] M. Lemistre, R. Gouyon, H. Kaczmarek and D. Balageas, *Damage localization in composite plates using wavelet transform processing on Lamb wave signals*. *Office National D Etudes Et De Recherches Aerospatiales Onera-Publications-TP*, 1999.

[5] M. Meo, U. Polimeno and G. Zumpano, *Detecting Damage in Composite Material Using Nonlinear Elastic Wave Spectroscopy Methods*. *Applied Composite Materials*, vol. **15**, pp. 115-126, 2008.

[6] K. Y. Jhang, *Nonlinear ultrasonic techniques for nondestructive assessment of micro damage in material: A review*. *International Journal of Precision Engineering and Manufacturing*, vol. **10**, pp. 123-135, 2009.

[7] J. Achenbach, W. Lin and L. Keer, *Mathematical modelling of ultrasonic wave scattering by sub-surface cracks*. *Ultrasonics*, vol. **24**, pp. 207-215, 1986.

[8] Y. Angel and J. Achenbach, *Reflection and transmission of elastic waves by a periodic array of cracks: oblique incidence*. *Wave motion*, vol. **7**, pp. 375-397, 1985.

[9] R. Green Jr and S. Letcher, *Treatise on Materials Science and Technology, Vol. 3: Ultrasonic Investigation of Mechanical Properties*. *Physics Today*, vol. **27**, p. 55, 1974.

[10] S. B. Kim and H. Sohn, *Instantaneous reference-free crack detection based on polarization characteristics of piezoelectric materials*. *Smart Materials and Structures*, vol. **16**, p. 2375, 2007.

[11] J. Krautkramer and H. Krautkramer, *Ultrasonic testing of materials*. *Springer- Verlag New York, Inc. 1977, 667 p(Book).* 1977.

[12] T. Kundu, *Ultrasonic nondestructive evaluation: engineering and biological material characterization*: CRC press, (*2004).*

[13] W. Morris, O. Buck and R. Inman, *Acoustic harmonic generation due to fatigue damage in high strength aluminum*. *Journal of Applied Physics*, vol. **50**, pp. 6737-6741, 2009.

[14] A. J. Hillis, S. A. Neild, B. W. Drinkwater and P. D. Wilcox, *Global crack detection using bispectral analysis*. *Proceedings of the Royal Society A: Mathematical, Physical and Engineering Science*, vol. **462**, p. 1515, 2006.

[15] D. M. Donskoy and A. M. Sutin, *Vibro-acoustic modulation nondestructive evaluation technique*. *Journal of Intelligent Material Systems and Structures*, vol. **9**, p. 765, 1998.

[16] D. Dutta, H. Sohn, K. A. Harries and P. Rizzo, *A Nonlinear Acoustic Technique for Crack Detection in Metallic Structures*. *Structural Health Monitoring-an International Journal*, vol. **8**, pp. 573-573, 2009.

[17] K. A. Van Den Abeele, P. Johnson and A. Sutin, *Nonlinear elastic wave spectroscopy (NEWS) techniques to discern material damage, part I: nonlinear wave modulation spectroscopy (NWMS)*. *Research in Nondestructive Evaluation*, vol. **12**, pp. 17-30, 2000.

[18] R. Truell, C. Elbaum and B. Chick, *Ultrasonic methods in solid state physics* vol. 13: Academic Press New York, (*1969).*

[19] J. Y. Kim, J. Qu, L. J. Jacobs, J. W. Littles and M. F. Savage, *Acoustic nonlinearity parameter due to microplasticity*. *Journal of Nondestructive Evaluation*, vol. **25**, pp. 29-37, 2006.

[20] T. Suzuki, A. Hikata and C. Elbaum, *Anharmonicity due to glide motion of dislocations*. *Journal of Applied Physics*, vol. **35**, pp. 2761-2766, 1964.

[21] A. Hikata, B. Chick and C. Elbaum, *Dislocation contribution to the second harmonic generation of ultrasonic waves*. *Journal of Applied Physics*, vol. **36**, pp. 229-236, 1964.

[22] P. Nagy, *Fatigue damage assessment by nonlinear ultrasonic materials characterization*. *Ultrasonics*, vol. **36**, pp. 375-381, 1998.

[23] J. Cantrell and W. Yost, *Acoustic harmonic generation from fatigue-induced dislocation dipoles*. *Philosophical magazine A*, vol. **69**, pp. 315-326, 1994.

[24] J. H. Cantrell, *Quantitative assessment of fatigue damage accumulation in wavy slip metals from acoustic harmonic generation*. *Philosophical Magazine*, vol. **86**, pp. 1539-1554, 2006.

[25] C. Pruell, J. Y. Kim, J. M. Qu and L. J. Jacobs, *Evaluation of fatigue damage using nonlinear guided waves*. *Smart Materials & Structures*, vol. **18**, pp. -, 2009.

[26] F. K. Chang, J. F. C. Markmiller, J. B. Ihn and K. Y. Cheng, *A potential link from damage diagnostics to health prognostics of composites through built-in sensors*. *Journal of Vibration and Acoustics*, vol. **129**, pp. 718-729, 2007.

[27] M. Lin and F. Chang, *Development of smart layer for built-in diagnostics for composite structures*. *Thirteenth Technical Conference of the American Society for Composites*, p. 1998, 1998.

[28] M. Tracy and F. Chang, *Identifying impacts in composite plates with piezoelectric strain sensors, part I: theory*. *Journal of Intelligent Material Systems and Structures*, vol. **9**, p. 920, 1998.

[29] Y. Roh and F. Chang, *Effect of impact damage on Lamb wave propagation in laminated composites*. *Dynamic response and behavior of composites*, pp. 127-138, 1995.

[30] S. Birch, *Aluminum space frame technology*. *Automotive Engineering;(United States)*, vol. **102**, 1994.

[31] C. Brotherhood, B. Drinkwater and S. Dixon, *The detectability of kissing bonds in adhesive joints using ultrasonic techniques*. *Ultrasonics*, vol. **41**, pp. 521-529, 2003.

[32] M. Klesnil and P. Lukáš, *Fatigue of metallic materials* vol. 71: Elsevier, (*1992).*

[33] J. D. N. Cheeke, *Fundamentals and applications of ultrasonic waves*. Boca Raton: CRC Press, (*2002).*

[34] B. J. W. S. Rayleigh, *The theory of sound*: Macmillan, (*1896).*

[35] L. Brillouin, *Tensors in mechanics and elasticity*: Academic Press New York, (*1964).*

[36] F. D. Murnaghan, *Finite deformations of an elastic solid*. *American Journal of Mathematics*, vol. **59**, pp. 235-260, 1937.

[37] A. Thuras, R. Jenkins and H. O'Neil, *Extraneous frequencies generated in air carrying intense sound waves*. *The Journal of the Acoustical Society of America*, vol. **6**, p. 57, 1934.

[38] I. Viktorov, *Effects of a second approximation in the propagation of waves through solids(Presence of growing second harmonics in finite amplitude wave propagation in solids)*. *SOVIET PHYSICS-ACOUSTICS*, vol. **9**, pp. 242-245, 1964.

[39] F. Rischbieter, *Messung der Nichtlinearen Schallverhltes von Aluminium mit Hilfe von Rayleighwellen*. *Acustica*, vol. **18**, pp. 109-112, 1967.

[40] P. Vella, T. Padmore, G. Stegeman and V. Ristic, *Nonlinear surface wave interactions: Parametric mixing and harmonic generation*. *Journal of Applied Physics*, vol. **45**, pp. 1993-2006, 2009.

[41] V. E. Gusev, W. Lauriks and J. Thoen, *New evolution equations for the nonlinear surface acoustic waves on an elastic solid of general anisotropy*. *The Journal of the Acoustical Society of America*, vol. **103**, p. 3203, 1998.

[42] R. E. Kumon and M. F. Hamilton, *Directional dependence of nonlinear surface acoustic waves in the (001) plane of cubic crystals*. *J Acoust Soc Am*, vol. **111**, pp. 2060-9, 2002.

[43] M. Deng, *Cumulative second-harmonic generation of Lamb-mode propagation in a solid plate*. *Journal of Applied Physics*, vol. **85**, pp. 3051-3058, 2009.

[44] W. de Lima and M. Hamilton, *Finite-amplitude waves in isotropic elastic plates*. *Journal of Sound and Vibration*, vol. **265**, pp. 819-839, 2003.

[45] T. H. Lee, C. IK-HWANG and K. Y. Jhang, *The nonlinearity of guided wave in an elastic plate*. *Modern Physics Letters B 22*, vol. **11**, pp. 1135-1140, 2008.

[46] J. L. Rose, *A baseline and vision of ultrasonic guided wave inspection potential*. *Transactions-American Society of Mechanical Engineers Journal of Pressure Vessel Technology*, vol. **124**, pp. 273-282, 2002.

[47] J. L. Rose and P. B. Nagy, *Ultrasonic waves in solid media*. *The Journal of the Acoustical Society of America*, vol. **107**, p. 1807, 2000.

[48] D. Hughes and J. Kelly, *Second-order elastic deformation of solids*. *Physical Review*, vol. **92**, pp. 1145-1149, 1953.

[49] R. Toupin and B. Bernstein, *Sound waves in deformed perfectly elastic materials. Acoustoelastic effect*. *The Journal of the Acoustical Society of America*, vol. **33**, p. 216, 1961.

[50] D. Crecraft, *The measurement of applied and residual stresses in metals using ultrasonic waves*. *Journal of Sound and Vibration*, vol. **5**, pp. 173-192, 1967.

[51] H. Fukuoka, H. Toda and T. Yamane, *Acoustoelastic stress analysis of residual stress in a patch-welded disk*. *Experimental Mechanics*, vol. **18**, pp. 277-280, 1978.

[52] M. Scott, D. Barnett and D. Ilic, *The Nondestructive Determination of Residual Stress in Extruded Billets from Acoustoelastic Measurements*. *1979 Ultrasonics Symposium*: IEEE, pp. 265-268, 1979.

[53] G. Johnson, *Acoustoelastic theory for elastic–plastic materials*. *The Journal of the Acoustical Society of America*, vol. **70**, p. 591, 1981.

[54] S. Suresh, *Fatigue of materials*: Cambridge University press, (*1998).*

[55] A. S. Birks, R. Greene and P. McIntire, *Nondestructive Testing Handbook*: American Society for Nondestructive Testing, (*1991).*

[56] E. A. Hanysz, *Ultrasonic transmission testing method*. U.S. Patent 2,912,853, issued November 17, 1959.

[57] A. Nielson, *Use of Acoustic Emission for Detection of Defects as They Arise During Fabrication*. *International Inst. Weld. Coll. on Acoustic Emission, 1976*, pp. 11-33, 1976.

[58] J. F. Couvreur and J. F. Thimus, *The properties of coupling agents in improving ultrasonic transmission*. *International journal of rock mechanics and mining sciences & geomechanics abstracts*, vol. **33**: Pergamon, pp. 417-424, 1996.

[59] A. Siggins, *Dynamic elastic tests for rock engineering*. *Comprehensive rock engineering*, vol. **3**, pp. 601–618, 1993.

[60] R. Nichols, *Acoustic emission*. *Applied Science Publishers Ltd., Barking, Essex, England*, p. 121, 1976.

[61] A. Best, C. McCann and J. Sothcott, *The relationships between the velocities, attenuations and petrophysical properties of reservoir sedimentary rocks1*. *Geophysical Prospecting*, vol. **42**, pp. 151-178, 1994.

[62] D. Lockner, J. Walsh and J. Byerlee, *Changes in seismic velocity and attenuation during deformation of granite*. *Journal of Geophysical Research*, vol. **82**, pp. 5374-5378, 1977.

[63] N. Klimis, *Geotechnical characterization of a thermally cracked marble*. *7th ISRM Congress, International Society for Rock Mechanics*, 1991.

[64] G. Tao and M. King, *Shear-wave velocity and Q anisotropy in rocks: a laboratory study*. *International Journal of Rock Mechanics and Mining Sciences & Geomechanics Abstracts*, vol. **27**: Pergamon, pp. 353-361, 1990.

[65] M. Toksöz, D. Johnston and A. Timur, *Attenuation of seismic waves in dry and saturated rocks: I. Laboratory measurements*. *Geophysics*, vol. **44**, p. 681, 1979.

[66] J. C. Spanner and J. W. McElroy, *Monitoring structural integrity by acoustic emission*: ASTM STP 571, (*1974).*

[67] T. Drouillard, R. Liptai and C. Tatro, *Industrial use of acoustic emission for nondestructive testing*. *Monitoring Structural Integrity by Acoustic Emission-STP 571*, p. 122, 1975.

[68] C. Morais and A. Green, *Establishing structural integrity using acoustic emission. Monitoring Structural Integrity Using Acoustic Emission*: ASTM STP 571, pp. 184-199, 1975.

[69] Y. Kikuta, T. Araki and T. Kuroda, *A study on mechanism of hydrogen embrittlement for iron and steel by means of electron fractography (Report - 1) - Relationship between delayed fracture and fracture morphology. J. Weld. Soc*, vol. **44**, pp. 168-75, 1975.

[70] H. Okada, K. Yukawa and H. Tamura, *Application of AE technique to the study of stress corrosion cracking in distinguishing between active path corrosion and hydrogen embrittlement. Corrosion* vol. **30**, pp. 235-5, 1974.

[71] Y. Sakamoto, K. Kinoshita, K. Nakanishi and K. Tsuruoka, *Basic studies on high temperature cracking in steel. Paper presented to Meeting of Iron and Steel Inst.*, p. 434, 1973.

[72] L. Graham and G. Alers, *Acoustic emission in the frequency domain. Monitoring Structural Integrity by Acoustic Emission, ASTM STP 571*: ASTM International, pp. 11-39, 1975.

[73] M. Kelly, D. Harris and A. Pollock, *Detection and location of flaw growth in metallic and composite structures. Monitoring Structural Integrity by Acoustic Emission-STP 571*, p. 221, 1975.

[74] P. J. Highmore and A. Rogerson, *Advances in Ultrasonic Flaw Characterisation*. Risley Nuclear Laboratories, UKAEA, Warrington, Cheshire, Uk, 1987.

[75] S. Kozakowski, *Measurements of the changes in the ultrasonic wave attenuation in spheroidal graphite iron test pieces subjected to fatigue load. Non-Destructive Testing--Proceedings of the 4 th European Conference*, vol. **4**, pp. 2212-2217, 1987.

[76] A. C. Duncumb and D. M. Keighley, *Inspection of Titanium Tubing using Ultrasonic Lamb Waves Generated by an Electromagnetic Acoustic Transducer. TI Research, Hinxton, Saffron Walden, Essex, UK*, 1987.

[77] M. Nakayama, K. Udagawa, K. Nishifuji, H. Hisakawa, H. Maruyama, Y. Nagakura, H. Yamaguchi, K. Fujisawa, Y. Iwasaki and A. Kondo, *Method of Ultrasonic Angle Beam Examination for Welds of Ferritic Steels with Acoustic Anisotropy. Transactions of the Iron and Steel Institute of Japan 27*, vol. **11**, pp. 898-909, 1987.

[78] J. A. Vogel and J. A. Bruinsma, *Contactless Ultrasonic Inspection with Fiber-optics. Technisch Physische Dienst TNO-TH, Institute of Appied Physics, Stieltjesweg 1, Delft, The Netherlands*, 1987.

[79] H. A. Crostack and H. K., *Flaw Size Estimation in Brazed Joints by Ultrasonic Testing. University of Dortmund, West Germany*, 1987.

[80] A. Lambert and B. Bossuat, *Automization of Inspection with Rayeigh Waves on Curved and Complex Surfaces. Non-Destructive Testing--Proceedings of the 4 th European Conference.*, vol. **4**, pp. 2358-2367, 1987.

[81] J. Rose, S. Pelts and M. Quarry, *A comb transducer model for guided wave NDE. Ultrasonics*, vol. **36**, pp. 163-169, 1998.

[82] J. L. Rose, Z. WENHAO and M. Zaidi, *Ultrasonic NDT of titanium diffusion bonding with guided waves. Materials evaluation*, vol. **56**, pp. 535-539, 1998.

[83] J. L. Rose and L. E. Soley, *Ultrasonic guided waves for anomaly detection in aircraft components*. *Materials evaluation*, vol. **58**, pp. 1080-1086, 2000.

[84] J. L. Rose, M. J. Avioli and Y. Cho, *Elastic wave analysis for broken rail detection*. *Quantitative Nondestructive Evaluation*, vol. **615**: AIP Publishing, pp. 1806-1812, 2002.

[85] J. L. Rose, V. S. Agarwala, L. E. Soley and T. L. Hay, *Ultrasonic guided waves for hidden corrosion detection in naval aircraft*. *CORROSION 2000*, 2000.

[86] J. L. Rose, *Guided wave nuances for ultrasonic nondestructive evaluation*. *Ultrasonics, Ferroelectrics and Frequency Control, IEEE Transactions on*, vol. **47**, pp. 575-583, 2002.

[87] J. Rose, M. Quarry, A. Bray and C. Corley, *Guided waves for corrosion detection potential in piping under insulation*. *Proceedings of the ASNT Fall Conference*, pp. 27-29, 1997.

[88] J. Li and J. L. Rose, *Implementing guided wave mode control by use of a phased transducer array*. *Ultrasonics, Ferroelectrics and Frequency Control, IEEE Transactions on*, vol. **48**, pp. 761-768, 2002.

[89] J. Li and R. L. Rose, *Excitation and propagation of non-axisymmetric guided waves in a hollow cylinder*. *J Acoust Soc Am*, vol. **109**, pp. 457-64, 2001.

[90] J. Li and J. Rose, *Guided wave inspection of containment structures*. *Materials evaluation*, vol. **59**, pp. 783-787, 2001.

[91] A. Bray, C. Corley, R. Fischer, J. Rose and M. Quarry, *Development of Guided Wave Ultrasonic Techniques for Detection of Corrosion Under Insulation in Metal Pipe*. *In Energy Sources Technology Conference and Exhibition*. ASME, 1998.

[92] U. Polimeno, M. Meo, D. Almond and S. Angioni, *Detecting Low Velocity Impact Damage in Composite Plate Using Nonlinear Acoustic/Ultrasound Methods*. *Applied Composite Materials*, pp. 1-8, 2010.

[93] T. Bateman, W. Mason and H. McSkimin, *Third Order Elastic Moduli of Germanium*. *Journal of Applied Physics*, vol. **32**, pp. 928-936, 2009.

[94] W. Yost and J. Cantrell, *The effects of fatigue on acoustic nonlinearity in aluminum alloys*. *Ultrasonics Symposium, 1992 Proceedings*: IEEE, pp. 947-955, 1992.

[95] J. Cantrell and K. Salama, *Acoustoelastic characterisation of materials*. *International Materials Reviews*, vol. **36**, pp. 125-145, 1991.

[96] W. Yost and J. Cantrell, *Absolute ultrasonic displacement amplitude measurements with a submersible electrostatic acoustic transducer*. *Review of Scientific Instruments*, vol. **63**, pp. 4182-4188, 1992.

[97] J. Antonopoulos, L. Brown and A. Winter, *Vacancy dipoles in fatigued copper*. *Philosophical Magazine*, vol. **34**, pp. 549-563, 1976.

[98] V. Nazarov and A. Sutin, *Nonlinear elastic constants of solids with cracks*. *The Journal of the Acoustical Society of America*, vol. **102**, p. 3349, 1997.

[99] K. Naugolnykh, L. Ostrovsky, O. Sapozhnikov and M. Hamilton, *Nonlinear wave processes in acoustics*. *The Journal of the Acoustical Society of America*, vol. **108**, p. 14, 2000.

[100] L. Ostrovsky, *Wave processes in media with strong acoustic nonlinearity*. *The Journal of the Acoustical Society of America*, vol. **90**, p. 3332, 1991.

[101] V. Nazarov, L. Ostrovsky, I. Soustova and A. Sutin, *Nonlinear acoustics of micro-inhomogeneous media*. *Physics of the Earth and Planetary Interiors*, vol. **50**, pp. 65-73, 1988.

[102] J. Cantrell and W. Yost, *Nonlinear ultrasonic characterization of fatigue microstructures*. *International Journal of Fatigue*, vol. **23**, pp. 487-490, 2001.

[103] M. Born and K. Huang, *Dynamical theory of crystal lattices*: Oxford University Press, USA, (*1988).*

[104] J. Cantrell, *Crystalline structure and symmetry dependence of acoustic nonlinearity parameters*. *Journal of Applied Physics*, vol. **76**, pp. 3372-3380, 2009.

[105] D. Wallace, *Thermoelastic Theory of Stressed Crystals and Higher-Order Elastic Constants*. Solid state physics*, vol. **25**, pp. 301-404, 1970.

[106] A. Winter, O. Pedersen and K. Rasmussen, *Dislocation microstructures in fatigued copper polycrystals*. *Acta Metallurgica*, vol. **29**, pp. 735-748, 1981.

[107] J. Na, J. Cantrell and W. Yost, *Linear and nonlinear ultrasonic properties of fatigued 410 Cb stainless steel*. *Review of progress in quantitative nondestructive evaluation*, vol. **30**: Springer US, pp. 1347-1352, 1996.

[108] J. Cantrell, *Substructural organization, dislocation plasticity and harmonic generation in cyclically stressed wavy slip metals*. *Proceedings of the Royal Society of London. Series A: Mathematical, Physical and Engineering Sciences*, vol. **460**, p. 757, 2004.

[109] J. Frouin, S. Sathish, T. Matikas and J. Na, *Ultrasonic linear and nonlinear behavior of fatigued Ti–6Al–4V*. *J. Mater. Res*, vol. **14**, pp. 1295–1298, 1999.

[110] J.K. Na, J.H. Cantrell and W. T. Yost, *Review of Progress in QNDE*. *Review of Progress in QND, Edited by DO Thompson and DE Chimenti*, vol. **15**, 1992.

[111] J. Antonopoulos and A. Winter, *Weak-beam study of dislocation structures in fatigued copper*. *Philosophical Magazine*, vol. **33**, pp. 87-95, 1976.

[112] P. Paris and F. Erdogan, *A critical analysis of crack propagation laws*. *Journal of Basic Engineering*, vol. **85**, pp. 528-534, 1963.

[113] J. M. Richardson, *Harmonic generation at an unbonded interface--I. Planar interface between semi-infinite elastic media*. *International Journal of Engineering Science*, vol. **17**, pp. 73-85, 1979.

[114] K. Kawashima, R. Omote, T. Ito, H. Fujita and T. Shima, *Nonlinear acoustic response through minute surface cracks: FEM simulation and experimentation*. *Ultrasonics*, vol. **40**, pp. 611-615, 2002.

[115] M. Friswell and J. Penny, *Crack modeling for structural health monitoring*. *Structural Health Monitoring*, vol. **1**, p. 139, 2002.

[116] C. Bermes, J. Y. Kim, J. Qu and L. J. Jacobs, *Experimental characterization of material nonlinearity using Lamb waves*. *Applied Physics Letters*, vol. **90**, p. 021901, 2007.

[117] C. Bermes, J. Y. Kim, J. Qu and L. J. Jacobs, *Nonlinear Lamb waves for the detection of material nonlinearity*. *Mechanical Systems and Signal Processing*, vol. **22**, pp. 638-646, 2008.

[118] M. Deng, P. Wang and X. Lv, *Experimental observation of cumulative second-harmonic generation of Lamb-wave propagation in an elastic plate*. *Journal of Physics D: Applied Physics*, vol. **38**, p. 344, 2005.

[119] J. Herrmann, J. Y. Kim, L. J. Jacobs, J. Qu, J. W. Littles and M. F. Savage, *Assessment of material damage in a nickel-base superalloy using nonlinear Rayleigh surface waves*. *Journal of Applied Physics*, vol. **99**, p. 124913, 2006.

[120] C. Pruell, J. Y. Kim, J. Qu and L. J. Jacobs, *Evaluation of plasticity driven material damage using Lamb waves*. *Applied Physics Letters*, vol. **91**, p. 231911, 2007.

[121] C. Pruell, J. Y. Kim, J. Qu and L. Jacobs, *A nonlinear-guided wave technique for evaluating plasticity-driven material damage in a metal plate*. *Ndt & E International*, vol. **42**, pp. 199-203, 2009.

[122] J. F. Martin, G. M. Sinclair and T. H. Topper, *Computer based simulation of cyclic stress-strain behavior with applications to fatigue (Cyclic stress-strain behavior prediction by mathematical model and computer simulation, applying to Al alloy fatigue)*. *Materials Research and Standards 11*, vol. **11**, pp. 23-28, 1971.

[123] L. Straka, Y. Yagodzinskyy, M. Landa and H. Hanninen, *Detection of structural damage of aluminum alloy 6082 using elastic wave modulation spectroscopy*. *Ndt & E International*, vol. **41**, pp. 554-563, 2008.

[124] N. Wilkie Chancellier and K. Van Den Abeele, *Experimental Detection of Structural Damage in Natural Building Stones Using Nonlinear Wave Modulation Spectroscopy*. *Review of Progress in Quantitative Nondestructive Evaluation*, vol. **760**: American Institute of Physics, p. 361, 2005.

[125] M. A. Meyers and K. K. Chawla, *Mechanical behavior of materials*. *Cambridge University Press*, 2009.

[126] H. Jeong, S. H. Nahm, K. Y. Jhang and Y. H. Nam, *A nondestructive method for estimation of the fracture toughness of CrMoV rotor steels based on ultrasonic nonlinearity*. *Ultrasonics*, vol. **41**, pp. 543-9, 2003.

[127] R. Viswanathan and S. Gehl, *A method for estimation of the fracture toughness of CrMoV rotor steels based on composition*. *Journal of Engineering Materials and Technology*, vol. **113**, p. 263, 1991.

[128] J. Kang, J. Qu, A. Saxena and L. Jacobs, *On the detection of creep damage in a directionally solidified nickel base superalloy using nonlinear ultrasound*. *Review of Progress in Quantitative Nondestructive Evaluation, Volume 23*, vol. **700**, pp. 1248-1255, 2004.

[129] T. Ohtani, K. Kawashima, M. Drew and P. Guagliard, *Nonlinear Acoustic Evaluation of Creep Damage in Boiler Heat Exchange Tubes*. *JAPANESE JOURNAL OF APPLIED PHYSICS PART 1 REGULAR PAPERS SHORT NOTES AND REVIEW PAPERS*, vol. **46**, p. 4577, 2007.

[130] S. Baby, B. Nagaraja Kowmudi, C. Omprakash, D. Satyanarayana, K. Balasubramaniam and V. Kumar, *Creep damage assessment in titanium alloy using a nonlinear ultrasonic technique*. *Scripta Materialia*, vol. **59**, pp. 818-821, 2008.

[131] J. S. Valluri, K. Balasubramaniam and R. V. Prakash, *Creep damage characterization using non-linear ultrasonic techniques*. *Acta Materialia*, vol. **58**, pp. 2079-2090, 2010.

[132] J. Rao, E. Kannan, R. V. Prakash and K. Balasubramaniam, *Fatigue damage characterization using surface acoustic wave nonlinearity in aluminum alloy AA7175-T7351*. *Journal of Applied Physics*, vol. **104**, p. 123508, 2009.

[133] D. Hurley, D. Balzar and P. Purtscher, *Nonlinear ultrasonic assessment of precipitation hardening in ASTM A 710 steel*. *Journal of Materials Research(USA)*, vol. **15**, pp. 2036-2042, 2000.

[134] Y. Choi, H. Kim, K. Jhang and I. Park, *Application of Nonlinear Acoustic Effect for Evaluation of Degradation of 2.25 Cr-1Mo Steel*. *Journal of KSNT*, vol. **22**, pp. 170-176, 2002.

[135] A. Metya, M. Ghosh, N. Parida and S. Palit Sagar, *Higher harmonic analysis of ultrasonic signal for ageing behaviour study of C-250 grade maraging steel*. *Ndt & E International*, vol. **41**, pp. 484-489, 2008.

[136] I. K. Park, H. M. Kim and K. Y. Jhang, *Nondestructive Evaluation of Degraded 2.25 Cr-1Mo Steel and Estimation of Nonlinear Acoustic Effect Using Bispectral Analysis*. *ASME 2003 Pressure Vessels and Piping Conference*: American Society of Mechanical Engineers, pp. 65-71, 2003.

[137] F. Matthews and R. Rawlings, *Composite materials: engineering and science*: Elsevier, (*1999).*

[138] B. Harris, *Fatigue in composites: science and technology of the fatigue response of fibre-reinforced plastics*: Woodhead Publishing Limited, Cambridge, England, (*2003).*

[139] D. Zenkert and M. Battley, *Foundations of Fibre Composites*. *Department of Aeronautics, Royal Institute of Technology, Sweden. Paper*, pp. 96-10, 2002.

[140] R. Talreja, *Internal variable damage mechanics of composite materials*. *Yielding, Damage, and Failure of Anisotropic Solids*, pp. 509-533, 1987.

[141] A. R. Oskouei and M. Ahmadi, *Acoustic Emission Characteristics of Mode I Delamination in Glass/Polyester Composites*. *Journal of Composite Materials*, vol. **44**, pp. 793-807, 2010.

[142] F. Dharmawan, G. Simpson and S. Herszbergand, *Mixed mode fracture toughness of GFRP composites*. *Composite Structures*, vol. **75**, pp. 328-338, 2006.

[143] A. De Morais and A. Pereira, *Mixed mode Iá+ áII interlaminar fracture of glass/epoxy multidirectional laminates-Part 1: Analysis*. *Composites Science and Technology*, vol. **66**, pp. 1889-1895, 2006.

[144] A. Brunner, B. Blackman and J. Williams, *Calculating a damage parameter and bridging stress from GIC delamination tests on fibre composites*. *Composites Science and Technology*, vol. **66**, pp. 785-795, 2006.

[145] D. ASTM, *5528-94a, Standard test method for mode I interlaminar fracture toughness of unidirectional fiber-reinforced polymer matrix composites*. *Annual book of ASTM standards*, 1994.

[146] F. Perrin, M. Bureau, J. Denault and J. Dickson, *Mode I interlaminar crack propagation in continuous glass fiber/polypropylene composites: temperature and molding condition dependence*. *Composites Science and Technology*, vol. **63**, pp. 597-607, 2003.

[147] R. Velmurugan and S. Solaimurugan, *Improvements in Mode I interlaminar fracture toughness and in-plane mechanical properties of stitched glass/polyester composites*. *Composites Science and Technology*, vol. **67**, pp. 61-69, 2007.

[148] S. Benmedakhene, M. Kenane and M. Benzeggagh, *Initiation and growth of delamination in glass/epoxy composites subjected to static and dynamic loading by acoustic emission monitoring*. *Composites Science and Technology*, vol. **59**, pp. 201-208, 1999.

[149] A. De Morais, M. De Moura, A. Marques and P. De Castro, *Mode-I interlaminar fracture of carbon/epoxy cross-ply composites*. *Composites Science and Technology*, vol. **62**, pp. 679-686, 2002.

[150] A. Refahi Oskouei, V. Ansari and M. Ahmadi, *Analyzing of AE Signals by Wavelet to Investigate Damage Mechanisms in Composite Materials*. *Proceedings of 3rd International Congress on Ultrasonics (ICU)*, pp. 190-194, 2007.

[151] S. Huguet, N. Godin, R. Gaertner, L. Salmon and D. Villard, *Use of acoustic emission to identify damage modes in glass fibre reinforced polyester*. *Composites Science and Technology*, vol. **62**, pp. 1433-1444, 2002.

[152] M. Johnson and P. Gudmundson, *Broad-band transient recording and characterization of acoustic emission events in composite laminates*. *Composites Science and Technology*, vol. **60**, pp. 2803-2818, 2000.

[153] J. Andersons, R. Joffe, M. Hojo and S. Ochiai, *Fibre fragment distribution in a single-fibre composite tension test*. *Composites Part B: Engineering*, vol. **32**, pp. 323-332, 2001.

[154] F. Cesari, V. Dal Re, G. Minak and A. Zucchelli, *Damage and residual strength of laminated carbon-epoxy composite circular plates loaded at the centre*. *Composites Part A: Applied Science and Manufacturing*, vol. **38**, pp. 1163-1173, 2007.

[155] M. R'Mili, M. Moevus and N. Godin, *Statistical fracture of E-glass fibres using a bundle tensile test and acoustic emission monitoring*. *Composites Science and Technology*, vol. **68**, pp. 1800-1808, 2008.

[156] I. Ndiaye, A. Maslouhi and J. Denault, *Characterization of interfacial properties of composite materials by acoustic emission*. *Polymer Composites*, vol. **21**, pp. 595-604, 2000.

[157] G. Zumpano and M. Meo, *Damage localization using transient non-linear elastic wave spectroscopy on composite structures*. *International Journal of Non-Linear Mechanics*, vol. **43**, pp. 217-230, 2008.

[158] L. Landau, E. Lifshitz, J. Sykes, W. Reid and E. H. Dill, *Theory of Elasticity: Vol. 7 of Course of Theoretical Physics*. *Physics Today*, vol. **13**, p. 44, 1960.

[159] R. A. Guyer and P. A. Johnson, *Nonlinear mesoscopic elasticity*. *Physics Today*, vol. **52**, pp. 30-6, 1999.

[160] P. Johnson, *New wave in acoustic testing*. *Mater. World*, vol. **7**, pp. 544-546, 1999.

[161] C. Campos-Pozuelo and J. Gallego-Juárez, *Experimental analysis of the nonlinear behaviour of fatigued metallic samples*. WCU, 2003.

[162] M. Meo, G. Zumpano, M. Piggott and G. Marengo, *Impact identification on a sandwich plate from wave propagation responses*. *Composite Structures*, vol. **71**, pp. 302-306, 2005.

[163] K. Van Den Abeele and J. De Visscher, *Damage assessment in reinforced concrete using spectral and temporal nonlinear vibration techniques*. *Cement and Concrete Research*, vol. **30**, pp. 1453-1464, 2000.

[164] K. Van Den Abeele, A. Sutin, J. Carmeliet and P. Johnson, *Micro-damage diagnostics using nonlinear elastic wave spectroscopy (NEWS)*. *Ndt & E International*, vol. **34**, pp. 239-248, 2001.

[165] K. McCall and R. Guyer, *Equation of state and wave propagation in hysteretic nonlinear elastic materials*. *J. Geophys. Res*, vol. **99**, p. 23, 1994.

[166] K. McCall and R. Guyer, *A new theoretical paradigm to describe hysteresis, discrete memory and nonlinear elastic wave propagation in rock*. *Nonlinear processes in geophysics*, vol. **3**, pp. 89-101, 1996.

[167] J. Bohse, *Acoustic emission characteristics of micro-failure processes in polymer blends and composites*. *Composites Science and Technology*, vol. **60**, pp. 1213-1226, 2000.

[168] B. B. Kang, *Excitation method for thermosonic non-destructive testing*. Imperial College London, 2008.

[169] D. P. Almond, B. Weekes, T. Li, S. G. Pickering, E. Kostson, J. Wilson, G. Tian, S. Dixon and S. Burrows, *Thermographic techniques for the detection of cracks in metallic components*. *Insight-Non-Destructive Testing and Condition Monitoring*, vol. **53**, pp. 614-620, 2011.

[170] R. Mignogna, R. Green, J. Duke, E. Henneke and K. Reifsnider, *Thermographic investigation of high-power ultrasonic heating in materials*. *Ultrasonics*, vol. **19**, pp. 159-163, 1981.

[171] K. Reifsnider, E. G. Henneke and W. Stinchcomb, *The mechanics of vibrothermography*. *Mechanics of nondestructive testing*: Springer, pp. 249-276, 1980.

[172] C. Pye and R. Adams, *Heat emission from damaged composite materials and its use in nondestructive testing*. *Journal of Physics D: Applied Physics*, vol. **14**, p. 927, 1981.

[173] X. Han, L. Favro and R. Thomas, *Sonic IR imaging and vibration pattern studies of cracks in an engine disk*. *AIP Conference Proceedings*, vol. **657**, p. 513, 2003.

[174] M. Morbidini and P. Cawley, *Reliable crack detection in thermosonics NDE*. *AIP Conference Proceedings*, vol. **975**, p. 536, 2008.

[175] J. Rantala, D. Wu and G. Busse, *NDT of polymer materials using lock-in thermography with water-coupled ultrasonic excitation*. *NDT & E International*, vol. **31**, pp. 43-49, 1998.

[176] C. Homma, M. Rothenfusser, J. Baumann and R. Shannon, *Study of the heat generation mechanism in acoustic thermography*. *AIP Conference Proceedings*, vol. **820**, p. 566, 2006.

[177] S. D. Holland, C. Uhl and J. B. Renshaw, *Toward a viable strategy for estimating vibrothermographic probability of detection*. 2007.

[178] M. Meo and G. Zumpano, *Nonlinear elastic wave spectroscopy identification of impact damage on a sandwich plate*. *Composite Structures*, vol. **71**, pp. 469-474, 2005.

[179] G. Zumpano and M. Meo, *Damage detection in an aircraft foam sandwich panel using nonlinear elastic wave spectroscopy*. *Computers & Structures*, vol. **86**, pp. 483-490, 2008.

[180] K. E. A. Van Den Abeele, A. Sutin, J. Carmeliet and P. A. Johnson, *Micro-damage diagnostics using nonlinear elastic wave spectroscopy (NEWS)*. *Ndt & E International*, vol. **34**, pp. 239-248, 2001.

[181] K. E. A. V. D. Abeele, J. Carmeliet, J. A. T. Cate and P. Johnson, *Nonlinear elastic wave spectroscopy (NEWS) techniques to discern material damage, part II: single-mode nonlinear resonance acoustic spectroscopy*. *Research in Nondestructive Evaluation*, vol. **12**, pp. 31-42, 2000.

[182] U. Polimeno and M. Meo, *Detecting barely visible impact damage detection on aircraft composites structures*. *Composite Structures*, vol. **91**, pp. 398-402, 2009.

[183] M. Holzmann, I. Dlouh , B. Vlach and J. Krumpos, *Degradation of mechanical properties of Cr---Mo---V and Cr---Mo---V---W steam turbine rotors after long-term operation at elevated temperatures. Part I: tensile properties, intergranular fracture strength and impact tests*. *International journal of pressure vessels and piping*, vol. **68**, pp. 99-111, 1996.

[184] I. Y. Solodov and B. A. Korshak, *Instability, Chaos, and "Memory" in Acoustic-Wave–Crack Interaction*. *Physical review letters*, vol. **88**, p. 14303, 2001.

[185] J. H. Cantrell, *Fundamentals and applications of non-linear ultrasonic nondestructive evaluation*. *Ultrasonic non-destructive evaluation*, vol. **vol. 6**, pp. p.363-434, 2004.

[186] M. Meo, F. Amerini and M. Amura, *Baseline-free estimation of residual fatigue life using third order acoustic nonlinear parameter*. *The Journal of the Acoustical Society of America* vol. **4**, pp. 1829-1837, 2010.

[187] H. Arabian-Hoseynabadi, H. Oraee and P. Tavner, *Failure modes and effects analysis (FMEA) for wind turbines*. *International Journal of Electrical Power & Energy Systems*, vol. **32**, pp. 817-824, 2010.

[188] C. C. Ciang, J.-R. Lee and H.-J. Bang, *Structural health monitoring for a wind turbine system: a review of damage detection methods*. *Measurement Science and Technology*, vol. **19**, p. 122001, 2008.

[189] Z. Hameed, Y. Hong, Y. Cho, S. Ahn and C. Song, *Condition monitoring and fault detection of wind turbines and related algorithms: A review*. *Renewable and Sustainable energy reviews*, vol. **13**, pp. 1-39, 2009.

[190] L. Germanischer, *Wind Energy, GL Wind.". Possible Wind Turbine Damage*, vol. **30**, 2007.

[191] M. M. Khan, M. T. Iqbal and F. Khan, *Reliability and condition monitoring of a wind turbine*. *Electrical and Computer Engineering, 2005. Canadian Conference on*: IEEE, pp. 1978-1981, 2005.

[192] M. Amura and M. Meo, *Prediction of residual fatigue life using nonlinear ultrasound*. *Smart Materials and Structures*, vol. **21**, p. 045001, 2012.

[193] D. P. Almond and P. Patel, *Photothermal science and techniques* vol. 10: Springer, (*1996).*

[194] J. Sarrate Ramos and A. Huerta, *An improved algorithm to smooth graded quadrilateral meshes preserving the prescribed element size*. *Department de Matematica Aplicada III, Universitat Politecnica de Catalunya*, 2011.

[195] K.-J. Bathe, *Finite element procedures*: Klaus-Jurgen Bathe, (*2006).*

[196] S. Vanaverbeke and K. Van Den Abeele, *Two-dimensional modeling of wave propagation in materials with hysteretic nonlinearity*. *The Journal of the Acoustical Society of America*, vol. **122**, p. 58, 2007.

[197] M. Scalerandi, V. Agostini, P. P. Delsanto, K. Van Den Abeele and P. A. Johnson, *Local interaction simulation approach to modelling nonclassical, nonlinear elastic behavior in solids*. *The Journal of the Acoustical Society of America*, vol. **113**, p. 3049, 2003.

[198] K.-Y. Jhang, *Nonlinear ultrasonic techniques for nondestructive assessment of micro damage in material: a review*. *International journal of precision engineering and manufacturing*, vol. **10**, pp. 123-135, 2009.

[199] K.-A. Van Den Abeele, P. A. Johnson and A. Sutin, *Nonlinear elastic wave spectroscopy (NEWS) techniques to discern material damage, part I: nonlinear wave modulation spectroscopy (NWMS)*. *Research in nondestructive evaluation*, vol. **12**, pp. 17-30, 2000.

[200] F. Amerini and M. Meo, *Structural health monitoring of bolted joints using linear and nonlinear acoustic/ultrasound methods*. *Structural Health Monitoring*, vol. **10**, pp. 659-672, 2011.

[201] M. Amura, M. Meo and F. Amerini, *Baseline-free estimation of residual fatigue life using a third order acoustic nonlinear parameter*. *The Journal of the Acoustical Society of America*, vol. **130**, p. 1829, 2011.

[202] D. Bates, G. Smith, D. Lu and J. Hewitt, *Rapid thermal non-destructive testing of aircraft components*. *Composites Part B: Engineering*, vol. **31**, pp. 175-185, 2000.

[203] L. Ostrovsky and P. Johnson, *Dynamic nonlinear elasticity in geomaterials*. *Rivista del nuovo cimento*, vol. **24**, pp. 1-46, 2001.

[204] P.-A. Johnson, *The Universality of Nonclassical Nonlinearity (with application to Nondestructive Evaluation and Ultrasonics)*. *Springer New York*, vol. **Chap. 4**, 2006.

[205] L. Landau and E. Lifshitz, *Theory of Elasticity, 3rd*. Pergamon Press, Oxford, UK, 1986.

[206] G. Zumpano and M. Meo, *A new damage detection technique based on wave propagation for rails*. *International journal of solids and structures*, vol. **43**, pp. 1023-1046, 2006.

[207] K. Helbig and P. N. Rasolofosaon, *A theoretical paradigm for describing hysteresis and nonlinear elasticity in arbitrary anisotropic rocks*. *Anisotropy*, pp. 383-398, 2000.

[208] P. Theocharis and D. Sokolis, *Spectral decomposition of the compliance fourth-rank tensor for orthotropic materials*. *Archive of Applied Mechanics*, vol. **70**, pp. 289-306, 2000.

[209] M. Meo and F. Ciampa, *Modelling of Multiscale Nonlinear Interaction of Elastic Waves with 3D Cracks. Manuscript submitted and accepted, Journal of Acoustical Society of America*, 2013.

[210] K.-J. Bathe, *Finite Element Procedures in Engineering Analysis*. *Prentice-Hall Inc.*, 1982.

[211] D. S. M. R.D. Cook, M.E. Plesha, *Concepts and applications of finite element analysis*. *third ed. John Wiley & Sons*, 1989.

[212] J. Donea, *Advanced Structural Dynamics*. *Applied Science Publishers, Barking. Essex*, 1980.

[213] J. Sarrate Ramos and A. Huerta, *An improved algorithm to smooth graded quadrilateral meshes preserving the prescribed element size*. 2012.

[214] O.T. Beata and S. Shepard, *Comparison of pulse phase and thermographic signal reconstruction processing methods, SPIE Defense, Security, and Sensing International Society for Optics and Photonics, Conference Volume 8705*, 2013

Appendix 1

Materials Investigated

Experiment Chapter:	Types of Materials:
Chapter 3.1.	**Material A: Aluminium Disks: AA2024-T6**
Chapter 3.2.	**Material A: Aluminium Disks: AA2024-T6** **Material B: Composite Plates: T300/914-CFRP [0°/90°/90°/0°]**
Chapter 3.3.	**Material C: Steel Joint Structure**
Chapter 4.1.	**Material D: Test Samples: AA6082-T6**
Chapter 4.2.	**Material D: Test Samples: AA6082-T6**
Chapter 5.	**Material E: T300/914-Composite Plates: CFRP Samples** **A22 $[0°/45°/90°/-45°/0°/45°/90°/-45°/0°/45°/90°/-45°]_s$** **A31 $[0°/15°/30/°/45°/60°/75°/90°/-75°/-60°/-45°/-30°/-15°]_s$**

Appendix 2

Nonlinear Ultrasound Modelling and Validation of Fatigue Damage

G.P. Malfense Fierro, F. Ciampa, D. Ginzburg, E. Onder, M. Meo*

Material Research Centre, Department of Mechanical Engineering, University of Bath, Bath, BA2 7AY, UK

*Corresponding author: m.meo@bath.ac.uk

Abstract

Nonlinear ultrasound techniques have shown greater sensitivity to microcracks and they can be used to detect structural damages at their early stages. However, there is still a lack of numerical models available in commercial finite element analysis (FEA) tools that are able to simulate the interaction of elastic waves with the materials nonlinear behaviour. In this study, a nonlinear constitutive material model was developed to predict the structural response under continuous harmonic excitation of a fatigued isotropic sample that showed anharmonic effects. Particularly, by means of Landau's theory and Kelvin tensorial representation, this model provided an understanding of the elastic nonlinear phenomena such as the second harmonic generation in three-dimensional solid media. The numerical scheme was implemented and evaluated using a commercially available FEA software LS-DYNA, and it showed a good numerical characterisation of the second harmonic amplitude generated by the damaged region known as the nonlinear response area (NRA). Since this process requires only the experimental second-order nonlinear parameter and rough damage size estimation as an input, it does not need any baseline testing with the undamaged structure or any dynamic modelling of the fatigue crack growth. To validate this numerical model, the second-order nonlinear parameter was experimentally evaluated at various points over the fatigue life of an Aluminium (AA6082-T6) coupon and the crack propagation was

measured using an optical microscope. A good correlation was achieved between the experimental set-up and the nonlinear constitutive model.

Keywords: Nondestructive Evaluation Techniques, Nonlinear Ultrasound, Finite Element Method, Fatigue Life.

Introduction

Ultrasound testing can be broken into two main fields: (i) linear acoustic/ultrasonic methods and (ii) nonlinear ultrasound methods. Linear methods analyse wave speed changes and amplitude variations due to reflections of waves caused by structural damages. These techniques work satisfactory in the presence of a significant impedance contrast. However, when micro-damages are present in the form of nonlinear elastic zones rather than a heterogeneous elastic medium, these methods have difficulties in determining the extent of the defect [1, 2]. To overcome this limitation, a greater sensitivity to damage presence is offered by a promising new class of Non-Destructive Evaluation (NDT) techniques and Structural Health Monitoring (SHM) systems based on the evaluation of material nonlinear elastic behaviour. These methods have proved their effectiveness by detecting early signs of material degradation long before changes of the linear acoustic properties become prominent [3-5]. Consequently, a deeper understanding of nonlinear behaviour of solids along with their microscopic structure and dynamics is essential to evaluate the integrity of the medium, hence the development of a nonlinear ultrasound model to predict damage. Ordinary materials such as aluminium, composites and numerous others, exhibit *anharmonic effects* that can be explained by the classical nonlinear theory of Landau [6], known as Classical Nonlinear Elasticity (CNE). Nonlinear elastic effects of damaged materials can be assessed with nonlinear elastic wave spectroscopy (NEWS) [4, 5, 7, 8] and phase symmetry analysis (PSA) techniques [9] which explicitly interrogate the material nonlinear elastic behaviour and its effect on wave propagation caused by the presence of defects.

The focus of this work was to develop a material constitutive model that would accurately predict the nonlinear ultrasound effects (modulation, sub-harmonic, and further harmonic production) produced by damaged or cracked regions of a material. In order to investigate whether

the nonlinear response of a material incorporating a crack could be simulated by means of numerical analysis, various methodologies using finite element modelling (FEM) techniques for damage representation were investigated [10, 11]. For this purpose, the commercial explicit finite element analysis (FEA) software LS-DYNA 971 was used.

Experimental tests were performed on the aluminium dogbone at various points during its fatigue life to determine the nonlinear behaviour caused by crack propagation. It has been shown in many studies [3, 12, 13] that the production of further harmonics (at twice and three times the fundamental frequency) can be directly related to damage or the increase in damage. It has also been shown that the second order nonlinearity parameter β, determined by relating the fundamental frequency and the nonlinear second harmonic responses, increases as crack propagation increases over the fatigue life of a component [14]. The generation of such harmonics can be attributed to the 'clapping or rubbing' of a damaged region, which are excited by small stresses generated by a waves propagation through the medium. The material constitutive model developed was used to determine the generation of these further harmonics by attributing nonlinear behaviour to a nonlinear response area (NRA) within a FEA model. The elements which would behave in such a nonlinear manner would be representative of a cracked or damaged region. By propagating a specific frequency through the modelled medium, elements that exhibited the nonlinear behaviour generated further harmonics.

The experimental design and setup was used to validate: (i) the further harmonic generation, (ii) the magnitude of β (second order nonlinearity parameter), (iii) the crack size, and (iv) the fatigue life percentage of the component. Using the constitutive model and the experimental β determined it was possible to evaluate the generation of further harmonic production in the modelled solution. The modelled magnitude of the second harmonic was compared with the experimental data to assess its accuracy. By increasing the size of the NRA it was possible to: (i) evaluate the increase of the modelled second harmonic, (ii) determine if the increase in harmonic generation corresponded to experimental results, and (iii) confirm that the implemented NRA's responded effectively to single frequency excitation in a comparable manner as actual damaged regions (in this case a propagating crack).

The results showed that the modelling of the nonlinear elastic effect using the determined model correlated well to experimental results. Therefore the model developed provides the first step in potential FEA methods which will allow: (i) the incorporation of nonlinear ultrasound effects in modeling, (ii) assessment of the generation and dispersion of nonlinearities due to damage in complex structures, (iii) the generation of more complex and realistic models, and (iv) estimation of residual fatigue life of components without baseline tests.

Nonlinear Constitutive Material Model

Linear stress-strain relationship defined in Hooke's law is usually inadequate to describe the nonlinear mechanical behaviour of solids with distributed damage (micro-cracks and micro voids) and with inelastic behaviour [15, 16]. Indeed, damaged materials such as aluminium, steel and composites that have atomic elasticity arising from atomic-level forces between atoms and molecules, exhibit classical nonlinear (also known as *anharmonic*) effects which can be described by the nonlinear elastic theory of Landau [17]. Particularly, the expression of the nonlinear elastic modulus K_C can be obtained through a one-dimensional (1D) power law expansion of the stress with respect to the strain ε:

$$K_C = K_0\left(1 + \beta\varepsilon + \delta\varepsilon^2 + \cdots\right) \tag{1}$$

where K_0 is the linear elastic modulus, β and δ are classical second order and third order nonlinear coefficients. In the up-scaling from microscopic to mesoscopic level (with dimensions of nearly 1-10 mm), both the linear elastic modulus and the nonlinear parameters can be assumed as constants within a solid element. Hence, Eq. (1) can be used to predict the nonlinear response of the material. However, for most solids the first nonlinear term β is sufficient to describe the nonlinear response. This coefficient can be experimentally obtained from the measurement of the second harmonic amplitude generated from a single pure tone input [18]. Since Eq. (1) represents a scalar model it cannot be used to investigate the three-dimensional (3D) material response of a cracked sample when different types of waves (bulk waves, guided waves, etc…) are applied.

Hence, to overcome this limitation, Kelvin notation was used to extend the standard Voigt stress-strain formulation in a tensorial equivalent form for the 3D Cartesian space [19]. Indeed, by

introducing Kelvin representation, the Voigt stress-strain relationship for a homogeneous elastic medium becomes:

$$\tilde{\boldsymbol{\sigma}} = \tilde{\mathbf{K}}\tilde{\boldsymbol{\varepsilon}} \tag{2}$$

where the new components of the 6D stress and strain vectors are:

$$\begin{aligned} \tilde{\boldsymbol{\sigma}} &= \left(\sigma_{11}, \sigma_{22}, \sigma_{33}, \sqrt{2}\sigma_{12}, \sqrt{2}\sigma_{13}, \sqrt{2}\sigma_{23}\right)^T \\ \tilde{\boldsymbol{\varepsilon}} &= \left(\varepsilon_{11}, \varepsilon_{22}, \varepsilon_{33}, \sqrt{2}\varepsilon_{12}, \sqrt{2}\varepsilon_{13}, \sqrt{2}\varepsilon_{23}\right)^T \end{aligned} \tag{3}$$

and $\tilde{\mathbf{K}}$ is the new six by six stiffness matrix defined by:

$$\tilde{\mathbf{K}} = \mathbf{TKT} \text{ with } \mathbf{T} = \begin{bmatrix} \mathbf{I} & 0 \\ 0 & \sqrt{2}\mathbf{I} \end{bmatrix} \tag{4}$$

where $\mathbf{K}$ is the stiffness matrix in Voigt formulation. The symmetric matrix $\tilde{\mathbf{K}}$ can be shown to represent the components of a second-rank tensor in the 6D space [20]. In accordance with Ciampa et al. [21, 22], the aim of this approach consists of determining the eigenmoduli $\boldsymbol{\Lambda}$ and the associated eigentensors $\tilde{\boldsymbol{\varepsilon}}$ of Eq. (2) in order to form an ortho-normalised basis for the stress and strain tensors of the second rank. In this manner, these tensors can be decomposed with respect to this basis in the six-dimensional (6D) space. In other words, we seek for the eigenvalues $\boldsymbol{\Lambda}$ (known as *Kelvin moduli*) that satisfy the following equation:

$$\left(\tilde{\mathbf{K}} - \boldsymbol{\Lambda}\mathbf{I}\right)\tilde{\boldsymbol{\varepsilon}} = 0. \tag{5}$$

Since the 6D linear transformation $\tilde{\mathbf{K}}$ is assumed to be symmetric and positive definite, there will be a maximum of six positive eigenelastic constants Λ_i $(i = 1,\ldots,6)$ associated to Eq. (5). In addition to the six values of $\boldsymbol{\Lambda}$, also six values of $\tilde{\boldsymbol{\varepsilon}}$ will be associated to the problem (5), which are denoted by the vector $\tilde{\boldsymbol{\varepsilon}}^{(i)}$ in the 6D space. The stresses $\tilde{\boldsymbol{\sigma}}^{(i)}$ obtained by multiplying $\tilde{\boldsymbol{\varepsilon}}^{(i)}$ by the eigenvalues Λ_i are called the stress eigentensors. Therefore, a Cartesian basis in the 6D space can be constructed from the normalised strain eigentensors, denoted by $\tilde{\mathbf{N}}$:

$$\tilde{\boldsymbol{\varepsilon}} = \tilde{\mathbf{N}}\left|\tilde{\boldsymbol{\varepsilon}}\right|; \quad \left|\tilde{\boldsymbol{\varepsilon}}\right|^2 = \tilde{\boldsymbol{\varepsilon}} \cdot \tilde{\boldsymbol{\varepsilon}}; \quad \tilde{\mathbf{N}} \cdot \tilde{\mathbf{N}} = 1. \tag{6}$$

Hence, the stress eigentensors can be written in terms of the normalised strain eigentensors using Eqs. (2), (5) and (6) as:

$$\tilde{\boldsymbol{\sigma}}^{(i)} = \Lambda_i \tilde{\boldsymbol{\varepsilon}}^{(i)}. \tag{7}$$

With respect to the 6D space, $\tilde{\boldsymbol{\sigma}}$, $\tilde{\boldsymbol{\varepsilon}}$ and $\tilde{\mathbf{K}}$ have the following representation:

$$\begin{aligned} \tilde{\boldsymbol{\sigma}} &= \sum_{i=1}^{6} \Lambda_i \tilde{\boldsymbol{\varepsilon}}^{(i)} = \sum_{i=1}^{6} \Lambda_i \left| \tilde{\boldsymbol{\varepsilon}}^{(i)} \right| \tilde{\mathbf{N}}^{(i)} \\ \tilde{\boldsymbol{\varepsilon}} &= \sum_{i=1}^{6} \tilde{\boldsymbol{\varepsilon}}^{(i)} = \sum_{i=1}^{6} \left| \tilde{\boldsymbol{\varepsilon}}^{(i)} \right| \tilde{\mathbf{N}}^{(i)} \end{aligned} \tag{8}$$

and:

$$\tilde{\mathbf{K}} = \sum_{i=1}^{6} \Lambda_i \tilde{\mathbf{N}}^{(i)} \otimes \tilde{\mathbf{N}}^{(i)} \tag{9}$$

where $\otimes$ indicated the tensor or dyadic product. The projection of the strain state given by Eq. (3) along the eigenvectors obtained using Eq. (8) defines the eigenstrain vector $\tilde{\varepsilon}_i$. Thereby, the total elastic modulus due to nonlinear material behaviour defined in Eq. (1) becomes:

$$\tilde{K}_{TOT,i} = \Lambda_i \left(1 + \beta \tilde{\varepsilon}_i + \delta \tilde{\varepsilon}_i^2 + \cdots\right) \tag{10}$$

Once the total elastic modulus $\tilde{K}_{TOT,i}$ $(i = 1,\ldots,6)$ is obtained, according to Eqs. (10) and (9), the 6 x 6 nonlinear stiffness matrix $\mathbf{K}_{TOT}$ can be then transformed from Kelvin to Voigt notation and it can be used for the implementation of the explicit FE numerical method at each individual time step.

Nonlinear Finite Element Model

The application of explicit FE analysis in wave propagation problems allows computing the nodal forces and displacements without recourse to a factorisation of the global stiffness matrix in a step-by-step solution. Let us consider a 3D solid domain Ω with boundary Γ discretized with three-dimensional elements. The weak form of the equilibrium equations for the continuum Ω can be derived from the displacement variational principle as follows [23]:

$$\mathbf{M}\ddot{\mathbf{u}} = \mathbf{F}^{ext} - \mathbf{F}^{\text{int}} \tag{11}$$

where the dots superscript denotes a second time derivative operation of the global displacement vector $\mathbf{u}$ and the external nodal forces vector $\mathbf{F}^{ext}$, the internal nodal forces vector $\mathbf{F}^{\text{int}}$ and the (lumped) diagonal mass matrix **M** are:

$$\mathbf{F}^{\text{int}} = \sum_{e=1}^{n_{el}} \mathbf{L}^{(e)T} \mathbf{C}^{(e)} \mathbf{L}^{(e)} \mathbf{u} \tag{12a}$$

$$\mathbf{F}^{ext} = \sum_{e=1}^{n_{el}} \mathbf{L}^{(e)T} \left[\int_{\Gamma^{(e)}} \mathbf{\Phi}^T \mathbf{t} d\Gamma + \int_{\Omega^{(e)}} \mathbf{\Phi}^T \mathbf{b}\, d\Omega \right] \tag{12b}$$

$$\mathbf{M} = \sum_{e=1}^{n_{el}} \mathbf{L}^{(e)T} \mathbf{m}^{(e)} \mathbf{L}^{(e)} \tag{12c}$$

where $\mathbf{L}^{(e)}$ is the Boolean connectivity matrix that gather the nodal displacement $\mathbf{d}^{(e)}$ of each element *e* to the global one over the entire domain Ω, n_{el} is the total number of elements, $\Omega^{(e)}$ and $\Gamma^{(e)}$ are the element domain and its boundary, $\mathbf{\Phi}^T$ is the transpose of the shape function matrix, $\mathbf{t}$ and $\mathbf{b}$ are the surface traction and body (inertial) force of the element, respectively. The element stiffness matrix $\mathbf{C}^{(e)}$ in Eq. (12a) can be expressed in terms of the nonlinear stiffness matrix $\mathbf{K}_{TOT}$ as follows [24]:

$$\mathbf{C}^{(e)} = \int_{\Omega^{(e)}} \mathbf{B}^T \mathbf{K}_{TOT} \mathbf{B}\, d\Omega \tag{13}$$

whilst the element mass matrix in Eq. (12c) is:

$$\mathbf{m}^{(e)} = \int_{\Omega^{(e)}} \rho \mathbf{\Phi}^T \mathbf{\Phi} d\Omega . \tag{14}$$

Finally, the strain nodal displacement matrix is defined by:

$$\boldsymbol{\varepsilon} = \mathbf{B}\mathbf{L}^{(e)}\mathbf{u} \tag{15}$$

The global displacement at the instant of time k+1 using the central difference method is given by:

$$\mathbf{u}_{k+1} = \Delta t^2 \mathbf{M}^{-1} \left(\mathbf{F}_k^{ext} - \mathbf{F}_k^{\text{int}} \right) + 2\mathbf{u}_k - \mathbf{u}_{k-1} . \tag{16}$$

where k=0, 1, 2, … corresponds to times $t = 0$, $t = T$, $t = 2T$, …, and T is the time increment. To guarantee numerical stability to the method, the time increment used for the simulation satisfy the following condition [25]:

$$\begin{aligned} &T < T_{cr} \\ &T_{cr} = \frac{1}{\pi} \frac{1}{f_{\max}} \end{aligned} \tag{17}$$

where f_{max} is the largest natural frequency of the system. The numerical scheme defined by Eq. (16) can be used by those elements that present either linear or nonlinear features. Whilst in the former case, the nonlinear elastic moduli are zero, in the nonlinear case the nonlinear stiffness matrix of the element has to be constantly updated at each time step due to the amplitude dependence with the material constants.

FE Model and Specimen Dimensions

Crack Representation Modelling

One way to represent a crack inside a specimen is to attempt to accurately model the crack geometry and interfaces and to define appropriate contact conditions. However, this approach requires discretising the volume into very small finite elements due to the geometrical complexity of the crack interfaces; this inherently leads to distortion of the elements within the model [26].

An alternative method, which was adopted in this study, was to replace a damaged zone of the material with a user defined constitutive material model (UMAT) incorporating a classical nonlinearity representation theory in order to simulate a dynamic response of a test specimen with a crack. An isotropic elastic material was chosen as a base material model and no plastic deformations took place during the experiment.

Equations detailed in the previous section were incorporated into a user defined isotropic elastic material model with nonlinear parameters (*UMAT41*) using FORTRAN. This model was then linked with LS-DYNA solver to simulate a NRA of the test specimen. In the numerical procedure of the FE solver, strains and stresses are evaluated at every time step and for each element, which are in turn used at the next time step to update the internal forces.

Pre-Processing

Pre-processing of FEA problem involves creating the geometry, discretising the geometry into finite elements (i.e. meshing) and applying boundary conditions and forces. For this purpose, LS-PrePost 4.0 software tool was utilised.

The geometry was created using the dimensions of the test specimen (Figure 1). As the geometry is three-dimensional, it is required to be meshed using 3D solid elements. The mesh size was determined by studying the numerical procedure used by LS-DYNA to calculate the time step size during the transient analysis. The solver uses Eq. (17) to determine the time step size during the simulation.

The time step was chosen to be the same value as the sampling rate required in order to achieve a good resolution of the sine wave signal applied to the specimen; the applied frequency was 100 kHz, for which the sampling rate was 10 MHz and therefore the time step size *T* was 1e-7 s. The speed of sound was calculated to be approximately 6000 m/s, and the following aluminium properties were used, i.e. *E* (Young's Modulus, GPa) = 70, ρ (Density, kg/mm^3) = 2.70e-6, ν (Poisson's Ratio) = 0.3. Having determined the time step and the speed of sound of the material, the element size was estimated to be 0.6 mm (i.e. length of a side of a cubic 3D solid element). Hence, the NRA of the specimen were meshed using 0.6 mm element size, whilst other features of the sample were meshed using element sizes up to 1.5 mm. *MAT001*, which is an isotropic elastic material, was used to represent the material of the specimen while the NRA was modelled using the user defined material *UMAT41*.

In the physical experiment, the specimen was simply supported at two ends. For the purpose of FE modelling, this was simulated by constraining the out-of-plane translational degrees of freedom (DOFs) of the nodes of the computational mesh of the test piece at two ends as shown in Figure 2 using **BOUNDARY_SPC_SET* card within LS-PrePost.

The sine wave load was modelled by means of **LOAD_NODE_SET* card applying a sine load in out-of-plane direction on the nodes covering the area where the transducer was placed in the experimental setup. The **DEFINE_CURVE* card was used to supply a continuous sine wave load curve:

$$s(t) = A\sin(2\pi f_0 t) \tag{18}$$

where A is the amplitude (equal to 1kN) and f_0 is the excitation frequency.

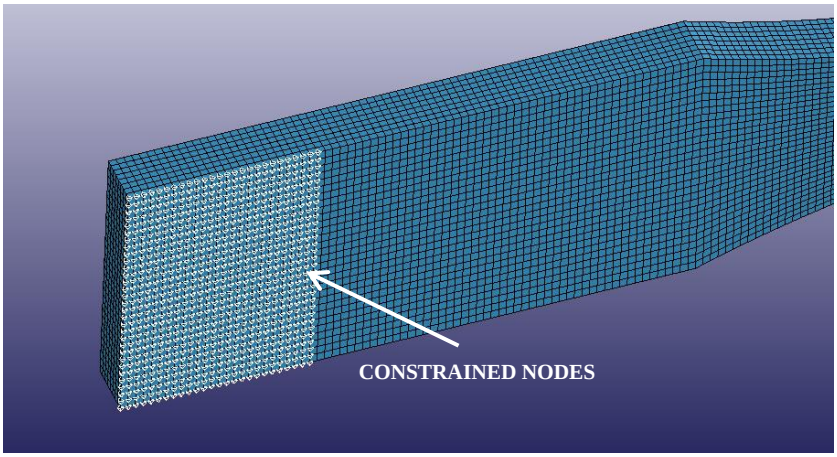

Figure 1: Selected nodes were constrained in out of plane direction in order to represent the experimental setup.

The final LS-DYNA deck contained approximately 72,000 3D solid elements modelled using *ELFORM=1* (i.e. constant stress element formulation) and nodal displacement histories were recorded at various locations throughout the specimen.

The simulation was run using a single precision SMP version of LS-DYNA on Intel Core i5 CPU utilising 4 cores clocked at 2.50GHz each. Wall clock computational time was 21 minutes.

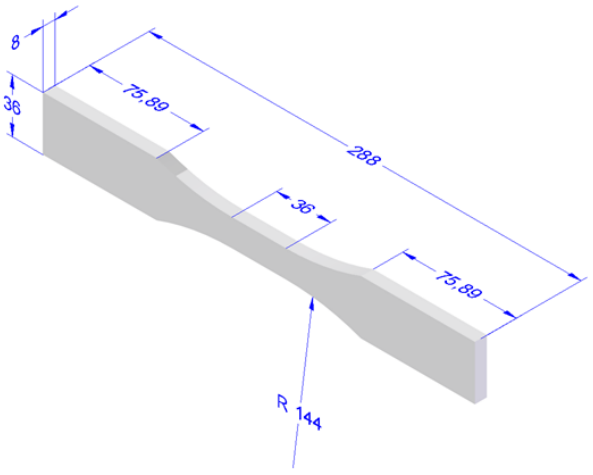

Figure 2: Dimensions of Dogbone specimen

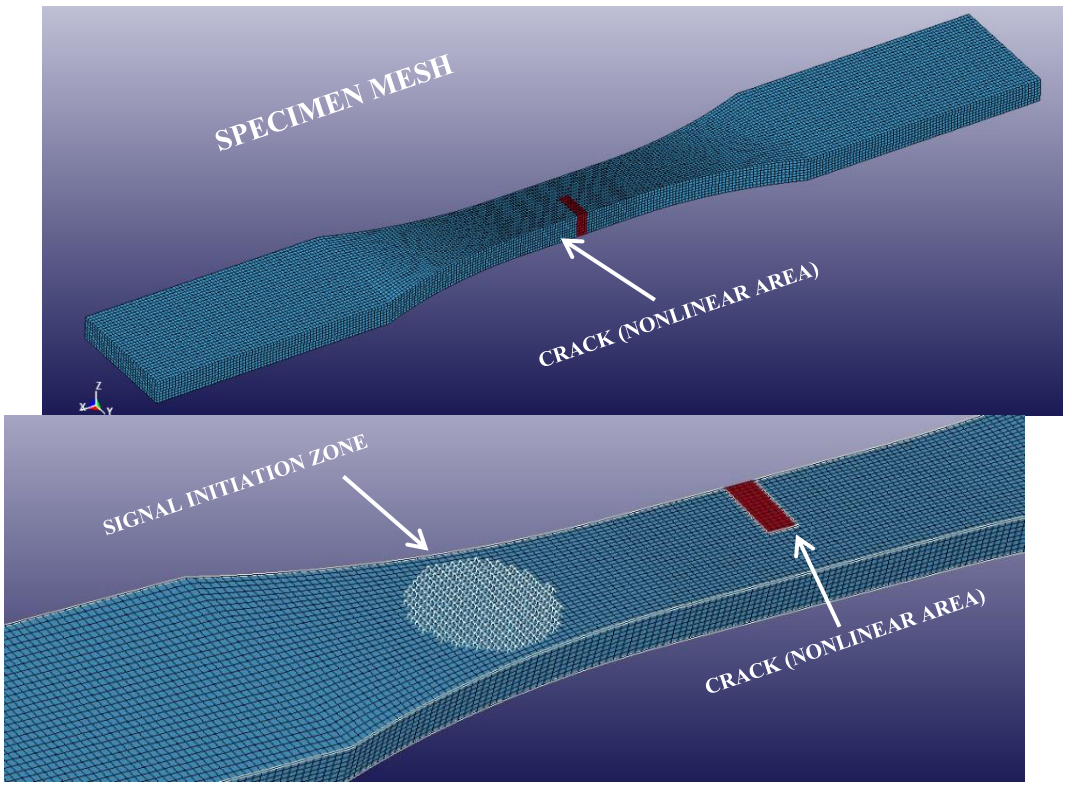

Figure 3: FEA model (elements, sensor and crack location)

Analytical Model

When exciting a structure using a single frequency excitation, the second-order (quadratic) nonlinear parameter (also known as β) generated by the presence of cracks or ruptures [27] can be defined as:

$$\beta = \frac{8A_2}{A_1^2 k^2 a_1} \tag{19}$$

where A_1 and A_2 are the amplitudes of the first and second harmonics of the recorded time domain waveforms, respectively, k is the wavenumber and a1 is the propagation distance. Eq. (19) was used to determine the experimental β, and was used within the constitutive model to determine the second harmonic ($2f_0$) produced by 'clapping/rubbing mechanisms' within the nonlinear response areas (NRA).

Experimental Setup

The experiment used a coupon that had been designed to allow for fatigue and crack growth. The samples geometry was representative of a classical dogbone for fatigue testing. The coupon was a high grade Aluminum 6082-T6, with a length of 288mm, thickness of 8mm, and breadth of 36mm. The design of the coupon ensured that: (i) high stress concentration areas existed, (ii) fatiguing of the sample focused on the initial crack region, and (iii) crack propagation occurred.

The piezoelectric sensor setup was determined by: (i) selecting the appropriate frequency, (ii) the use of broadband piezoelectric sensors, and (iii) assessing the production of harmonics at various piezoelectric sensor locations on the specimen. The piezoelectric sensors used (APC transducers) were glued in place and thus were attached to the coupon during the fatigue testing. This allowed evaluation of permanently installed transducers and evaluation of the proposed techniques in real-life conditions. The sending piezoelectric sensor was driven directly by an arbitrary waveform generator (TTi-TGA12104), and the receiving sensor was not amplified. The frequencies used were carefully selected. The arbitrary waveform generator was used to perform a sweep of the frequencies for various frequency ranges in order to determine the peaks of the second harmonic in the sample response. In this manner, the excitation frequency (f_0) used was 100 kHz. The specimen was tested at various intervals throughout its fatigue life using the excitation frequency in order to determine the nonlinear behaviour of the propagating crack.

The acquired signal, captured by Sensor 2 (Figure 4), was recorded using an oscilloscope (Picoscope 4224) in the time domain and then converted into the frequency domain (using a Fast-Fourier transform) to evaluate the production of further harmonics (second harmonic). This data was then analyzed over the fatigue life of the specimen. The sampling frequency used was 20 MHz.

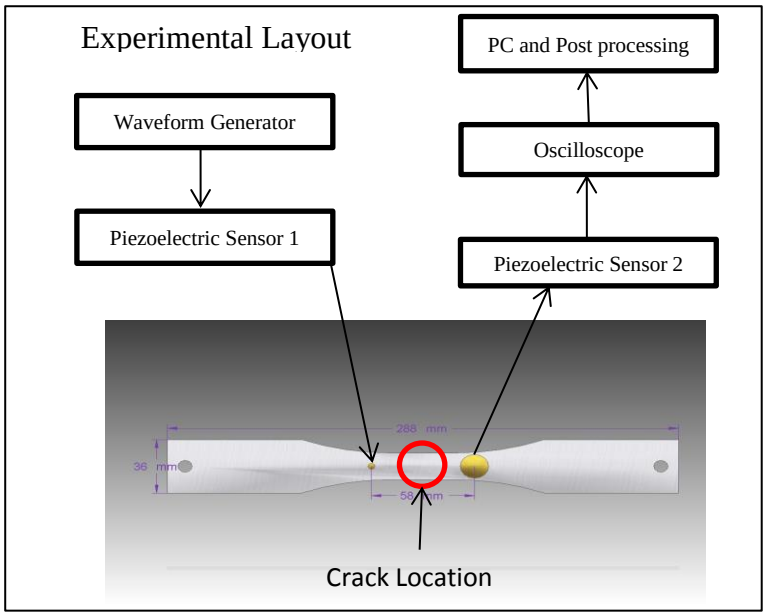

Figure 4: Experimental Layout

Numerical and Analytical Results

Crack Growth

The specimen was fatigued and tested using ultrasound at various points during its fatigue life. Figure 5 (below) shows the crack propagation length at 40000 cycles (90% of fatigue life) and the initial crack, measured using a microscope. The fatigue test was conducted using an Instron machine and was cyclic fatigued using sinusoidal tension with a stress ratio of 0.027 and amplitude of 18.5 kN. The material properties were carefully characterised before conducting the fatigue test to ensure crack propagation and specimen failure. The specimens showed consistent failure just above 40000 cycles. The consistency of the failure allowed accurate measurement of further harmonic production due to crack propagation.

Fatigue Life	0%, 25%, 32%, 40%, 87%, 99%
Number of Cycles	0, 10000, 13000, 16000, 35000, 40000
Stress Ratio ($\sigma_{min}/\sigma_{max}$)	0.027
Amplitude	18.5kN

Table III: Fatigue Characteristics

At each stage throughout the fatigue life of the specimen the second harmonic generation was assessed and compared with the fundamental frequencies amplitude in order to determine the second order nonlinearity parameter.

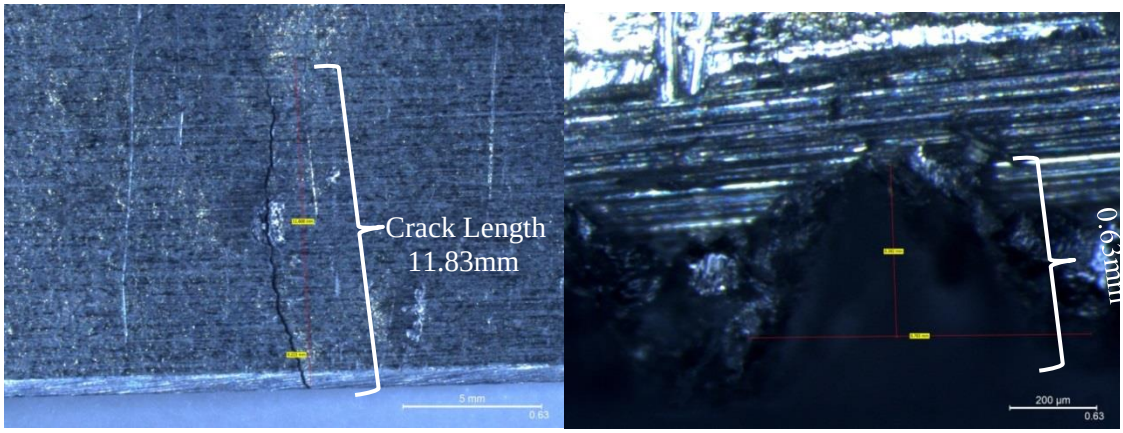

Figure 5: Crack propagation: 40000cycles (Left) and initial crack (Right)

Experimental and Numerical Results

The experimental β was used within the constitutive model in order to determine the level of the second harmonic. By applying the constitutive model and the experimental β to the NRA (areas of interest, representing damaged zones/crack propagation areas) it was possible to simulate the nonlinear material response.

During the post-processing step, the evolution of nodal displacements (recorded at various locations) through the specimen were plotted in the frequency domain by means of a Fast Fourier Transfer (FFT) using MATLAB software. These results (Figure 6) were initially computed for a stationary crack with dimensions of 5 x 5 x 2 mm in order to determine whether the computational model could be used to estimate the second harmonic level using the application of the material constitutive model.

The specimen was then fatigue tested using the ultrasound methodology discussed earlier. The experimental results (Figure 6a) show the amplitude of the second harmonic at 200 kHz ($2f_0$) relative to the amplitude of the fundamental frequency (f_0) whilst the computational analysis (Figure 6b) results show a normalised frequency domain plot. Figure 6b, was determined by using

the experimental value of β within the numeric model in order to evaluate the second harmonic. The numeric model was able to estimate the level of the second harmonic with good accuracy.

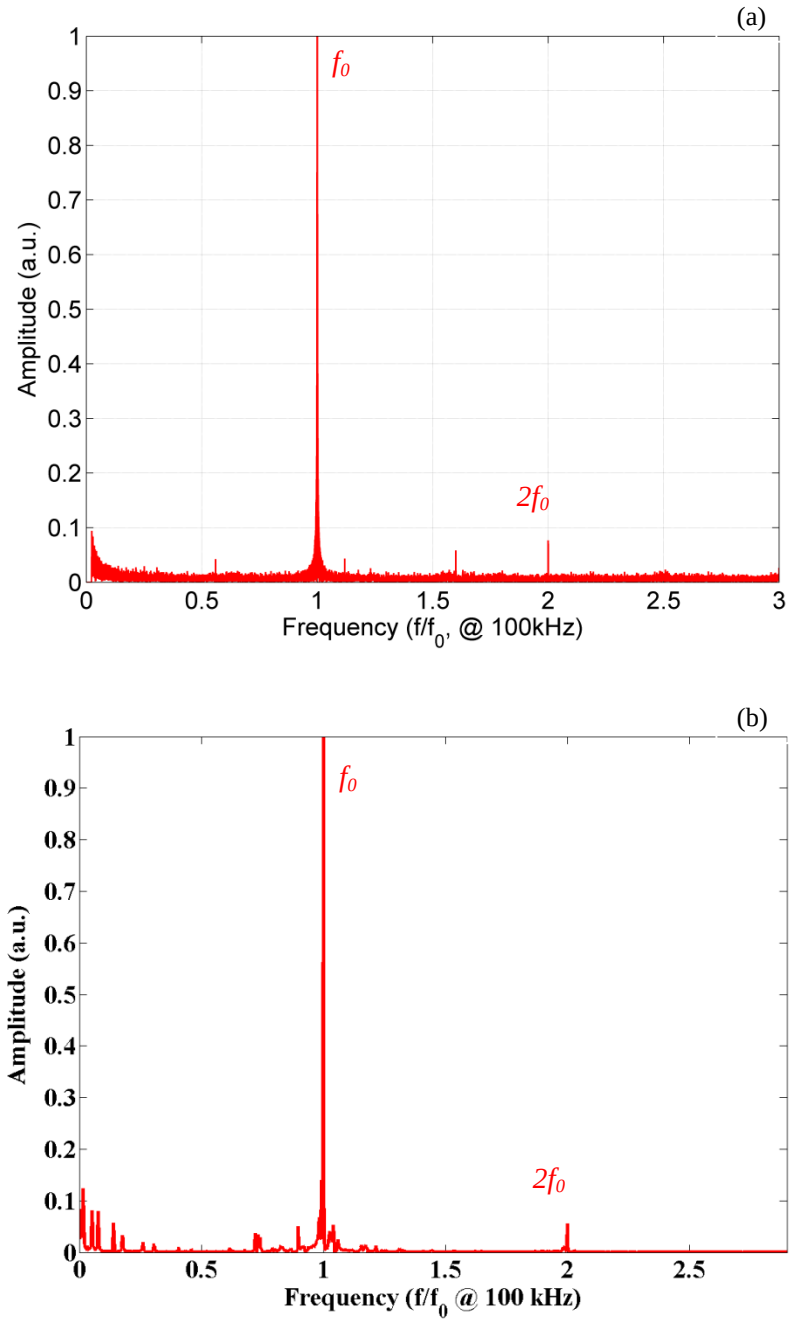

Figure 6: Normalised Experimental (a) vs. Normalised Numerical (b) Results (10000 cycles)

After the initial comparison between the constitutive model and the experimental results showed good correlation, the model was run with increasing NRA's to determine whether this increase would results in larger second harmonics.

Experimental results for the frequency tested confirmed a clear increase of the second order nonlinearity parameter (β) as fatigue life (and crack length) increased. The relationship between β and fatigue life showed that: (i) the increase in β was directly related to the fatigue life, resulting from a reduction in f_0 and increase in $2f_0$, (ii) the production of harmonics are directly related to the 'clapping/rubbing' mechanisms (i.e. cracks), as cracks increased in length so did the $2f_0$ generation, (iii) the growth of such mechanisms resulted in an increase in further harmonic production, and (iv) β can be used to estimate fatigue life.

In order to analyse the behaviour of the fundamental and second harmonics with crack propagation, images were taken using a microscope at each fatigue interval to determine the crack length. This allowed for visual confirmation that the second harmonic as well as β increased relative to the crack length. Taking into account that the production of the second harmonic allowed for the second order nonlinear parameter to be determined, a constitutive model that could predict $2f_0$ as crack length grows (increase in NRA) would provide valuable insight into the nonlinear, failure, and fatigue life mechanics of a component.

The model developed (Figure 7-dotted line) showed $2f_0$ increased as the NRA's grew representing the fatigue of the structure over its useful life. The increase in the numeric second harmonic showed good correlation with experimental results (solid line); as the NRA's were increased to represent larger cracks. It should be noted that element sizes were kept relatively large (in order to reduce computational times), but it is expected that greater accuracy could be achieved with finer meshes.

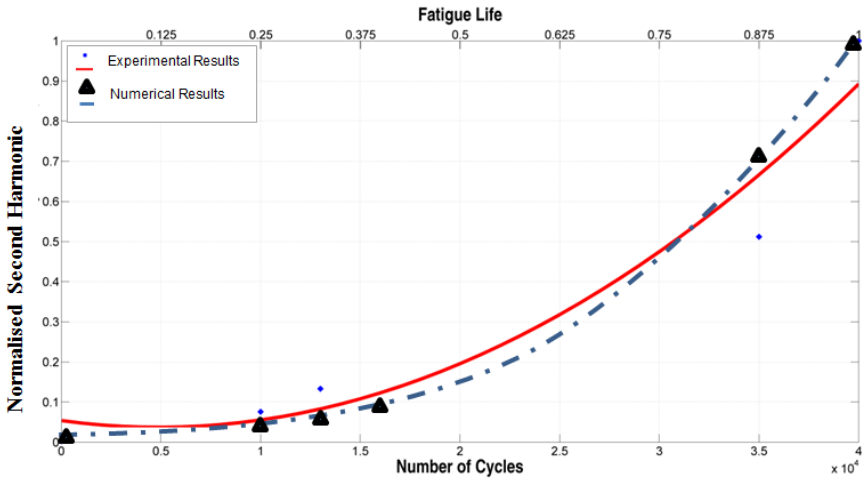

Figure 7: Normalised Second Harmonic vs. Fatigue life (Number of Cycles) at 100 kHz

The behaviour of NRA's using the developed constitutive model showed that: (i) the nonlinear behaviour which is directly correlated to the size of damaged regions can be modelled, (ii) element distortion is not an issue as the model developed does not require complicated design of cracks or other damage types, (iii) correlation between the model and experimental results were good, and (iv) it can be a useful tool to estimate the nonlinear behaviour of damaged regions at various stages over the fatigue life of a material.

A few considerations that should be taken into account regarding the developed model are: (i) the growth and propagation area of the crack were know, (ii) the specimen was designed to exhibit high stress concentration areas in known locations, (iii) fatiguing of the material was done accurately and used sinusoidal cycling, which would not be the case during the life cycle of a component, and (iv) simplicity of the shape of the specimen aids the developed model.

Conclusion

The work looked at developing a nonlinear constitutive material model that could predict the production of further harmonics which can be directly related to the extent of damage within a material. Nonlinear ultrasound methods have also been shown to be highly sensitive to damage compared with traditional methods such as linear ultrasound techniques. A material constitutive model was developed in LS-DYNA that could replicate and relate the production of further harmonics to a predefined nonlinear response area (NRA); this allowed for: (i) the estimation of the second harmonic after taking into account the experimental β value, and (ii) an estimation of damage progression related to the numeric generation of the second harmonic.

The experimental generation of harmonics and the increase of β as damaged increased showed that: (i) the results followed the expected theory that material damage results in further harmonics, (ii) the production of these further harmonics relative to the fundamental frequency increases with damage, and (iii) β can be used to estimate the fatigue life of the material.

The direct correlation between the generation of the second harmonic, damage, and the ability of the model to calculate the second harmonic showed that it can provide useful information about the growth of damage within a component. The β derived experimentally was used within the

model in order to assign nonlinear characteristics to known high stress regions or damaged regions, this allowed for the estimation of the second harmonic for various sized NRA's. Good correlation between the numerical prediction and experimental results were found for the prediction of the second harmonic.

The results of this work suggest that it is possible to generate FEA models based on nonlinear ultrasound theory and material models that would be able to estimate damage without the need of baseline tests of components. The robustness of the method relies on the comparison of the experimental and the numerical results, which showed good correlation.

References

[1] E.N., Janssen, K.V.D., Abeele, "Dual energy time reversed elastic wave propagation and nonlinear signal processing for localisation and depth-profiling of near-surface defects: A simulation study", *Ultrasonics* **51** (8), pp. 1036-1043, (2011)

[2] W., de Lima, M., Hamilton, "Finite-amplitude waves in isotropic elastic plates", *Journal of Sound and Vibration* **265** (4), pp. 819-839, (2003)

[3] K.-A., Van Den Abeele, P.A., Johnson, A., Sutin, "Nonlinear elastic wave spectroscopy (NEWS) techniques to discern material damage, part I: nonlinear wave modulation spectroscopy (NWMS)", *Research in nondestructive evaluation* **12** (1), pp. 17-30, (2000)

[4] M., Meo, G., Zumpano, "Nonlinear elastic wave spectroscopy identification of impact damage on a sandwich plate", *Composite Structures* **71** (3-4), pp. 469-474, (2005)

[5] G., Zumpano, M., Meo, "Damage localization using transient non-linear elastic wave spectroscopy on composite structures", *International Journal of Non-Linear Mechanics* **43** (3), pp. 217-230, (2008)

[6] L.-D., Landau, E.-M., Lifchits, A.-M., Kosevitch, L.-P., Pitaevski, J.-B., Sykes, W., Reid, L.-D., Landaou, L.-P., Pitaevski, Course of theoretical physics: Theory of elasticity, Butterworth-Heinemann, 1986.

[7] K. A., Van Den Abeele, P., Johnson, A., Sutin, "Nonlinear elastic wave spectroscopy (NEWS) techniques to discern material damage, part I: nonlinear wave modulation spectroscopy (NWMS)", *Res Nondestruct Eval* **12** (1), pp. 17-30, (2000)

[8] P., Johnson, "New wave in acoustic testing", *Mater. World* 7 (9), pp. 544-546, (1999)

[9] F., Ciampa, M., Meo, "Nonlinear elastic imaging using reciprocal time reversal and third order symmetry analysis", *The Journal of the Acoustical Society of America* 131, pp. 4316, (2012)

[10] S., Vanaverbeke, K., Van Den Abeele, "Two-dimensional modeling of wave propagation in materials with hysteretic nonlinearity", *The Journal of the Acoustical Society of America* 122, pp. 58, (2007)

[11] M., Scalerandi, V., Agostini, P.-P., Delsanto, K., Van Den Abeele, P.A., Johnson, "Local interaction simulation approach to modelling nonclassical, nonlinear elastic behavior in solids", *The Journal of the Acoustical Society of America* 113, pp. 3049, (2003)

[12] K.-Y., Jhang, "Nonlinear ultrasonic techniques for nondestructive assessment of micro damage in material: a review", *International journal of precision engineering and manufacturing* 10 (1), pp. 123-135, (2009)

[13] F., Amerini, M., Meo, "Structural health monitoring of bolted joints using linear and nonlinear acoustic/ultrasound methods", *Structural Health Monitoring* 10 (6), pp. 659-672, (2011)

[14] M., Amura, M., Meo, F., Amerini, "Baseline-free estimation of residual fatigue life using a third order acoustic nonlinear parameter", *The Journal of the Acoustical Society of America* 130, pp. 1829, (2011)

[15] L., Ostrovsky, P., Johnson, "Dynamic nonlinear elasticity in geomaterials", *Rivista del nuovo cimento* 24 (7), pp. 1-46, (2001)

[16] P.-A., Johnson, "The Universality of Nonclassical Nonlinearity (with application to Nondestructive Evaluation and Ultrasonics)", *Springer New York* Chap. 4 (49-69), (2006)

[17] L., Landau, E., Lifshitz, Pergamon Press, Oxford, UK, 1986.

[18] G., Zumpano, M., Meo, "A new damage detection technique based on wave propagation for rails", *International journal of solids and structures* 43 (5), pp. 1023-1046, (2006)

[19] K., Helbig, P.-N., Rasolofosaon, "A theoretical paradigm for describing hysteresis and nonlinear elasticity in arbitrary anisotropic rocks", *Anisotropy*, pp. 383-398, (2000)

[20] P., Theocharis, D., Sokolis, "Spectral decomposition of the compliance fourth-rank tensor for orthotropic materials", *Archive of Applied Mechanics* 70 (4), pp. 289-306, (2000)

[21] F., Ciampa, E., Barbieri, M., Meo, "Modelling of Multiscale Nonlinear Interaction of Elastic Waves with three dimenisonal Cracks", *J. Acoust. Soc. Am. 135 (4),* (2014) *doi: 10.1121/1.4868476*

[22] F., Ciampa, E., Onder, E., Barbieri, M., Meo, "Detection and Modelling of Nonlinear Elastic Response in Damage Composite Structures", *J. Nondestruct Eval.* (2014) *doi: 10.1007/s10921-014-0247-7*

[23] K.-J., Bathe, "Finite Element Procedures in Engineering Analysis", *Prentice-Hall Inc.*, (1982)

[24]. R.-D., Cook, D.-S, Malkus, M.E. Plesha, "Concepts and applications of finite element analysis", *third ed. John Wiley & Sons*, Hoboken, (1989)

[25] J., Donea, "Advanced Structural Dynamics", *Applied Science Publishers, Barking. Essex*, (1980)

[26] J., Sarrate Ramos, A., Huerta, "An improved algorithm to smooth graded quadrilateral meshes preserving the prescribed element size", Commun. Numer. Methods Eng. **17**(2):89–99 (2001)

[27] J.-H., Cantrell, "Fundamentals and applications of non-linear ultrasonic nondestructive evaluation", *Ultrasonic non-destructive evaluation* vol. 6 (Boca Raton (FL): CRC Press), pp. p.363-434, (2004)